APPLICATION OF SYNTHETIC MOLECULAR SIEVE ZEOLITES AND SILICA GEL TOWARDS THE SEPARATION OF SULFUR DIOXIDE FROM COMBUSTION GASES

by

George Todd Wright

Dissertation submitted to the Graduate Faculty of the

Virginia Polytechnic Institute and State University

in partial fulfillment of the requirements for the degree of

DOCTOR OF PHILOSOPHY

in

Mechanical Engineering

APPROVED:

F. J. Pierce, Chairman

H. M. McNair

H. L. Wood

W. C. Thomas

C. H. Long

May, 1979

Blacksburg, Virginia

ACKNOWLEDGEMENTS

I would like to express my sincere appreciation to the members of my advisory and examination committee: Professors W. C. Thomas, H. L. Wood, C. H. Long, H. M. McNair, and F. J. Pierce. I would especially like to thank Professor McNair for his guidance and advice throughout the investigation.

I am endebted to Professor Pierce, my committee chairman, for his invaluable counsel, assistance, and friendship throughout my graduate endeavors.

I extend thanks to for assisting in x-ray spectroscopy data acquisition.

Support of this investigation by the National Science Foundation is gratefully acknowledged.

I would also like to acknowledge the support and encouragement of and my mother during the course of this investigation.

Finally, I sincerely appreciate the support of my wife whose encouragement and tremendous patience lead to the completion of this dissertation.

TABLE OF CONTENTS

Table of Contents (Cont.)

Table of Contents (Cont.)

LIST OF FIGURES

List of Figures (Cont.)

List of Figures (Cont.)

List of Figures (Cont.)

LIST OF TABLES

NOMENCLATURE

a	effective area for heat and mass transfer
B	HETP constant
c	gas phase adsorbate concentration
D_B	adsorption column diameter
D_g	gas phase diffusivity
D_p	particle diameter
D_e	effective particle diffusivity
g	gravitational constant
HETP	height equivalent of theoretical plate
h	convective heat transfer coefficient
K	isotherm constant
k	thermal conductivity
L	bed depth
N_p	number of theoretical plates
n	isotherm exponent
p	pressure
PH	chromatograph response (peak height)
ppmv	concentration, parts-per-million
q	solid phase adsorbate concentration
q_m	asymptotic adsorbate solid phase concentration
q^*	equilibrium adsorbate concentration
q_{st}	isosteric heat of adsorption
R	gas constant

RH	relative humidity
s	entropy
T	temperature
V	gas velocity
X	axial position

Greek Symbols

β	dimensionless mass transfer coefficient
ΔH	heat of adsorption
ε	adsorption column porosity
λ	tortuosity factor
ρ_g	gas density
ρ_p	pellet density
σ	standard deviation
σ_m	standard deviation of mean

I. INTRODUCTION

The demand for economical, reliable, and environmentally acceptable energy sources has led to the development of several new processes and methods for electric power generation. In most cases these processes and methods are still in the early stages of development and application is not expected for many years. Fusion, wind, geothermal, and solar power are all promising but more research and/or development is needed. As a result, emphasis continues on the widespread application of proven methods or more readily adaptable systems which will be economically competitive.

Combustion processes associated with power generation have received considerable renewed attention because of strict air pollution emission standards. Presently, sulfur and nitrogen oxides represent the most important control problem. Sulfur oxide (SO_x) control is especially important since there has been renewed emphasis in the use of coal because of the oil embargo of 1973. The present state of sulfur oxide emission control is passive and relies heavily upon the use of low sulfur coal. Consequently, the vast high sulfur content coal reserves have not been fully utilized. Methods for the efficient control of sulfur oxides from combustion processes must be developed if full utilization of current coal reserves is to be realized within present day legislated environmental constraints.

1.1 Origin of Sulfur Oxides

Sulfur dioxide (SO_2) is the predominate oxide of sulfur formed by the combustion of sulfur laden fuels. Even when oxygen is present in large stoichiometric excess, sulfur trioxide (SO_3) is seldom found in amounts greater than a few percent of sulfur dioxide. SO_2 and SO_3 are collectively denoted by SO_x but SO_2 represents the most important control problem. The oxidation reaction for sulfur trioxide formation

$$SO_2 + \frac{1}{2}O_2 \rightleftarrows SO_3 \qquad (1.1)$$

forms SO_3 at equilibrium temperatures below 500°C (932 F) but, in the absence of a suitable catalyst, the rate of the forward reaction is extremely slow [1]. The formation of sulfur trioxide (SO_3) would be desired since the removal of dilute concentrations of SO_3 may be accomplished much easier than for other sulfur oxides (primarily SO_2).

The problem of sulfur dioxide removal is not really a new problem. Inhabitants of areas close to ore smelters, ore roasters, and sulfuric acid manufacturing plants have been aware of this problem for decades. It was not until the disastrous incidents in Belgium, London, and Donora, Pa., that the hazardous effects of sulfur oxide-related air pollution were realized. The most convincing case was in the December 1952, London air pollution disaster where total deaths for a two-week period from all causes exceeded the seasonal norm by

a factor of nearly three. Almost one thousand deaths occurred on the day of maximum sulfur dioxide concentration (3830 $\mu g/m^3$).

Toxicity of sulfur dioxide to the human respiratory system has been studied extensively. It is extremely irritating to the upper respiratory tract and complicated by the fact that the gas is readily absorbed by the protective mucous lining of the esophagus and the lungs' air passages. Once absorbed, SO_2 readily enters the blood-stream and alternation of carbohydrate metabolism, destruction of insulin, and reduction of liver glycogenesis have been verified [2].

Presently, there is little disagreement over the potential hazards associated with SO_2 pollution however; controversy exists over realistic values for concentrations and times of exposure.

1.2 SO_2 Emission Standards

In an effort to accelerate implementation of air pollution control, Congress amended the Clean Air Act in 1970 and established strict requirements and timetables for compliance. As a result, the Environmental Protection Agency (EPA) has published primary and secondary ambient-air-quality standards as shown in Table 1.1. Sulfur dioxide limitations were set at 0.52 Kg SO_2/MJ (1.2 lbm/MBtu) for coal-fired plants and 0.34 Kg SO_2/MJ (0.8 lbm/MBtu) for oil-fired plants. These values are commonly referred to as the New Source Performance Standards.

Since sulfur dioxide originates within the boiler proper and emission standards are based on the sulfur content and heating

Table 1.1 National Sulfur Dioxide Ambient Air Standards [3]

Standard	Concentration		Description
	$\mu g/m^3$	ppmv	
primary	80	0.03	annual arithmetic mean
	365	0.14	24-hr maximum not to be exceeded more than once per year
secondary	60	0.02	annual arithmetic mean
	260	0.1	24-hr maximum not to be exceeded more than once per year
	1300	0.5	3-hr maximum not to be exceeded more than once per year

value of the fuel, the most obvious solution would be to use a low sulfur, high-heating value fuel. However, this leaves the vast amounts of domestic high sulfur coal relatively unused. Reference to Table 1.2 shows estimates of known recoverable reserves of coal and indicates that portion of the total reserves that would comply with the New Source Performance Standards. The estimated reserve of high sulfur coal represents 87.7 percent of the remaining recoverable domestic coals.

As utilities begin to comply with the new emission standards, low sulfur coal will command a premium price. Consider, for example, that the entire growth potential for coal is based on low sulfur coal. Based on a conservative contemplated production growth rate of 7 percent per year through 1985, Rieber [5] concludes that by 1985 known recoverable reserves of low sulfur coal would be insufficient by a total of 1.27 billion metric tons (1.4 billion short tons) or 2.47 percent of the known domestic reserves.

Aside from the demand for low sulfur coal, there are also other factors to consider. First, most of the available low sulfur coal is found in the West while the largest consumers of coal are in the East. Second, low sulfur coals generally have a lower heating value and higher ash content consequently, even though a low sulfur coal is consumed, emission standards will not necessarily be met.

Table 1.2 Estimates of Remaining High and Low Sulfur Coals (Millions of Short Tons) [4]

	Deep Coal to 1,000 ft.	Sub-bituminous	Bituminous	Lignite	Capable of Compliance	Total
Total within Continental U.S.	288,267.0	62,168.0	39,360.8	27,867.5	51,513.0	417,663.9
Percent	69	14.9	9.4	6.7	12.3	100

Does not include Anthracite reserves totaling 7,294 tons.

Methods of Sulfur Dioxide Control

Several possible methods have been proposed for reducing SO_2 emissions. These control methods may be summarized as follows:

(1) Fuel selection--use of low sulfur fuel (depending upon meterological conditions);

(2) Coal gasification--conversion of high sulfur coal to low sulfur oil and gas (reduction of SO_2 to H_2S);

(3) Fluidized bed combusion--removal of SO_2 within the boiler by calcinated limestone;

(4) Coal cleaning--removing pyritic sulfur (Fe_2S) by chemical treatment;

(5) Gas dispersion control--use of tall stacks to insure low ground level concentrations of SO_2;

(6) Flue gas desulfurization (FGD)--post combustion process where SO_2 is removed from the combustion gas before the stack.

The gasification and coal cleaning processes both require the consumption of a portion of the input coal feedstock. It has been estimated [6, 7] that the energy penalty for gasification is roughly 25 percent compared to only three to seven percent for FGD. Coal washing processes can provide coal that will meet emission standards but only about 40 percent of the coal feedstock is cleaned. This is too expensive for most utilities [8]. Fluidized bed combustion has received considerable attention towards application in air pollution

control. However, fluidized bed combustion requires a redesign of the boiler and commercial availability is not expected until 1984-86 [9]. The use of fuel selection and tall stacks are not considered as solutions by the EPA. While several utilities are pursuing this approach, the installation of some means of control that will be compatible with EPA emission standards is inevitable. A case in point is the approach in England where ground level SO_2 concentrations have been substantially reduced by using tall stacks [10]. No response from neighboring countries was noted. Present U.S. emission standards are based on stack emissions and not ground level concentrations.

Of the six methods above, flue gas desulfurization is considered the leading sulfur dioxide control technique that will likely have large spread application in the next ten to fifteen years [11]. The current trend in fossil fuel central station installations has been towards larger capacity and by 1980, most new stations will provide a generating capacity in excess of 1000 MW [12]. This current trend and the fact that implementation of sulfur dioxide control equipment will eventually become mandatory has led to the popularity of FGD systems.

1.3 Flue Gas Desulfurization (FGD) Systems

A basic division in FGD systems is non-recovery versus recovery, which refers to the end product resulting from gas treatment. Non-recovery processes usually produce a sludge which either must be stored at the plant site or transported to an environmentally acceptable disposal site. These processes essentially convert an air

pollution problem to a solid waste disposal problem. Recovery processes produce a marketable product such as sulfuric acid, fertilizer, or elemental sulfur. The advantage of recovery processes is that the cost for gas treatment may be reduced.

Regenerable and non-regenerable refer to the material used to contact the gas. Either term may apply to a recovery or non-recoverable process. For example, the double-alkali liquid scrubbing process is non-recoverable and regenerable. The reason for this is that the end product from the process is a non-recoverable sludge but the material used for contacting the flue gas is regenerable.

The separation of sulfur dioxide from flue gas may be accomplished by three principal methods:

(1) Absorption-diffusion of SO_2 molecules through a gas into a liquid film or droplet through the gas-liquid interface;

(2) Adsorption-retention of the SO_2 molecules on a solid phase by physical (van der Waals) and/or chemical (chemisorption) forces;

(3) Catalysis-catalytic oxidation or reduction (preceded by adsorption of SO_2 for the eventual formation of hydrogen sulfide (H_2S) or sulfuric acid (H_2SO_4).

Within the division of non-recovery versus recovery processes the media used for gas contacting may be either 'wet' or 'dry'. A 'wet' process involves mixing or scrubbing the gas intimately with a

liquid. Removal of SO_2 is accomplished by reacting the SO_2 absorbed in the liquid with a suitable chemical, usually calcium carbonate (limestone). The liquid effluent is then conveyed to a holding tank where the SO_2 reactions go to completion and the wastes are separated by precipitation or other means. A 'dry' process involves contacting the SO_2-laden gas with a solid material that either combines chemically with SO_2, catalyzes SO_2 in the presence of O_2 to form SO_3, or simply retains the SO_2 on the surface by adsorption.

Recovery processes can also be applied to wet or dry systems. Presently wet, non-regenerable, non-recoverable (wet scrubbing) methods are highly favored [13]. Despite this fact, the universal acceptance of liquid scrubbing processes has not been achieved owing to the fact that several unsolved problems continue to prevent efficient operation. Lime-limestone scrubbers are the favored processes by the utility industry because it is considered that less risk (both economic and operational) is involved. The four main problems with wet, non-regenerable, non-recoverable, lime-limestone slurry scrubbers have been:

(1) Corrosion of carbon steel from low pH and high chloride content scrubbing liquor;

(2) Erosion of valves, nozzles, pumps, and auxiliary equipment by the abrasive slurry;

(3) Scaling and plugging (soft-scale formation) in pipes, pumps, and gas-contacting towers (especially wet-dry interfaces);

(4) Disposal of very large quantities of waste (approximately 900 tons/day for 1000 MW plant burning 3 percent sulfur coal).

Dry processes, although not as well developed, possess several important advantages. First, cooling of the flue gas is generally not required. Liquid systems usually require prehumidification and, consequently, gas cooling to help maintain proper chemistry in the scrubber circuit and to prevent water loss from the cycle. Cooling of the flue gas is highly undesirable because the stack gas has lost buoyancy which can lead to excessive ground level concentrations. In one instance, excessive ground level concentration occurred even through 92 percent of the SO_2 has been removed [14]. Second, process design is usually simplified since the amount of physical equipment is reduced. The degree of simplification is influenced by the process selection, i.e., recovery or non-recovery. The general differences between recovery and non-recovery processes are shown schematically in Fig. 1.1.

A major drawback of non-recovery processes is the problem of disposing of substantial quantities of waste (usually a thixotropic slurry material). Figure 1.2 demonstrates the distinct advantage of a recovery operation based on the weight of by-products for a 600 MW plant burning three percent sulfur coal. Based on current removal standards, about 0.9 million metric tons (1.0 million short tons) of sulfur would be removed from the flue gas over a 30-year period. A recovery process for sulfur production would produce

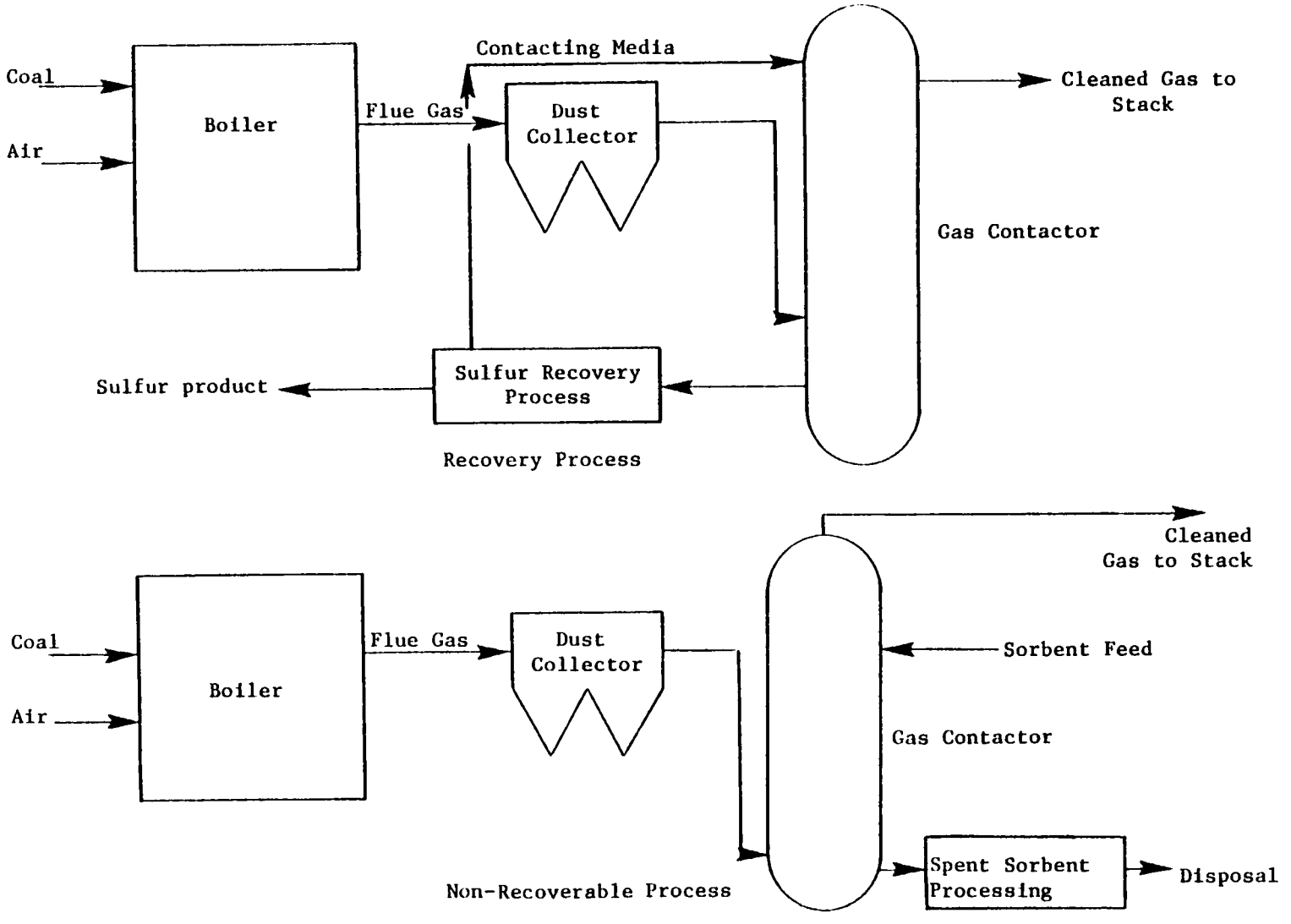

Figure 1.1 Comparison of Recovery and Non-Recoverable Processes for Flue Gas Desulfurization.

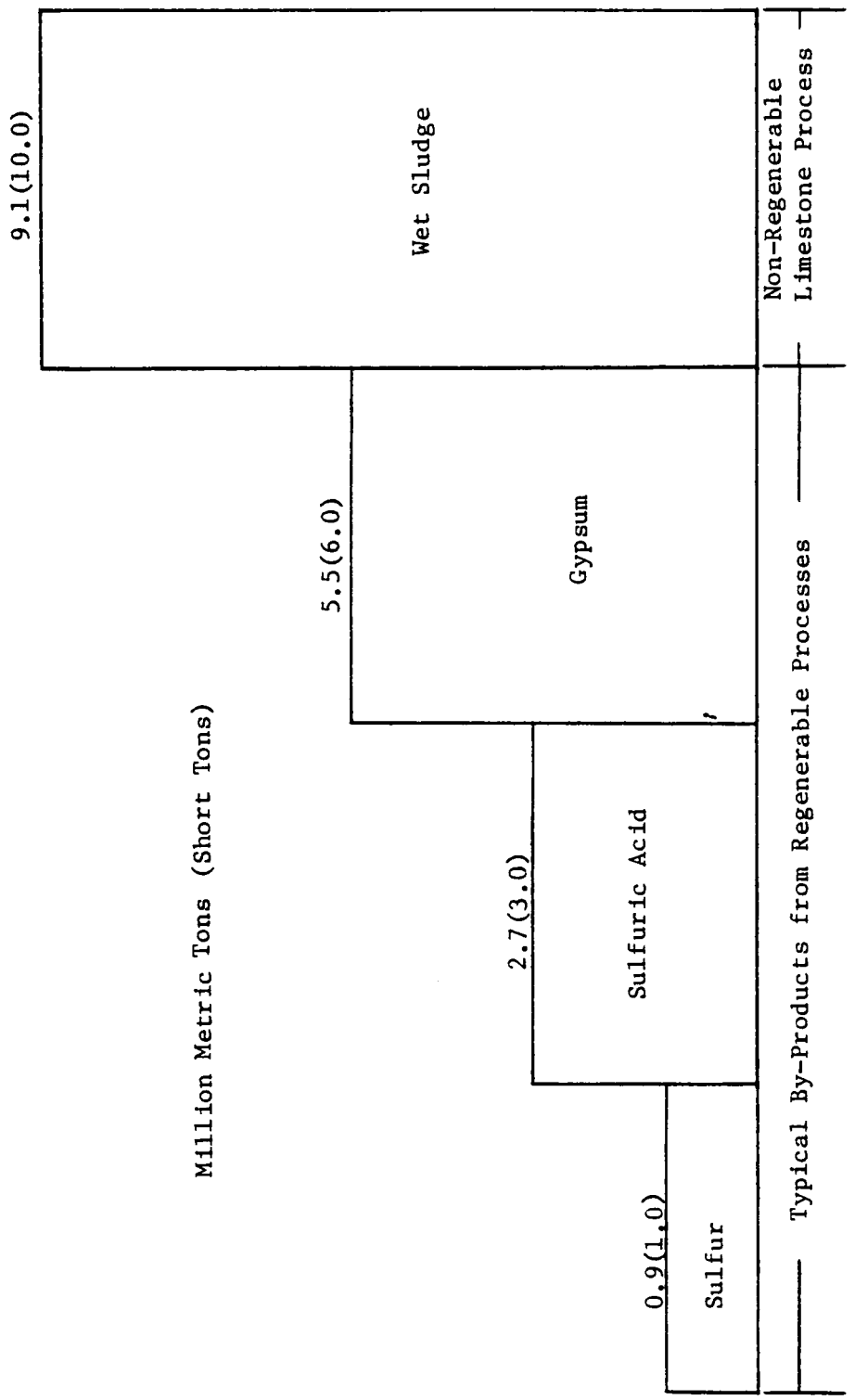

Figure 1.2 By-Product Generation from FGD Systems from a 600 MW Plant Burning 3 per cent Sulfur Coal [15].

one-tenth the by-products of a comparable non-regenerable process. Similarly, production of sulfuric acid would represent about one-third the amount of waste produced by a non-regenerable wet process. Aside from the advantage of decreased by-products production, recovery by-products may be marketed in an effort to offset the gas treatment cost. The by-products formed usually depends upon the nature of the recovery process. Since the processes are designed for SO_2 removal by oxidation or reduction, the usual form of sulfur by-product removed requires no further processing. For this reason several recovery processes have received considerable attention. Only a few of the several recovery processes developed have been cited by EPA [16] as being developed to the point of large scale industrial application in sulfur dioxide control processes. Table 1.3 gives a summary of these processes and the stages of development. Of these processes, only the Wellman-Lord process has been selected for installation by a utility [17]. It is interesting to note that all of the processes in development possess possible hazards, aside from their questionable performance in large scale industrial installations. Since either hydrogen or methane sidestreams are required to accomplish the necessary regeneration, this means that additional, often stringent, safety precautions must be taken because large gas volumes are used and the potential hazards could be significant.

Table 1.3 Status of Regenerable Desulfurization Process [8].

Wet Processes	Licensee or Identification	Number	Status as of April 1977
Sodium scrubbing	Wellman-Lord	2	1 in service, 1 under construction
Magnesium oxide	Chemico-Basic	3	all demonstrator down
Citrate	U.S. Bureau of Mines	1	demonstrator shutdown September 1974
Aqueous carbonate	Atomics International	1	shutdown in 1972
Dry Processes			
Activated carbon	Foster Wheeler/Bergbau-Forschung	1	started January 1975
Activated carbon	Westvaco	1	shutdown in 1974
Copper oxide	Shell/Universal Oil Products	1	tests in progress

1.4 Adsorption Processes for Flue Gas Desulfurization

Adsorption is one possible means for accomplishing combustion gas desulfurization which has not received considerable attention. It offers the following advantages:

(1) No humidification or gas cooling is required;

(2) Regeneration is usually simpler compared to chemical absorbents;

(3) Gas contactor design is usually much simpler.

The disadvantage of adsorption is that the processes tend to become uneconomical due to attrition of expensive adsorbents and loss in adsorption capacity due to fouling over many cycles of regeneration. Of the many adsorbents that have been investigated, processes using alkalized aluminum, copper oxide, and activated carbon have been the most thoroughly developed.

The alkalized alumina process shown schematically in Fig. 1.3 was originally patented by the U.S. Bureau of Mines [19]. Equilibrium capacities for SO_2 are about 15-20 percent by weight [20] when contacted with flue gas at 330°C (625 F). Regeneration is accomplished at 650°-705°C (1200-1300 F) with hydrogen as the reducing gas. The hydrogen sulfide (H_2S) produced may then be readily processed to elemental sulfur by the Claus process.

The copper oxide process proposed by the U.S. Bureau of Mines and shown in Fig. 1.4 uses porous alumina impregnated with copper oxide. The alumina acts as a support for the copper oxide adsorbent which otherwise could not withstand repeated use. Regeneration

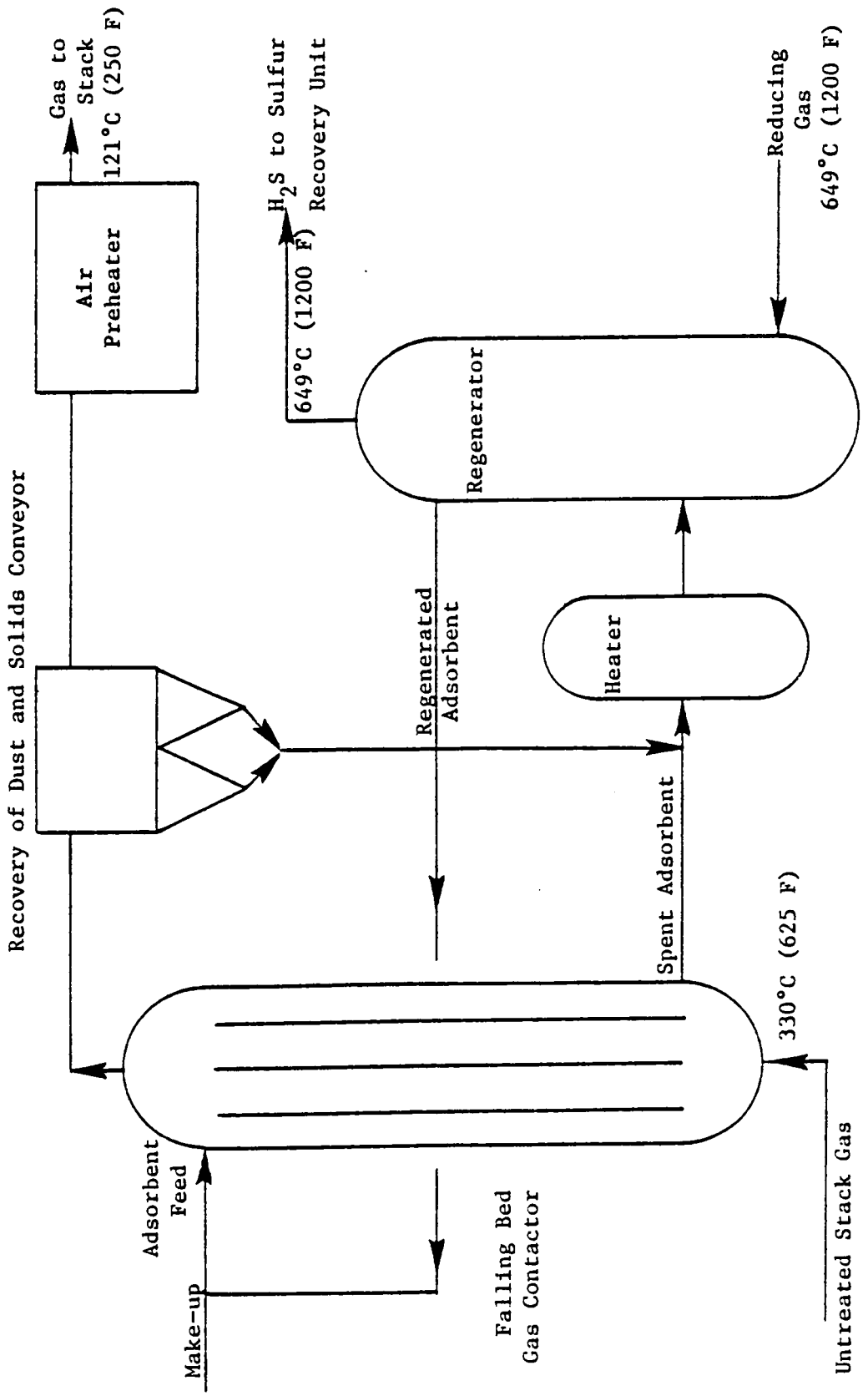

Figure 1.3 Alkalized Alumina Process Proposed by U.S. Bureau of Mines.

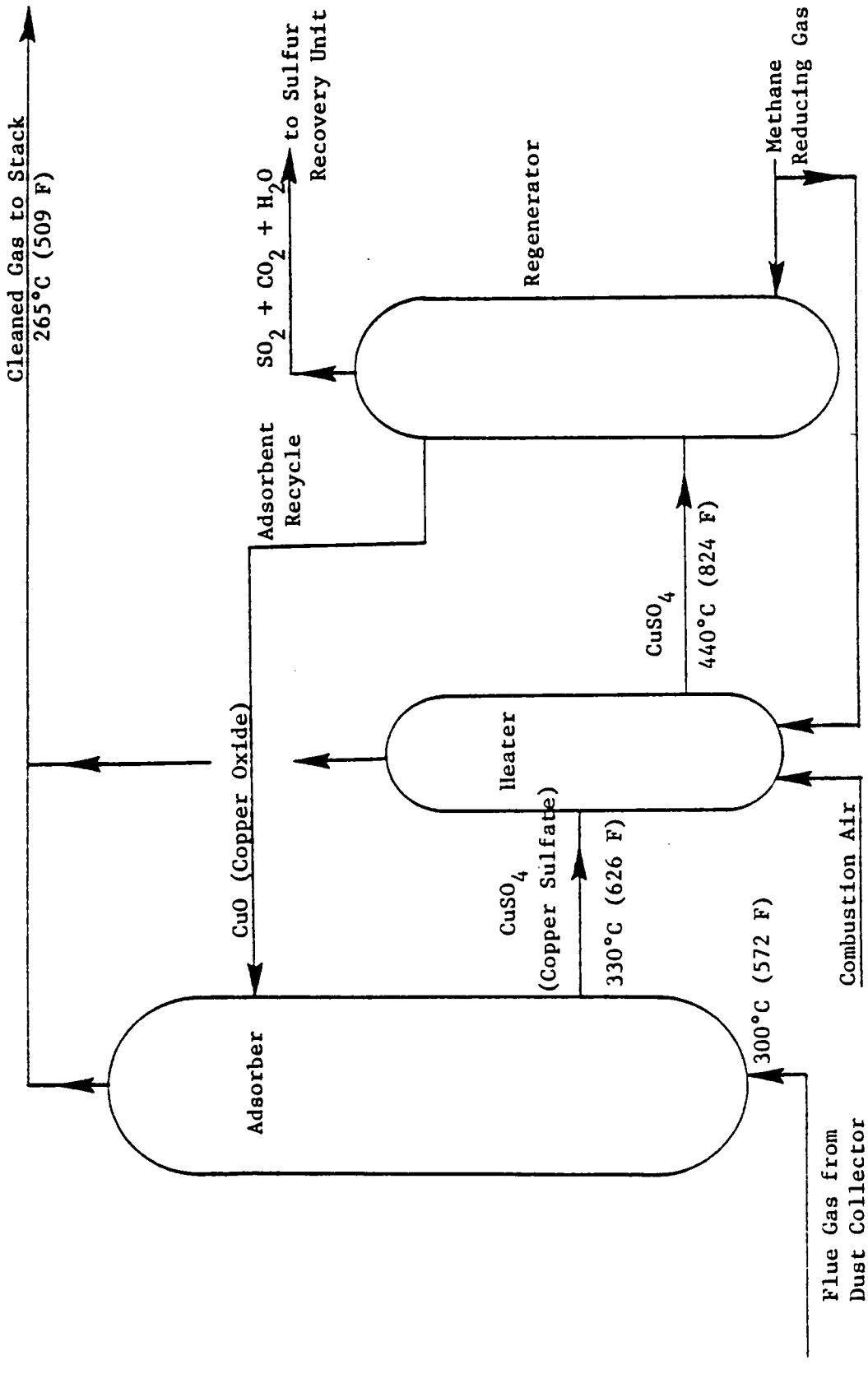

Figure 1.4 U.S. Bureau of Mines Copper Oxide Process for Flue Gas Desulfurization.

is accomplished at approximately 420°C (788 F) with methane used as the reducing gas. A similar process is presently being developed by Univeral Oil Products under license from Shell Oil Company. The main difference is that in the latter portion of the process the solid adsorbent is not transferred from the adsorber to the regenerator but instead is a fixed bed where regeneration and adsorption take place in the same contactor [21].

Foster Wheeler Corporation/Bergbau-Forschung and Westvaco Corporation are independently developing processes based on the use of activated carbon for SO_2 adsorption [22, 23]. A flow sheet for the FW-BF process is shown in Fig. 1.5. Equilibrium capacity for SO_2 by activated carbon is about five to twelve percent SO_2 by weight at approximately 100°C (212 F). The difference between the two processes is primarily in the method used to accomplish regeneration. In the Westvaco process regeneration of the activated carbon is obtained by using side streams of natural gas or hydrogen at temperatures of 149°C and 538°C (300 and 1000 F) to purge the bed of elemental sulfur and form hydrogen sulfide (H_2S). The FW-BF process utilizes sand at 816°C (1500 F) mixed with the carbon to reverse reactions that occur during adsorption.

The main drawback of the above four processes is that the regeneration is carried out at high temperatures and this would result in a substantial energy penalty. Additionally, the reducing gas used for some of the processes is flammable posing additional problems of safety. In light of these problems an effort was

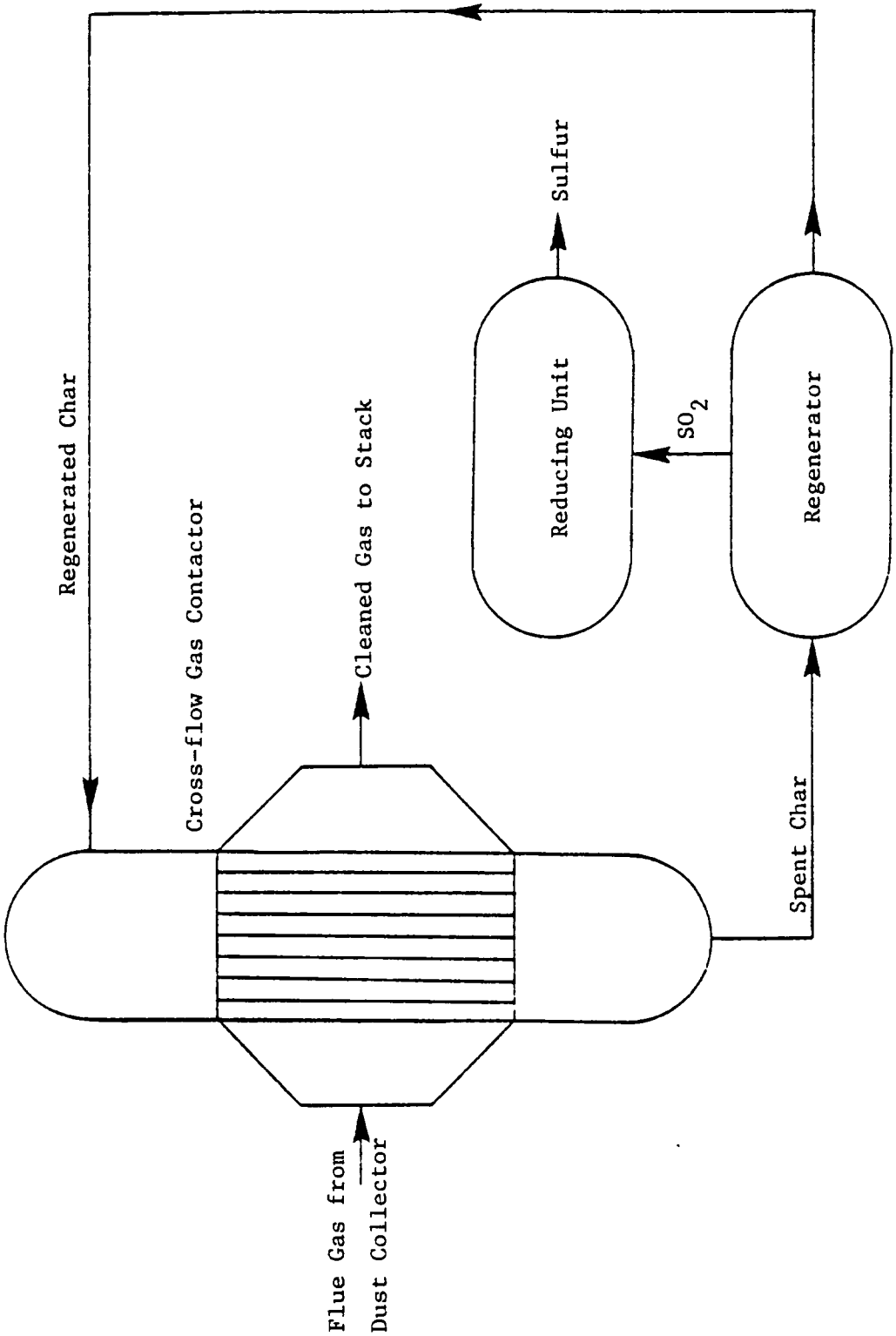

Figure 1.5 Foster Wheeler-Bergbau Forschung (FW-BF) Dry Adsorption Process for SO_2 Removal.

undertaken in this study to investigate several adsorbents and process variations that would accomplish the necessary SO_2 removal without being susceptible to the two serious problems of energy penalty and safety. The desired characteristics of such an adsorption process would be that it would:

(1) Require minimum energy for regeneration;

(2) Not require complex processes or chemical treatment for removal or regeneration;

(3) Operation restricted to similar operating conditions of existing units (similar flow, temperature, and pressure drop conditions).

A novel, preliminary-design disclosure [24] was used as the basis for evaluation. The process, shown in Fig. 1.6 involves the continuous movement of an adsorbent material through an SO_2-contaminated gas stream. Regeneration is accomplished by passing a purge gas at approximately 260°C (500 F) with supplemental radial heating for regeneration. The adsorbent is arranged as a fixed bed-matrix assembly such that adsorbent attrition would not be a problem. Since the bed is transported continuously the switching of large gas volumetric flows is unnecessary. The design is similar to rotary air preheaters currently used successfully on large central stations.

Using this as a basis for study, the next step was selection of the adsorbent. Because of the low regeneration energy, high adsorption capacity requirement, the selection of a suitable adsorbent was

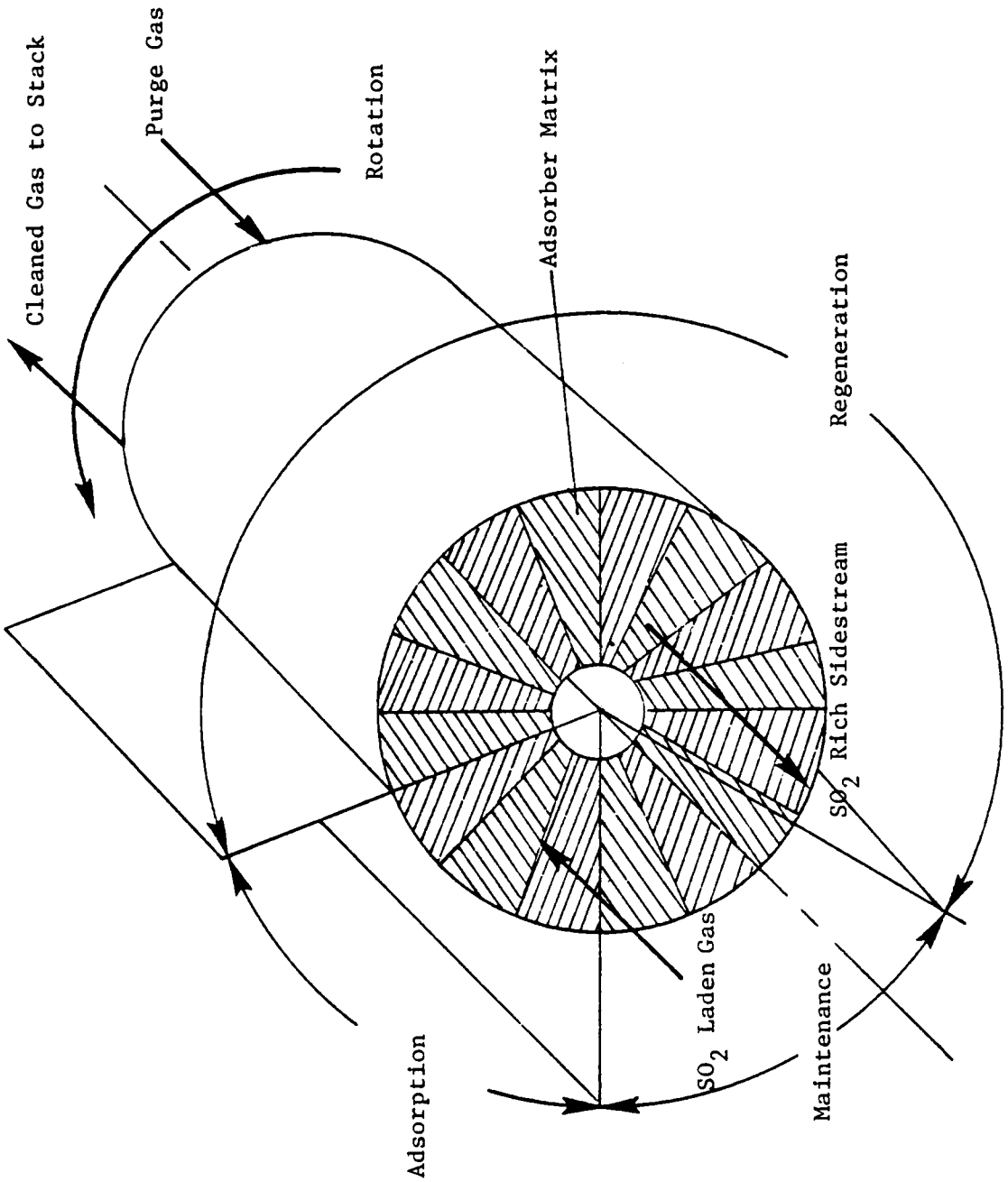

Figure 1.6 Rotary Adsorber Design for Flue Gas Desulfurization.

limited. After careful evaluation, molecular sieves and silica gel were selected for study. Both adsorbents have shown promise based on equilibrium data but necessary kinetic information does not appear to exist in the literature.

1.5 Goals and Scope of the Research Effort

In view of the current problems associated with FGD dry adsorption systems, an investigation was performed with the following specific goals:

(1) Evaluate kinetic performance of adsorbents under conditions similar to other FGD systems;

(2) Evaluate interference effects by competitive adsorption with other gases;

(3) Determine the stability of the adsorbent under the acidic conditions that would occur within the FG train;

(4) Evaluate the effects of various methods of regeneration on stability and adsorbent life;

(5) Provide a basis for adsorbent evaluation based upon selectivity;

(6) Compare experimental results with one-component adsorption models that could be used for scaling of the device.

An experimental system was designed to study the effects of temperature, gas volume flow, and water vapor concentration on the removal efficiency of the previously mentioned adsorbents. Since

the continuous bed configuration operates in the transient mode from the adsorbent point of view, the transient performance of the adsorber beds is a key to the successful engineering design of such a large scale continous bed device.

The purpose of this investigation was to establish process feasibility of the concept and obtain preliminary chemical kinetic data of the adsorption process. Adsorbent regeneration studies were used to identify process parameters that could significantly reduce adsorbent life.

II. THEORY OF ADSORPTION

Adsorption is a rather complex subject that requires a knowledge of several fields of study. At present, many theories have been proposed to explain the mechanism of equilibrium and dynamic adsorption. The purpose of the following section is to review the theories of adsorption used as a basis for evaluating the proposed FGD system.

The process of adsorption may be considered to take place in three steps. First, the adsorbate is transferred through the gas phase by molecular and/or turbulent diffusion to the external surface of the solid. The next step is diffusion of the adsorbate into the pores of the adsorbent. The third step is the actual adsorption of the adsorbate at a site within the adsorbent surface layer. The overall rate of adsorption will be limited by the slowest step of the overall three-step transport process. Diffusion through macro- and micropores is a property of the adsorbent material while the external transfer process is hydrodynamically controlled.

The occurrence of adsorption is manifest in two ways:

(1) The adsorbate is bound to the adsorbent by the same forces that account for the non-ideal behavior of gases--viz., classic van der Waals attractive forces; or

(2) Electrons are shared or transferred between the adsorbate and adsorbent; thus a chemical reaction has occurred.

Case (1) is referred to as physical adsorption, case (2) is generally referred to as chemisorption. The fundamental difference between physical adsorption and chemisorption lies in the nature of the attractive forces involved. The forces in chemisorption arise due to the exchange or sharing of electrons, while physical adsorption forces are the classical electrostatic van der Waals forces. Because of these differences in forces a certain 'activation energy' is associated with chemisorption.

The most consistent difference between physical adsorption and chemisorption is the magnitude of the heat of adsorption released during the solid-gas interaction. Heat of adsorption is defined simply as the energy released during adsorption. The release of energy (heat of adsorption) for physical adsorption is on the same order of magnitude as the energy transfer required to condense a gas at constant pressure and temperature. The energy release during chemisorption is much higher and is on the order of the energy of the chemical bonds. While this is not always true, it does indicate the presence of different kinds of attractive forces.

Additionally, these two types of adsorption differ in the temperature interval of adsorption. Physical adsorption generally occurs at temperatures in the neighborhood of the boiling temperature of the adsorbate, while the temperature interval for chemisorption is generally over a larger range.

Finally, physical adsorption requires no activation energy for the process to occur, while the rate of chemisorption varies with temperature and is very dependent on activation energy [25].

2.1 Adsorption Equilibrium and Surface Retention

Adsorption equilibrium leads to the important concept of the adsorption isotherm. At the point that adsorbtion equilibrium is established the number of molecules leaving the surface is equal to the number striking the surface.

For a given condition of adsorption equilibrium the amount adsorbed, q, is represented by

$$q = q(p,T)$$

where p is the equilibrium pressure of the adsorbate and T is the adsorbate temperature.

If the temperature remains constant during adsorption and the pressure is varied, the variation of the amount adsorbed for this constant temperature is known as the adsorption isotherm. Functionally, the relation is written

$$dq = \frac{\partial q}{\partial p}\bigg|_T dp \qquad (2.1)$$

The concept of an adsorption isotherm is very important. It is the most used characteristic of an equilibrium adsorption system and is used in the solution of kinetic adsorption problems, pore volume,

magnitude of heat of adsorption, and affinity coefficient (which relates the relative adsorbability to a given standard) studies.

Several semi-empirical relations have been proposed to represent adsorption isotherms. These are presented in Fig. 2.1 and are defined as

(A) Henry's Law--simple equation which relates amount of adsorbate adsorbed, q, as a function of equilibrium pressure,

$$q = Kp \tag{2.2}$$

where K is temperature dependent and p is the equilibrium pressure.

(B) Freundlich's Equation--the amount of adsorbate that is adsorbed, q, is proportional to the gas pressure p raised to $\frac{1}{n}$, where n is a factor that depends on temperature.

$$q = Kp^{1/n} \tag{2.3}$$

The Freundlich Equation is of importance for chemisorption processes because it fits experimental data very well.

(C) Langmuir Equation--this theory is based on the dynamic equilibrium concept whereby there are equal rates of adsorption and desorption. Thus, for a single adsorbate

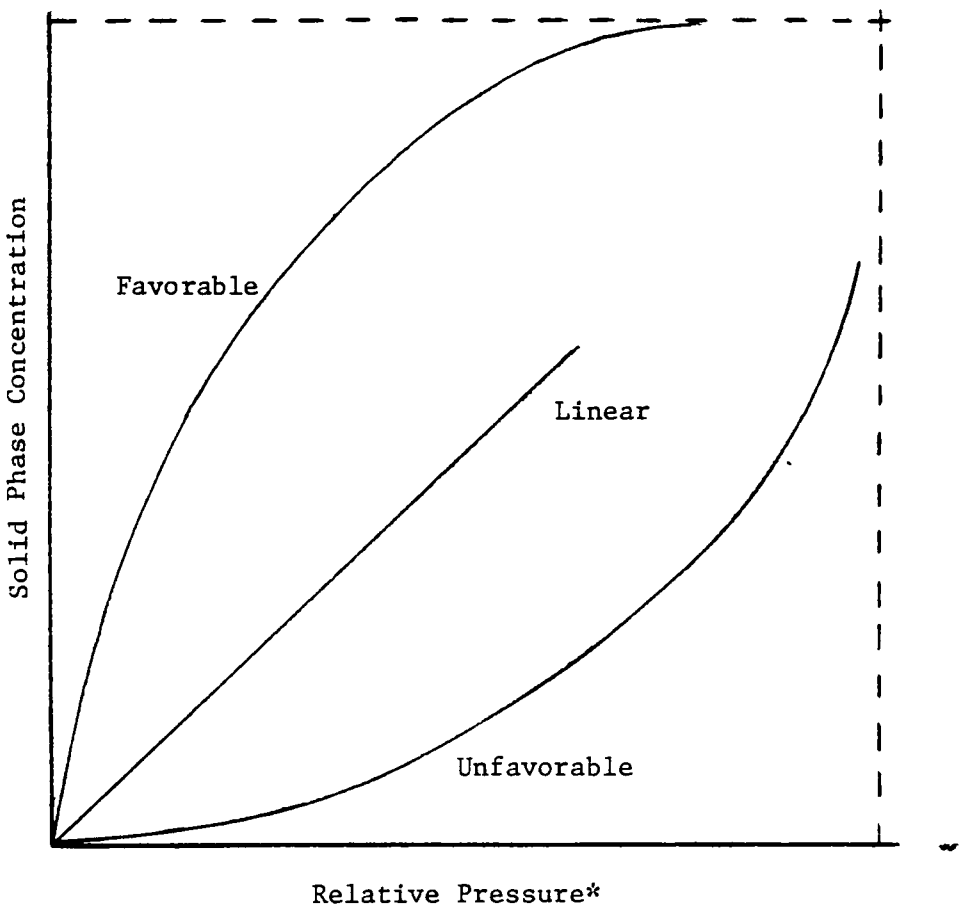

Figure 2.1 Representative Adsorption Isotherms.

*Ratio of absolute to saturation pressure.

$$q = q_m Kc/(1 + Kc) \qquad (2.4)$$

where q_m is the asymptotic maximum solid-phase concentration, K is the equilibrium constant and c is the adsorbent concentration in the gaseous or mobile phase.

The derivation of the Langmuir equation is based on three assumptions: 1) the molecule can only by adsorbed on the free surface, thus a portion of the surface that adsorbs a molecule cannot adsorb another, 2) all molecules have the same probability of being adsorbed, and 3) the forces between adsorbed molecules are assumed negligible in comparison with the forces of attraction (adsorption).

The terms 'favorable' and 'unfavorable' in Fig. 2.1 refer to the adsorption process with respect to removal efficiency. A favorable isotherm indicates that high loadings are possible for low partial pressures. The opposite is true for an unfavorable isotherm. During regeneration a favorable isotherm is not desired since very high vacuums, high regeneration temperatures, or very pure (adsorbate free) purge gases are needed.

While equilibrium data is of significant importance for screening purposes, kinetic studies are necessary to evaluate rate controlling steps in the overall transport process. The ability to successfully predict adsorbent performance usually becomes more difficult

when binary and multicomponent adsorption occur and the adsorption process is adiabatic. Because of insufficient data in the open literature and lack of sophisticated mathematical models, the evaluation of adsorbents must be performed experimentally.

III. REVIEW OF THE LITERATURE

3.1 Molecular Sieve Zeolites

Molecular sieve zeolites are crystalline aluminosilicates that possess the ability to selectively adsorb gases and liquids. The crystal structure of zeolites is three-dimensional which, when dehydrated, consists of a matrix of channels and pores. Since these pores and channels occur within the crystal, very high surface area to volume ratios result. Unlike other industrial adsorbents, the pore size distribution is discreet and therefore certain molecules are excluded from the crystal based on the size of the molecule alone. McBain [26] noticed this effect in 1926 and thus coined the term "molecular sieve" indicating the sieving property of zeolites. The combined properties of molecular selectivity and high affinity for polar molecules combine to yield a class of adsorbents that can selectively separate gases from complex gas mixtures.

Zeolites were first recognized by Cronstedt as a new group of minerals consisting of hydrated aluminosilicates of alkali and alkali earths with his discovery of stilbite in 1756 [27]. For centuries, more natural zeolites and zeolite deposits were located but lack of demand hindered their widespread utilization. In 1948, Union Carbide Corporation's Linde Division became interested in the use of zeolites for gas purification and separation. Until this time utilization of natural zeolites had been hindered because their physical and chemical variability made applications difficult. Therefore, research was begun to develop and synthesize zeolites that could yield more

reliable performance. By 1953, more than 30 distinct pure zeolites had been prepared with possible applications for such diverse uses as air separation and drying, large-scale separation of normal paraffins from branched chain and cyclic hydrocarbons, high altitude atmospheric sampling, acid gas drying, and liquid hydrocarbon and natural gas sweetening by H_2S and mercaptan removal [28].

3.2 Properties of Zeolites

The general chemical formula for molecular sieves is

$$M_{2/n}O \cdot Al_2O_3 \cdot xSiO_2 \cdot yH_2O$$

where M is the cation of valence n. Of particular importance in zeolite manufacture and chemistry is the mole ratio of SiO_2/Al_2O_3. By controlling this ratio, zeolites of differing properties are possible. Usually, as the mole ratio is increased, the stability of the zeolite to low pH attack is reduced. The adsorbents chosen for this study have unit cell formulas:

$$\text{type 13X:} \quad Na_{86}[(AlO_2)_{86}(SiO_2)_{106}] \cdot 276H_2O$$

$$\text{type AW500:} \quad Ca_{4.5}[(AlO_2)_9 (SiO_2)_{27}] \cdot 27H_2O$$

Type 13X is used commercially for general gas drying and natural gas sweetening. Type AW500 is a so-called acid stable zeolite that resists change in chemical composition and crystal structure when exposed to low pH environments.

Molecular sieves not only separate molecules based on molecular size but they also will preferentially adsorb molecules based on polarity and degree of saturation (gas phase concentration). The strong adsorptive forces in zeolites are largely due to the cation and cation concentration. The cations act as strong, localized sites that attract the negative end of a polar molecule. Thus a polar molecule of strong dipole moment is preferentially adsorbed to a non-polar molecule.

The forces responsible for adsorption in zeolites are physical in nature [29]. This means that a chemical reaction (i.e., sharing or transfer of electrons) does not occur between the adsorbent and adsorbate. The importance of this is that during regeneration considerably less energy is required to desorb the adsorbate since the bonding responsible for chemisorption results in much greater forces than the bonding forces of physical adsorption.

3.3 Sulfur Dioxide Adsorption Using Zeolites

The selection of an adsorbent for the conditions that prevail in a typical flue gas stream should be based on zeolites that possess the following properties:

(1) high rates of adsorption coupled with high equilibrium capacity;

(2) resistance to acid attack and/or poisoning by the complex flue gas;

(3) multiple regeneration capabilities without significant deterioration in ultimate capacity;

(4) physical integrity to insure low attrition;

(5) low energy input required for regeneration.

Several investigators have studied the equilibrium capacity of zeolites for SO_2. Sameshima and Hemmi [30] first studied the equilibrium adsorption of natural zeolites in 1934. They found that the equilibrium adsorption capacity of N-mordenite for SO_2 was about 20 percent by weight but 24 hours was required to attain equilibrium. Bienstock, Field and Myers [31] evaluated several industrial adsorbents including zeolites, activated carbon, and copper oxide. They found that Linde Molecular Sieves Types 4A, 5A and 13X adsorbed 2.3, 1.8 and 7.0g SO_2 (0.08, 0.06 and 0.2 ounces) per 100g (3.5 ounces) of adsorbent, respectively, at 130°C (265 F). The results obtained for zeolites were comparable to results obtained for activated and impregnated carbons. They concluded that the higher equilibrium capacity of type 13X zeolite could be attributed to the pore size. The type 4A pore size is roughly 4×10^{-10}m (4Å) which is approximately the same diameter as the critical diameter of the SO_2 molecule [3.7×10^{-10}m(3.7Å)].

The experiments of Bienstock, et al. were carried out in a gas stream of the following composition:

Constituent	Volume Percent
SO_2	0.3
CO_2	13.0
O_2	6.0
H_2O	6.0
N_2	74.7
	100.0

Since the bed effluent concentration was measured by adsorption in standard iodine and titration with sodium thiosulfate, no indication of the effect of water vapor on the equilibrium capacity could be ascertained. This should have been considered due to the strong affinity of zeolites for water. The importance of the work of Bienstock and Field with respect to this study is the comparable performance between zeolites and activated carbons. As noted previously, activated carbons have received considerable attention and currently are being considered for full scale development.

Martin and Brantley [32] evaluated the performance of Linde Molecular Sieves type 13X, AW500, 3A, 4A and 5A. Tests were performed in a 2.5 cm (1.0 in.) ID glass pipe and exposed to SO_2 concentrations of 1, 3 and 9 percent SO_2 by volume at 2m/min (6fpm). The simulated flue gas was composed of SO_2, CO_2, and N_2. Tests were performed at 26°C (79 F) and 89.3 kPa (26.5 in. Hg). Of the adsorbents tested, types 13X and 4A had the greatest selectivity for SO_2 adsorbing 29.5g (1.04 ounces) and 27.6g (0.974 ounces) of SO_2 per 100g (3.5 ounces), respectively. Their tests were performed under very dry conditions so that the effects of water vapor were not considered. Regeneration studies were performed by exposing the adsorbent bed to a 9 percent by volume SO_2 gas stream until the bed was saturated. The flow rate was then reduced and bed heating commenced while the flow of SO_2 was stopped. The effluent concentration from the bed was measured at discreet time intervals and the effluent SO_2 concentration recorded. The regeneration temperature was limited to below 400°C (752 F) which

is below the critical operating temperature of this zeolite. The significance of their results is that a relatively concentrated (approximately 90 percent by volume) SO_2 stream was obtained. This effluent then could be processed more easily that the original 9 percent by volume stream.

Regeneration tests were performed for several cycles and the reduction in capacity noted. Martin and Brantley found that the 13X zeolite lost approximately 57 percent of the original adsorption capacity after 13 cycles compared to type 4A which lost 40 percent. No effort was made to determine if the residual SO_2 was bound to the crystalline zeolite or if a possible side reaction with the zeolite, zeolite binder, or complex adsorption with subsequent chemical reaction resulted in the irreversible adsorption of SO_2.

Tamboli [33] evaluated the equilibrium capacity of several natural and synthetic zeolites and also determined their acid stability on exposure to sulfuric acid (H_2SO_4). In a one-normal acid solution, 10 to 1 acid to adsorbent ratio (10 mℓ to 1g), natural and synthetic large-port mordenite, natural ferrierite, natural phillipsite, and Linde AW300 molecular sieves are acid stable. X-ray diffraction patterns for the unstable adsorbents showed a noticeable change indicating a rearrangement in the zeolite crystal structure. The acid stable zeolites, Norton H mordenite powder, and Linde AW300 pellets were found to adsorb 17.4 and 9.2g SO_2 (0.6 and 0.3 ounces) per 100g (3.5 ounces) of adsorbent, respectively.

Anurov, et al. [34, 35] evaluated the kinetics of adsorption of SO_2 on natural zeolites. The three zeolites studied were composed of 80 percent clinoptilolite, 70 percent clinoptilolite, and synthetic CaY zeolite. Rate parameters were studied by using single grain samples on a McBain balance. The results confirmed the variation of solid phase diffusivity could be described by the Arrhenius relation

$$D_e \propto \exp(A\gamma) \tag{3.1}$$

where γ is the normalized temperature and A is a constant. Based on kinetic data, Glueckauf's equation [35]

$$\frac{dq}{dt} = \beta \frac{(q^*)^2 - q^2}{2q} \tag{3.2}$$

gave the best prediction of SO_2 sorption kinetics on CaY synthetic zeolites.

Friedman [36] performed an exhaustive study of several industrial adsorbents. Of particular interest were the results obtained for clays and zeolites. He found that Bentonite clay could adsorb about 2 percent by weight SO_2. No effort was made to determine the adsorption mechanism. Norton H zeolite was found to reversibly adsorb SO_2 at 200°C (392 F). Norton zeolites with copper and nickel cations were found to have low capacities (less than 1 percent by weight). Friedman attributed the low capacities at temperatures above 125°C (257 F) to the premise that purely physical adsorption is not possible near the critical point of the adsorbate.

Vinnikov, et al. [37] conducted tests on activated charcoal, NaX, N-mordenite zeolites, and silica gel to determine the effect of SO_2 and water vapor on the relative adsorption capacity of the adsorbent. The testing method consisted of quantitatively measuring the SO_2 and water vapor released from a thermodesorption apparatus. Thermodesorption data was obtained which showed the dependence of the quantity of SO_2 adsorbed with time. The relative equilibrium capacities for SO_2 and water vapor were essentially the same for both the NaX and N-mordenite zeolites.

Strong displacements of SO_2 occurred as the water vapor concentration was increased above 0.5 percent by volume. Although the reported adsorption data seemed promising, the validity of the thermodesorption technique is questionable based on evidences of previous investigators [33] who report that, even in the absence of H_2O, irreversible adsorption of SO_2 occurs.

Brown [38] conducted experiments on several dry adsorbents after it was suspected that drying agents used in sampling systems of stack gas monitoring instrumentation were causing erroneous results. Dry adsorbents tested included molecular sieves, dehydrated gypsum (Drierite), and calcium chloride. It was found that both nitric and sulfur oxide concentrations were reduced by the adsorbents, with molecular sieves responsible for the greatest reduction. Since results were for the simultaneous removal of NO and SO_2, estimates of the removal capacity for SO_2 alone by the adsorbents was not possible.

3.4 Silica Gel

Silica gel is a porous, amorphous form of silica synthetically manufactured from the chemical reaction between sulfuric acid and sodium silicate. Silica gel is relatively inert, reacting only with strong alkalies and hydrofluoric acid. It is slightly softer than ordinary window glass having a hardness of No. 5 on Moh's Mineralogical Scale. Silica gel has selective affinity for moisture and is also efficient in selectively adsorbing certain types of compounds from hydrocarbon mixtures [39].

Only a few investigations have been concerned with measurement of the equilibrium adsorption capability of silica gel for SO_2. The first investigation was performed by McGavack and Patrick [40] in 1920 as a result of previous work to obtain materials that could be used against poisonous war gases, especially mustard gas. This is the only known equilibrium study, aside from the work of Friedman [36], that was found in the literature. Cole and Shulman [41] evaluated isosteric heats of adsorption based on the data of McGavack and Patrick and compared the results to SO_2 ultimate adsorption capacities of several anion exchange resins. A representative isotherm for the adsorption of SO_2 on silica gel is shown in Fig. 3.1. For comparison, an isotherm for SO_2 adsorption on Davison Type 13X zeolite, measured by Joubert [42], is also presented. Both adsorption isotherms are 'favorable' but the 13X isotherm exhibits far greater loadings for lower partial pressures. Silica gel is of interest,

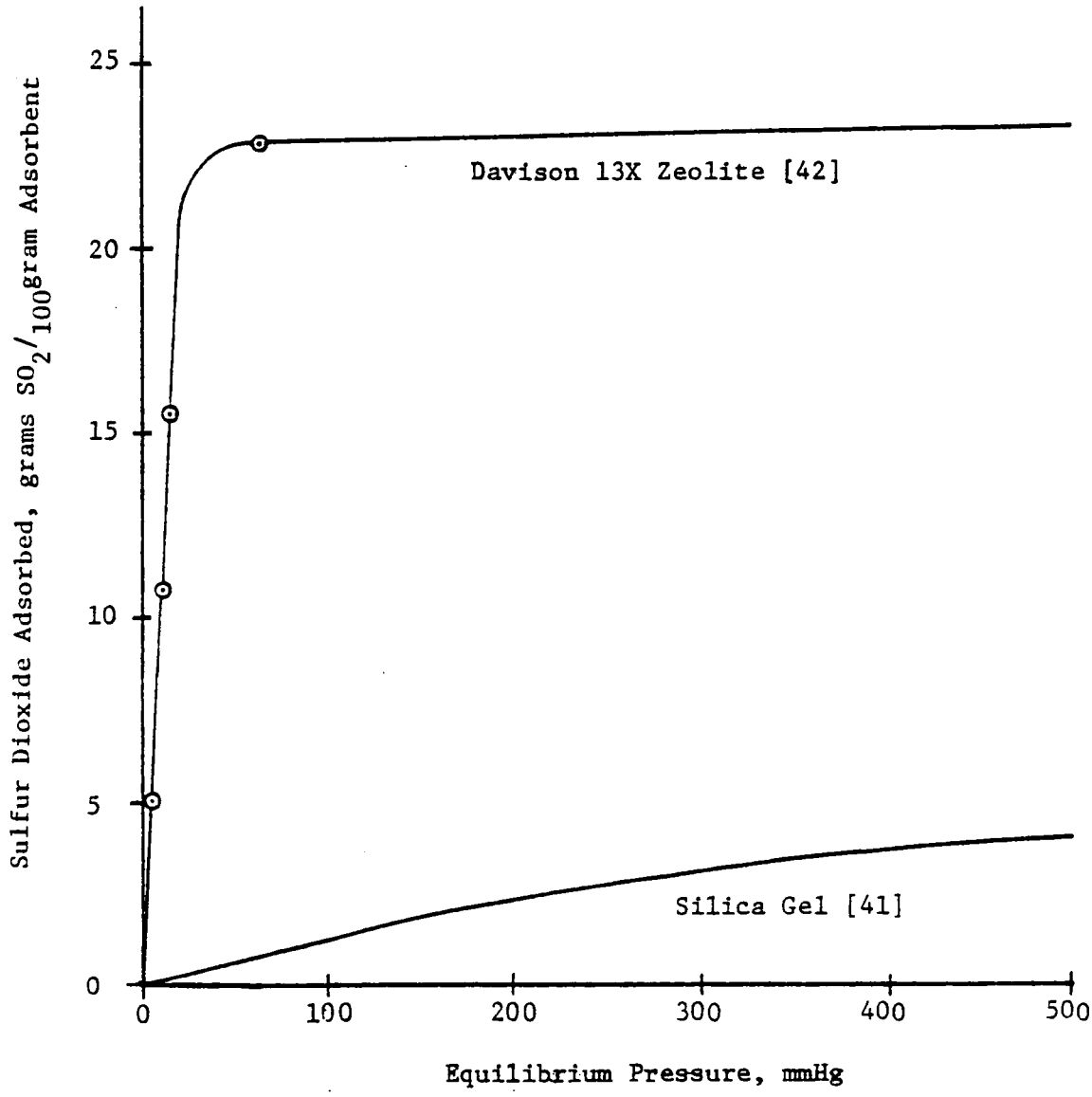

Figure 3.1. Equilibrium Adsorption Capacities of 13X Zeolite and Silica Gel for Sulfur Dioxide.

though, because of its known stability in acid environments and physical integrity which would be beneficial if low adsorbent attritioning was important. Jones and Ross [43] measured adsorption isotherms and isosteric heats of adsorption for chromatographic grade silica gels for the temperature range -10 to 50°C (14 to 122 F). The partial pressures used correspond to SO_2 concentrations much greater than those usually encountered in a combustion gas stream. Galan and Smith [44] used a pulsed-response chromatographic method to measure adsorption and intraparticle mass transfer of sulfur dioxide in silica gel at 1 atmosphere and a temperature range of 175 to 270°C (347 to 518 F). Adsorption was nearly reversible in the temperature range 175-270°C but irreversible below 150°C (302 F). Also, it was found that intraparticle mass transfer significantly affected the overall rate of adsorption.

3.5 Adsorbent Selection and Justification

A summary of known measurements for SO_2 adsorption on zeolites is presented in Table 3.1. Presently, kinetic data necessary to develop or design a large-scale adsorber does not exist. Aside from the work of Vinnikov [37], the existence of kinetic data for the simultaneous removal of SO_2 and water vapor was not found. As a preliminary step, the screening of adsorbents based on equilibrium capacities is justified but further dynamic testing is essential to insure that

Table 3.1 Sulfur Dioxide Adsortpion on Molecular Sieves and Silica Gel.

Adsorbent	SO_2 Concentration	Composition of Carrier				SO_2 Adsorbed	Temp.	Equilibrium Time	Investigator
	Vol. pct.	N_2	CO_2	O_2	H_2O	g/100g	C	min.	
(Molecular Sieves)									
Linde 13X									Martin and
	9	81	10	-	-	27.6	26	70	Brantley [32]
	3	87	10	-	-	23.9	26	-	
	1	97	10	-	-	22.2	26	-	
Linde 5A	9	81	10	-	-	18.9	26	41-45	
Linde AW500	9	81	10	-	-	18.4	26	50	
	3	87	10	-	-	16.5	26	-	
	1	89	10	-	-	14.2	26	-	
Linde 13X	9	81	10	-	-	29.5	26	35-37	
	3	87	10	-	-	27.5	26	-	
	1	89	10	-	-	25.5	26	-	
Davison 13X	0.35	82.7	14.9	-	-	6	125	-	Friedman [36]
Norton--H(cation)	0.35	82.7	14.9	-	-	1-2	125	-	
Norton--Cu(cation)	0.35	82.7	14.9	-	-	1-2	125	-	
Norton--Ni(cation)	0.35	82.7	14.9	-	-	1-2	125	-	
Norton--H(cation)	0.35	82.7	14.9	-	-	3.9	23	-	
Natural Mordenite	100	-	-	-	-	10.223	28	150	Tamboli [33]
Linde AW300	100	-	-	-	-	9.721	28	100	
Linde 4A	0.3	74.7	13.0	6.0	6.0	2.3	130	-	Bienstock and
Linde 5A	0.3	74.7	13.0	6.0	6.0	1.8	130	-	Field [31]
Linde 13X	0.3	74.7	13.0	6.0	6.0	7.0	130	-	
Zeolite (NaX)	0.37	78.0	21.0	0.45	-	2.2	-	-	Vinnikov [37]
Zeolite N-Mordenite	0.37	78.0	21.0	0.45	-	1.8	-	-	
(Silica gel)									
Gel (ShSM)	0.37	-	-	-	0.45	1.0	-	-	
Gel(ShSM)	0.59	-	-	-	0.01	2.2	-	-	
Gel (ShSM)	0.30	-	-	-	2.5	2.0	-	-	
						cc/g			
Silica Gel (labora-	110	-	-	-	-	110	25	-	McGavack and
tory sample)	100	-	-	-	-	25	100	-	Patrick [40]

(1) adsorber design is compatible with central station operating conditions (turndown ratio, variable SO_2 release);

(2) promising equilibrium data is accompanied with high rates of adsorption.

It is known that zeolites possess a great affinity for polar molecules such as water vapor and SO_2. Since a typical flue gas stream is composed of relatively high H_2O concentrations (usually about 8 to 10 percent by volume), the evaluation of the effects of water vapor on the dynamics of SO_2 removal by zeolites and silica gel was considered.

Zeolite type 13X (faujasite) was chosen for study based on the relatively high rates of adsorption evidenced by the work of Martin and Brantley [32]. This would serve as a comparison with other zeolites. Due to the acidic nature of the flue gas environment, Linde Molecule Sieve Type AW500 (erionite) was chosen since it is an acid stable zeolite. Adsorbent selection also considered the possible effects of non-adsorbate particulates that possibly could 'plug' the zeolite pores. Both types of zeolites have been used successfully for various liquid and gaseous hydrocarbon separations while techniques are available for zeolite cleaning and recovery. The possibility of coking and fouling within the structure exist but a strong oxidizing stream has been found to be very useful for zeolite re-activation [45]. Plugging and fouling of the AW500 zeolite may not be a problem since the pore openings are small enough to exclude heavy hydrocarbons [46].

Another aspect of this investigation was to obtain a better understanding of the adsorption process with respect to regeneration. Investigators who have studied this problem have failed to consider adsorbent degradation within the realm of actual application. For example, Tamboli [33] performed acid stability tests on type 13X zeolites and found that on exposure to a one-normal solution of sulfuric acid, the SO_2 sorption properties were completely destroyed. The eventual application of a zeolite would not result in exposure to such a harsh environment. Thus, a more suitable criteria for evaluation would be one based on the adsorbent degradation per regeneration cycle.

Sulfuric acid does exist in the flue gas train but the concentration is low (< 10 ppmv). The formation of sulfuric acid is limited by two factors:

(1) initial formation of the sulfate ion, $SO_3^{=}$;

(2) catalysis of the sulfurous acid (H_2SO_3) already formed.

The stability of the zeolite therefore will depend on time of exposure, pH of acid media, method of regeneration, and type of acid. No evidence of studies on the stability of these zeolites in sulfurous-sulfuric acid environments could be found. Consideration of acid stability should also include an explanation of the irreversible adsorption of SO_2. Theories to explain this have ranged from the suggestion that the SO_2 is chemisorbed with the cation of the zeolite [36], to the theory that a very strong dipole interaction with the SO_2 molecule exists [26].

Since the adsorption of both SO_2 and H_2O on the adsorbent surface occurs, the probability for H_2SO_3 or even H_2SO_4 formation exists. Oxidation of H_2SO_3 is rather complex and still not fully understood. In the early work of Johnstone [47], several materials were found to act as catalysts for the formation of H_2SO_4. But of particular significance was that even a dilute mixture of H_2O and H_2SO_3 heated above 62.7°C (145 F) resulted in an increase of H_2SO_3 oxidation. The significance of this is crucial since regeneration is performed by thermal means. Thus the important question to answer is 'Does formation of H_2SO_4 occur before the decomposition of H_2SO_3?' To help elucidate the complex mechanism of irreversible adsorption, an investigation into the effect of the regeneration scheme on the amount of SO_2 irreversible adsorbed was considered. These tests were based on the premise that if the residual sulfur content and the bonding mechanism (held as SO_3 or SO_2 on the surface) are known, the regeneration process could be re-designed.

IV. EXPERIMENTAL APPARATUS

The proper design of the gas contactor and selection of gas analysis instrumentation is necessary to obtain breakthrough curve information. 'Breakthrough curve' refers to the bed effluent concentration variation with time. This information is very useful because many parameters associated with mass transport can be qualitatively identified based on the shape of the breakthrough curve alone. Of primary importance in this investigation was the rate of SO_2 flow from an adsorption bed for a fixed input concentration. An apparatus was designed to obtain the kinetic SO_2 sorption behavior of molecular sieves and silica gel. The system was constructed so that the effects of gas velocity, temperature, and water vapor content could be investigated.

While methods for the scale-up of equilibrium adsorption data do exist, these are restricted by certain idealized conditions--linear adsorption isotherm, single component adsorption, isothermal flow, etc. As noted previously, equilibrium data has been obtained for a few cases but in general these data are insufficient to properly evaluate the adsorbents. Even if the necessary single component isotherm information existed, predicting binary adsorption behavior would be difficult because of surface reactions between SO_2 and H_2O.

4.1 Selection of Gas Contacting Scheme

An important consideration in adsorber design is the selection of the means by which the gas is contacted with the adsorbent. Fluidized

bed, packed bed, or radial flow bed configurations are possible designs for the gas contactor. Large central stations usually can withstand an additional 12.7 cm (5 in.) of water pressure loss downstream of the economizer. This has generally been adopted as the criteria for adsorber/adsorption flue gas desulfurization systems.

A packed bed was selected as the basis for study because of its simpler design and because results obtained can be better scaled to predict the behavior of the other bed configurations. A fluidized bed was not considered because of pressure drop and adsorbent attritioning restrictions.

Reiterating, the prediction of SO_2 adsorption in the presence of water vapor requires measurement of the effluent concentration history of the bed. The successful application of the adsorption process will require that its test conditions be similar to those conditions that exist in large central stations. To ensure valid scale-up information a appropriate design criteria must be established.

Therefore, the following parameters were selected as the basis for investigation:

(1) superficial gas velocity (gas velocity in the unobstructed flow area)--the gas velocity was chosen such that for a given bed depth, high pressure drop would be avoided. Gas velocity also affects the overall resistance to mass transfer but the selection is an optimization between contactor size and bed pressure drop. Typical adsorber gas velocities

employed to date range from 0.31 to 0.61 m/sec (1 to 2 ft/sec). Thus, gas velocities in this range were considered.

(2) gas temperature--the equilibrium capacity for constant molar concentrations of the solute (adsorbate) is related to temperature by the adsorption isotherm. The rate of adsorption will be controlled by the slowest mass transfer step. Since rate of diffusion increases with temperature and equilibrium capacity decreases, dynamic measurements are necessary to evaluate the actual adsorption rates.

(3) SO_2 concentration--SO_2 concentration emitted by large central stations burning high sulfur coal is roughly 3000 ppmv. This is a representative value and should serve as a suitable basis for evaluating the adsorbents.

(4) water vapor concentration--water vapor concentration usually represents 8 to 10 percent by volume of the effluent combustion stream. Water vapor content is of particular interest for this investigation because of the great affinity of zeolites and silica gel for water. Water vapor concentration was varied so that the competitive adsorption of H_2O and SO_2 and possible displacement (chromatographic) effects could be studied.

(5) gas pressure drop--gas pressure drop is a function of bed porosity, particle shape, and superficial gas

velocity. Pressure drop was chosen such that the adsorption test conditions were similar to pressure drop values of existing flue gas desulfurization units. Selection of pressure drop may be considered an optimization problem except the bed length must be sufficiently long to prevent adsorbent by-passing.

(6) bed diameter--bed diameter was chosen to reduce difficulties that occur in scaling. Charm et al. [48] attempted to scale-up an elution column based on modified Reynolds number while maintaining the same bed geometry (bed length to bed diameter ratio). This is not valid unless geometric similarity exists. Geometric similarity does not exist since the length to diameter ratio may be changed while maintaining the same packing material. This is further complicated because of a radial porosity variation that arises due to the inability to tightly pack the particles close to the bed wall. To avoid these problems associated with scale-up, it was necessary to adopt a criteria that would help eliminate the flow distribution problem and at the same time not require large amounts of adsorbents. Schwartz and Smith [49] found that for

$$D_P/D_B > 30$$

where D_P = particle diameter

D_B = bed diameter,

the resulting effluent velocity profile would be approximately uniform or a plug flow. Thus, a more representative indication of the performance of a large scale, large diameter device could be obtained.

(7) isothermal or adiabatic testing--adiabatic operation was chosen for study because in actual application a large diameter adsorber would be difficult to maintain at constant temperature. The adsorbents characteristically have low thermal conductivities and high heats of adsorption, thus the adiabatic case would be reasonable.

Based on these design parameters, a system was designed and constructed. The details of design and operation of the unit are presented.

4.2 Main Air Supply System--Dehumidifier Assembly

The bulk gas chosen for use in this investigation was air because the composition is similar to the bulk constituents of flue gas. Also, it is readily available and would not interfere with the adsorption process. In order to properly evaluate the kinetic behavior of the adsorbents, certain air feed requirements must be met. These are

(1) proper air conditioning to ensure minimization of possible side reactions caused by contaminants such as compressor oil in the feed line and/or water vapor;

(2) constant gas flowrate and temperature.

The air purification system is shown in Fig. 4.1. Air purification was accomplished by three principle methods:

(1) centrifugal separation;

(2) impaction and filtering, and;

(3) adsorption.

Plant air was first filtered using a centrifugal type air filter. The air then passed through a 10.23 cm (4.03 in.) ID steel pipe 91.4 cm (36 in.) long pipe packed with glass wool and acetate filter media to help reduce dust and oil loads on the next purification stage. The filtered air was then routed to a large capacity drying column. The drying column was fabricated from a 20.3 cm (7.98 in.) ID, 137.2 cm (4.5 ft) long steel pipe. Both ends of the pipe were capped with 1.27 cm (0.5 in.) aluminum plate. A helical coil of 1.27 cm (0.5 in.) copper tubing was secured within the pipe and used to supply steam for activating the adsorbents. Provisions were made for cold water to be passed through the helical coil to increase adsorbent loadings. The column was then filled with three different commercial adsorbents. Three different adsorbents were used because removal of both water vapor and oil mist was required. Since adsorbents preferentially adsorb one component over another, careful adsorbent selection is necessary for efficient operation. Activated silica gel (Davison, Tell-Tale, Type IV, code no. 44-08-237-3-8 mesh) was used because of its high equilibrium capacity for water vapor in moderately high relative humidity environments. Activated charcoal (Fisher, code no. 5-685B, 6-14 mesh) comprised the second stage adsorption layer.

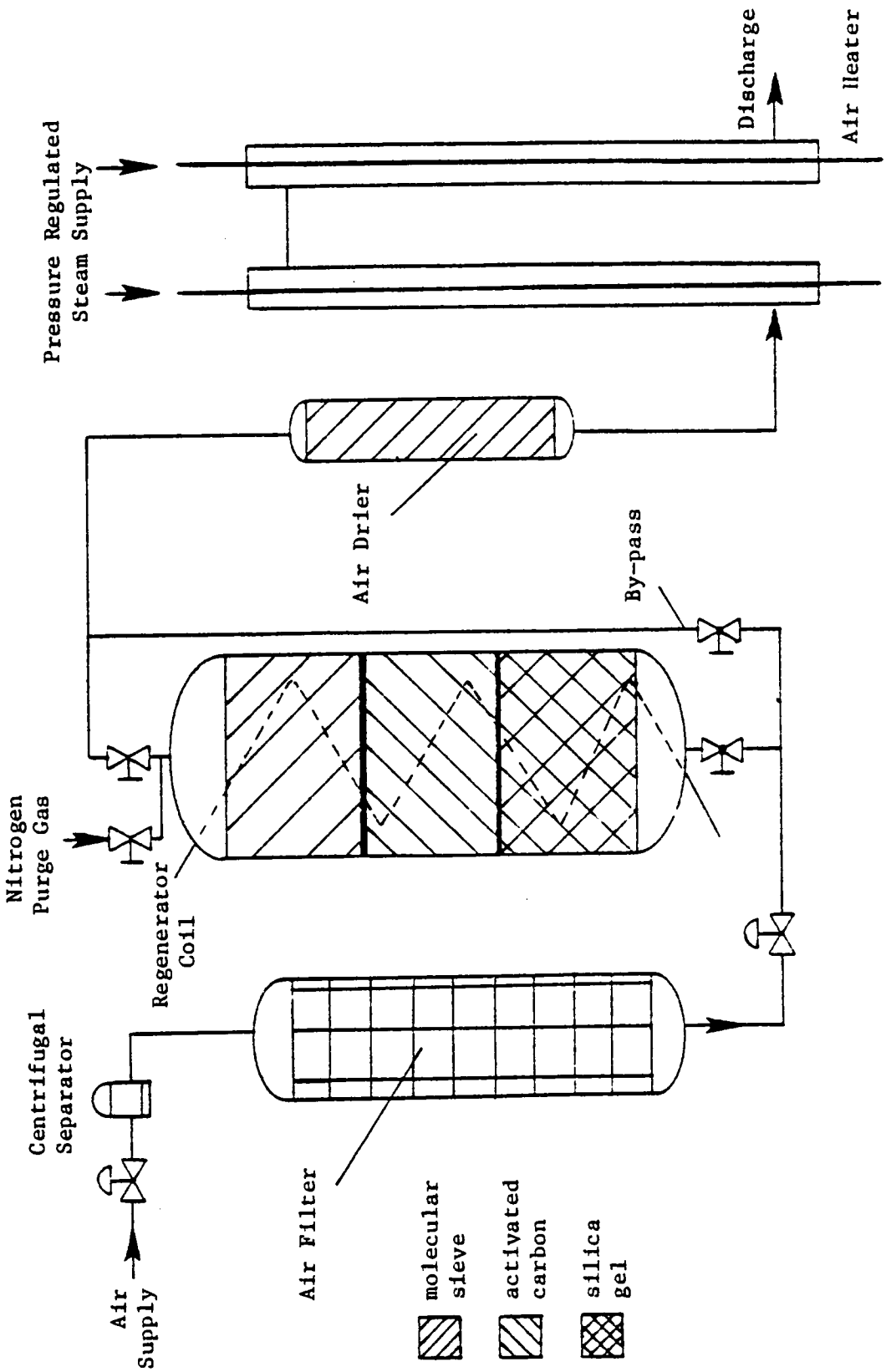

Figure 4.1 Air Dehumidification and Purification System.

Activated charcoal will adsorb both hydrocarbons and water vapor but, since water vapor could decrease hydrocarbon loadings, the carbon bed was placed downstream from the silica gel. Type 13X molecular sieve (Union Carbide Linde Co., lot no. 13945450036) comprised the final adsorbent layer which was used to remove trace amounts of oil and water. Once filling of the adsorption column was complete, the aluminum caps were secured and sealed with high temperature resistant silicone rubber (General Electric, stock no. GE2562-01DP) and neoprene (Polychloroprene) gaskets. The adsorbents were supported within the column by a stainless steel screen-glass wool grid. The entire dehumidifier assembly was insulated with 2.54 cm (1 in.) fiberglass.

A second stage trimming bed, shown in Fig. 4.1, was installed after initial testing revealed that the large column failed to remove water vapor adequately. The trimming bed contained approximately 4.53 kg (10 lbm) of Type 13X molecular sieve. Water vapor removal was substantially increased as was evidenced by continuous operation of the system at about 0.283 m^3/min (10 scfm) for 72 hours with no measurable water vapor in the bulk gas stream. Sizing of the water vapor removal unit is presented in Appendix A. The column was activated by heating the bed to 149-160°C (300-320 F) and purging with dry nitrogen (Airco Industrial Gases, grade 4.5, pre-purified, maximum H_2O content 10 ppmv). The trimming bed was regenerated by disconnecting the unit and heating the adsorbent to 260°C (500 F).

The heat exchange assembly depicted in Fig. 4.1 was fabricated from 2.54 cm (1 in.) standard steel pipe and 1.27 cm (0.5 in.) copper

tubing. The total heat exchanger length was 4.37 m (12 ft). Incoming air was contacted in annular flow with the center copper tube. Exit gas temperature was maintained by varying the gas flowrate and center pipe temperature. The center pipe temperature was controlled with a steam controller (Fisher Governor Co., Type 4160, serial no. 4686960) used to maintain constant pressure and therefore constant temperature. All piping was insulated and long pipe runs were wrapped with resistance heating tapes to reduce system preparation time.

4.3 Gas Flow Control and Metering

The experimental gas adsorption unit with attendant instrumentation is shown in Fig. 4.2 and schematically in Fig. 4.3. The gas adsorption unit consisted of a gas metering section, gas mixing and adsorption section, and an effluent gas sampling system.

The gas metering section was provided to supply the bulk air, SO_2, and air-water vapor mixture flowrates. The bulk gas flowrate was measured with a rotameter (Brooks, 250 mm scale, type 1321-1110, serial no. 6408-69887/1) located downstream from a 2.54 cm (1 in.) standard globe valve used to set the air flowrate. SO_2 flowrates were measured using a ball-float type rotameter (Air Products and Chemicals, code no. E21-G-150mm42, tube no. E29-C-150mm2) which has a maximum flowrate of 0.661 liter/min. The accuracy of the flowmeter (± 5 percent full scale) was judged not sufficient for setting the SO_2 flow to establish a given and constant concentration. The metered flow from the rotameter was corrected using a bubble flowmeter shown in Fig. 4.4.

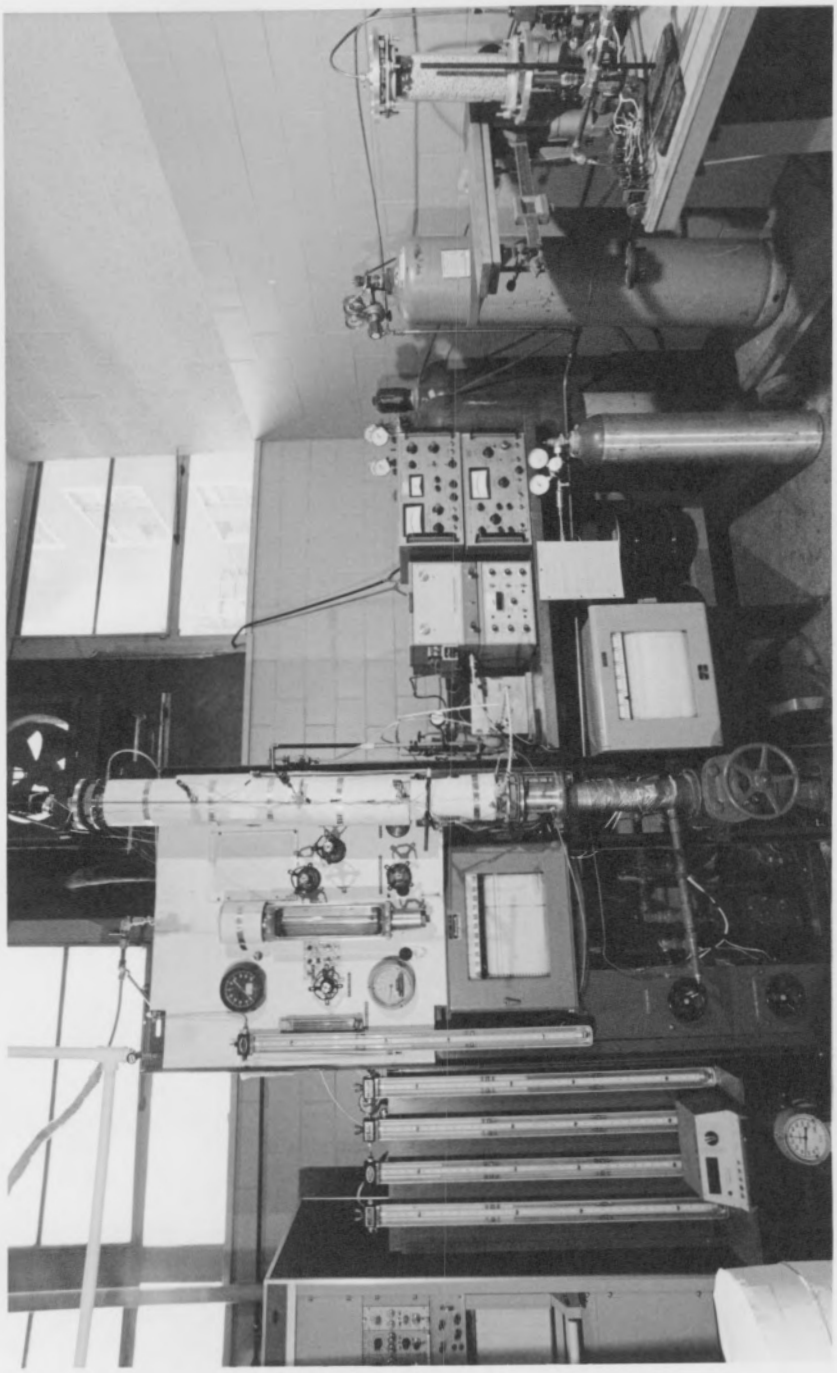

Figure 4.2 Gas Contacting Apparatus for Dynamic Adsorption Measurements.

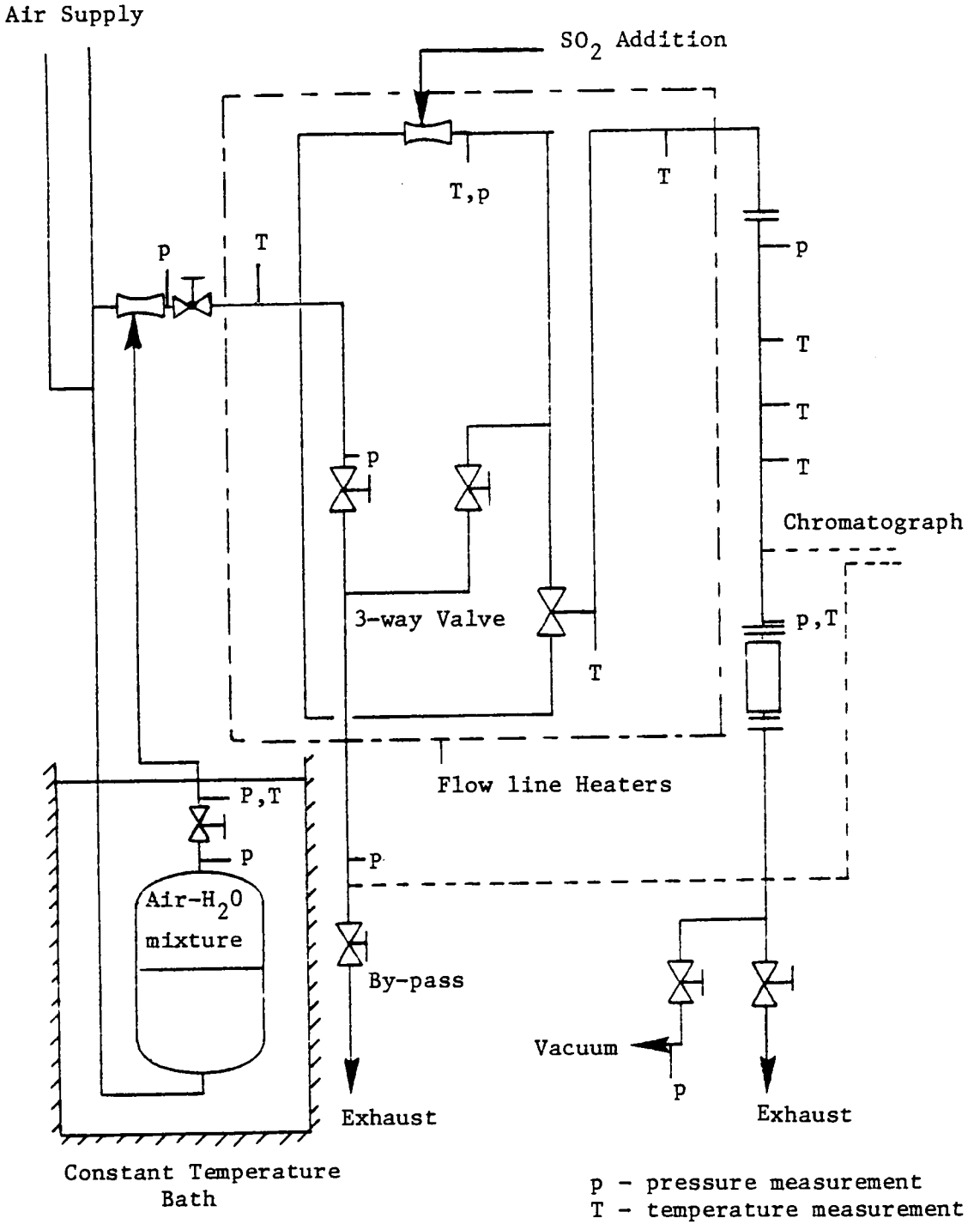

Figure 4.3 Schematic of Gas Contacting Apparatus.

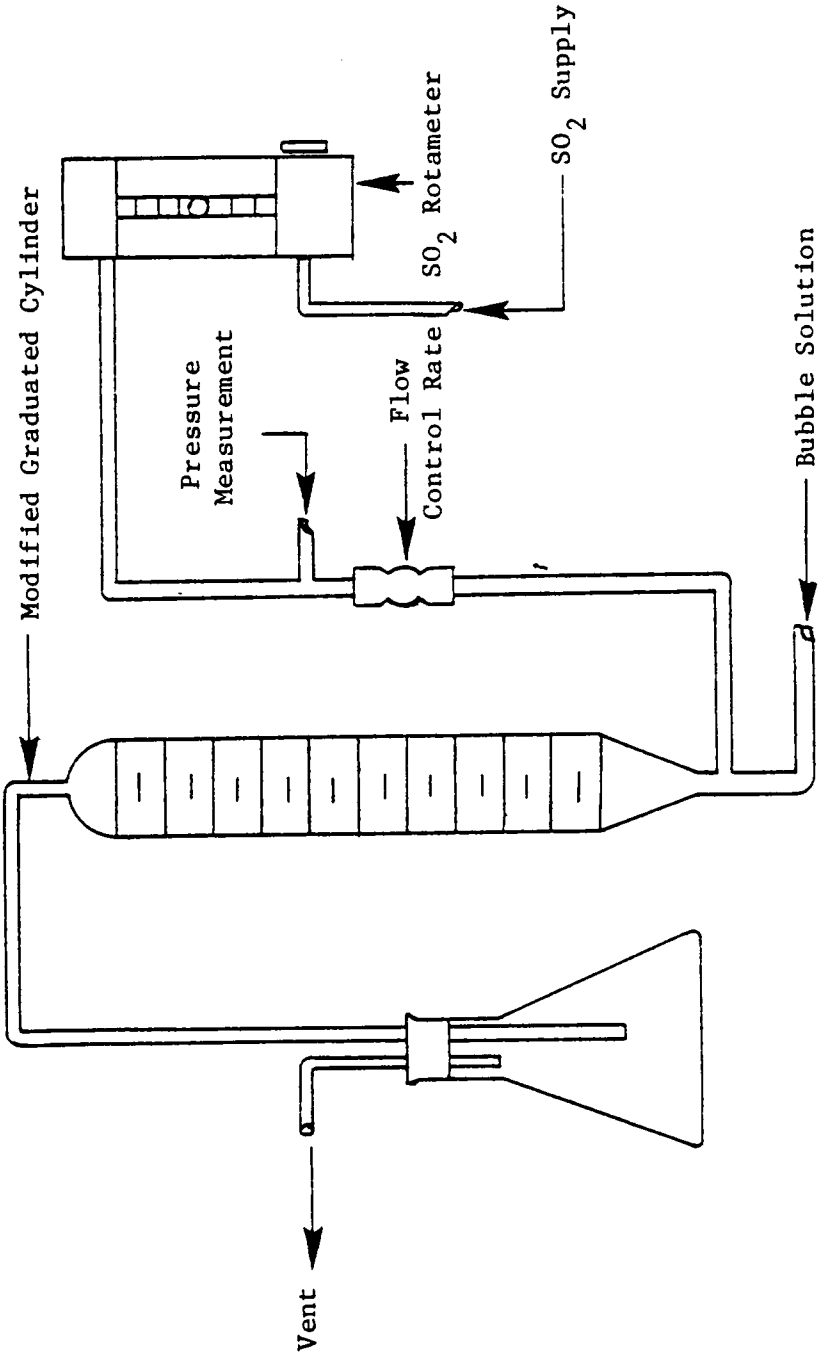

Figure 4.4 Bubble Flowmeter Apparatus.

The accuracy of the bubble flowmeter depends on the accuracy of the time measurement, accuracy of bubblemeter volume, and amount of bubble dehydration. Bubble dehydration could account for an apparent increase in the observed flowrate but this was found to be insignificant. Unlike the ball-float rotameter, the bubble flowmeter is independent of fluid viscosity effects.

The SO_2 used for all adsorbent testing was obtained from Union Carbide [69 Kg (150 lbm) anhydrous SO_2, minimum purity 99.98 percent]. Gas delivery was maintained using a corrosion resistant gas regulator (Union Carbide, part no. C12G30-660). SO_2 poses a material selection problem from the standpoint of corrosion. Therefore, connecting tubing which supplied SO_2 was 316 stainless steel and flow switching and cut-off valves were 304 stainless steel with teflon seats and seals. The use of stainless steel piping was not deemed necessary after the concentrated SO_2 had been mixed with the bulk gas flow. Slowik [50] has found that carbon steel pipe may be used for sampling low concentrations of SO_2 with no loss due to adsorption by the pipe. This was demonstrated with the present apparatus by establishing a flow of air and SO_2 and monitoring the concentration over a long period of time. Measured concentrations were found not to vary over a 24-hour period.

Operating conditions require that the system be able to simulate a step change in SO_2 concentration. Since water vapor and SO_2 in known concentrations must be injected simultaneously, a method to obtain specific gas mixtures was required. A three-way valve was used to control the main air flow through the test apparatus. Once the flow

conditions through the adsorption column had been established (pressure drop, back pressure, and temperature), the flow was then diverted to a straight run of pipe with two 2.54 (1 in.) standard globe valves that could be adjusted to simulate the flow conditions in the adsorption column. The SO_2 and water vapor content were adjusted until the desired gas composition was obtained. The three-way valve was then used to 'inject' the gas stream back into the adsorption column.

4.4 Adsorption Column

The adsorption column, shown in Fig. 4.5, was fabricated from 75 cm (2.95 in.) ID Pyrex glass pipe, 127 cm (50 in.) long. Five 1.27 cm (0.5 in.) OD glass stems 4.45 cm (1.75 in.) long were attached to the column at 30.5 cm (12 in.) intervals to facilitate insertation of thermocouple and gas sampling lines. Two 0.635 cm (0.25 in.) glass stems with rubber septum caps were attached to allow gas sampling with syringes. Connections with the 1.27 cm (0.5 in.) OD glass stems was accomplished by using 1.27 cm (0.5 in.) ID Swaglok 316 stainless steel unions with Teflon ferrules. Hand-tightening only was required to achieve a leak-proof seal. The adsorbent bed was supported in the column by a 304 stainless steel screen (10 x 10 mesh, 64 percent open area) secured to an adjustable center post. The column was installed in a vertical position and fastened to a 1.27 cm (0.5 in.) thick aluminum plate. An O-ring seal was used to prevent leakage. Flange connectors for the glass pipe were fabricated from Bakelite that was machined to fit the glass pipe flange contour. After the top of the column was secured, the bottom of the column was connected to a 7.62 cm

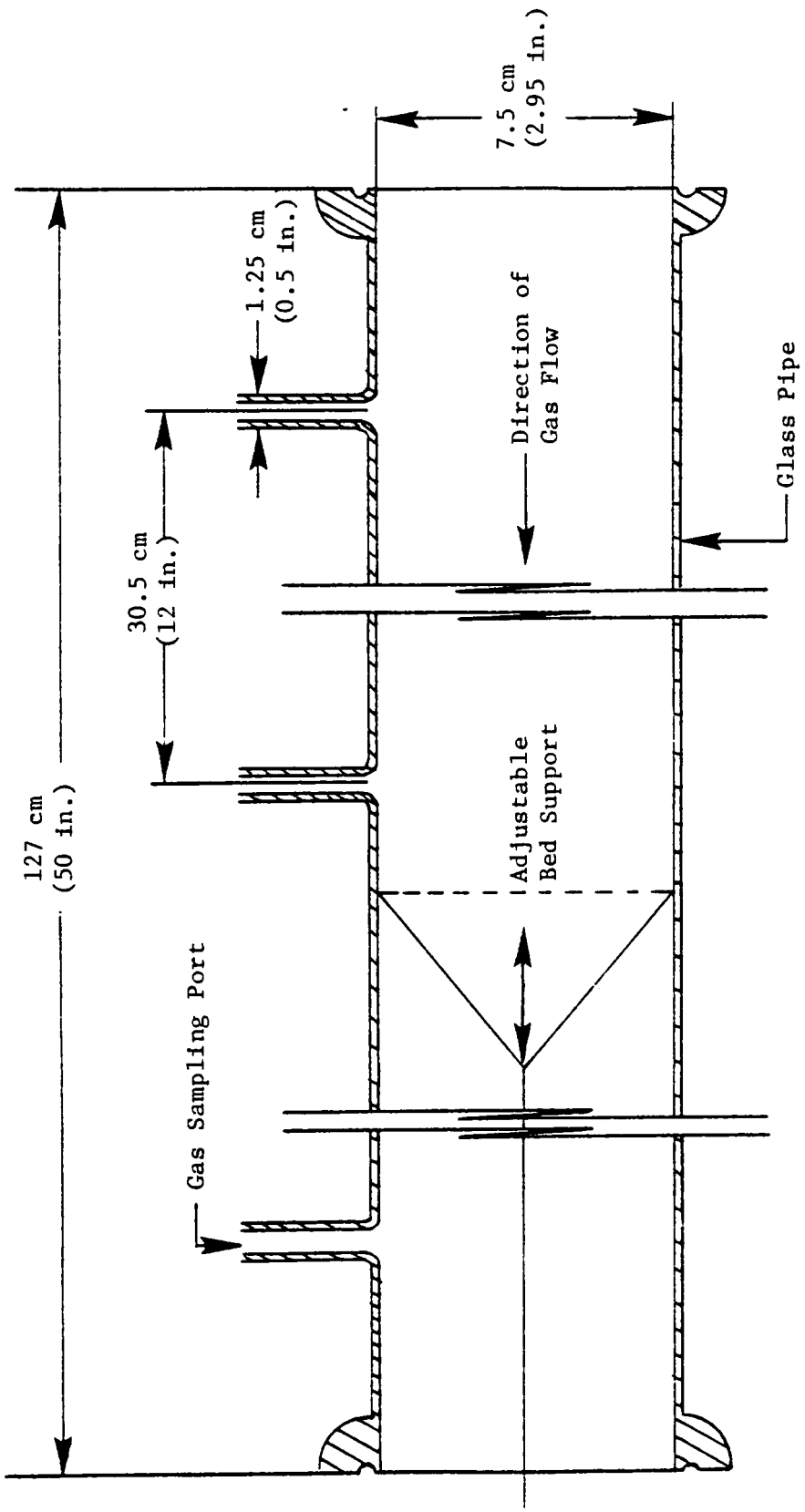

Figure 4.5 Details of Gas Adsorption Column.

(3.0 in.) ID Teflon-lined flexible pipe. The flexible pipe was in turn connected to a 7.62 cm (3.0 in.) gate valve which was used to regulate the back pressure of the adsorption column. Once the column had been properly aligned, two springs were attached to the base of the column to provide additional support. This design allowed the adsorption column to accommodate dimensional changes due to thermal expansion. For adiabatic operation, the entire column was covered with a 2.54 cm (1.0 in.) fiberglass insulation.

The effluent gas from the adsorption column was sent to a window mounted exhaust unit which mixed the column effluent with room air and discharged to the atmosphere. The exhaust unit maintained a negative pressure within the laboratory to minimize SO_2 concentrations. As a precautionary measure, the SO_2 concentration of the room was periodically measured with a Bendix Gastek gas monitor which permits immediate determination of atmospheric SO_2 concentrations.

4.5 Temperature Measurement

The measurement of gas temperature at the adsorption column inlet, outlet, and within the bed was obtained using three 0.16 cm (0.063 in.) 304 stainless steel sheathed, ungrounded, iron-constantan thermocouples (Omega ICSS-116U-12) connected to a temperature recorder (Honeywell Brown Electronik, model no. Y153X62-P(S)-16-II-III-22, serial no. 5161). The temperatures at several locations on the test rig were also monitored using 16 24-gauge copper-constantan thermocouples connected to a 16-channel temperature recorder.

4.6 Selection of Gas Analysis Equipment

The measurement of dilute concentrations of SO_2 and water vapor poses several problems with respect to instrument selection. Instruments are available for measuring both SO_2 and water vapor but their flexibility is limited since usually only one of the constituents can be measured by a single detector. The main difficulty arises due to the corrosive nature of the gas sample itself. Gas analysis could be performed by non-dispersive infrared analysis, gas chromatography, mass spectrometry, electrochemical analysis, or ultraviolet analysis.

Gas chromatography was selected because SO_2 and water vapor may be measured simultaneously and wide flexibility in operating conditions make analysis of more complex gas streams possible. Gas chromatography represents an area of analytical chemistry that deals with the separation of gas mixtures. Chromatographic separations can be obtained for gases, solids, and liquids.

The basic components of a gas chromatographic system are shown in Fig. 4.6. The operation of the system may be described as follows: an inert carrier gas, such as helium, continuously purges a column that contains an adsorbent material. The sample to be analyzed is injected and swept through the column by the carrier gas. As the sample passes through the column, a component of the injected sample is retained by the solid and the remainder of the sample is convected away. Depending on the column temperature and pressure, the adsorbed component is desorbed at a fixed rate. This process is continued until the sample

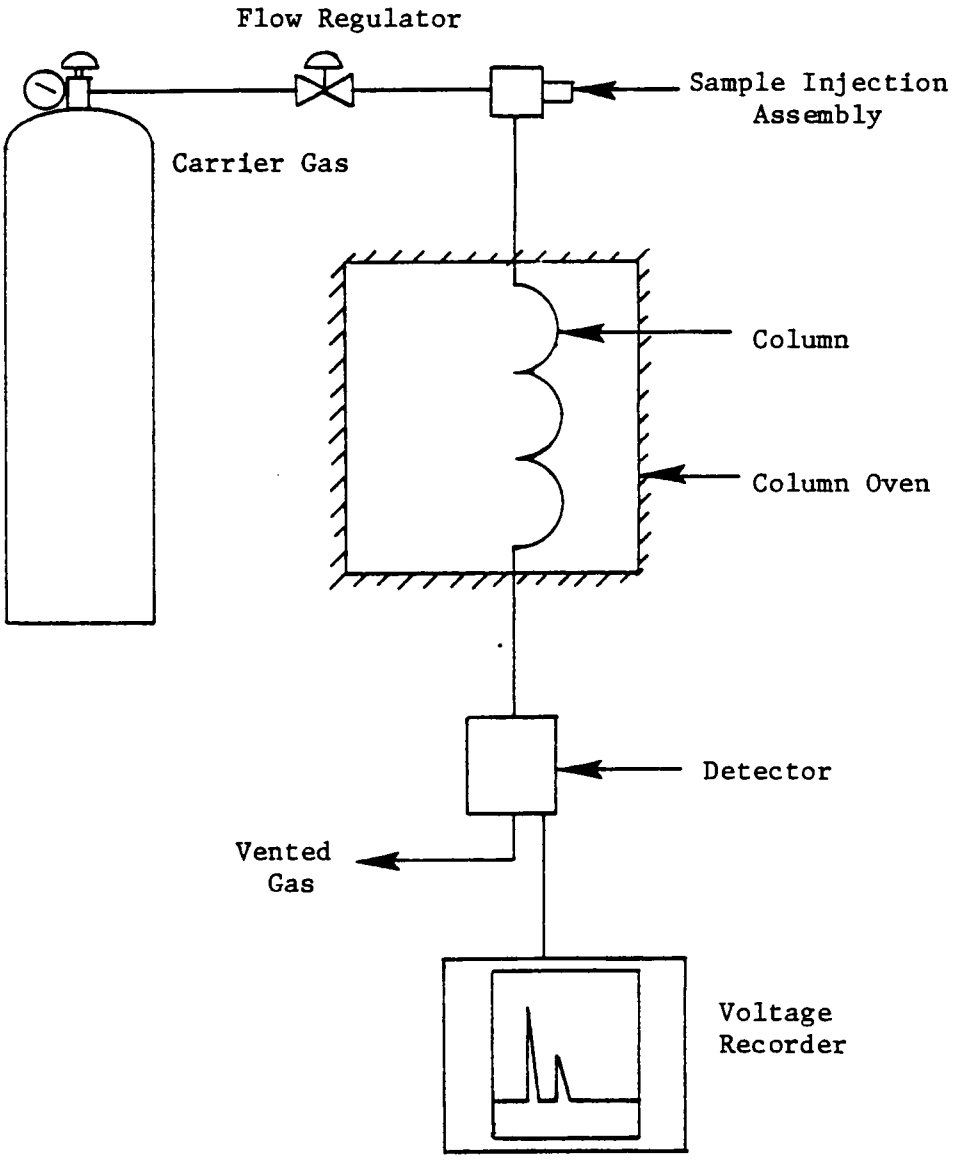

Figure 4.6 Basic Components of Gas Chromatograph System.

and the separated component are eluted from the column. The change in carrier gas composition is then detected by a suitable detector such as thermal conductivity, flame ionization, or electron capture detector.

For a given set of operation conditions, the elution time for specific constituents is the same and usually not dependent on concentration. Therefore, qualitative analysis may be performed when retention times are known. Quantitative analysis is obtained by recording the detector output variation with time and by either measuring the height of the effluent peak or the area under the peak, with the latter directly proportional to the component concentration.

4.7 Selection of Gas Chromatograph and Components

One of the most important considerations in chromatography is, 'Which column is best suited to accomplish the separation?' For this investigation the problem was to select a column that would separate both SO_2 and water vapor and require minimum analysis time. With polar molecules, such as water vapor and SO_2, eluted peaks are usually characterized by tailing. This alone could necessarily require long analysis time. Also, water vapor and SO_2 may be corrosive, which could be detrimental to the column. The first consideration was selection of the column material. At the parts-per-billion level, loss of the sample is controlled by careful selection of the column and the packing material. Villalobos [51] recommends Teflon tubing for trace analysis of sulfur compounds but stainless steel columns have proven to be effective for SO_2 measurements at the part-per-million level.

Thus, stainless steel was selected as the column material. Next, the selection of the packing material for obtaining separation of SO_2 and water vapor from air was required.

Several packing materials have been identified as possible materials suitable for identifying volatile sulfur compounds. Silica gel is suitable for separating SO_2, H_2S, and CS_2, but if water vapor is present in concentrations greater than 100 ppmv, it will elute as a broad band long after sulfur compounds [52] which could interfere with subsequent analysis. Because of the difficult separations required and the shortcomings of existing columns, commercial development of new packing materials was begun and eventually led to several promising supports. Powdered Teflon supports were found to be excellent packing materials. Presently, several column materials (Carbopack B-HT-100, Chromosil 310, Chromosorb T/Polyphenylether, Supelpak-S, and Porapak QS) have proved successful in sulfur gas analysis.

Porapak QS was selected as the packing material because polar components are eluted rapidly and with little or no tailing [53]. Porapak QS is the silanized version of Porapak Q. Porapaks are commercial chromatograph packing materials that are porous polymers with very distinct pore size openings that require no mobile phase.

The sampling system selected consisted of a sampling valve-sampling line arrangement instead of syringe injection. Syringe injection would have been cumbersome, less accurate, and expensive. The sampling system, depicted in Fig. 4.7, consists of a 0.635 cm (0.25 in.) OD aluminum probe and a 316 stainless steel rotary sampling

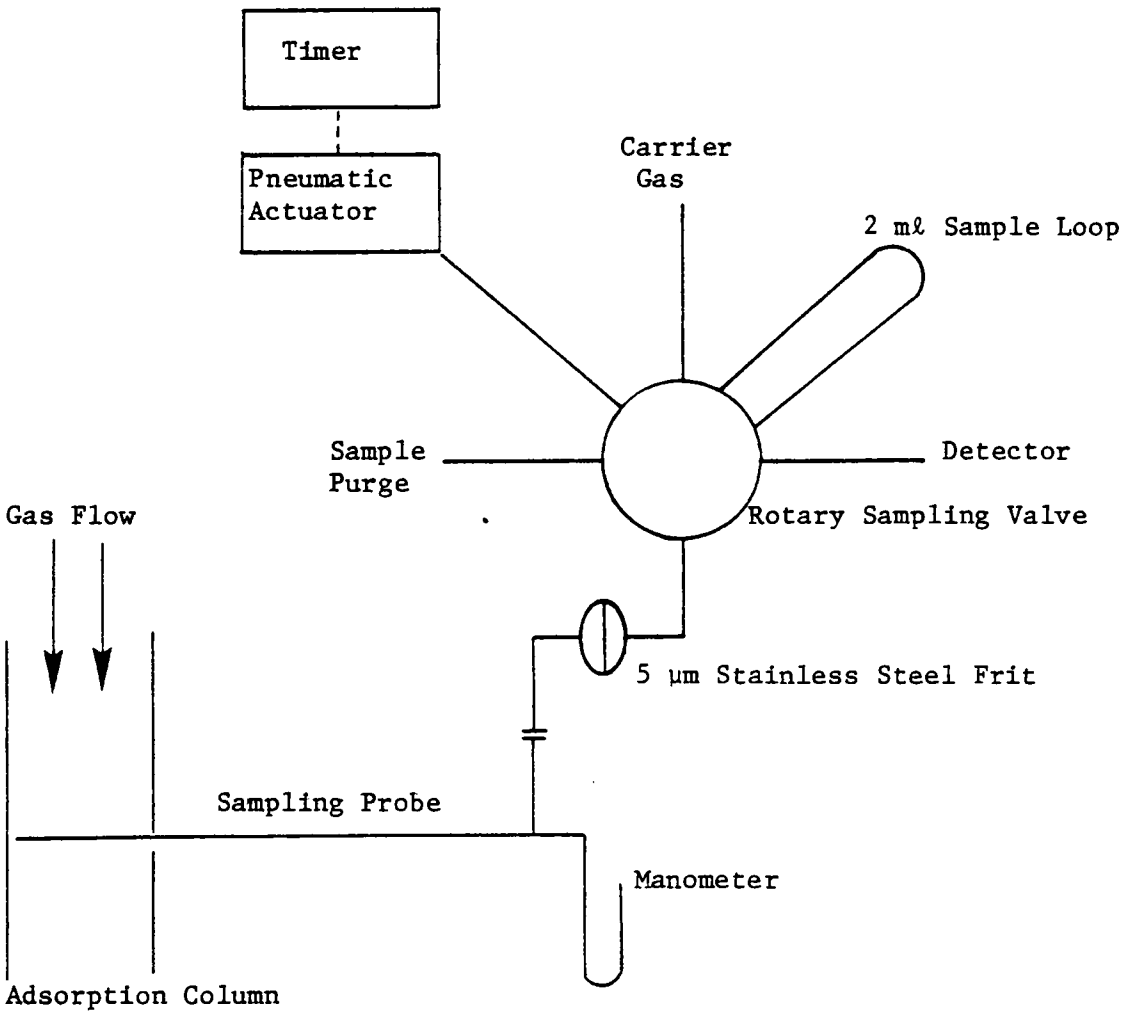

Figure 4.7 Gas Sampling System.

valve with a pneumatic actuator and timer. A 5 μm stainless steel porous frit was placed upstream of the sampling valve to prevent accumulation of particulates within the valve. The system was arranged so that residual gas in the sampling line was vented and sample flow from the test section was continuous and not interrupted by the sampling valve sequential operation. To verify the stability of the selected sampling materials with respect to reproducibility, several diagnostic studies were performed with glass and stainless steel tubings. For the range of gaseous concentrations studied, aluminum tubing was satisfactory and was preferred because of its flexibility.

The gas chromatograph-gas sampling system is shown in Fig. 4.8. A Gow-Mac 550 Gas Chromatograph (serial no. 49504R) with a thermal conductivity detector and an installed 8-port rotary sampling valve with two 2 mℓ demountable loop pairs and pneumatic actuator was used to analyze SO_2 and water vapor in air samples. A 0.3175 cm (1/8 in.) x 1.219 m (4 ft) 316 stainless steel column packed with 80/100 mesh Porapak QS was used to achieve separation of both water vapor and SO_2. Helium (Airco Industrial Gases, Grade 4.5) was used as the carrier gas. A 0.635 cm (0.25 1/4 in.) x 3 m (10 ft) aluminum column packed with 60/80 mesh 13X zeolite molecular sieve was used to pre-condition the carrier gas.

4.8 Miscellaneous Instrumentation

Provisions were made so that the inlet and outlet velocity profiles from the adsorption column could be measured. A constant

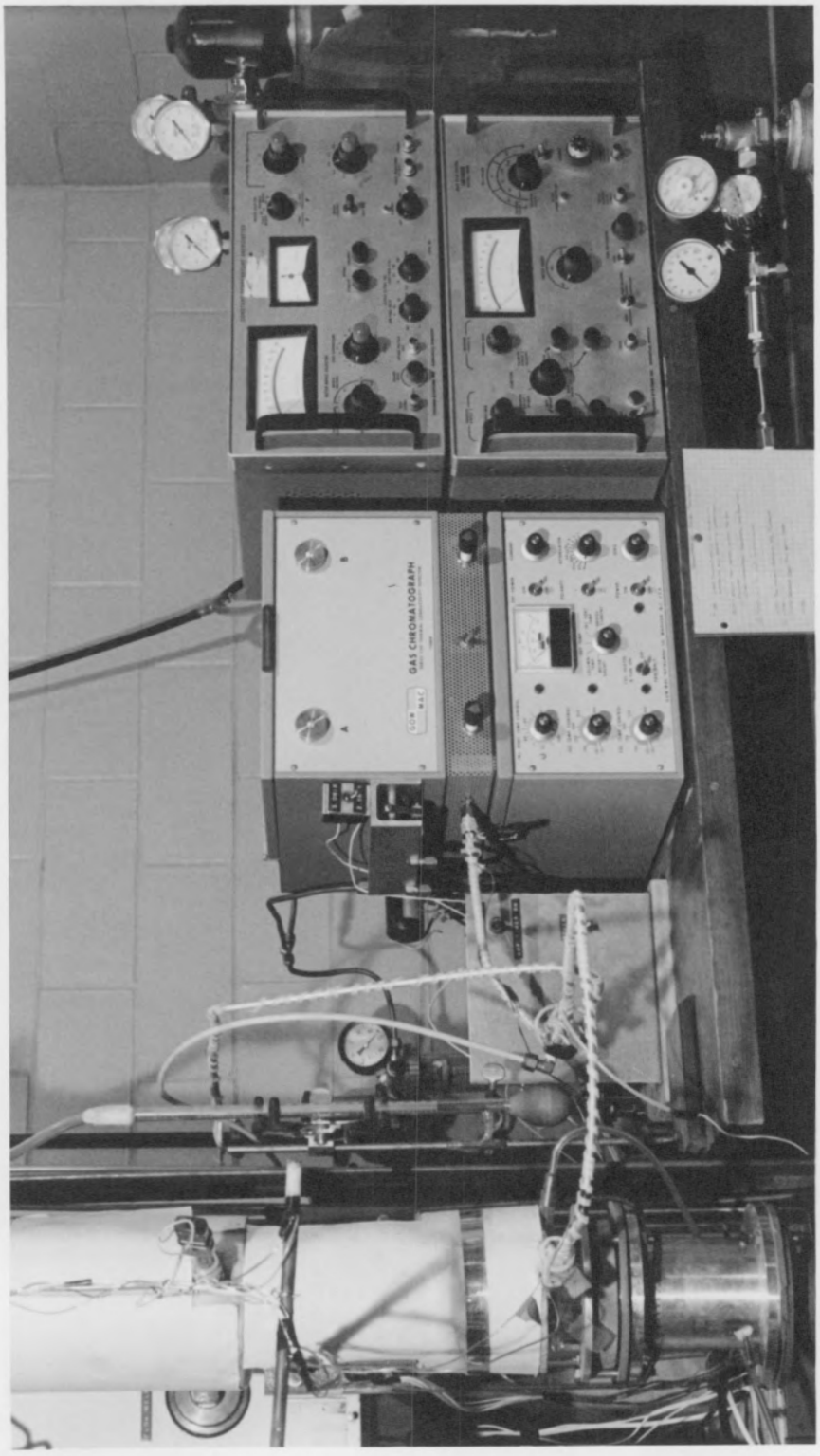

Figure 4.8 Gas Chromatograph System.

temperature anemometer with hot film sensor (TSI, Model 1010A, Probe model 1210) was used to measure gas velocities at several radial positions. Bed pressure drop, bed back-pressure, sampling line pressure, main air flow, and SO_2 rotameter pressure were measured with U-tube manometers (Merium Instruments, Model 10AA35WM).

One problem with breakthrough curve analysis is determining at what time the SO_2 gas front reaches the bed. This was solved by placing a small amount of sodium hydroxide with phenol red indicator on a piece of adhesive tape within the adsorption column and upstream of the bed. By observing the color of the material, arrival of SO_2 was indicated when the color changed from pink to yellow. An event marker was used to reference all chromatograms using this method.

Time resolution was roughly ± 5 sec with respect to the arrival of the gas 'front'.

Other instrumentation was utilized during the course of the investigation. Electron microscopy and the regeneration and adsorption isotherm instrumentation will be discussed in subsequent chapters.

V. CALIBRATION AND INITIAL TESTING

A considerable amount of time and effort was necessary to obtain and insure consistent results from the entire test facility. While the details of preliminary testing are unimportant, initial system calibration and performance deserve attention. Calibration of the gas chromatograph for SO_2 and water vapor and response testing are presented.

5.1 Calibration of Gas Chromatograph--SO_2

It has been well documented that the accuracy and stability of gases such as oxides of nitrogen, carbon monoxide, and surfur dioxide are questionnable when stored in pressurized gas cylinders for a period of time. The instability is partially a function of gas adsorption or reaction with the cylinder walls [54].

Airco Industrial Gases has developed specially treated aluminum cylinders that retain blended concentrations within ±2 percent. Thus, calibration of the gas chromatograph system was accomplished by using two Airco cylinders (no. LL1990 and CC5785) with nitrogen-SO_2 mixtures containing 2880 and 921.1 ppmv SO_2, respectively.

The calibration procedure involved connecting the gas cylinders to the gas chromatograph and establishing a flow of gas through the sampling system using a pressure regulator.

The restraints imposed on the gas chromatograph were minimum analysis time and minimum detector cell current to prevent filament

oxidation. The four parameters that may be varied to optimize the system are

(1) carrier gas flowrate

(2) cell current

(3) column oven temperature

(4) column length.

Because of the difficulty with changing column length, only the first three above were considered at this time. Several diagnostic tests were performed so that the effect of changes in carrier gas flow, column temperature, and cell current on system response could be ascertained. Column oven temperature and cell current demonstrated the most significant effect on gas chromatograph response. Column temperature was varied from 60 to 120°C (140 to 248 F) to determine the effect on the resolution of SO_2 and water vapor. Cell current was varied from 75 to 150 ma. Sensitivity was very poor for low cell currents at 75 ma and high cell currents must be avoided if cell contamination, drift, and long filament life are considered. A cell current of 100 ma and column temperature of 100°C (212 F) gave an acceptable response. In tests where ambient conditions changed drastically (room temperature, drafts, etc.), the gas chromatograph was found to operate reproducibly.

The calibration tanks provided a two-point calibration but to establish linearity of the calibration curve, several techniques were used. A syringe injection method was used whereby a change in SO_2 concentration could be accomplished by changing the sample volume.

For example, a syringe size of 2 mℓ corresponded to an SO_2 concentration of 2880 ppmv. Likewise, a 1 mℓ sample would correspond to a concentration of 1440 ppmv. By repeating this procedure for different sample volumes a calibration curve was obtained. The data was evaluated by the method of least squares and is shown in Fig. 4.8. The relative standard deviations for the two calibration tank valves were 0.45 and 2.7 percent, respectively. This should not imply that variability was a function of SO_2 concentration. Since peak height values could only be read to the nearest 0.5 mm, and the relative error is of the same order of magnitude, it may be argued that the high relative standard deviations for the low concentration was not attributable to the gas chromatograph.

Additional testing was performed by utilizing a rather simple dynamic scheme so that the calibration could be verified without disconnecting gas sampling lines. The method consisted of establishing a main air flow rate of about 0.13 to 0.19 m^3/min (5 to 7 scfm) and adjusting the SO_2 flowrate until the SO_2 peak height corresponded to either calibration tank value. Without changing the main airflow rate, the SO_2 flowrate could be varied and measured using the bubble flowmeter apparatus previously discussed. The concentration of SO_2 is given by

$$c_{SO_2} = \frac{\dot{v}_{SO_2}}{\dot{v}_{air} + \dot{v}_{SO_2}} \times 10^6 \qquad (5.1)$$

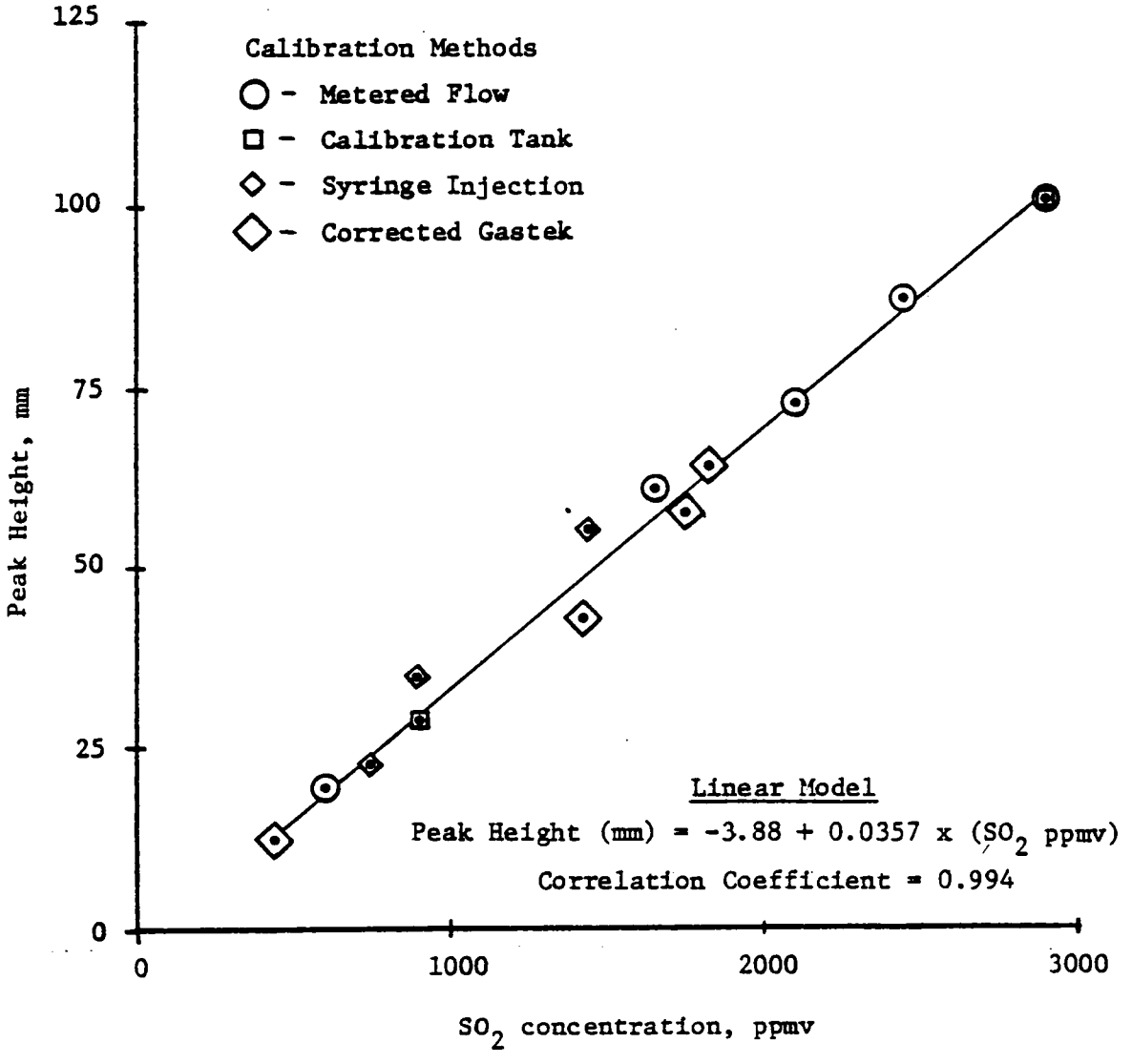

Figure 4.8 Gas Chromatograph Calibration for SO_2.

where

c_{SO_2} = concentration of SO_2, ppmv

$\dot{v}_{SO_2}$ = volumetric flowrate of SO_2, mℓ/min

$\dot{v}_{air}$ = volumetric flowrate of air, mℓ/min

The air flowrate could not be measured as accurately as the SO_2, thus the air flowrate was inferred by knowing the SO_2 flowrate and concentration. Using this method, agreement with the calibration curve was obtained. The utility of this method is that during adsorption tests, points on the calibration curve may readily be verified. Since the air flowrate must remain constant throughout the tests, the initial reference point using the calibration tank was checked before each data was obtained.

Several readings were obtained before and after each adsorption run to insure calibration curve validity. The detailed procedure that was used during adsorption runs is presented in Appendix C.

5.2 Gas Chromatograph Calibration--Water Vapor

The calibration technique for water vapor was considerably more complicated than SO_2. Because stable (non-condensable) gas mixtures of water vapor in pressurized cylinders are not available, another source must be used. The problem is to select a source that would yield accurate and reproducible water vapor-air mixtures. Wexler [55] has developed several methods for producing accurate water vapor-air mixtures. One method developed by Wexler is capable of attaining

relative humidities to within ±1/4 percent. The device, referred to as a 'pressure humidity apparatus', consists of saturating a gas at elevated pressure and then expanding isothermally to a lower pressure. If the process of saturation and expansion occurs isothermally and the ideal gas law is assumed, then the relative humidity from the device is related to the delivery pressure by

$$RH = P_d/P_s \times 100 \tag{5.2}$$

where RH = relative humidity, percent

P_d = delivery pressure

P_s = saturation pressure

which requires that saturation conditions exist at pressure P_s. Since water vapor-air mixtures depart from ideal gas behavior, Weaver [56] has shown that an empirical equation of the form

$$RH = 100 \times \frac{P_d}{P_s} \frac{(1 - KP_d + K'P_d^2)}{(1 - KP_s + K'P_s^2)} \tag{5.3}$$

where $K = 1.9 \times 10^{-4}$

$K' = 1.4 \times 10^{-8}$

When P_d is expressed in the units of psi, Eq. 5.3 may be used to correct for non-ideal gas behavior.

Attempts to use the pressure humidity device as a means for calibrating the gas chromatograph were futile. The results were either significantly larger or smaller than results obtained using other

methods. The device was used, however, to supply air-water mixtures to the adsorption column during breakthrough tests. Several methods were investigated for supplying constant water vapor concentrations and the pressure humidity apparatus was the only method found that could supply constant concentrations of water vapor for three to six hours.

As a preliminary step, several calibration values were established by connecting a vacuum pump to the gas sampling line exit. Ambient air was drawn into the sampling system and injected into the chromatograph. Approximate water vapor concentrations were obtained by measuring the water vapor content with a sling psychrometer.

Since the range and accuracy of water vapor concentrations using the psychrometer were limited, a method that would provide direct calibration was needed. The next method [57] investigated required injecting known weights (volumes) of water into a known volume of dry gas. The apparatus is depicted in Appendix C. After the flask had been evacuated for 30 min, dry gas was then used to purge the flask. The purge gas effluent was routed to the gas chromatograph so that an indication of residual water vapor content could be obtained. After no response of the gas chromatograph was observed, the purge gas was allowed to continue flowing for two hours to insure removal of trace water vapor. Next, a known volume of water vapor was injected into the flask and allowed to evaporate. At least eight hours were allowed for equilibrium to be established. By using very low purge gas flowrates (5 to 10 mℓ/min), a constant water vapor peak was observed on the gas chromatograph output. Usually, after approximately 15 minutes, the

peak height would decrease as the dry purge gas became mixed with the water vapor-gas mixture in the flask. A Bendix Gastek gas monitor was used to verify the results obtained for several air-water vapor mixtures. Unlike the SO_2 measurements, the values obtained using the Gastek device were in agreement with the calibration values. A representative calibration curve is shown in Fig. 5.2.

5.3 Response Testing

Before testing adsorbents, the behavior of the system without the adsorption bed must be studied so that dispersion effects associated with the bed alone will not be confused with effects due to the sampling apparatus. Since the volume of the sampling line and sample line flowrate may affect the chromatograph response, several diagnostic tests were performed to determine the response characteristics of the sampling system.

The response of the system to a step change in SO_2 concentration is shown in Fig. 5.3. Notice that there is a lag between the time of injection and chromatograph response. The reason for this is that the sampling system performs a 'batch' analysis of the gas flowing through the sampling system. Since 2.5 minutes is required to analyze a single sample, the sample valve was activated only every 2.5 minutes. The tests were performed with different time intervals before sample valve activation. By doing this, the actual response could be obtained. The significance of Fig. 5.3 is that the sampling system does not contribute to excessive axial dispersion. It was suspected that the stainless steel frit used to filter the sampling gas may have caused

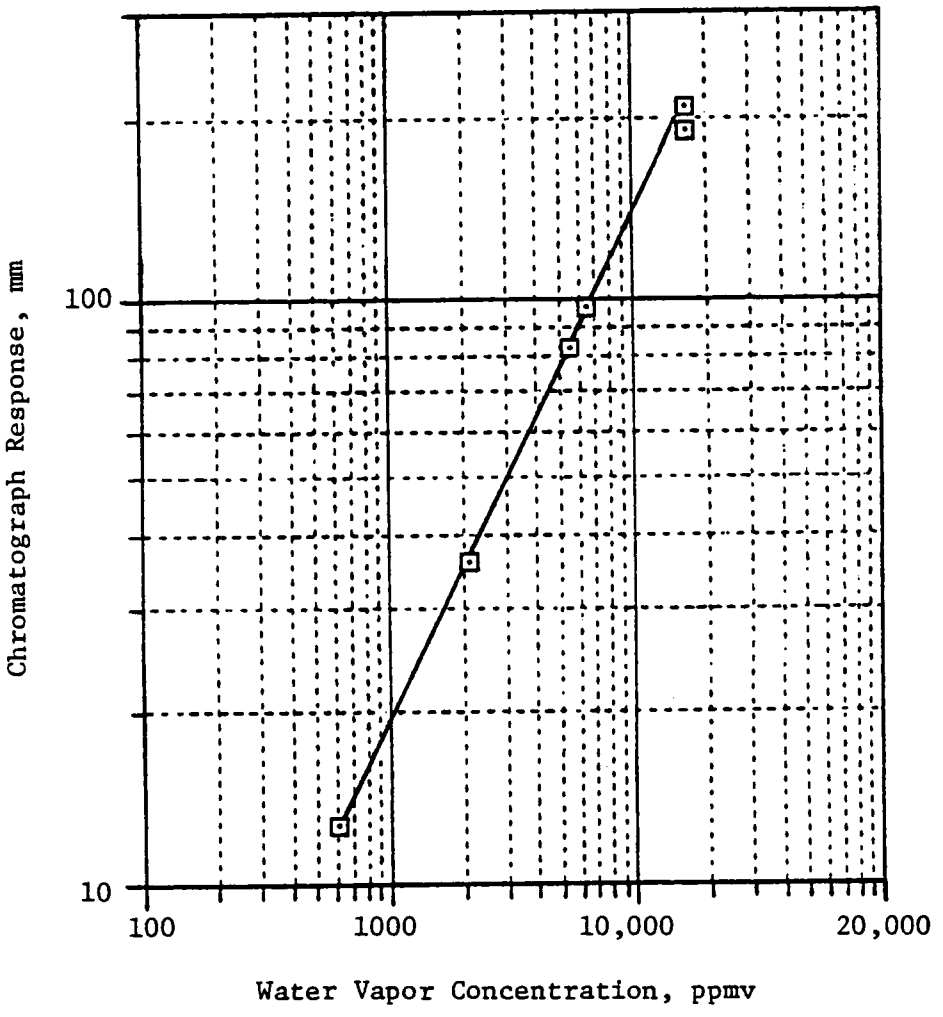

Figure 5.2 Gas Chromatograph Calibration Curve for Water Vapor.

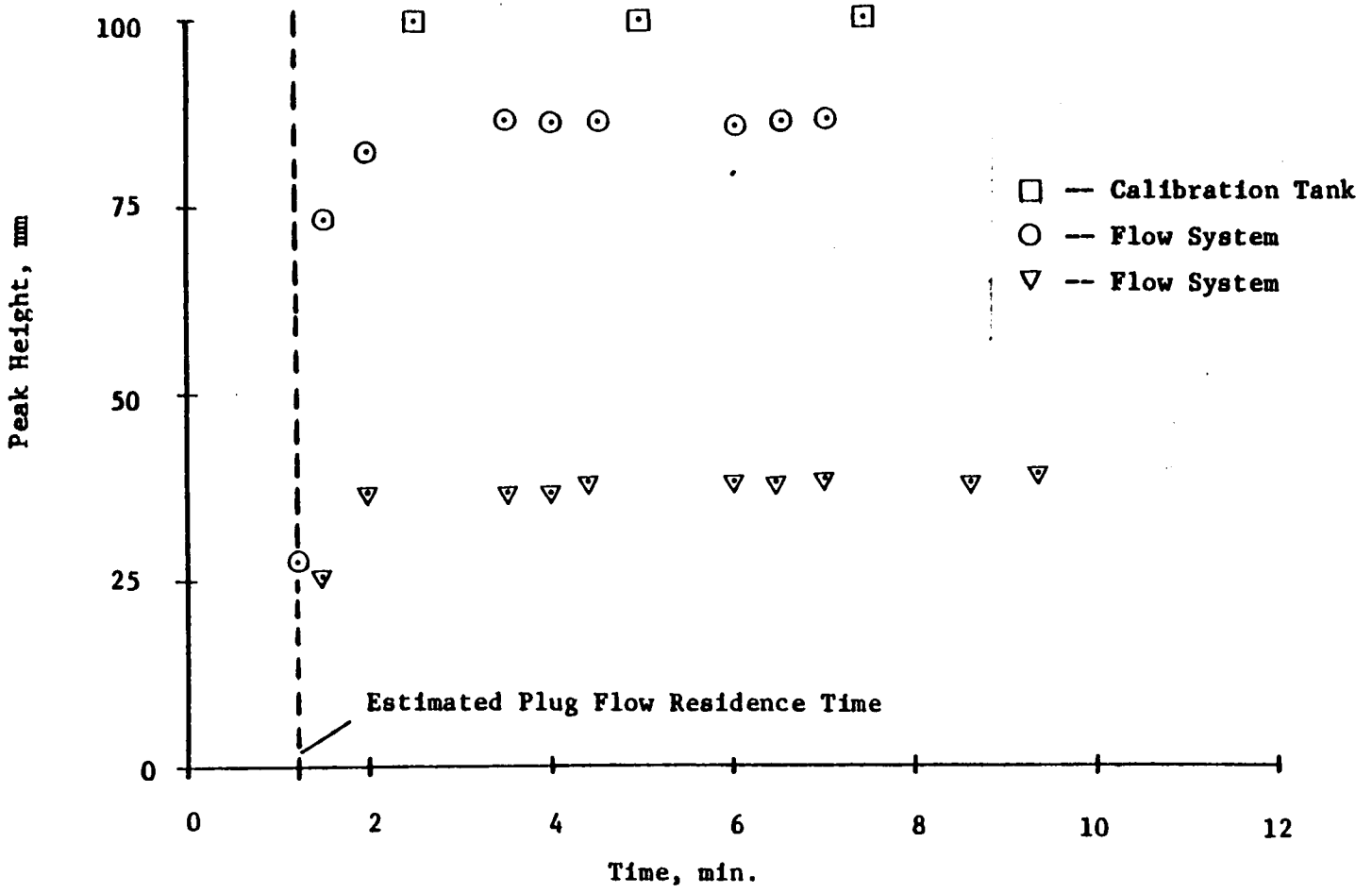

Figure 5.3 Response of Gas Chromatograph System to Step Change in Concentration.

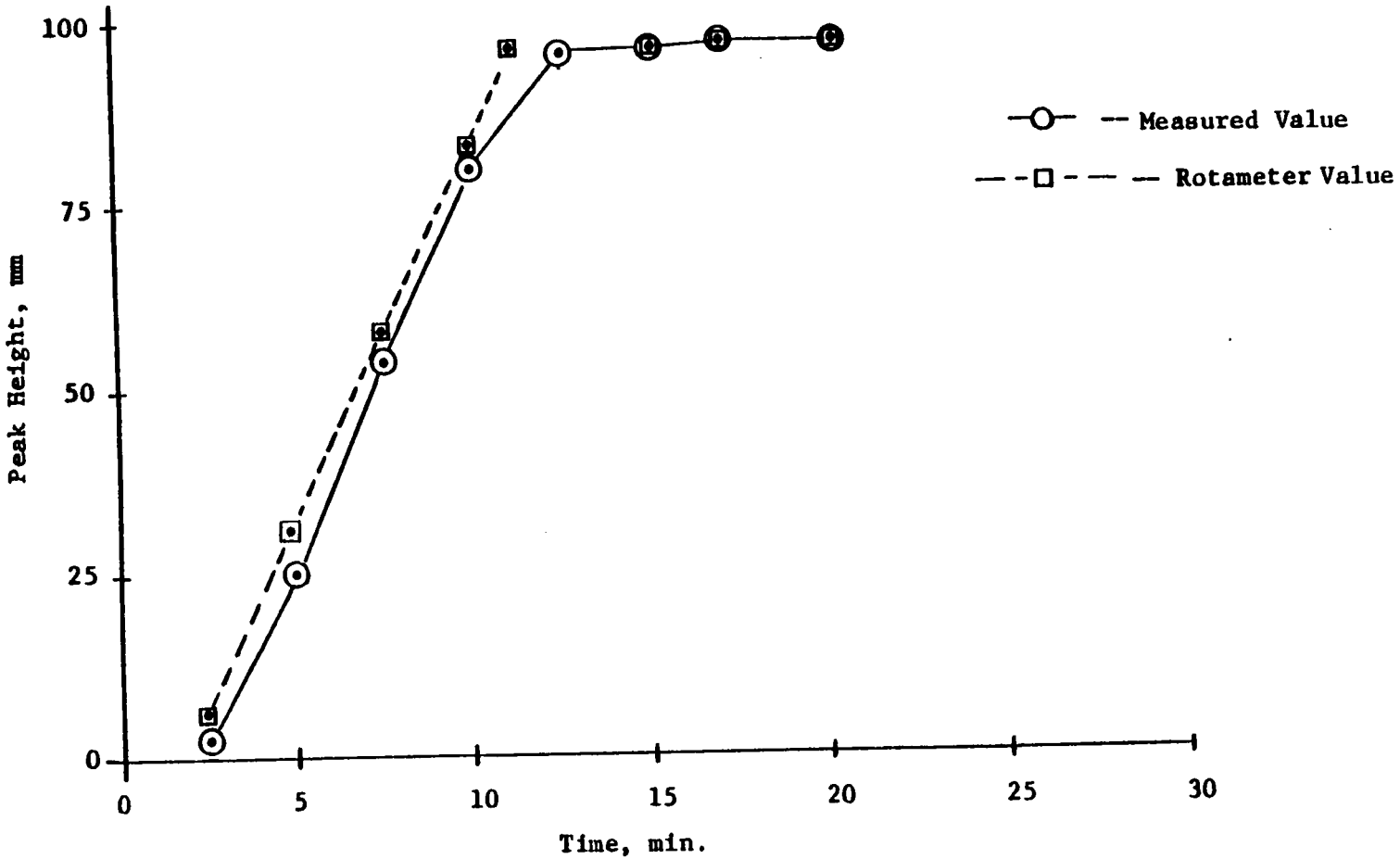

Figure 5.4 Response of Gas Chromatograph System to Linear Change in Concentration.

dispersion. This was not supported by the results obtained. To quantify the effects caused by the frit, a continuous detection system would be required. The time lag shown in Fig. 5.3 is the time required for the gas sample to reach the sampling valve after the SO_2 was injected into the main gas stream.

The purpose of the second series of tests was to determine if the sampling system would modify the breakthrough curve shape. A simulated breakthrough curve was obtained by adjusting the SO_2 rotameter to the desired concentration. By using a series of rotameter settings, the desired concentration curve shape could be obtained (linear or non-linear). Figure 5.4 depicts the response of the chromatograph for a linear input. The chromatograph response lags the SO_2 input by approximately 0.5 minutes. This is in agreement with the value obtained in the step change in concentration runs.

The response to a non-linear SO_2 concentration is shown in Fig. 5.5. The significance of Fig. 5.5 is that the response of the chromatograph was in agreement with the input concentration. Therefore, it was concluded that aside from the time lag associated with the sampling line, the measured concentration represented the actual concentration in the adsorption column.

With the preliminary tests complete, the system could now be used to measure SO_2 and SO_2-water vapor breakthrough curves.

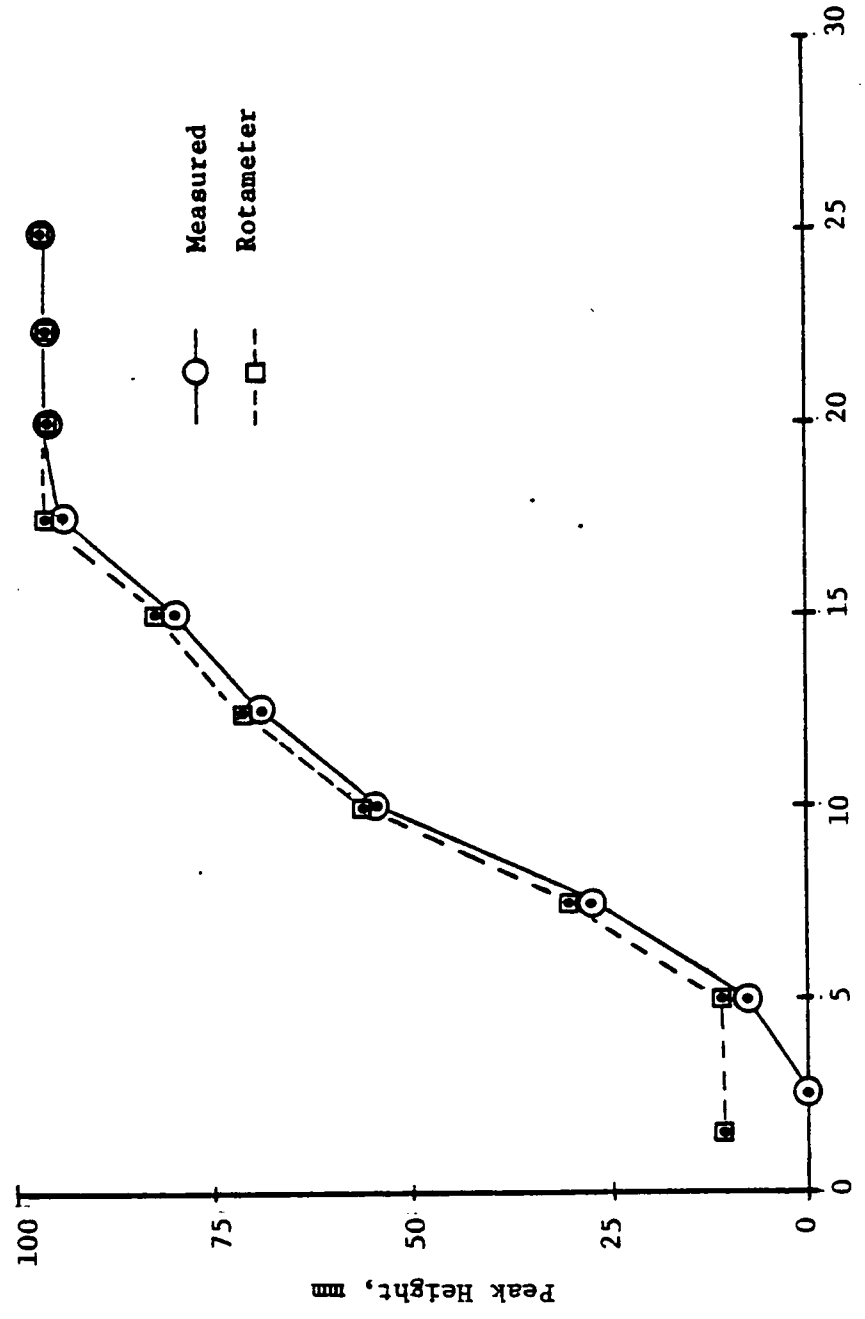

Figure 5.12 Response of Gas Chromatograph System to Non-linear Change in Concentration.

VI. MEASUREMENT OF ADSORPTION BREAKTHROUGH CURVES

The adsorption breakthrough curves for SO_2 on Linde molecular sieves type 13X, AW500, and Davison silica gel were measured and the effects of gas throughput and temperature investigated. Activated charcoal and montmorillonite were also tested. Activated charcoal served as an important comparison because flue gas desulfurization processes using this material are actively being developed.

Binary adsorption performance was obtained for constant SO_2 and variable water vapor concentration. In this way the effects of co-adsorption of water vapor on SO_2 breakthrough curves could be studied.

6.1 Measurement of Single Adsorbate Breakthrough Curves

The breakthrough curve experiments for single adsorbates were performed to serve as a comparison to the SO_2-water vapor breakthrough curve tests. For each measured breakthrough curve, inlet gas composition was held constant and either gas volumetric flowrate or gas temperature was varied. Effluent gas concentrations were normalized with respect to the inlet concentration and recorded as a function of actual elapsed time.

A representative breakthrough curve for SO_2 adsorption on Linde molecular sieve type 13X is shown in Fig. 6.1. The effluent concentration represents a characteristic sigmoidal curve. The effluent profile shape is determined by the mechanisms for mass transfer and

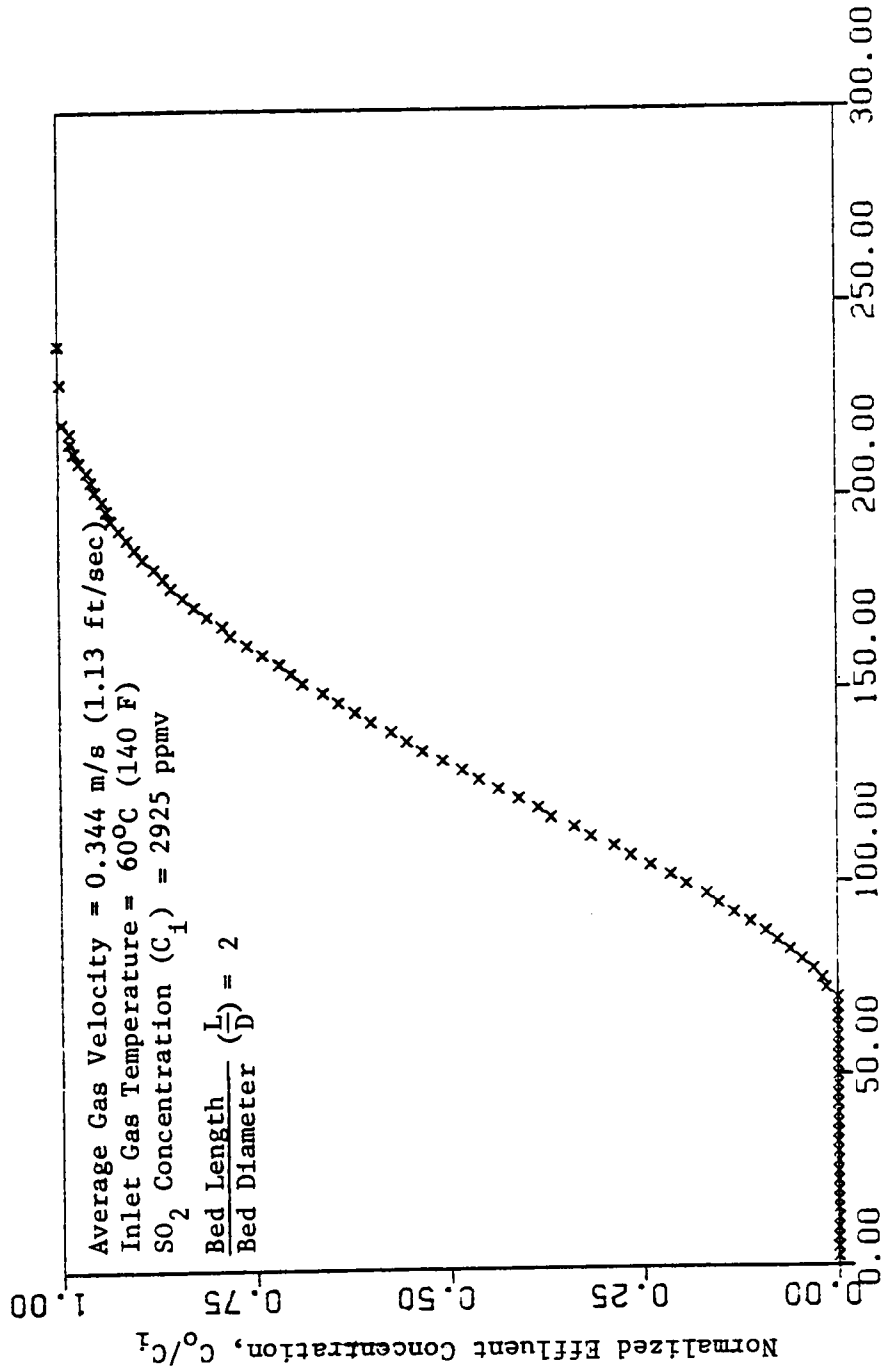

Figure 6.1. Representative Breakthrough Curve for SO_2 Adsorption on Type 13X Molecular Sieve Zeolite.

is commonly referred to as profile or zone spreading. These may be classed according to the following:

1) sorption kinetics--refers to mass transport processes that occur within the porous pellet. The rate of adsorption at the surface is rapid but rate of mass transport of the adsorbate can be slow. Referring to Fig. 6.1, internal diffusion is not controlling based on the shape of the measured effluent profile and the retention time. Intra-partical diffusion processes are characterized by very broad sigmoidal curves that asymptotically approach the inlet concentration.

2) hydrodynamic effects--refers to mass transport processes that occur external to the adsorbent. Because of the very complex nature of flow paths established through a porous bed, describing the flow distribution would be a considerable task. Since the bed packing assumes a random orientation, a range of flow paths are formed that offer different resistances. The net result is the formation of eddys that contribute to altering the effluent concentration profile. Also the flow regime (laminar or turbulent) will affect the rate of mass transport.

3) thermal effects--as adsorption occurs, energy is released in an amount depending on the heat of adsorption. Consequently the ultimate adsorption capacity will be decreased depending on the adsorption isotherm.

Ultimate capacities were obtained for each run by performing a mass balance on the adsorption column. The total SO_2 adsorption was obtained from the expression

$$Q_{AD} = \frac{1}{\rho_B V_B} \int_o^{t_{sat}} [\rho_g Q_g C_i - \rho_g Q_g c(t)]dt \qquad (6.1)$$

where the change in bulk gas flowrate is assumed to be negligible due to adsorption. The expression above was solved by trapezoidal integration.

An energy balance was performed on the adsorption column to obtain the heat released during adsorption. The expression

$$Q_H = \int_o^{t_{sat}} [\rho_a Q_a T_a(t) - \rho_a Q_a T_a(t_o)]dt \qquad (6.2)$$

was integrated numerically for the temperature data obtained during an adsorption test. The upper limit of integration, t_{sat}, was the time when the effluent gas concentration equaled the inlet gas concentration. Recalling Fig. 6.1, the measured ultimate adsorption capacity was 12.5g/100g adsorbent compared to an equilibrium value of 18g/100g obtained during isothermal adsorption conditions. The

discrepancy between ultimate and equilibrium values is attributed to the uncertainty in bulk gas flowrate and primarily to non-isothermal conditions. Adiabatic adsorption leads to decreased loadings depending on the adsorption isotherm. Thus equilibrium between free stream and adsorbent concentration was not obtained.

The measure of adsorption column efficiency is usually indicated by HETP (acronym meaning height equivalent of a theoretical plate) which was obtained by van Deemter et al. [58] to simplify the mathematical results of Lapidus and Amundson [59]. The plate height or HETP is widely used and accepted as a parameter for characterizing 'zone' spreading and resolution. 'Zone' refers to the length of the adsorption column required to attain equilibrium with the adsorbate. HETP is related to the adsorption column parameters through the expression

$$\text{HETP} = A + B/u + Cu \tag{6.3}$$

where A, B, and C are constants and u is the average gas velocity. In the expanded form

$$\text{HETP} = 2\lambda d_p + \frac{2\gamma D_g}{u} + \frac{8}{\pi^2}\left(\frac{k}{1+k}\right)^2 \frac{d_p^2}{D_g} u + \frac{2k}{2(1+k)^2} \frac{d_f^2}{D_e} u \tag{6.4}$$

The difficulty in applying the HETP expression to this investigation is determining the number of theoretical plates, N_p. Robell and Merrill [60] have shown that for frontal chromatography (constant input of adsorbate) the number of theoretical plates is given by

$$N_p = 16\left(\frac{t_s}{W_f(2)\sqrt{\frac{2}{\pi}}}\right)^2 \qquad (6.5)$$

where

t_s = stoichiometric time

W_f = frontal curve width

N_p = number of theoretical plates.

The stoichiometric time, t_s, is defined as the time when the following integration equality is satisfied

$$\int_0^{t_s} c(t)dt = \int_{t_s}^{\infty} [c_i - c(t)]dt \qquad (6.6)$$

The frontal curve width was obtained by constructing a tangent to the frontal curve at the stoichiometric time and extending this line until the abscissa and line of effluent saturation were intersected. Stoichiometric time and frontal curve width measurements are shown in Fig. 6.2. Because of the shallow bed depths employed in this investigation conclusions based on HETP results alone would be subject to considerable doubt. Since low bed depths result in poorly developed fronts, inferences made on profile shape alone must be carefully made. However, HETP does provide a means for comparing 'trends' in adsorption column behavior.

Figure 6.3 depicts the variation in SO_2 adsorption performance on Linde molecular sieve type 13X with superficial gas velocity. The lower gas velocity, case 1V, results in the discharge of a characteristic sigmoidal curve. The 'c' shaped profile of case 2V does

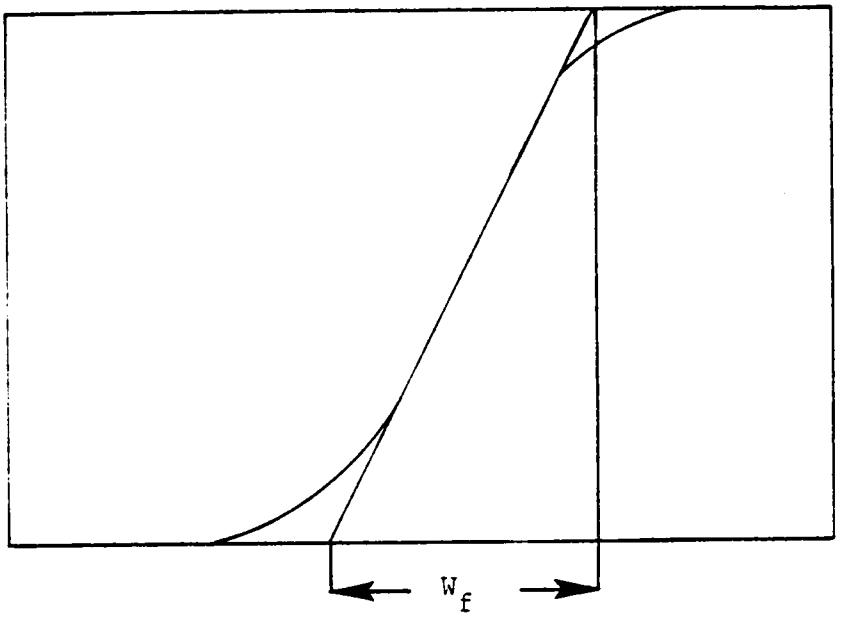

Frontal Curve Width Measurement

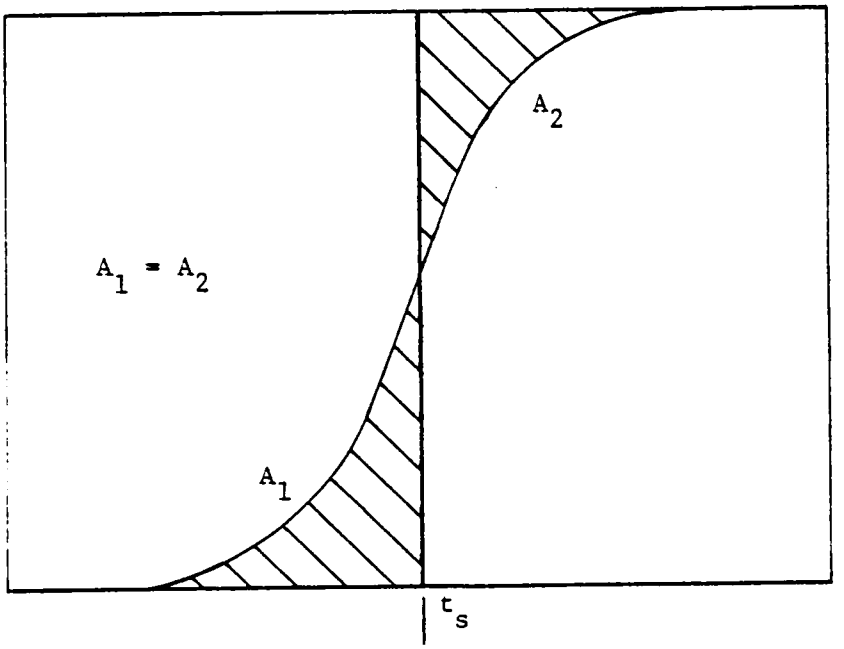

Location of Stoichiometric Time, t_s, with Respect to Effluent Profile

Figure 6.2. Measurement of Stoichiometric Time and Frontal Curve Width.

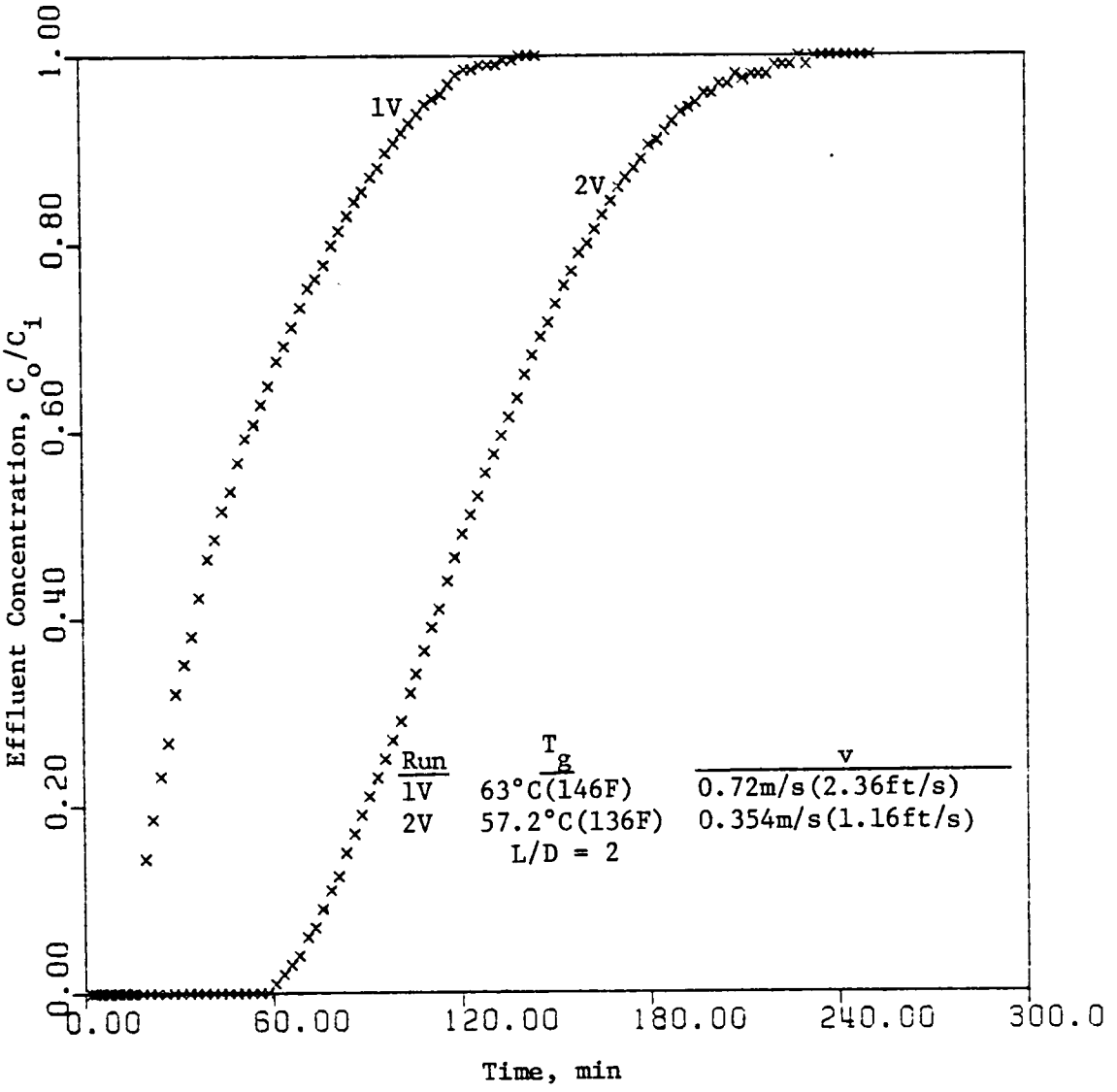

Figure 6.3 Variation of SO_2 Adsorption Performance on 13X Molecular Sieve with Gas Velocity.

exhibit sigmoidal characteristics but not as developed as in case 1V. Referring to Table 6.1, the HETP values were 0.35 cm (1.16 in.) and 13.3 cm (5.25 in.), respectively. This would explain why the profile for case 2V was poorly developed since only one theoretical plate occurred compared to 7.3 for case 1V.

The calculated ultimate capacities showed that for case 1V the SO_2 removal was 15.7g/100g adsorbent compared to 12.5g/100g adsorbed for case 2V. The lower ultimate capacity for case 2V was attributed to shorter gas contact time (equilibrium time). Since the adsorption process here is adiabatic, this phenomena would be expected.

For P_e (Peclet number) greater than 1000, mass transfer is either external controlled or pore or particle diffusion controlled. For P_e in the range of 1 to 10, axial dispersion is controlling. The P_e numbers for cases 1V and 2V were 709 and 1060 respectively. The fact that axial dispersion is not significant was demonstrated by the system response test for non-adsorbing media which was discussed in Chapter 5. Since mass transfer data for the adsorbents was not available measurement of actual mass transport was necessary.

Figure 6.4 is a comparison between a low and high temperature breakthrough curve test. Case 1T depicts the characteristic sigmoidal curve. Case 2T is a 'c'-shaped profile but it resembles a developing sigmoidal curve. The ultimate adsorption capacities for SO_2 were 12.0 and 16.0g/100g for cases 2T and 2T, respectively. As gas temperature was increased, the breakthrough time was reduced.

Table 6.1 Summary of SO_2 Adsorption on Fixed Beds of Molecular Sieve Zeolites and Silica Gel

Adsorbent	Temperature °C	(F)	Gas Velocity m/s	(ft/s)	HETP cm	(in.)	N_p	Bed Pressure Drop cm H_2O	(in. H_2O)	SO_2 Adsorbed g/100g	Stoichiometric Time, min
Linde 13X	25.5	(78)	0.316	(1.04)	1.5	(0.60)	9.97	4.6	(1.85)	16	141
	31.1	(88)	0.832	(2.73)	9.2	(3.6)	1.66	17	(6.75	21	70
	57.2	(135)	0.353	(1.16)	2.08	(0.82)	7.29	3.8	(1.5)	16	128
	60.0	(140)	0.344	(1.13)	1.67	(0.6)	9.08	3.9	(1.55)	16	137
	63.3	(146)	0.719	(2.36)	13.3	(5.2)	1.14	13	(5.45)	12	52
	82.2	(180)	0.957	(3.14)	14.3	(5.6)	1.06	13	(5.25)	12	39
Linde AW500	28.8	(84)	0.316	(1.04)	18.3	(7.2)	0.828	3.3	(1.3)	11	87.5
	65.5	(150)	0.902	(2.96)	57.1	(22.5)	0.266	13	(5.5)	8.2	31
	57.2	(135)	0.356	(1.17)	21.7	(8.56)	0.70	3.6	(1.45)	8.9	78
	27.2	(81)	0.829	(2.72)	43.1	(16.9)	0.354	14	(5.9)	12	40
	82.2	(180)	1.18	(3.9)	33.6	(13.3)	0.453	9.9	(3.9)	4.2	14.5
Davison Silica Gel	56.1	(133)	0.314	(1.12)	29.7	(11.7)	0.513	5.5	(2.20)	0.72	7.5
	57.2	(135)	0.877	(2.88)	31.1	(122)	0.045	14	(5.60)	1.80	7.3
	27.7	(82)	0.316	(1.04)	--	--	--	5.3	(2.10)	1.43	14.4

*SO_2 concentration : 2800 ppmv ± 100 ppmv Bed Length : 15.2 cm (6 in.)

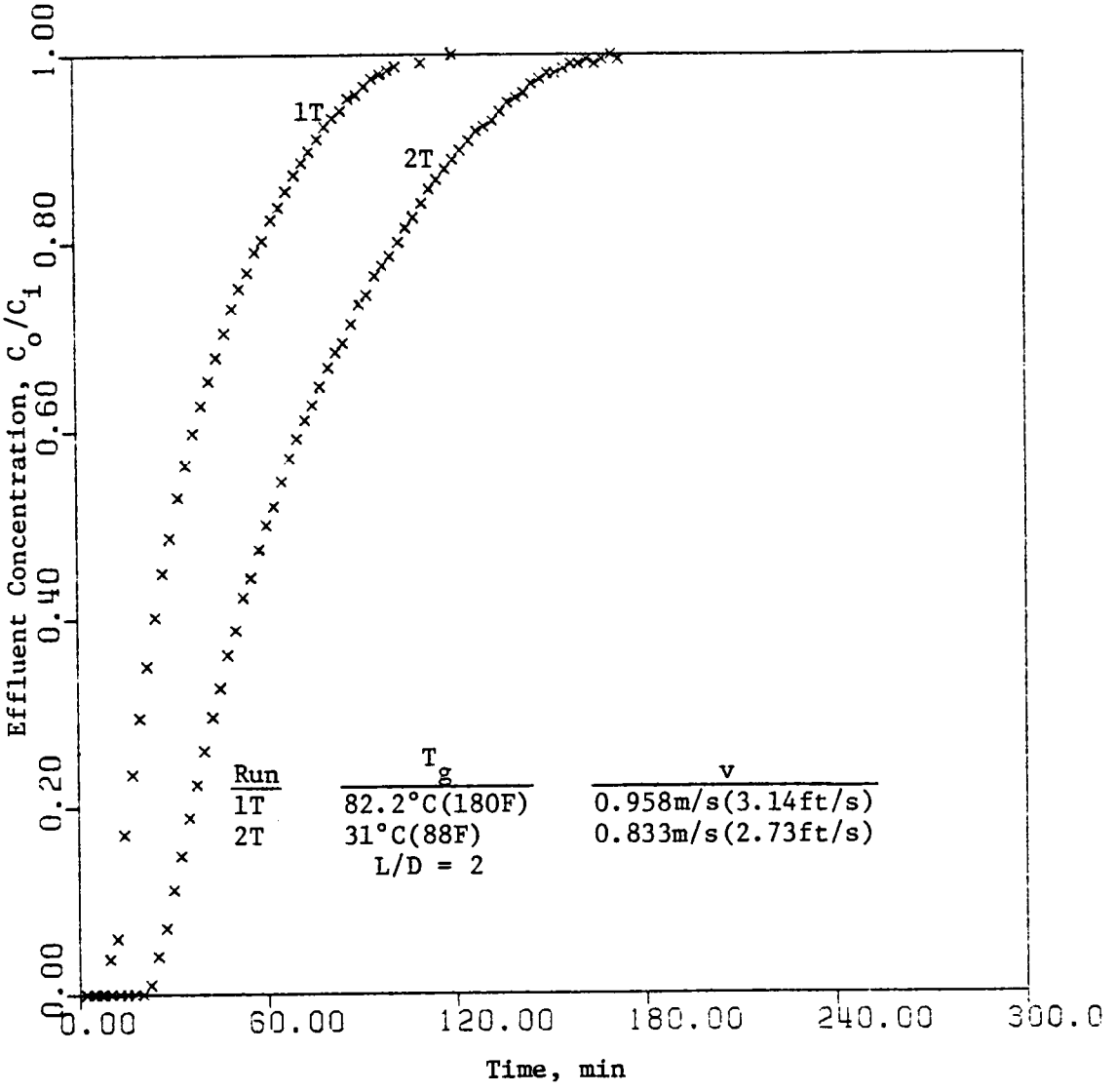

Figure 6.4 Variation of SO_2 Adsorption Performance on 13X Molecular Sieve with Temperature.

Profile 'spreading' of the type exhibited in Figs. 6.3 and 6.4 was expected because SO_2 adsorption on 13X molecular sieves may be represented by a 'favorable' Langmuir adsorption isotherm. In general, a concave or favorable isotherm leads to profile spreading since removal for low concentrations is favored. The converse is true of a 'non-favorable' Langmuir isotherm. For sufficiently long columns with fully developed adsorption profiles and negligible axial dispersion, a symmetrical sigmoidal curve would result.

In the design of a large scale adsorber, an important parameter to consider is the 'sharpness' of the profile which is defined as the slope of the breakthrough curve for a specified effluent concentration. For comparison, the derivative of the breakthrough curve at $c_o/c_i = 0.5$ is presented in Table 6.2. As superficial gas velocity increased, profiles became steeper and breakthrough times decreased. A 2.6-fold increase in velocity caused a reduction in breakthrough time by 43 percent or approximately 1/3. For constant velocity, an increase in gas temperature produced a similar effect.

The next tests to consider were the SO_2 adsorption behavior of type AW500 molecular sieves. A comparison of SO_2 adsorption variation with gas temperature is shown in Fig. 6.5. Unlike the sigmoidal curves for the type 13X molecular sieve, the effluent profile had a definite 'c' profile shape. The profile was characterized by a sharp front that extended over approximately 70 percent of the profile followed by a very broad tail. The long equilibration time was of

Table 6.2 Comparison of Breakthrough Curves at Half-Maximum Effluent Concentration

Adsorbent	Gas Velocity m/s (ft/s)	Breakthrough Time min	Curve Width min	Slope of Breakthrough Curve $_{-1}$ min
Linde 13X	0.316 (1.04)	134	117	0.0086
	0.719 (2.36)	43	82	0.012
	0.957 (3.14)	29.5	47	0.0213
	0.344 (1.13)	130	97.5	0.0102
	0.353 (1.16)	120	98.5	0.0101
	0.832 (2.73)	57.5	70.5	0.0142
Linde AW500	0.316 (1.04)	62	98.5	0.0101
	0.902 (2.96)	15	28	0.0357
	0.356 (1.17)	49	65.5	0.0153
	0.829 (2.72)	19	33	0.0303
	1.18 (3.9)	8	25.5	0.0392
Silica Gel	0.314 (1.12)	4	14	0.072
	0.877 (2.88)	1.5	17	0.0588

Prediction of Effluent Profiles

13X Molecular Sieve

$$C_o/C_i = \frac{t - [e^{(5.576 - 0.669v)} - \frac{1}{2}e^{(5.028 - 0.3226v)}]}{e^{(5.028 - 0.3226v)}}$$

AW500 Molecular Sieve

$$C_o/C_i = \frac{t - [e^{(4.773 - 0.689v)} - \frac{1}{2}e^{(4.847 - 0.459v)}]}{e^{(4.847 - 0.459v)}}$$

where C_o/C_i = effluent concentration/inlet concentration

t = time, min

V = superficial gas velocity, ft/sec

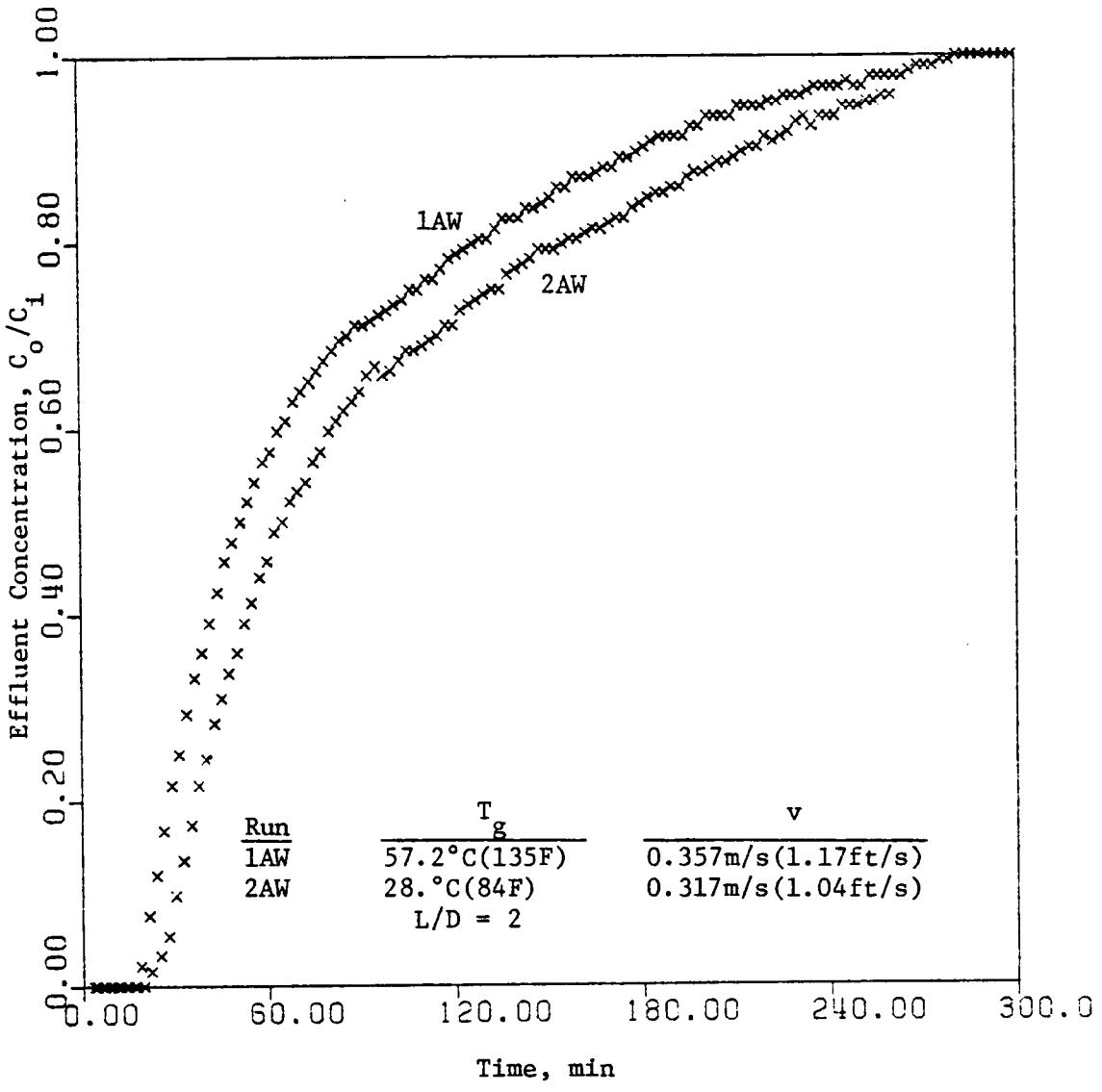

Figure 6.5 Variation of SO_2 Adsorption Performance on Type AW500 Molecular Sieve with Temperature.

considerable concern because this implies a possible reaction with the adsorbent. The other possible effect would be intraparticle diffusion controlling. The ultimate adsorption capacity was 8.19 and 11.8g/100g adsorbent. These removal rates represent approximately one-half the amount removed by the type 13X sieves operating under similar conditions.

The effect of gas velocity on profile shape is depicted in Fig. 6.6. The results obtained were similar to those previously discussed for Fig. 6.5. The ultimate capacities were 8.9 and 8.19g/100g for cases 1AV and 2AV, respectively. The HETP was 57.1 cm (22.5 in.) and 21.7 cm (8.56 in.). Care must be used when calculating HETP values since the stoichiometric time is not the best criteria. Since the profile may be characterized by two profiles of different slopes, certainly one should not necessarily obtain results comparable to the other.

Silica gel gave the lowest removal capacity for SO_2 even when low velocity, low temperature runs were performed. Figure 6.7 depicts the profile obtained for superficial gas velocities of 0.314 m/s (1.12 ft/s) and 0.877 m/s (2.88 ft/s). The adsorption capacities were 0.72 and 1.80g/100g adsorbent. Saturation tests (Chapter 8) showed that silica gel and 13X molecular sieve had approximately the same adsorption capacity for SO_2 concentrations of 100 percent. Thus SO_2 adsorption capacity of silica gel is much lower for the adsorbate concentrations for the range considered in this investigation.

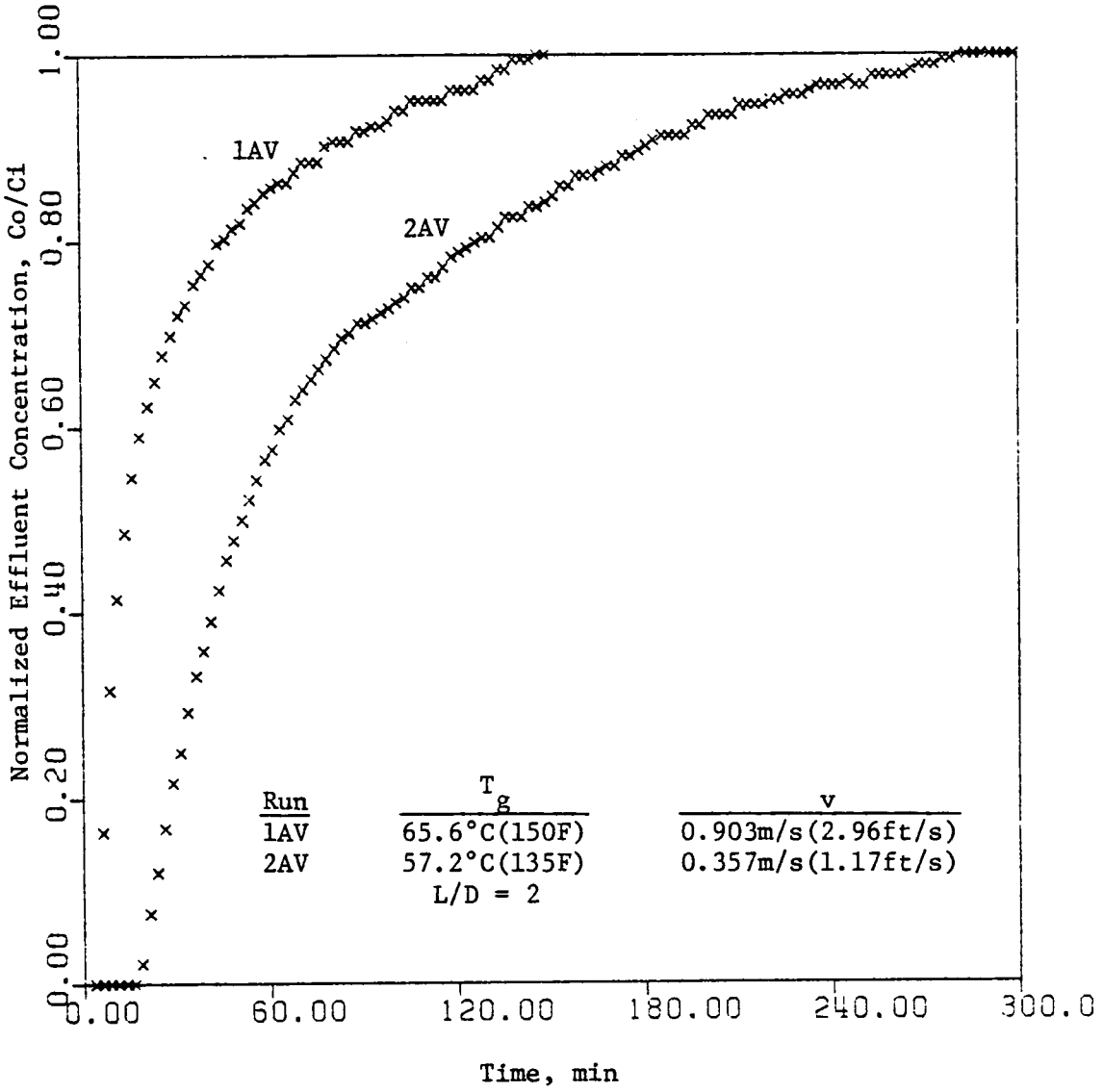

Figure 6.6 Variation of SO_2 Adsorption Performance on Type AW500 Molecular Sieve with Gas Velocity.

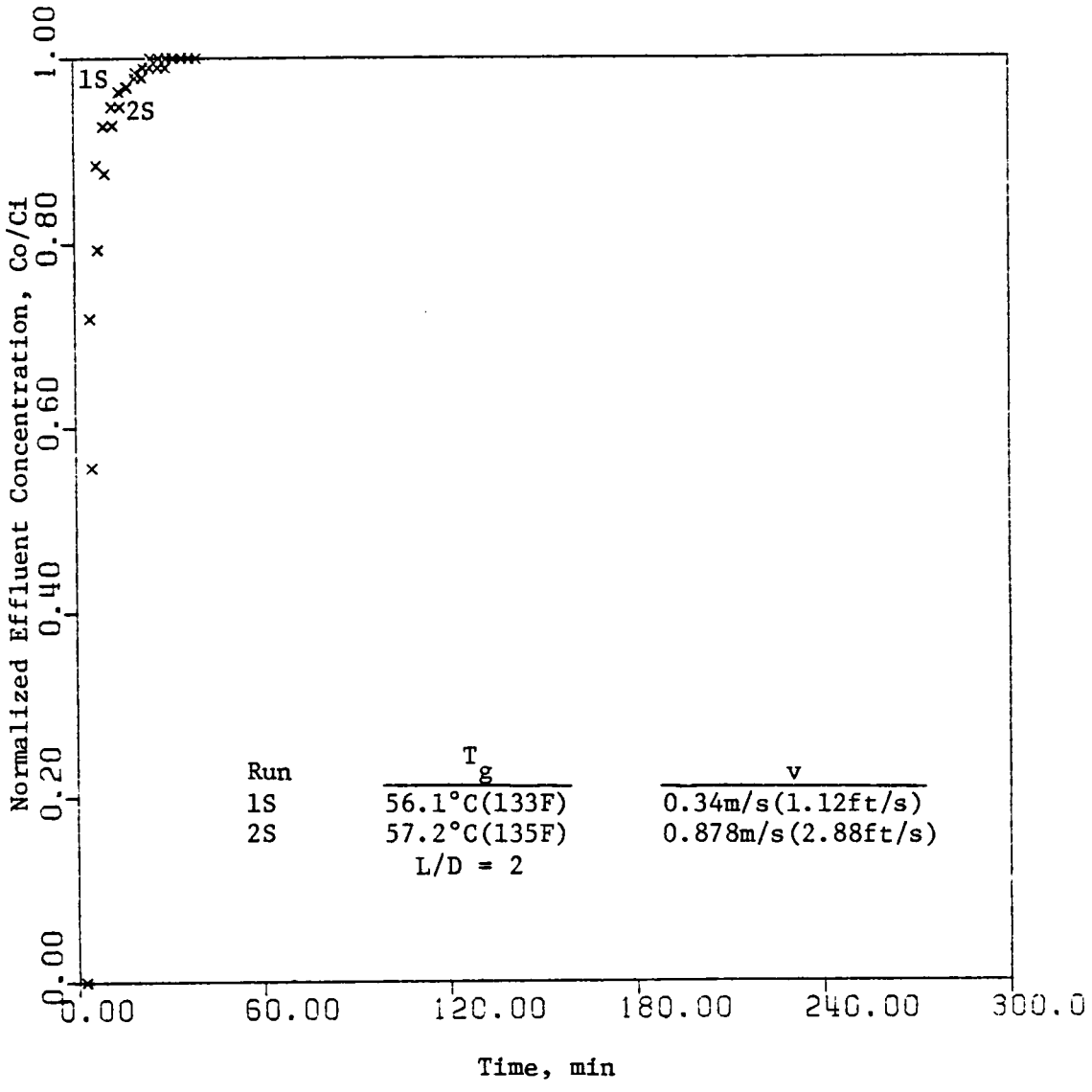

Figure 6.7 Variation of SO_2 Adsorption Performance on Davison GR1 Silica Gel.

A summary of the cases considered is presented in Table 6.1 and the significant results are that it:

1) Demonstrates SO_2 adsorption in single dilute adsorbate flow;
2) In general, breakthrough times were greatest for adsorbents in the order 13X > AW500 > silica gel;
3) Provides contact times necessary to achieve a specific removal for selected gas temperatures and velocities;
4) Performance is based on shallow beds that could be staged and scaled for a specific separation problem;
5) 13X and silica gel have the greatest ultimate capacity for SO_2 but silica gel SO_2 adsorption was significantly lower in low adsorbate flows;
6) AW500 required the longest time to achieve saturation. Integrated breakthrough curves did not agree with equilibrium adsorption capacity tests which indicates a particle side or rate-limiting adsorption step.

6.2 Binary Adsorption of SO_2 and Water Vapor

The procedure used to obtain binary adsorption results was similar to the single adsorbate case except extreme care was necessary to insure proper SO_2-water vapor mixture fractions were maintained during tests. The pressure-humidity device previously described in Chapter 5 was used to provide the desired water vapor concentration.

The results for the binary adsorption tests on 13X molecular sieve are summarized in Table 6.3. The measured breakthrough curves for different SO_2 water vapor mixture fractions are shown in Figs. 6.8-6.11. Figure 6.8 shows the results for a high SO_2 water vapor mixture fraction (5.28 ppmv H_2O/ppmv SO_2). The interesting phenomenon to notice in Fig. 6.8 is that the effluent SO_2 peak actually exceeds the inlet concentration. In fact, the effluent peak represents a desorption of 18.5 percent of the initial SO_2 adsorbed. The reason for this behavior is that water vapor is more strongly attracted and held by the adsorbent than SO_2. Consequently, water vapor is being adsorbed in the first few adsorbent layers of the bed. As the water vapor mass transfer 'zone' moves through the bed the adsorbed SO_2 is displaced and consequently raises the free stream SO_2 concentration. The SO_2 adsorbed was 6.38g/100g adsorbent compared to 16.1/100g for the water vapor free case. Desorption also was influenced by the temperature rise of the bed. Since ultimate adsorption capacity is influenced by temperature, this also contributes to decreased adsorbate loadings.

Figure 6.9 shows the effect of decreasing water vapor concentration. The SO_2 adsorbed was 10.2g/100g adsorbent and desorption was 41.4 percent of the initial SO_2 removed. As gas temperature was increased, adsorbent capacity also decreased. Figure 6.10 shows the breakthrough curve results for a gas temperature of 60°C (140 F). SO_2 adsorption was 4.54g/100g adsorbent compared to 12.4g/100g for the

Table 6.3 Summary of Binary Adsorption Tests

Adsorbent	Gas Temperature °C(F)	Gas Velocity m/s (ft/s)	SO_2 Concentration ppmv	H_2O Concentration ppmv	Effluent Time at Half-Maximum t_{SO_2}	Effluent Time at Half-Maximum t_{H_2O}	SO_2 Adsorption g/100g	SO_2 Desorption percent
13X	26 (80)	0.34 (1.1)	2480	13,100	59.5	113	6.38	19
	23 (75)	0.33 (1.1)	2800	3,960	87.5	231	10.2	41
	60 (140)	0.89 (2.9)	2800	14,900	10.5	38.5	4.54	8.6
	77 (170)	0.96 (3.2)	2800	11,400	14	42	6.3	0.2
AW500	23 (73)	0.34 (1.1)	2930	4,180	36	240	5.3	17
	29 (85)	0.34 (1.1)	2660	12,700	24.5	98	2.6	51
	77 (170)	0.96 (3.2)	3000	11,300	7	32	1.4	29
	31 (88)	0.86 (2.8)	2680	9,990	7	45.5	1.7	15
Silica Gel	25 (78)	0.018(0.06)	2630	10,600	1.8	35	0.02	2.1
	34 (93)	0.86 (2.8)	3150	13,800	5.3	21	0.66	4.8
	25 (78)	0.85 (2.8)	2750	5,300	7	47	1.8	47

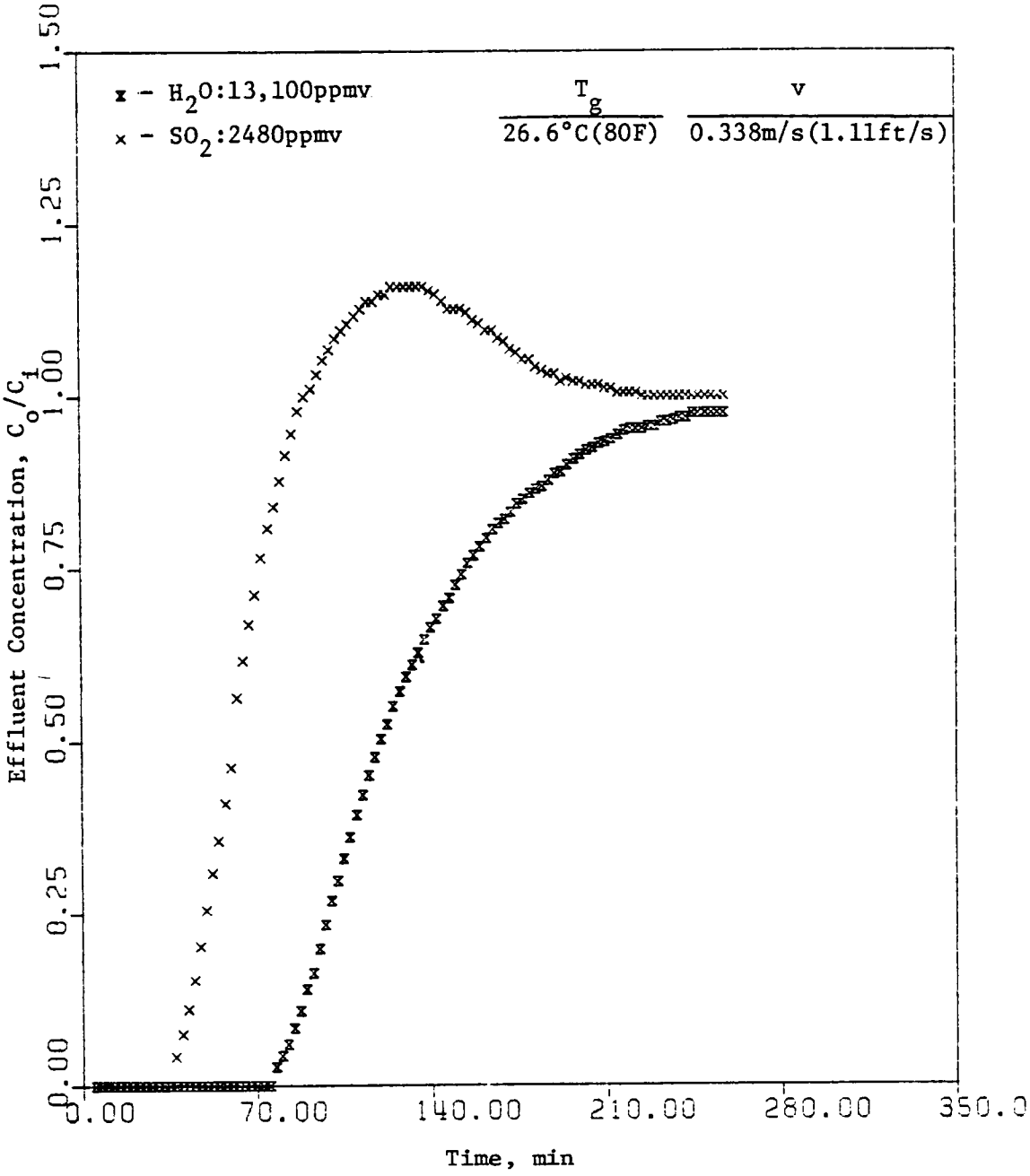

Figure 6.8 Binary Adsorption Performance of SO_2 and Water Vapor on 13X Molecular Sieve--High Water Vapor Content.

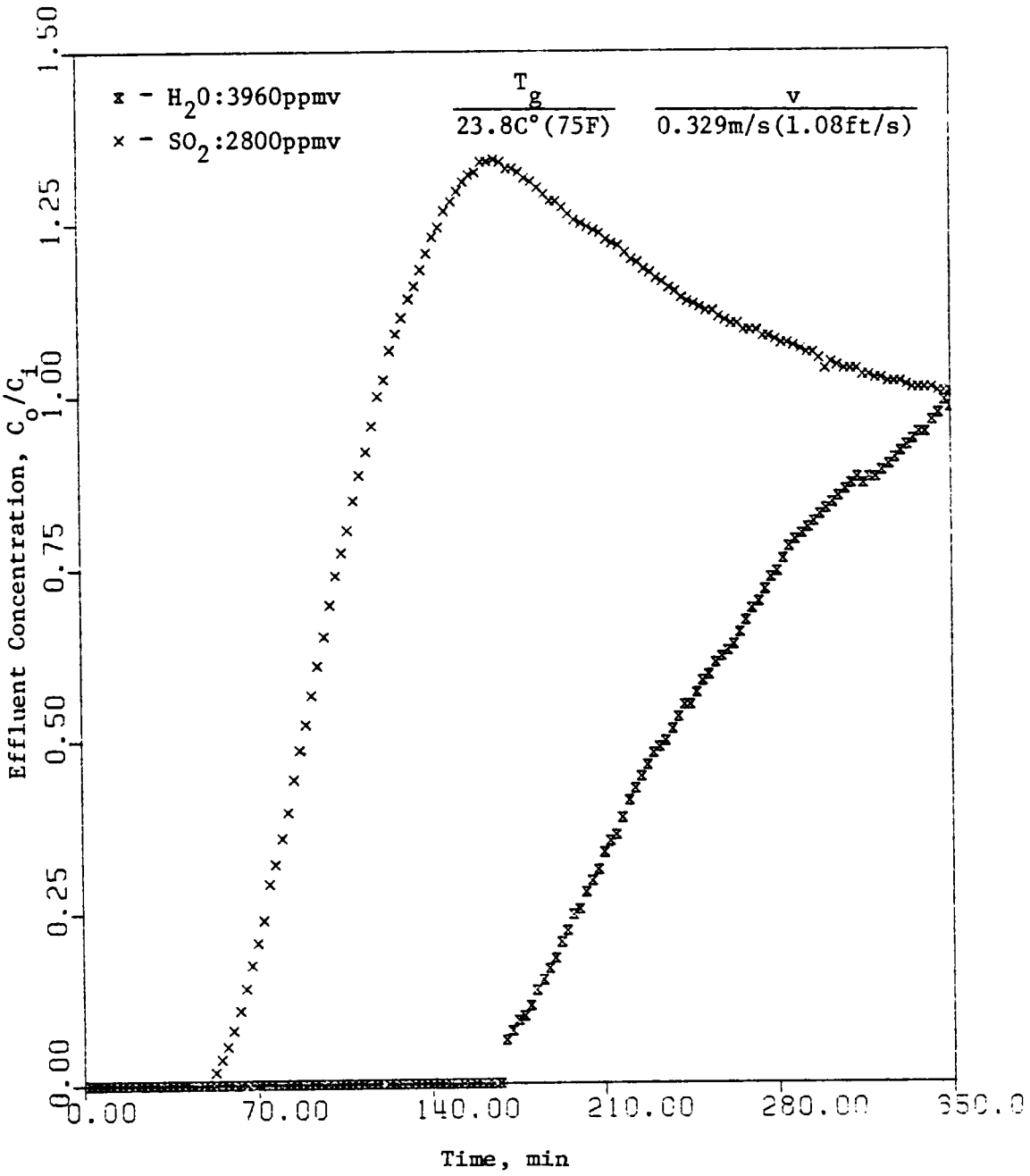

Figure 6.9 Binary Adsorption Performance of SO_2 and Water Vapor on 13X Molecular Sieve--Low Water Vapor Content.

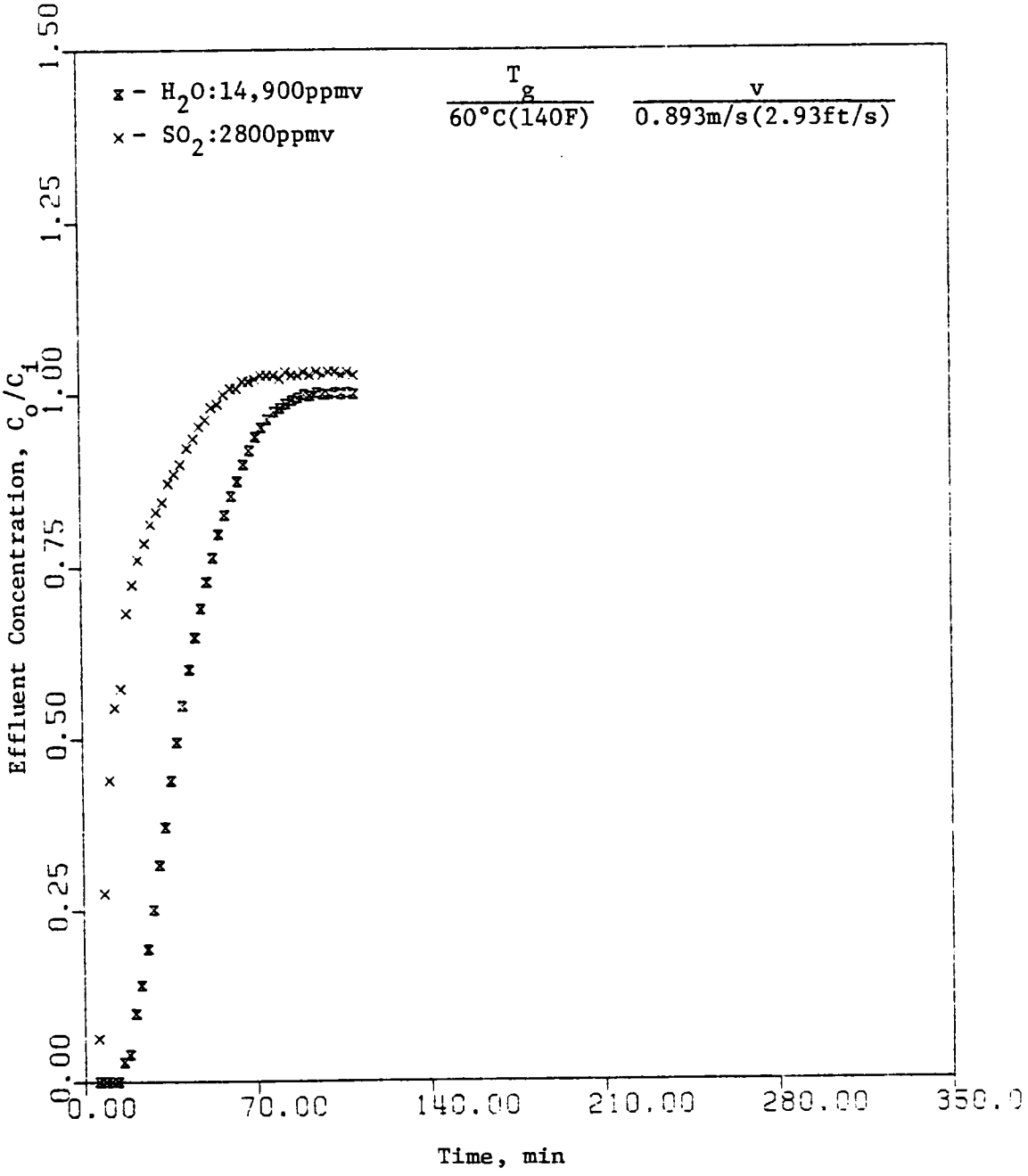

Figure 6.10 Binary Adsorption Performance of SO_2 and Water Vapor on 13X Molecular Sieve--High Water Vapor Content.

water vapor free conditions. SO_2 desorption represented only 8.6 percent of the inlet SO_2 concentration.

Figure 6.11 depicts the SO_2 sorption behavior at the maximum test temperature, 76.6°C (170 F). The most notable effect in Fig. 6.11 is the breakthrough curve shape exhibited by SO_2. Water vapor was eluted as a relatively sharp front while the SO_2 curve consisted of a sharp front followed by a long tail. This does not represent the sigmoidal curves previously obtained. It is also important to note the very short breakthrough times for SO_2 and water vapor (14 and 42 minutes, respectively).

The binary adsorption results for type AW500 molecular sieves are shown in Figs. 6.12-6.15. Figure 6.12 shows the breakthrough curves for constant velocity, constant water vapor concentration For the low water vapor test (4183 ppmv) the SO_2 adsorbed was 5.28g/100g adsorbent and the desorption was 16.5 percent. Figure 6.13 shows that for a water vapor concentration of 12,700 ppmv the SO_2 adsorption was 2.62g/100g but SO_2 desorption was 50.7 percent.

The desorbed SO_2 was substantially increased as water vapor concentration increased from 4200 to 12,700 ppmv. Desorption increased by a factor of 3 for a three-fold increase in water vapor concentration. Thus, a three-fold increase in water vapor concentration reduced SO_2 adsorption by one-half and SO_2 desorption increased by a factor of 3.

Figure 6.14 shows the adsorption of water vapor and SO_2 on type AW500 molecular sieves at 76.6°C (170 F). Only 1.44g/100g adsorbent

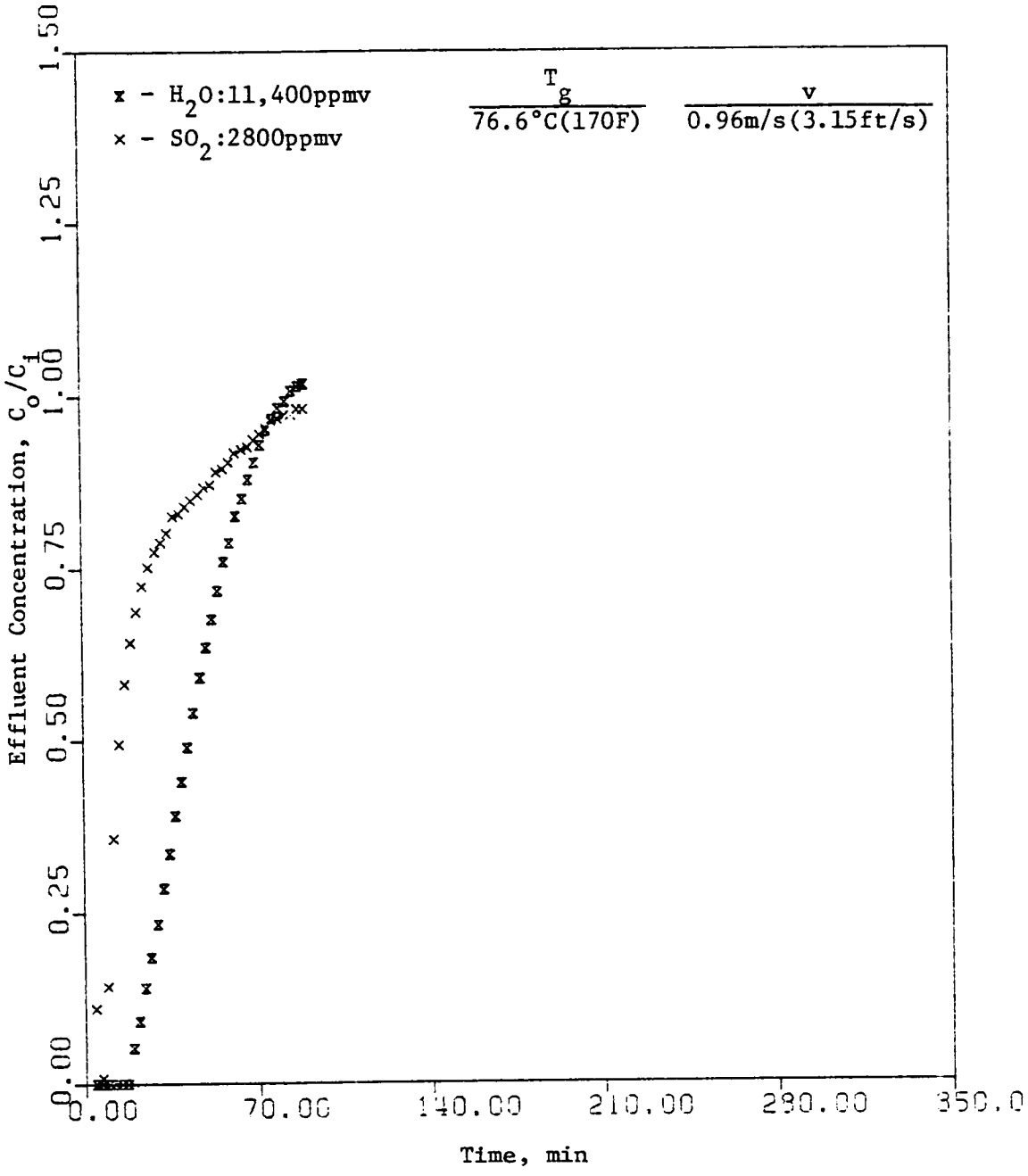

Figure 6.11 Binary Adsorption Performance of SO_2 and Water Vapor on 13X Molecular Sieve--High Water Vapor Content.

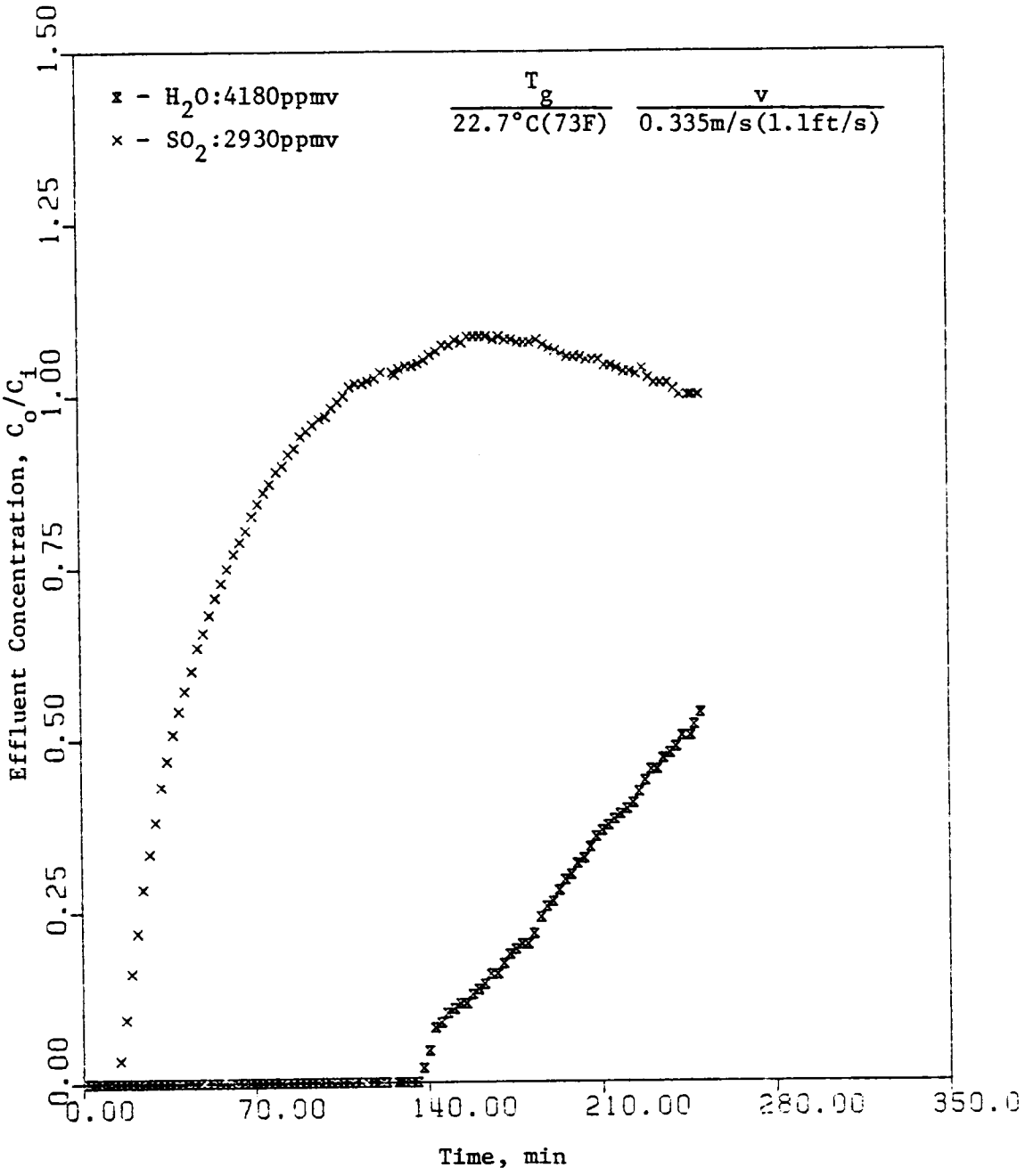

Figure 6.12 Binary Adsorption Performance of SO_2 and Water Vapor on AW500 Molecular Sieve--Low Water Vapor Content.

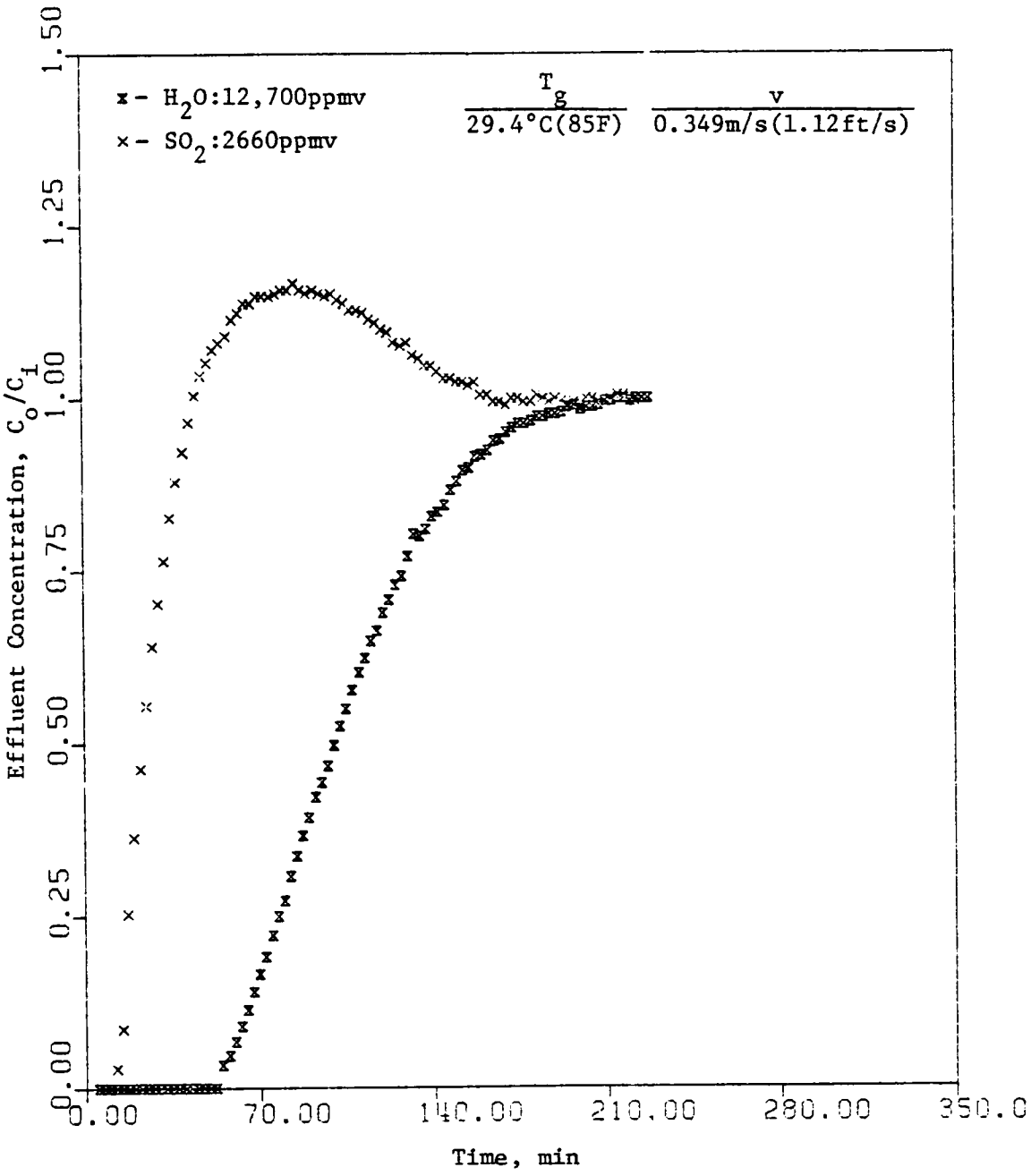

Figure 6.13 Binary Adsorption Performance of SO_2 and Water Vapor on AW500 Molecular Sieve--High Water Vapor Content.

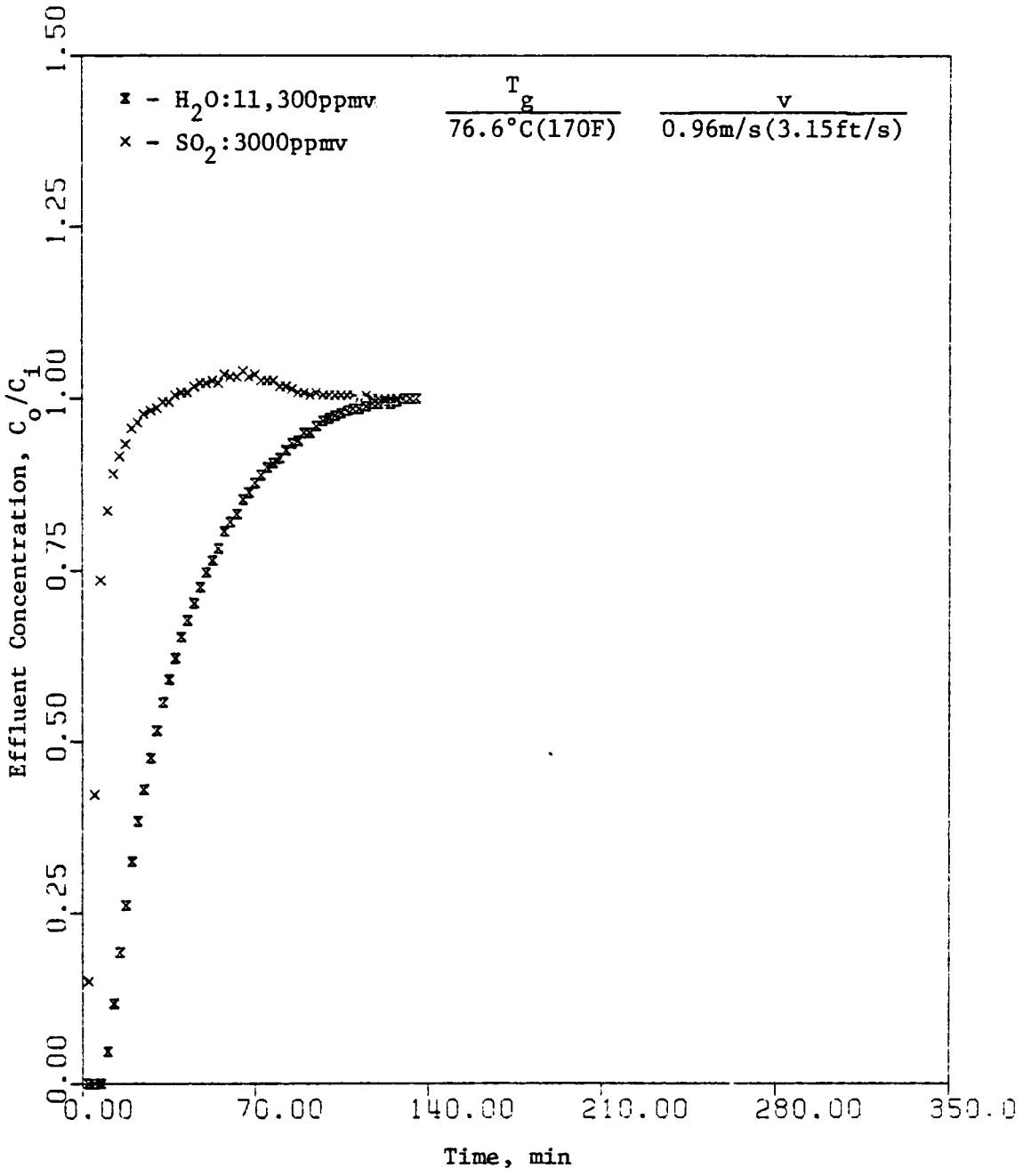

Figure 6.14 Binary Adsorption Performance of SO_2 and Water Vapor on AW500 Molecular Sieve—High Water Vapor Content.

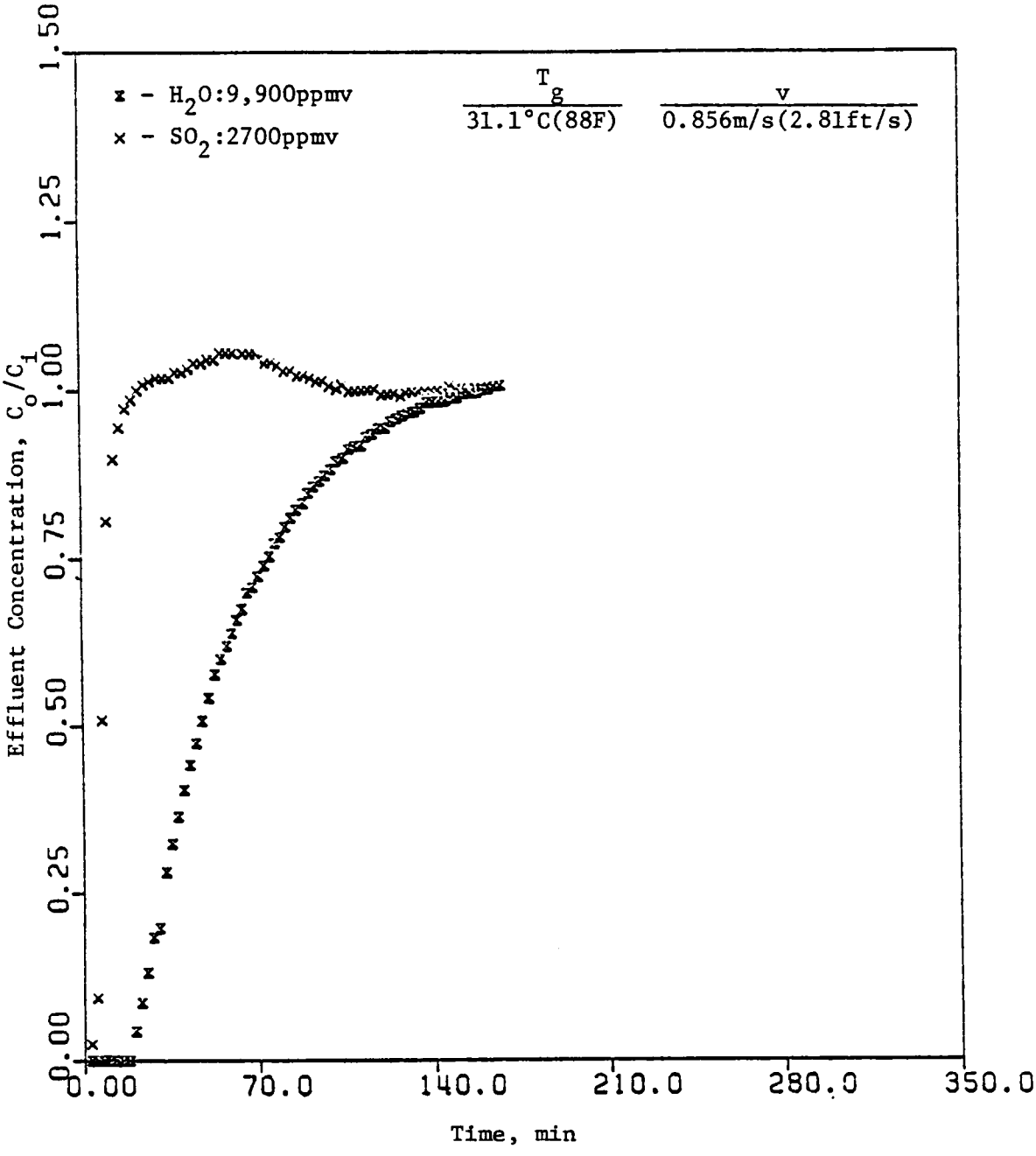

Figure 6.15 Binary Adsorption Performance on AW500 Molecular Sieve--High Water Vapor Content.

of SO_2 was adsorbed compared to 4.18g/100g adsorbent for the water vapor free test. SO_2 desorption was 28 percent for a water vapor concentration of 11,300 ppmv.

Figures 6.16 and 6.17 show the results for tests performed on silica gel. SO_2 adsorption was significantly reduced by water vapor co-adsorption as is shown in Fig. 6.16. SO_2 adsorption was 0.02g/100g adsorbent and water vapor adsorption was 0.0026 m^3 (0.08 ft^3). A measure of separation capability of silica gel is given by the time at one-half the effluent concentration. SO_2 breakthrough time was 1.75 min and water vapor breakthrough time was 37 min.

The results for both water vapor free and variable water vapor concentration tests are summarized in Table 6.4. The significance of these results are:

1) breakthrough curves for simultaneous SO_2 and water vapor adsorption on 13X and AW500 molecular sieves and silica gel have been measured;
2) water vapor adsorption reduced SO_2 adsorption and consequently breakthrough time;
3) the greatest selectivity for SO_2 in the SO_2-water vapor tests occurred in the following order 13X > AW500 > silica gel;
4) as inlet water vapor concentration increased, the effluent SO_2 concentration profile was sharpened.

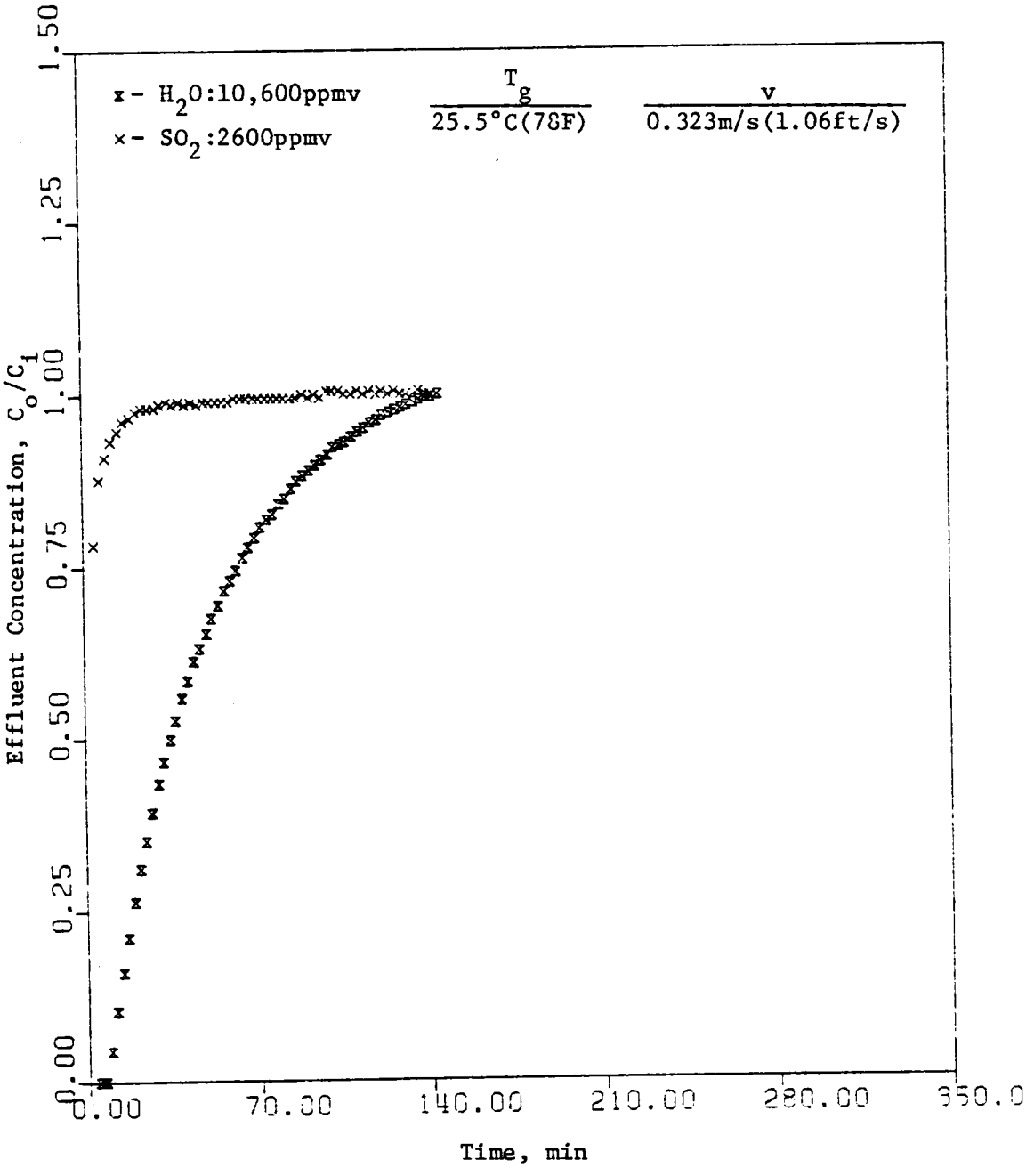

Figure 6.16 Binary Adsorption Performance of SO_2 and Water Vapor on Silica Gel--High Water Vapor Content.

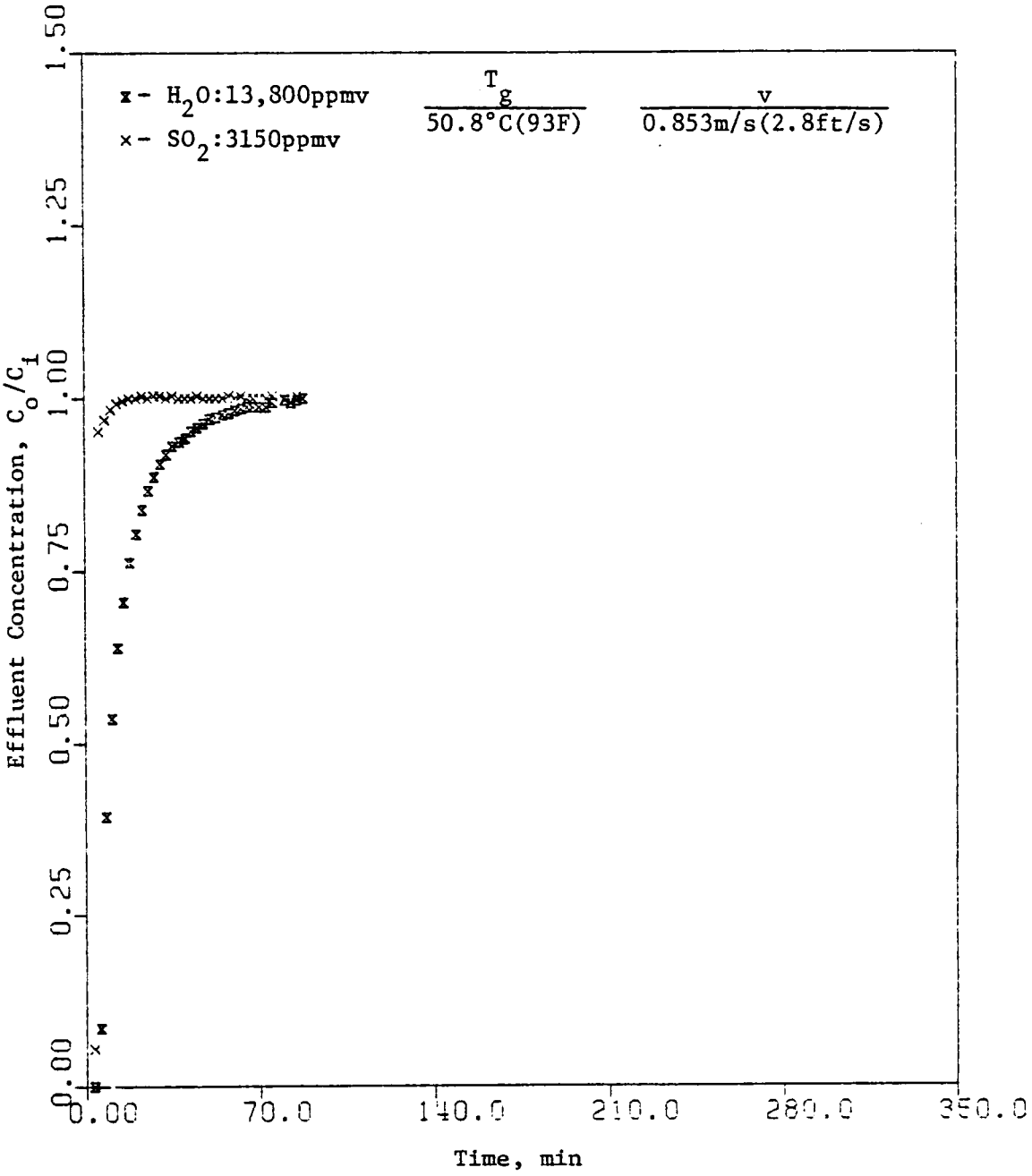

Figure 6.17 Binary Adsorption Performance of SO_2 and Water Vapor on Silica Gel--High Water Vapor Content.

5) a correlation was obtained that can be used to predict SO_2 breakthrough times in types 13X and AW500 molecular sieves.

6.3 Adsorption Performance for Activated Charcoal and Montmorillinite

A comparison between the relative adsorption performances of molecular sieves to activated charcoal would be useful in determining the possible implementation of molecular sieves in combustion gas desulfurization processes. Therefore tests were performed to obtain SO_2 breakthrough curve data for activated charcoal under the conditions used to test the molecular sieves. Activated charcoal serves as an important comparison material because large scale processes utilizing this material presently are being evaluated.

The results for SO_2 adsorption on 3-8 mesh activated charcoal are depicted in Fig. 6.16. Also breakthrough curves for SO_2 adsorption on types 13X and AW500 molecular sieves are shown. The effluent SO_2 breakthrough curve on activated charcoal was characterized by a relatively sharp front compared to the molecular sieves. The tests represent SO_2 removal based on equivalent adsorbent weights. The measured breakthrough times at half-maximum of the effluent concentration were

Adsorbent	Breakthrough Time, min
13X Molecular Sieve	134
AW500 Molecular Sieve	62
Activated Charcoal	26.6
Silica Gel	4

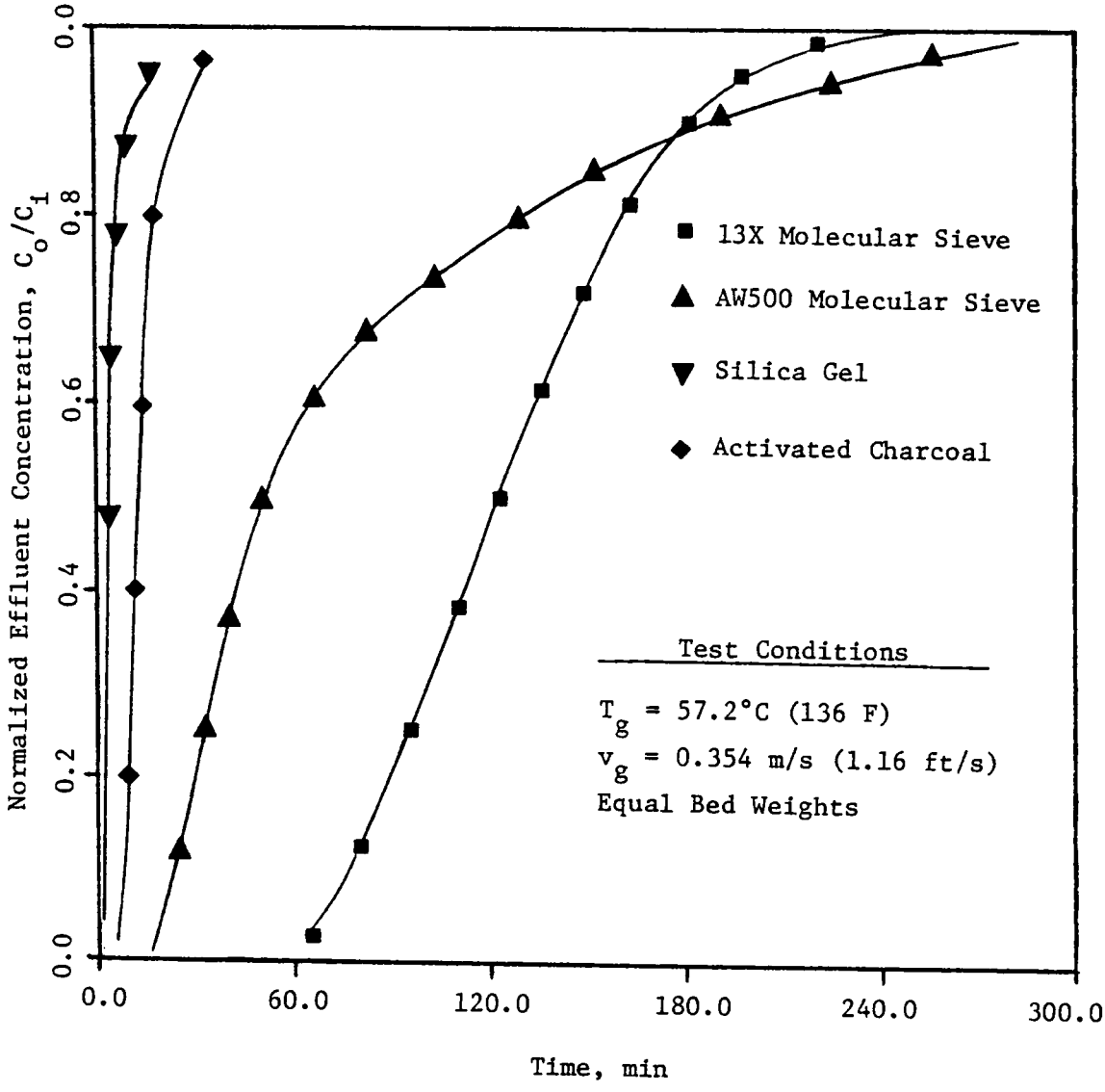

Figure 6.18 Comparison of SO_2 Breakthrough Curves for Activated Charcoal and Synthetic Molecular Sieve Zeolites.

Thus, for equal bed weights, the type 13X molecular sieve has roughly 5 times the SO_2 adsorption capacity of activated charcoal.

Water vapor reduces the breakthrough time for SO_2 since SO_2 adsorption is reduced because the adsorption 'sites' have a greater affinity for SO_2 and adsorbent temperature is increased by high adsorbate loadings. The effect of inlet water on SO_2 breakthrough time is presented in Appendix E. For both type 13X and AW500 molecular sieves breakthrough time was inversely proportional to the inlet water vapor concentration.

VII. MEASUREMENT OF ADSORPTION EQUILIBRIUM PARAMETERS

The design of a large scale SO_2 adsorber system will require the ability to predict how various design parameters affect performance Therefore, a general theoretical description of the adsorption process is necessary to describe the adsorption of SO_2 and the related transport processes.

7.1 Theoretical Description of Adiabatic Fixed Bed Adsorption

The subject of adiabatic adsorption has received considerable attention by several investigators. Numerous analytical and numerical results have been proposed to describe the effluent composition profile from a fixed bed adsorber.

Acrivos [61] used the method of characteristics to solve several heat and mass transfer problems that could be described by hyperbolic differential equations. Bullock et al. [62] investigated the adiabatic adsorption of water vapor on silica gel. Rachinskii [63] describes several solutions to isothermal adsorption for both linear and nonlinear equilibrium relationships. The main difficulty in applying the previous investigators results to the present study is that most are limited to a linear adsorption isotherm and not simultaneous, multicomponent adsorption.

The primary goal here is to obtain an expression to predict the gaseous concentration distribution throughout the adsorption bed as a function of elapsed time. Since the predictive capability will depend on the proper identification of significant controlling effects, a complete documentation of observations during data acquisition was

necessary to ensure the validity of assumptions made in the problem formulation. One aspect of fixed bed adsorption that has not received attention is the effect of the velocity profile distribution at the packed bed exit. To ensure proper gas flow distribution through the packed bed several measurements were made of the gas velocity at the bed exit. Figure 7.1 depicts a representative velocity profile for a packed bed with 0.3175cm (1/8in.) 13X molecular sieve pellets. As expected the velocity near the wall was greater than the velocity near the center of the column. In fact, the velocity near the wall was approximately twice the centerline velocity. The net effect of this with respect to SO_2 removal is that adsorbent pellets located around the circumference of the bed will become saturated before the rest of the bed. Consequently, the width of the SO_2 effluent breakthrough curve will increase. To account for this behavior the adsorbent bed was considered to consist of two regions of different porosity as shown in Fig. 7.2. If the thermal and mass transport across this interface are neglected then the problem may now be considered as the formulation of two 1-dimensional adsorption problems.

Applying a material balance on the adsorbate

$$\varepsilon\rho_g v\frac{\partial c}{\partial x} + (1 - \varepsilon)\rho_s\left(\frac{\partial q}{\partial t}\right) + \varepsilon\rho_g\frac{\partial c}{\partial t} = \mathcal{D}\varepsilon\frac{\partial^2 c}{\partial x^2} \qquad (7.1)$$

For Reynolds number (based on particle diameter) greater than 2, axial dispersion may be neglected [64]. Equation 7.1 may be written

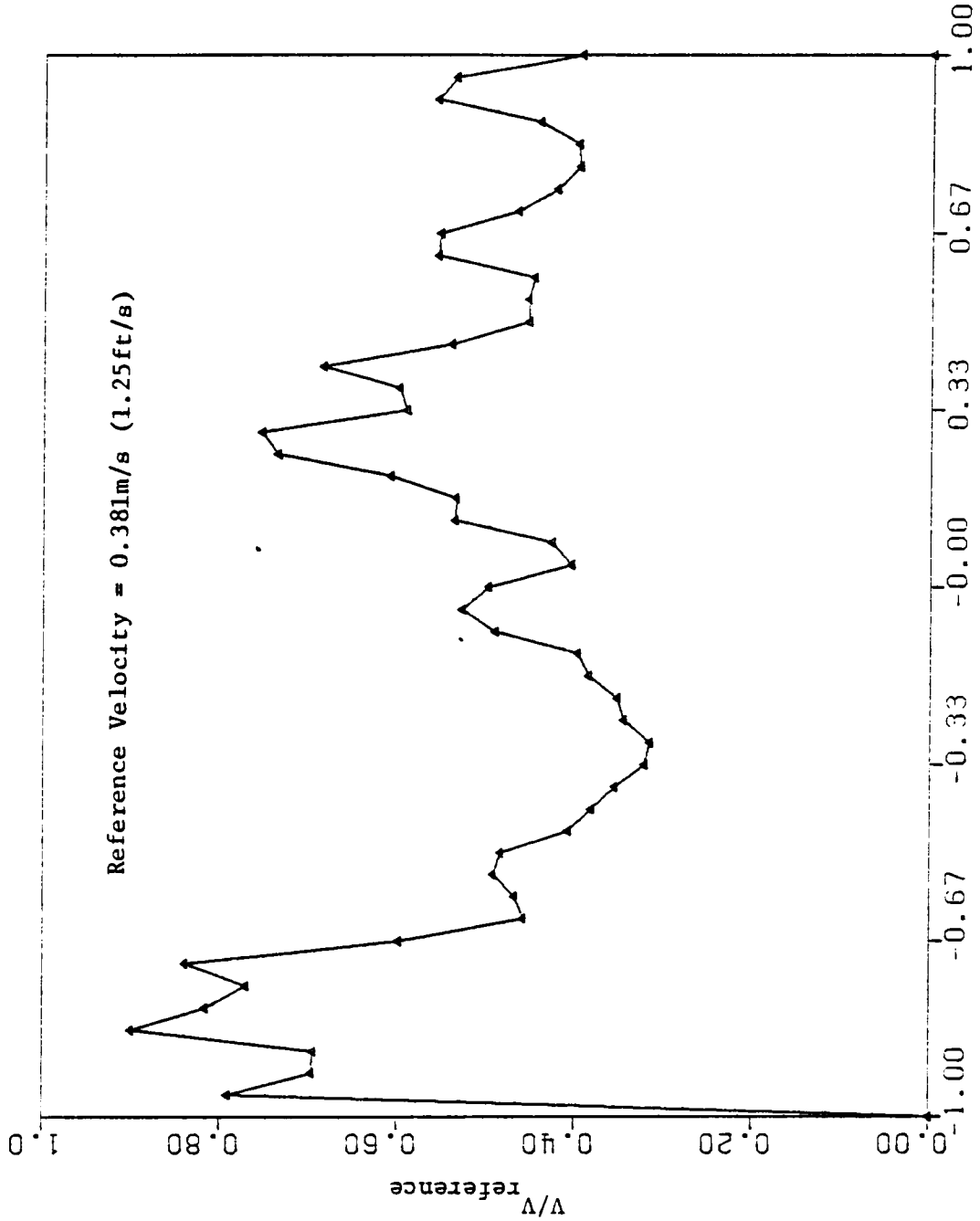

Figure 7.1 Representative Exit Velocity Profile from Fixed Bed Adsorption Column.

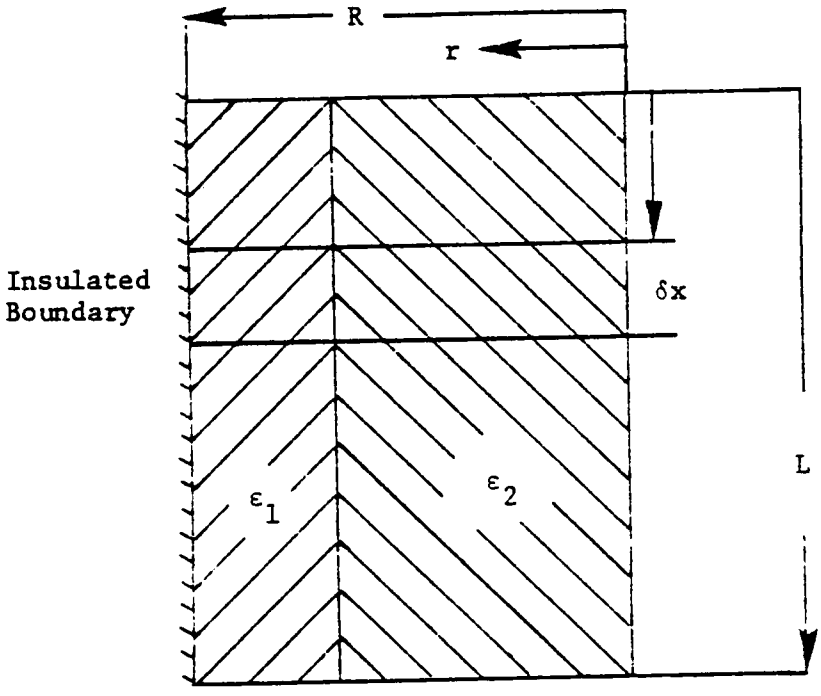

Two Porosity Region Representation of
Fixed Bed Adsorber

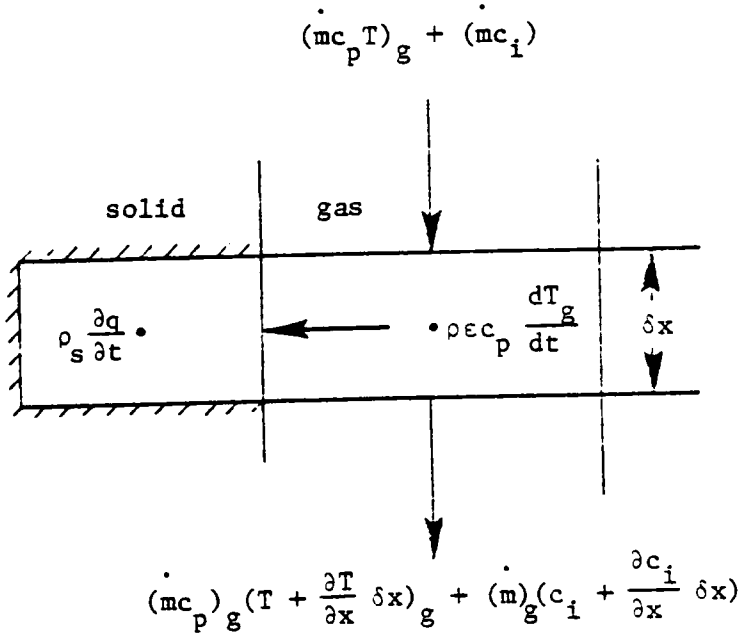

Adsorbate Material Balance

Figure 7.2 Configuration Depicting Adsorbate Material Balance and Energy Balance for Gaseous Heat Transfer.

$$v\frac{\partial c}{\partial x} + \frac{(1 - \varepsilon)}{\varepsilon}\frac{\rho s}{\rho g}\frac{\partial q}{\partial t} + \frac{\partial c}{\partial t} = 0 \qquad (7.2)$$

If the rate of mass transfer is represented by a linear function of the overall driving force, then a mass balance for the adsorbent yields

$$\frac{\partial q}{\partial t} = \frac{K_m a}{\rho_s}(q^* - q) \qquad (7.3)$$

The mass transfer was considered to have been solid-side controlling based on the breakthrough curve data obtained in Chapter 6.

To obtain the temperature distribution throughout the bed an energy balance was performed on a differential element. The gas-side energy equation for the packed bed is

$$k_g\varepsilon\frac{\partial^2 T_g}{\partial x^2} + h_g a(T_s - T_g) = \rho_g c_p \varepsilon\frac{\partial T_g}{\partial t} + \rho_g c_p \varepsilon v\frac{\partial T_g}{\partial x} \qquad (7.4)$$

The solid-side energy equation is

$$k_s(1 - \varepsilon)\frac{\partial^2 T_s}{\partial x^2} + h_g a(T_g - T_s) + u''' = \rho_s c_{p_s}(1 - \varepsilon)\frac{\partial T_s}{\partial t} \qquad (7.5)$$

where the volumetric heat generation term, u''', is related to the heat of adsorption. For packed beds, the effective thermal conductivity of the packing material is small (<10 percent) compared to the convective contribution [65]. Therefore, equations 7.4 and 7.5 may be combined to give

$$u''' + K_g\varepsilon\frac{\partial^2 T_g}{\partial x^2} = \rho c_p v\frac{\partial T_g}{\partial x} + \rho_g c_p \varepsilon\frac{\partial T_g}{\partial x} + \rho_s c_{p_s}(1 - \varepsilon)\frac{\partial T_s}{\partial t} \qquad (7.6)$$

Applying an energy balance around the adsorbent

$$\rho_s c_{p_s}(1 - \varepsilon)\frac{\partial T_s}{\partial t} = [\rho_s(1 - \varepsilon)\frac{\partial q}{\partial t}]\Delta H - h_g a(T_s - T_g) \qquad (7.7)$$

where ΔH is the heat of adsorption.

The equations describing adsorption and heat transfer in a packed bed may be written as

$$v\frac{\partial c}{\partial x} + \frac{(1 - \varepsilon)}{\varepsilon}\frac{\rho s}{\rho g}\frac{\partial q}{\partial t} + \frac{\partial c}{\partial t} = 0 \qquad (7.8)$$

$$v\frac{\partial T_g}{\partial x} + \frac{\partial T_g}{\partial t} + \frac{h_g a}{\rho_g c_p \varepsilon}(T_g - T_s) = 0 \qquad (7.9)$$

$$\frac{\partial q}{\partial t} = \frac{K_m a}{\rho_s}(q^* - q) \qquad (7.10)$$

$$\frac{\partial T_s}{\partial t} = \frac{1}{c_{ps}}\left[\frac{\partial q}{\partial t}\right]\Delta H - \frac{h_g a}{\rho_s c_{ps}(1 - \varepsilon)}(T_s - T_g) \qquad (7.11)$$

where q^* represents the equilibrium solid-phase concentration based on the adsorbate concentration, c.

Equations 7.8-7.11 comprise a set of coupled differential equations which are linear as written but will become nonlinear when q* is written to represent nonlinear equilibrium behavior.

Boundary conditions for equations 7.8-7.11 are based on subjecting the bed to a step change in inlet adsorbate concentration. The boundary conditions are

$$q(x,0),\ c(x,0) = 0 \qquad 0 < x \leq L \tag{7.12}$$

$$c(0,t) = 1.0 \qquad t \geq 0 \tag{7.13}$$

$$T_g(x,0),\ T_s(x,0) = T \qquad 0 < x \leq L \tag{7.14}$$

$$T_g(0,t) = T_{g_i} \tag{7.15}$$

$$\left.\frac{\partial T}{\partial x}\right|_{x = L} = 0 \qquad t \geq 0 \tag{7.16}$$

For the adsorption of SO_2 on molecular sieves three unknowns prevent solution of the equations above. The equilibrium relationship and the heat of adsorption must be known before the equations can be solved. Once these relationships are known, the mass transfer coefficient may be varied until convergence with experimental data is obtained.

Therefore, additional investigations were required to obtain the equilibrium adsorbate relationship and the heat of adsorption.

7.2 Measurement of SO_2 Adsorption Equilibria

Knowledge of adsorption equilibria is useful in evaluation of the adsorbate loading capacity and also for estimating adsorption column behavior. As discussed in Chapter 2, the isotherm shape serves as an indication of the effluent concentration profile shape.

Numerous theories and equations describing adsorption equilibrium for pure and multicomponent systems exist in the literature however many of these relationships lack sufficient rigor to be applicable for certain gas adsorption problems. Of interest with respect to this investigation was the adsorption of SO_2 on synthetic molecular sieves zeolites. While these relationships aid in the correlation of measured data little insight into the physical and thermodynamic properties of the adsorbate and adsorbent can be obtained.

Of the several relationships to describe adsorption Langmuir's expression [66]

$$q = \frac{q_m Kc}{(1 + Kc)} \tag{7.17}$$

where q = solid phase concentration

q_m = asymptotic solid phase concentration

K = isotherm constant

c = adsorbate concentration

is probably the most well known. This expression was obtained by assuming that molecules were adsorbed at definite points on the surface of the adsorbent and that surface coverage did not proceed beyond monolayer coverage. Also, no interaction between adsorbed molecules was assumed.

The Langmuir equation has been found to correlate a wide variety of adsorption isotherm data--even for cases that violate the assumptions for which the equation was derived. Acceptance has largely been based on the fact that it has been successful in describing many adsorption isotherms.

Since the correlation of both pure and multicomponent data would be necessary the isotherm expression should be chosen accordingly. Several empirical and thermodynamic expressions have been developed but selection of the isotherm expression should be based on the particular adsorbate-adsorbent system.

Molecular sieves possess strong attractive forces for polar molecules (SO_2, H_2O, etc.) thereby necessitating the need for a suitable isotherm expression. For this reason adsorption of SO_2 on molecular sieves could not be correlated with existing expressions.

Joubert [67] considered the binary adsorption of SO_2 and CO_2 on H-mordinite. Several expressions for correlating binary adsorption data were considered. No one expression was found to be entirely applicable though the total amount adsorbed was predicted by the Ideal Solution Theory of Myers and Prausnitz [68].

Most of the existing theories and isotherm expressions are not able to fully represent adsorption on molecular sieves. Several theories may be neglected based on the fact that adsorption on molecular sieves is limited by the volume of the intracrystalline structure. Thus, molecular sieve adsorbents are characterized by a maximum attainable adsorbate loading that cannot be correlated by unbounded isotherms such as the Freundlich isotherm,

$$N = KP^{1/n} \tag{7.18}$$

the infinite layer BET (Brunaer, Emmett, Teller)

$$\frac{N}{N_m} = \frac{K_\chi[1 - (L - 1)\chi^L + L\chi^{L+2}]}{(1 - \chi)[1 - (1 - k)\chi - k_{\chi L + 1}]} \tag{7.19}$$

where $\chi \equiv P/P_o$

and the modified Langmuir expression of Peterson and Redlich

$$N = KP/(1 + KP^{1/n}) \tag{7.20}$$

Therefore an expression was desired that would correlate the data and also be capable of extension to multicomponent systems. The basic Langmuir relationship has been rederived for several less stringent assumptions as noted by Yon and Turnock [69]. Even Langmuir suggested that the equation be modified. Thus the expression

$$\frac{q}{q_m} = \frac{Kp^{1/n}}{(1 + Kp^{1/n})} \tag{7.21}$$

where $K = Aexp^{E/RT}$ (7.22)

was used to correlate SO_2 adsorption on types 13X and AW500 molecular sieve. This expression is similar to the relationship used by Yon and Turnock for correlating adsorption of nitrogen and methane on molecular sieves [68].

The adsorption isotherm data was obtained by measuring the weight gains of type 13X and AW500 molecular sieves on exposure to known concentrations of SO_2-nitrogen mixtures. Nitrogen adsorption was found to be negligible for the range of temperatures and pressures used in this investigation. Also adsorption of nitrogen would not be expected to affect SO_2 adsorption appreciably because adsorption of the polar SO_2 molecule is favored. After exposure of the adsorbents to known SO_2 mixtures, the adsorption flask was then weighted on an electronic balance and the adsorbent weight gain recorded. At least three replications of each data were performed to assure consistency.

Figures 7.3-4 depict the measured adsorption isotherms for type 13X and AW500 molecular sieves. The success in the application of equation 7.21 is demonstrated by the correlation between data for different adsorbate pressures and temperatures. Since the adsorption equilibria may now be suitably represented, the isosteric heat of adsorption can be determined.

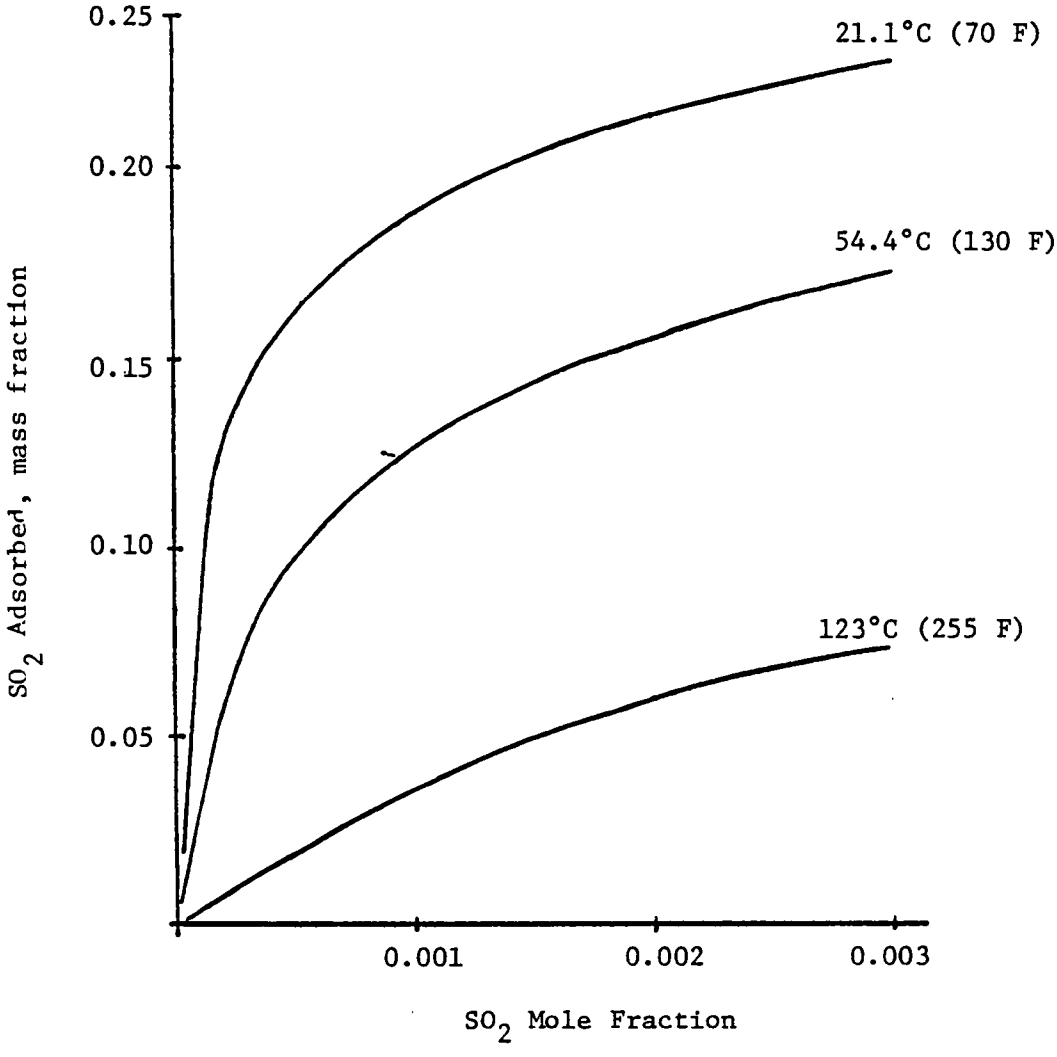

Figure 7.3 SO_2 Adsorption Isotherm for Type 13X Molecular Sieve.

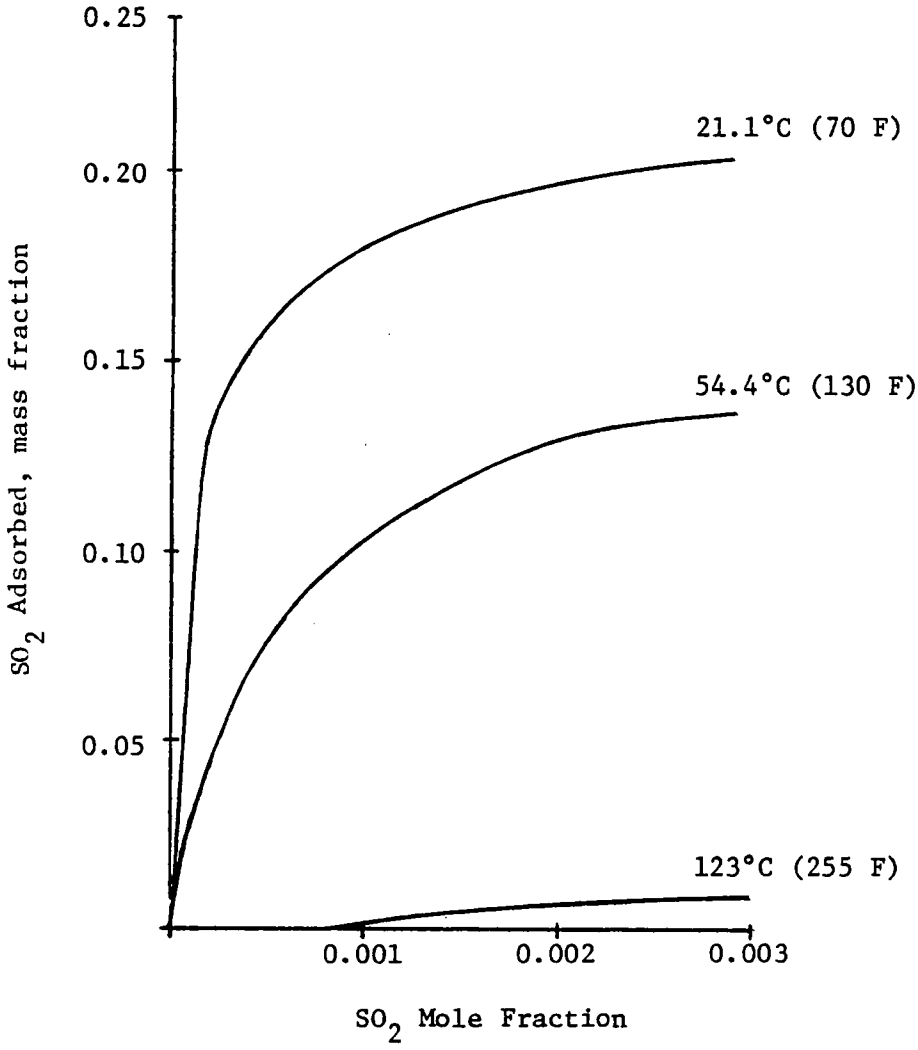

Figure 7.4 SO_2 Adsorption Isotherm for Type AW500 Molecular Sieve.

7.3 Determination of SO_2 Heat of Adsorption

As adsorption occurs heat is released in an amount that can be related to the adsorbate gas pressure and temperature by the relationship

$$q_{st} = -R \left[\frac{\partial \ln P}{\partial 1/T}\right]_{\theta} \tag{7.23}$$

The heat released, q_{st}, is termed the 'isosteric heat' of adsorption because equation 7.23 involves the temperature dependence of the equilibrium pressure for constant coverage, θ. The isosteric heat may be derived by applying a thermodynamic description of the adsorption process. Rewritting equation 7.23 in terms of an equivalent form of the Clausius-Clapeyron equation

$$\left.\frac{\partial \ln P}{\partial T}\right|_{\theta} = \frac{S_G - \bar{S}_s}{RT} = \frac{h_G - \bar{h}_s}{RT^2} = \frac{q_{st}}{RT^2} \tag{7.24}$$

where S_G = molar entropy

$\bar{S}_s$ = partial molar entropy of bound adsorbate

h_G = molar enthalpy

$\bar{h}_s$ = partial molar enthalpy of bound adsorbate

For small temperature variations, q_{st} does not vary significantly, hence offers a 'check' of measured isotherm data.

The isosteric heat of adsorption was determined for both type 13X and AW500 molecular sieves by substituting the appropriate

isotherm expression into equation 7.23. For the isotherm model used, the asymptotic SO_2 loading could adequately be expressed as a function of adsorbate temperature by the relationship

$$q_m = A_1 + A_2T \tag{7.25}$$

Using the definition of the isotherm exponent given by Yon and Turnock [69]

$$n = A_3 + A_4/T \tag{7.26}$$

Substituting the general isotherm expression

$$q = \frac{(A_1 + A_2T)K[(c)^{1/(A_3 + A_4/T)}]}{[1 + K[(c)^{1/(A_3 + A_4/T)}]]}$$

into equation 7.23 and performing the indicated operation, the isosteric heat can be written in the form

$$\frac{-q_{st}}{R} = n\left[\frac{1}{\frac{q_m}{q} - 1}\right]\frac{A_2}{q}\left[\frac{1}{T^2}\right] + A_4 \ln\left[\frac{1}{\frac{q_m}{Kq} - K}\right] \tag{7.27}$$

The calculated isosteric heat values are presented in Table 7.1. The results for both type 13X and AW500 varied with adsorbate loading

Table 7.1 Calculated Isosteric Heats of Adsorption

Adsorbent	SO_2 Adsorbed mass fraction	Temperature °C	(F)	Isosteric Heat Kg-cal/Kg	(Btu/lbm)
13X	0.02	18	(65)	204	(367.2)
Molecular	0.02	110	(230)	197.2	(354.9)
Sieve	0.1	18	(65)	142.8	(257.)
	0.1	110	(230)	133.1	(239.6)
	0.2	18	(65)	101.4	(182.6)
	0.2	110	(230)	80.8	(145.4)
AW500	0.02	18	(65)	345.7	(622.3)
Molecular	0.02	93	(200)	331.8	(597.2)
Sieve	0.1	18	(65)	241.2	(434.1)
	0.1	93	(200)	217.3	(391.1)
	0.2	18	(65)	147.6	(265.6)
	0.2	93	(200)	--	--

Polynomial Representation of Isosteric Heats

$$-\Delta H_{13X} = [367.79 - 912.42q] + [-0.06171 - 0.61971q + 4.95388q^2]T$$

$$-\Delta H_{AW500} = [684.82 - 3196.2q + 8572.6q^2] + [1/(-5.9639 + 27.5735q)]T$$

ΔH = isosteric heat, Btu/lbm

T = equilibrium temperature, F

q = adsorbate loading, mass fraction

Adsorption Isotherm Constants

Adsorbent	n	K	q_m
13X	-1.3952 + 1853.5/T	39.5	0.5059 - 0.0003514(T)
AW500	-3.473 + 2970.5/T	75.6	0.4586 - 0.0004025(T)

T = equilibrium temperature, R

and adsorbate gas temperature. As loading increased, the isosteric heat of adsorption decreased. For constant coverage, both molecular sieves were characterized by an approximate 20 percent decrease in isosteric heat as adsorbate temperature was increased. The consistency of isosteric heat data further supports the validity of the isotherm expression.

VIII. ADSORBENT REGENERATION

The success of an adsorption process for flue gas desulfurization will not only depend on the adsorption loading capacity of the adsorbent but also the degree of desorption that can be obtained. This could pose a severe problem in the utilization of synthetic zeolite molecular sieves for desulfurization since replacement materials are relatively expensive and therefore regeneration would be necessary.

Recalling Chapter 3, Martin and Brantley [32] found that the adsorption capacity of type 13X molecular sieves for SO_2 decreased by 57 percent after only two regenerations. The AW500 molecular sieves were found to decrease in adsorption capacity by 40 percent. Tamboli [33] found that in a one-normal solution of sulfuric acid the SO_2 sorption capacity of type 13X molecular sieve was completely destroyed. The significance of these results is that under the SO_2 and water vapor exposures that would occur in an actual application adsorbent degradation would be of importance. Because of the necessity for a regenerable adsorbent, it was deemed necessary to study the regeneration process in more detail to provide additional information for the regeneration scheme. Since the tests of Tamboli were considered too harsh and unrealistic and the regeneration studies of Martin and Brantley were based on using a single maximum regeneration temperature of 375°C (707 F), results for desorption characteristics were desired for conditions that would more closely represent those of actual use.

8.1 Equilibrium Adsorption Capacity and Regenerability

Because of the importance of adsorbent regeneration, it was decided that a pure component test using the adsorbate gas only would be a valid basis for evaluating the adsorption-desorption behavior because

1) effects (such as catalysis) due to other gases would be avoided;
2) interactions with other adsorbed gases, such as water, could be qualitatively evaluated;
3) interactions between adsorbate and the adsorbent could be identified.

The apparatus used to obtain the regeneration and ultimate adsorption capacity data is shown in Fig. 8.1. The apparatus consisted of an adsorption flask, purge gas and SO_2 gas cylinders, and a timer-actuator controlled furnace used for thermally cycling the adsorbents. Gas flowrate was controlled by adjusting the pressure regulator for that cylinder. All gases were vented first through a bubble flowmeter and then the atmosphere. The sampling line from the gas chromatograph was used to establish gas mixtures for low adsorbate concentration tests.

The results for the ultimate adsorption tests are summarized in Table 8.1. Activated charcoal had the highest capacity, 51.4 weight percent for SO_2 followed by Davison Silica Gel. Montmorillinite exhibited the lowest capacity, 4.4 percent by weight, for SO_2 adsorption. It is interesting to note that silica gel had a high

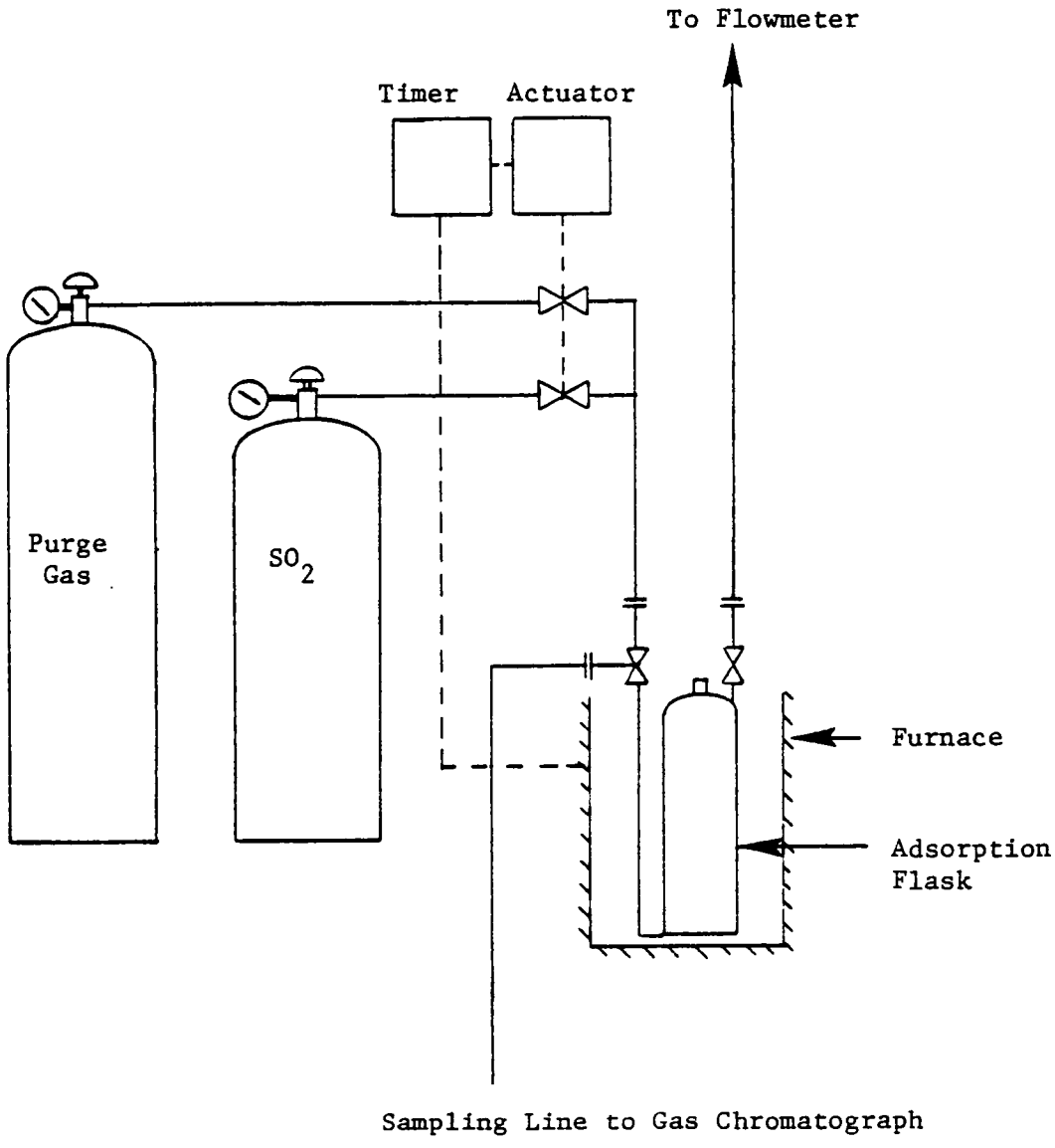

Figure 8.1. Regeneration Apparatus.

Table 8.1 Summary of Measured SO_2 Equilibrium Adsorption Capacities

Adsorbent	Manufacturer	Lot No.	Test Gas Temperature °C	(F)	SO_2 Adsorbed weight percent
13X Molecular Sieve	Linde	13945477003	24	(76)	31.6±0.09
		13945450038	26	(78)	31.6±0.07
			71.1	(160)	29.05±0.12
			87.7	(190)	27.6±0.16
			113	(235)	26.11±0.11
AW500 Molecular Sieve	Linde	5943556040	26	(78)	24.17±0.12
			71.1	(160)	20.53±0.09
			87.7	(190)	19.13±0.121
			11.3	(235)	17.18±0.1
Silica Gel	Davison	Gr-01-08-05-215	26	(78)	33.7±0.28
Activated Charcoal	Fisher	5-685B	26	(79)	51.4±0.7
Montmorillinite*			26	(79)	4.4±0.8

*ore obtained from Paris, Tennessee

adsorption capacity in a 100 percent SO_2 atmosphere but the dynamic testing performed in Chapter 6 showed that it had the least capacity in a low adsorbate concentration flow. As expected, the ultimate adsorption capacities for types 13X and AW500 decreased as adsorbent temperature increased.

The next series of tests were performed to obtain regeneration results and compare these to the data of Martin and Brantley. The procedure was to first saturate the adsorbents under isothermal conditions. The adsorption flask was then weighed and the SO_2 adsorbed determined. Next, a flow of dry purge gas (Nitrogen) was then used to purge the flask while the flask was heated. The flask was then weighted to determine the residual weight gain or loss. The results for the regeneration tests on Linde type 13X and AW500 molecular sieves are presented in Table 8.2. Table 8.2 shows that, unlike the results of Martin and Brantley, only a 24.6 percent decrease in adsorption capacity was noted. In tests performed at various temperatures it was found that at low regeneration temperatures 148°C (300 F), the adsorbate was not completely desorbed. At higher temperatures and very low purge gas flowrates the 13X pellets were observed to change to a pale yellow color. This would indicate possible reduction with formation of a sulfur based compound. Thus, it can be argued that Martin and Brantley possibly caused a reaction to occur that led to reduced SO_2 loadings. Results for the type AW500 molecular sieves showed that the ultimate adsorption capacity decreased by 11.3 percent compared to approximately 40 percent obtained by Martin and Brantley.

Table 8.2 Summary of Molecular Sieve Regeneration Tests--SO_2 and N_2 Exposure

Adsorbent	Regeneration Cycle No.	SO_2 Adsorbed weight percent	Desorption percent of adsorption	Desorption Conditions
13X Molecular Sieve*	1	31.7±0.19	83.2±6.2	Purged with N_2 at 260°C (500°F) for 3 hours
	2	25.8±1.6	94.9±1.4	
	3	23.9±0.75		
AW500 Molecular Sieve**	1	24.25±0.11	94.76±0.15	Purged with N_2 at 260°C (500°F) for 3 hours
	2	22.99±0.09	96.7±0.19	
	3	21.5±0.46		

		Extrapolated Adsorbent Life SO_2 Adsorbed weight percent x 100	
		Martin & Brantley[1]	Wright[2]
13X Molecular Sieve	1	29.8	31.6
	2	19.9	25.8
	3	16.6	23.8
	5	14.1	22.3
	10	12.1	21.1
	20	11.1	20.6
AW500 Molecular Sieve	1	19.8	24.3
	2	16.9	22.9
	3	16.	21.5
	5	15.3	19.3
	10	14.7	15.4
	20	14.4	10.9

* Linde Lot No. 13945450038 0.3175 cm (1/8 in.) pellets
**Linde Lot No. 5943556040 0.3175 cm (1/8 in.) pellets
1 Regeneration Conditions: 375°C (707 F), N_2 purge
2 Regeneration Conditions: 260°C (500 F), N_2 purge

Water vapor adsorption in the presence of SO_2 is of extreme importance because both are present in the products of coal combustion and are readily adsorbed by molecular sieves and silica gel. The possibility then exist for a reaction between the adsorbed SO_2 and water vapor which subsequently could lead to a reaction between the adsorbed SO_2 and water vapor which subsequently could lead to a reaction with and possible destruction of the adsorbent. Therefore, additional regeneration tests were performed to determine the effect of the simultaneous adsorption of SO_2 and water vapor on adsorbent degradation. The next series of tests were performed by saturating the adsorbent with SO_2 and then passing a mixture of air and water vapor over the adsorbent. The purpose of this was to simulate the conditions that occurred during the dynamic adsorption tests and also determine the reduction in adsorption capacity. Table 8.3 shows the results obtained for regeneration tests performed on 13X and AW500 molecular sieves. The loss in adsorption capacity results obtained were similar to those obtained by Martin and Brantley for the first two regeneration cycles. Unlike the results obtained in their work, the SO_2 adsorption capacity was decreased by 37.3 percent but adsorption capacity was constant for subsequent loadings. Results obtained for the type AW500 molecular sieve did not compare with those of Martin and Brantley. Only a 8.7 percent decrease in SO_2 adsorption capacity was measured compared to 12.5 percent measured by Martin and Brantley.

It has been demonstrated that high regeneration temperatures [375°C (707 F)] and low regeneration temperatures are responsible for

Table 8.3 Regeneration of 13X and AW500 Molecular Sieves after Exposure to SO_2 and Moist Air

Adsorbent	Regeneration Cycle No.	SO_2 Adsorbed weight percent	SO_2 Desorbed percent of Adsorption	Desorption by water vapor percent of adsorption	Desorption Conditions
13X	1	31.6	87.9	27.2	adsorbent bed heated to 260°C (500 F) and purged with dry N_2 for three hours
	2	20.9	92.1	92.1	
	3	19.8	99.8	99.8	
AW500	1	24.2	84.8	37.26	
	2	22.1	94.8	42.93	
	3	18.1	90.1	40.1	
13X	1	31.3	--	--	adsorbent bed washed in distilled water (ratio of 100 ml to 1 gram) three times and regenerated at 260°C (500 F) with dry N_2 purge gas for three hours.
	2	13.2	--	--	
	3	10.1	--	--	
AW500	1	24.75	--	--	
	2	24.17	--	--	
	3	23.8	--	--	

Extrapolated Adsorbent Life

		SO_2 Adsorbed weight percent	SO_2 Adsorbed (water wash) weight percent
13X	5	18.1	4.71
	10	17.2	1.42
	20	16.7	0.0
AW500	5	16.8	22.89
	10	12.1	20.95
	20	7.8	17.9

decreased SO_2 adsorbent loadings after regeneration. For low adsorbate temperatures desorption is limited by the adsorption isotherm. At elevated temperatures the conditions for desorption are favorable but the chance for possible reactions and the extent of these reactions between adsorbed water and SO_2 and the zeolite could be enhanced. Figure 8.2 depicts the variation in SO_2 adsorption with regeneration cycle and regeneration conditions. All curves are characterized by a decrease in SO_2 loading after the first regeneration step followed by a gradual decrease in SO_2 adsorption capacity to a constant value. Exposure to dry Nitrogen and SO_2 atmospheres resulted in minimum adsorbent degradation. Exposure to water vapor-air-SO_2 mixtures increased adsorbent degradation by roughly 19 percent.

The results obtained in the previous section have shown the effect of several 'interfering' parameters on adsorbent regeneration but if the mechanism for adsorbent degradation could be ascertained, the process or adsorbent could be designed for minimum degradation. Thus the problem is to determine how the SO_2 molecule is bound to the adsorbent surface.

X-ray diffraction analysis is a method commonly used in crystallography to study the structure of crystalline materials. Tamboli [33] used x-ray diffraction to study the change in zeolite structure after exposure to SO_2. But even when exposed to acidic environments, adsorption may be diminished while x-ray diffraction patterns remain essentially unchanged [65]. Thus quantitative data concerning zeolite attack cannot be obtained. In view of this it was decided to use an

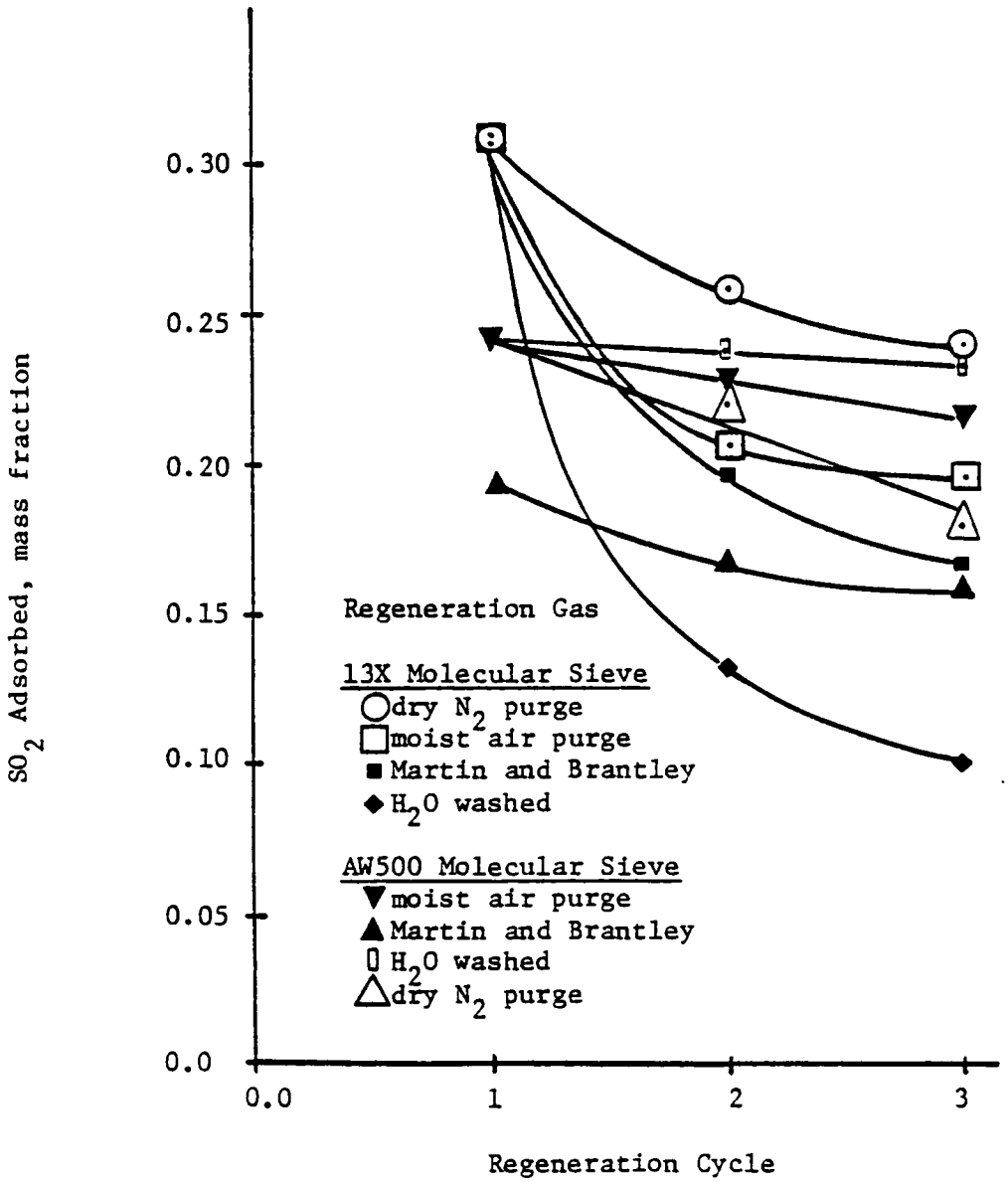

Figure 8.2 Variation of SO_2 Adsorption with Regeneration Cycle.

electron microprobe x-ray analyzer to determine how the SO_2 was distributed in the adsorbent pellets. The next section explains details of tests performed using the electron microprobe analyzer.

8.2 Electron Microprobe X-ray Analyzer Investigations

The electron microprobe x-ray analyzer is a device that permits quantitative and qualitative measurements of very small volumes (1-10 μm^3) to be obtained. The instrument is widely used to solve mineralogical, petrological, and geochemical problems. For this investigation the electron microprobe was desired because

1) Analysis of grains a few microns in diameter are possible. The effective volume analyzed may be only 1-10 μm^3;
2) The sample may be viewed during analysis which allows correlation between chemical composition and sample morphology;
3) Analysis can be considered non-destructive (no surface modifications);
4) By comparison with a suitable standard a large number of quantitative analysis are possible.

Operation of the microprobe requires focusing an electron beam on a flat surface and measuring the x-ray emission spectra produced. Because of interactions between high-energy electrons with atoms of elements present in the sample, a characteristic x-ray spectra of these elements is given off. Using x-ray spectrometers these

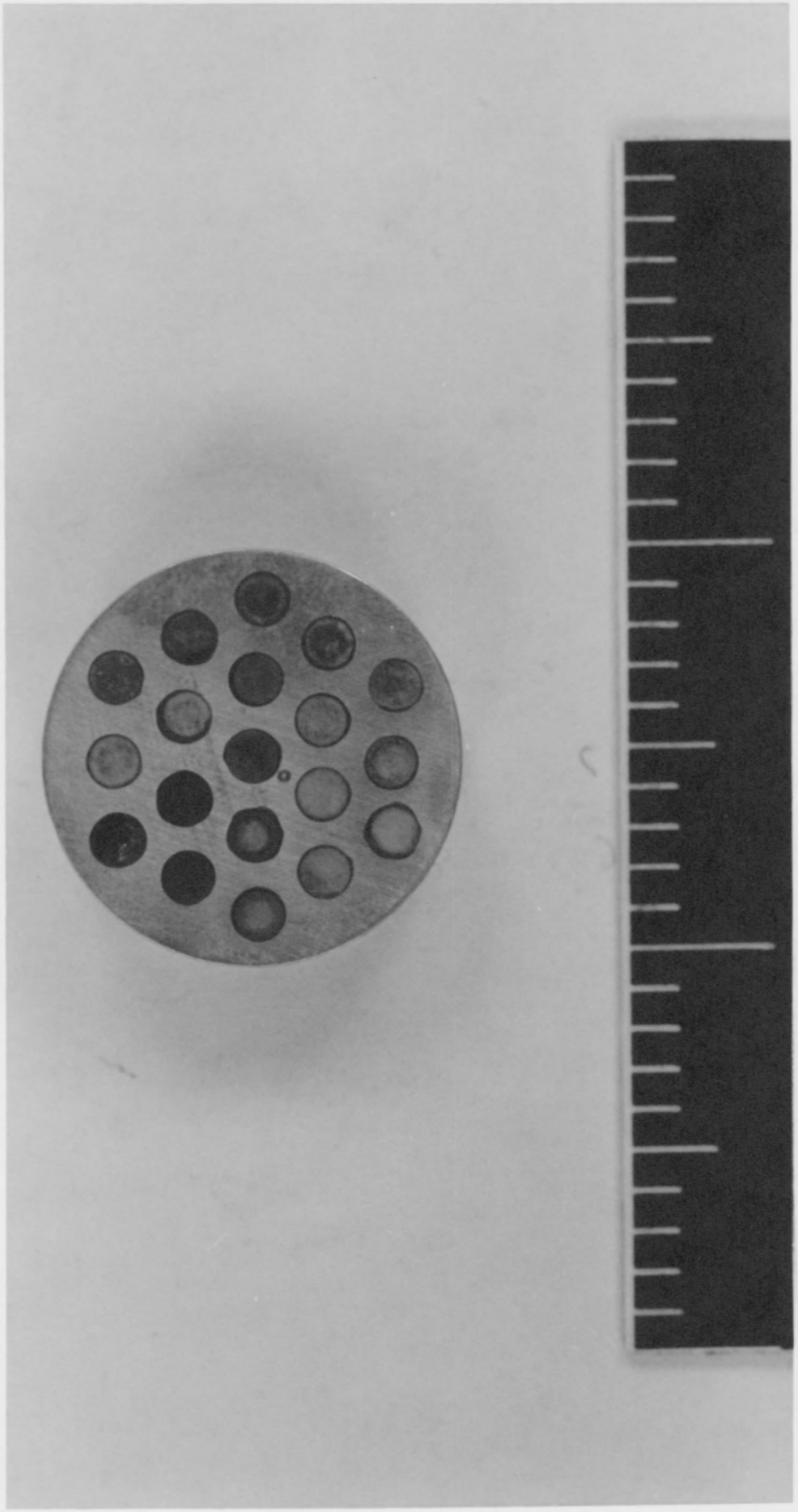

Figure 8.3 Photograph of Pellets Mounted in Aluminum Support.

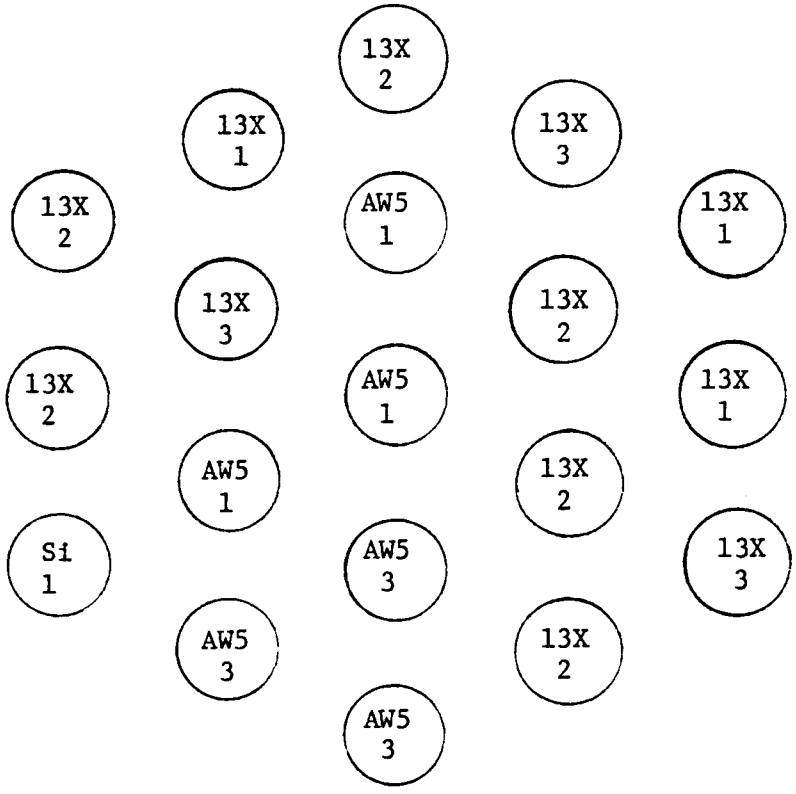

1 - as received
2 - exposure to SO_2 and water vapor
3 - exposure to H_2SO_4

Figure 8.4 Identification and Exposure Conditions of Mounted Molecular Sieve Samples.

spectra are then analyzed for wavelength and intensity. Quantitative analysis can be obtained by comparing the intensity reading with the intensity reading from a standard of known composition.

The first series of tests were performed to determine possible contamination caused by sample preparation. Samples were prepared by placing the adsorbent pellets into a cylindrical cap and imbedding one end in epoxy. The pellets were then sliced in half (radial cut) and carbon coated. Because of out-gassing, long periods of time were required before prepared samples could be analyzed. Coated samples were then placed in the microprobe and radial composition profiles were obtained. The effects of different surface preparations could then be determined by comparing radial composition profiles. Different methods of surface polishing were used to determine the effect of sample smearing and reduction in resolution. The best sample preparation was obtained by mounting the pellets in an aluminum support and embedding the pellet in epoxy. The surface to be studied was then successively polished with 600 grit silicon carbide. The pellets, mounted and ready for analysis, are depicted in Fig. 8.3. Figure 8.4 shows the identity of the pellets mounted in Fig. 8.3.

The purpose of the next series of tests was to determine how the residual SO_2 was distributed throughout the pellet. It would be expected that only the zeolite material itself could contribute to SO_2 retention. However certain materials (clays) can exhibit a weak attraction for polar molecules. Hence the need to determine the

sulfur distribution between the zeolite crystal and clay binder. In addition, residual sulfur distributions can give an insight into adsorbent utilization.

Figure 8.5 is a photograph of molecular sieve zeolites types AW500 and 13X. Notice that the 13X sieve is characterized by spherical particles that are approximately 2μm in diameter. The type AW500 structure suggest a non-uniform zeolite crystal distribution. Figure 8.4 demonstrates the success of the sample preparation technique since voids and distinct zeolite crystals are discernable.

Figure 8.6 shows the surface of a type 13X molecular sieve after exposure to SO_2 and thermal regeneration at 260°C (500 F). X-ray imaging was used to indicate residual sulfur. Figure 8.6 shows the same surface but images for Na were obtained (Na because 13X is Na based). Comparing Figs. 8.6 and 8.7 shows that for the 13X molecular sieve, the zeolite was uniformly distributed and the SO_2 appears bound with the zeolite.

Figure 8.8 shows the surface of a type AW500 molecular sieve after exposure to SO_2 and thermal regeneration at 260°C (500 F). Also shown is the x-ray image of the residual sulfur on the surface. Note that regions of high sulfur concentration were not as uniformly distributed as it was with the type 13X molecular sieve. Figure 8.9 shows similar results except for calcium. By comparing Figs. 8.8 and 8.9 there is a correlation between residual sulfur and calcium which was expected for a calcium based zeolite. Figure 8.9 shows an x-ray

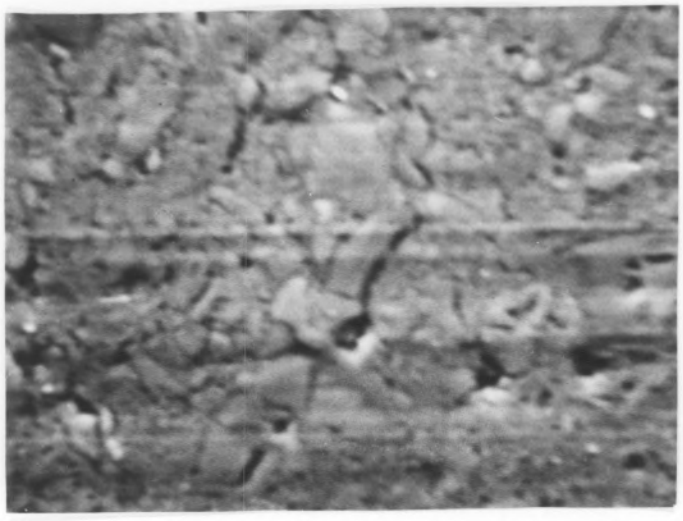

Type AW500 Molecular Sieve Surface (10.5μm/cm)

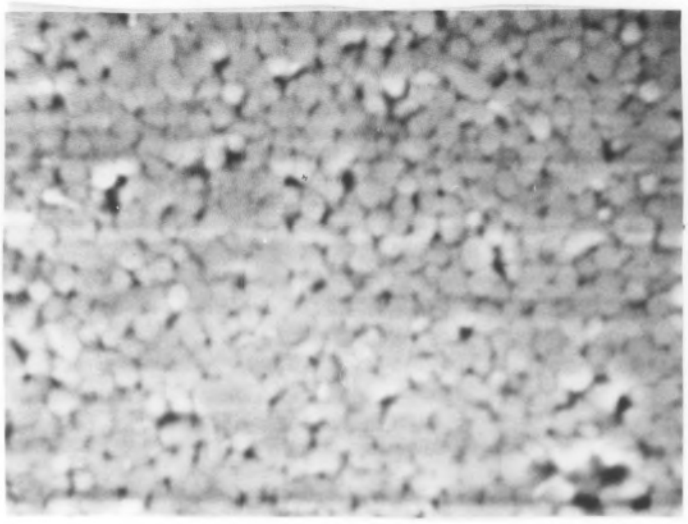

Type 13X Molecular Sieve Surface (11.2μm/cm)

Figure 8.5 Photograph of Type 13X and AW500 Molecular Sieve Surfaces.

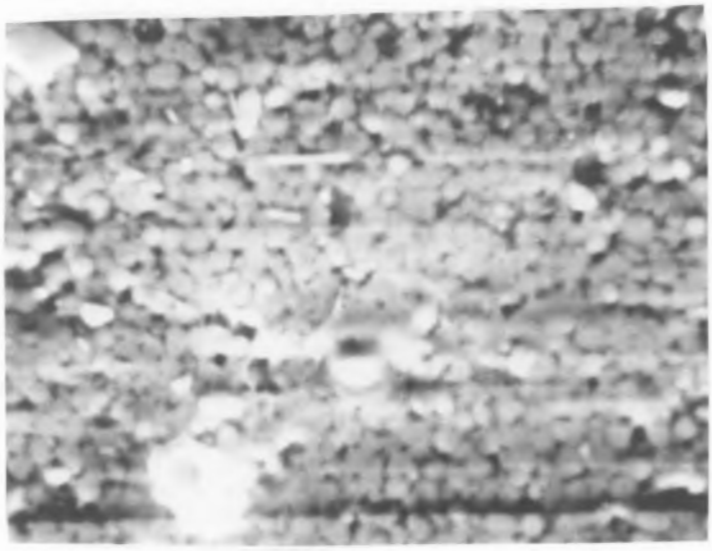

13X Molecular Sieve Surface (11μm/cm)

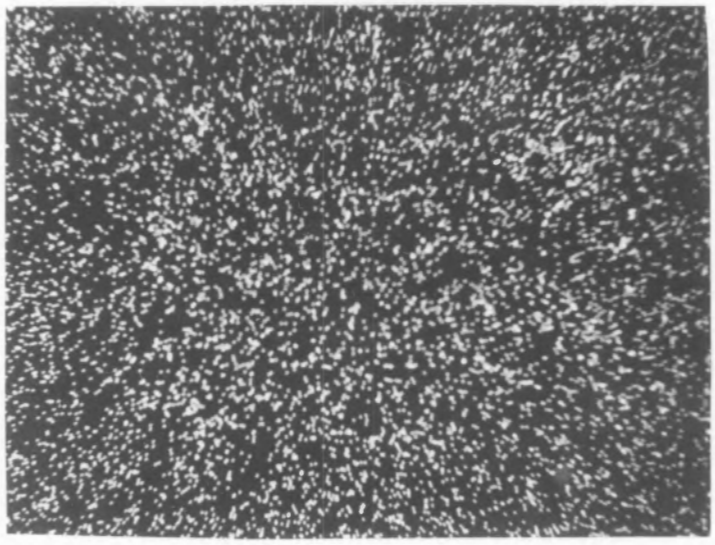

Sulfur Image (11μm/cm)

Figure 8.6 Comparison Between Sulfur Image and Actual Surface of Type 13X Molecular Sieve.

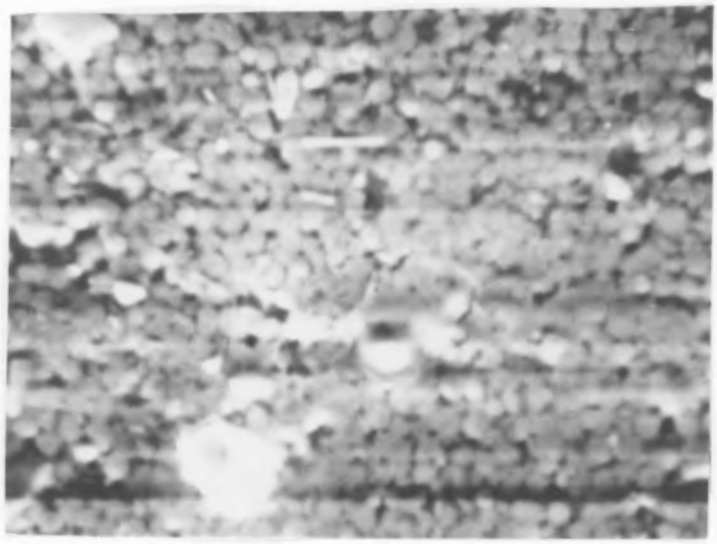

13X Molecular Sieve Surface (11μm/cm)

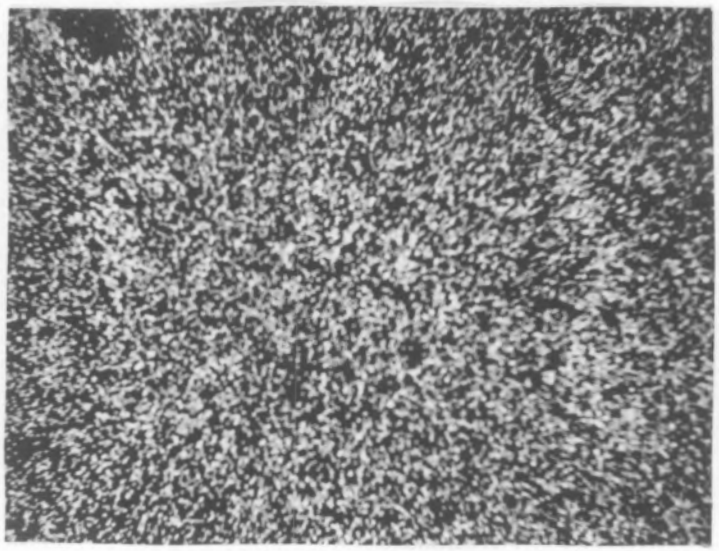

Sodium Image (11μm/cm)

Figure 8.7 Comparison Between Sodium Images and Actual Surface of Type 13X Molecular Sieve.

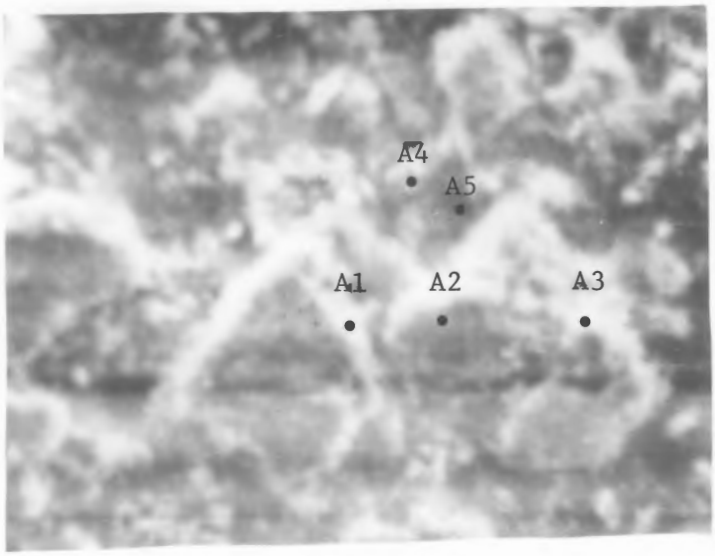

Type AW500 Molecular Sieve Surface (11μm/cm)

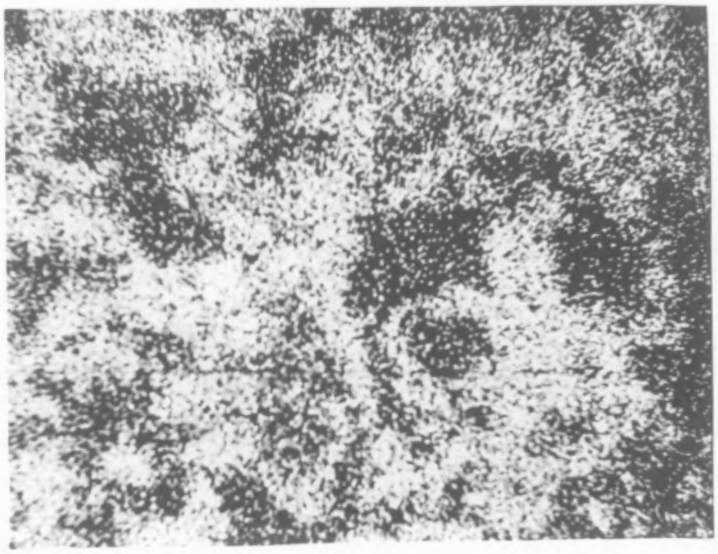

Sulfur Images (11μm/cm)

Figure 8.8 Comparison Between Sulfur Images and Actual Surface of Type AW500 Molecular Sieve.

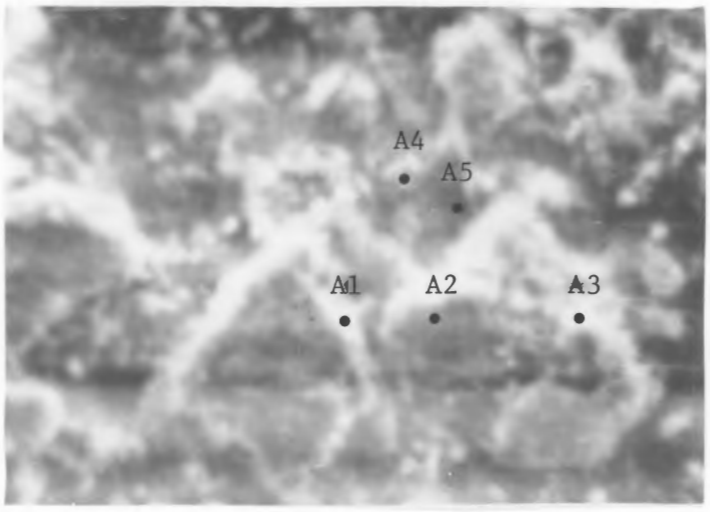

Type AW500 Molecular Sieve Surface (10.8μm/cm)

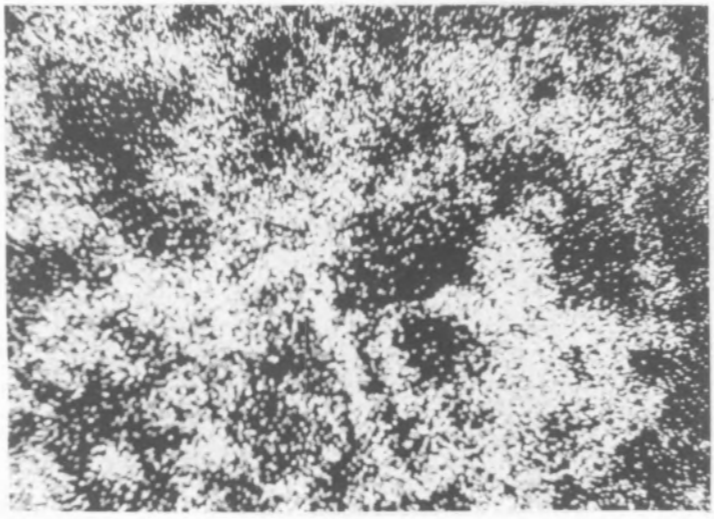

Calcium Images (10.8μm/cm)

Figure 8.9 Comparison Between Calcium Images and Actual Surface of Type AW500 Molecular Sieve.

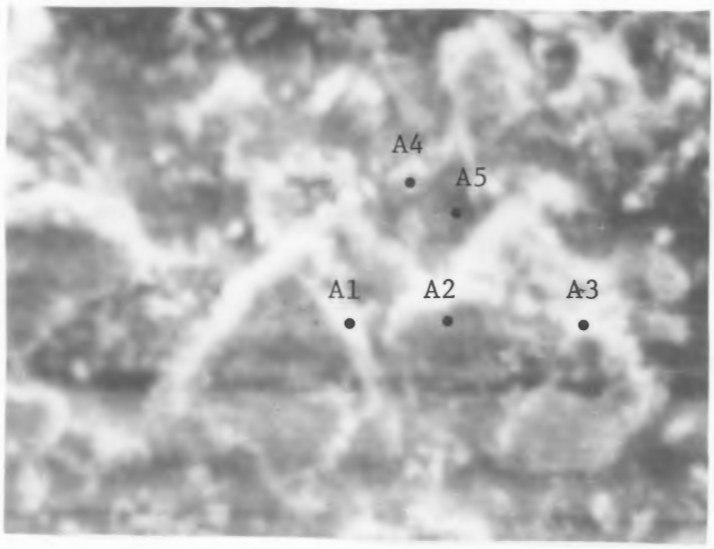

Type AW500 Molecular Sieve Surface (10.8μm/cm)

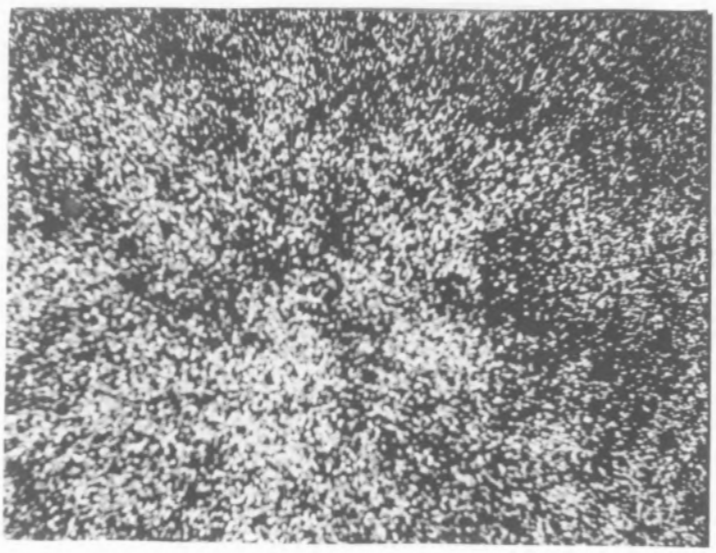

Silica Images (10.8μm/cm)

Figure 8.10 Comparison Between Silica Images and Actual Surface of Type AW500 Molecular Sieve.

image for silica. The silica distribution was much more uniform than sulfur or calcium but regions of high silica content were discernable.

Table 8.4 is a summary of quantitative analysis that were performed at locations A1, A2, A3, A4, and A5 as shown in Fig. 8.7. The dark regions (A2, A4, A5) were characterized by high SiO_2/Al_2O_3 ratios. The lighter regions (A1, A3) were characterized by low SiO_2/Al_2O_3 ratios.

Since the lighter regions (A1, A3) were also characterized by high sulfur and calcium contents it may be inferred that these locations corresponded to the location of the zeolite and the darker, high silica regions were composed primarily of binder material.

To verify the results obtained in the previous analysis the effect of surface roughness must be ascertained. Figure 8.11 shows a radial distribution of sulfur for a Type 13X molecular sieve. The sodium distribution is similar (corresponding peaks) thus confirming the validity of the previous analysis. Note that the sulfur profile is essentially uniform indicating the homogeneity of sulphur distribution within the pellet. Figure 8.12 depicts similar characteristics for a Type AW500 sieve. The sulfur distribution is more distorted corresponding to the non-uniformity of the zeolite distribution in the pellet.

8.3 Adsorbent Degradation

The first sections of this chapter were concerned with the measurement and identification of the conditions necessary to reduce

Table 8.4 Summary of Quantitative Analysis* Performed at Various Locations Depicted in Fig. 8.7.

Location	Region Description	Ca wt %	CaO wt %	SiO_2/Al_2O_3	SO_3 wt %	S wt %
A1	Light (boundary)	19.4	27.2	2.82	23.5	1.98
A2	Dark (core)	3.49	3.49	4.13	1.01	0.085
A3	Light (boundary)	19.2	26.9	3.31	31.3	2.64
A4	Dark (core)	2.46	3.44	2.74	3.56	0.30
A5	Dark (core)	3.37	4.72	3.15	4.79	0.404

*Limit of Detectibility: $50ppm_m$

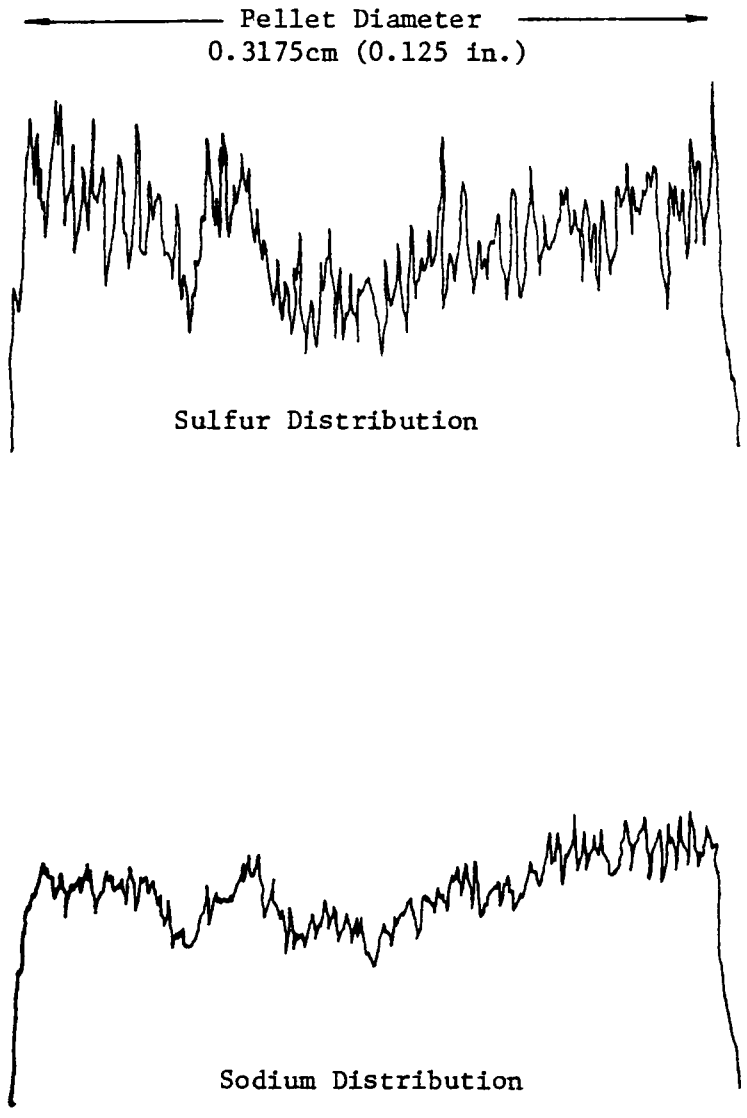

Figure 8.11 Comparison of Spectrometer Responses for Radial Sulfur and Sodium Distributions--Type 13X Molecular Sieve.

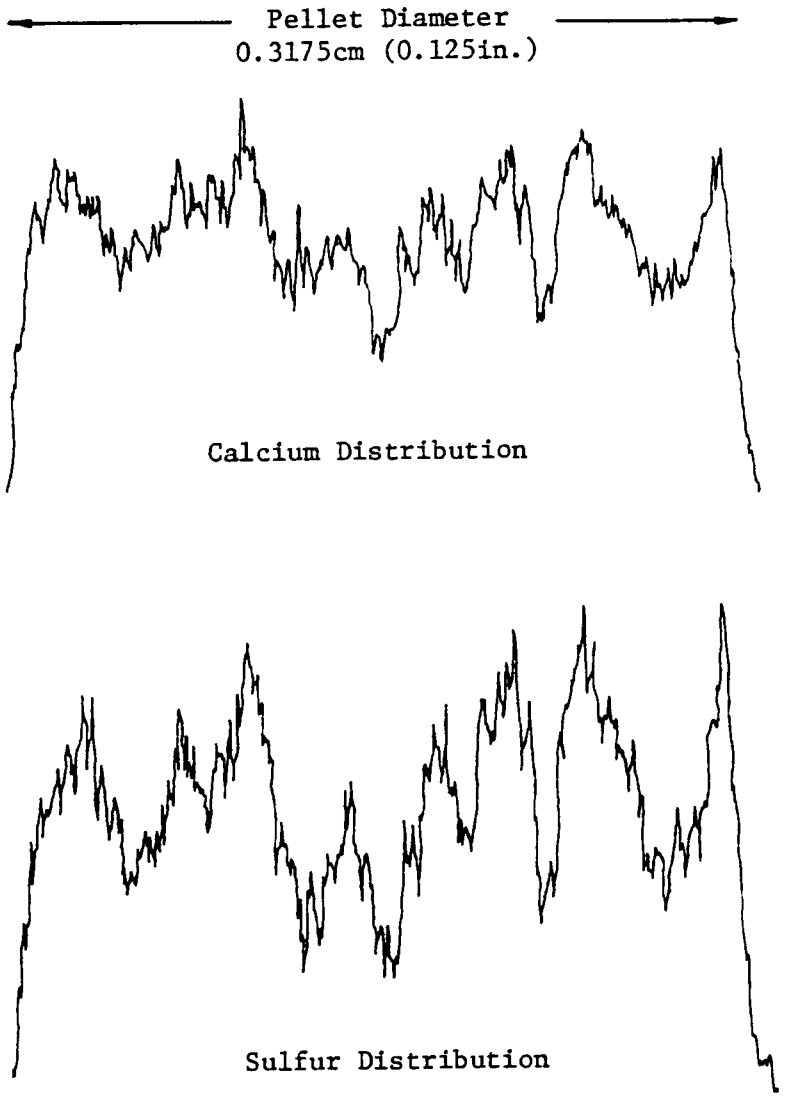

Figure 8.12 Comparison of Spectrometer Responses for Radial Sulfur and Calcium—Distributions Type AW500 Molecular Sieve.

adsorbent degradation. During the course of these investigations one primary observation was the cause of considerable concern with respect to molecular sieve behavior. Recall the variation of adsorption performance depicted in Fig. 8.2 where all adsorption capacity curves were characterized by a sharp decrease in capacity followed by a gradual change, approaching a constant value. Regardless of the regeneration conditions, the maximum loss in adsorption capacity occurred after the first regeneration cycle. Also, as the regeneration conditions were changed, ultimate adsorption capacity for several regeneration cycles could be altered. To help elucidate the mechanisms responsible for this behavior a series of SO_2 bonding mechanism tests were performed. A complete investigation of all possible adsorbent degradation effects was beyond the scope of this investigation, however an attempt was made to explain gross adsorbent degradation.

The study of zeolite behavior with respect to variations in adsorption performance is generally referred to as 'zeolite stability'. Instability does not necessarily imply total destruction but instead an irreversible change or alteration of the zeolite crystal structure. Adsorbent stability is affected primarily by chemical, mechanical, and/or thermal conditions. Since regeneration temperatures were relatively low, 425°C (797 F), thermal stability was not considered. Chemical stability was considered since simultaneous adsorption of SO_2 and water vapor occurred.

Zeolite materials have limited stability in acidic environments because of the solubility of aluminum away from the structure. As

aluminum 'leaves' the zeolite structure, the remaining voids can lead to a collapse of the remaining zeolite crystal. Zeolites are especially susceptible to acid attack because the aluminum is essentially all surface aluminum and receives little protection by being inaccessible in the crystal structure. It is known [70] that some clays resist acid leeching because the aluminum is located between silicate layers and therefore is inaccessible. Some zeolites can tolerate removal of framework aluminum without structural collapse. Mordenite zeolites can withstand almost complete removal of framework aluminum with very little change in structure. However mordenite structure is one dimensional compared to the very open three dimensional structure of 13X molecular sieves. Thus, mordenite would be more probable to suffer from pore blockage by the impurities in a combustion gas stream. Exposure to high temperatures can also be detrimental because some zeolites structures may delaminate thereby exposing embedded aluminum.

Generally, the action of acids on zeolites ranges from complete structural collapse of the zeolite crystal to simple dealumination. Regardless of the extent of aluminum extraction degradation depends on a variety of factors including the type and strength of the acid, exposure time, exposure temperature and thermal history of the zeolite.

Attempts to determine the nature of the SO_2 bonding mechanism with zeolite materials Linde 13X and AW500 have not been made. Several investigators have observed this (irreversible adsorption) behavior of SO_2 and other polar molecules but have not pursued the type, if

any, of reaction that occurs. Therefore a series of experiments were performed to determine the bonding mechanism between the zeolite and SO_2.

The experiments consisted of analyzing SO_2 exposed and as received molecular sieves by use of x-ray photoelectron spectroscopy (ESCA). Electron spectroscopy consists of using x-rays to excite core level photoemission in the samples to be analyzed. Analysis of measured electron energy spectra identifies elemental constituents and the bonding energies in the material. Previous electron-microprobe studies confirmed the existance of surface retained sulfur, even in a high vacuum. Long vacuum periods assured removal of physically adsorbed SO_2. Measurements made by ESCA revealed no presence of sulfur. Both powder and pelletized samples yielded the same results. The significance of this is that either the irreversibly adsorbed SO_2 was retained within the zeolite framework 'cage' and thus escaped detection or the sulfur concentration was not significant for detection.

It may be expected that a strong interaction between the zeolite cation and SO_2 occurred because of the large measured isosteric heat of adsorption for low adsorbate concentrations (low surface coverage). While quantitative measurements of SO_2 bonding mechanisms were not successful, a relationship between the ultimate adsorption capacity and the Al_2O_3/SiO_2 ratio of the molecular sieve was obtained. The ultimate adsorption capacity is related to the Al_2O_3/SiO_2 by

$$q_{u,r} = (1 - Al_2O_3/SiO_2)q_u \qquad (8.1)$$

where $q_{u,r}$ = ultimate adsorption capacity after adsorbent regeneration

q_u = maximum ultimate adsorption capacity

Al_2O_3/SiO_2 = aluminum oxide--silica dioxide mash ratio.

Regenerations performed in the absence of water vapor were found to correlate well for the type AW500 molecular sieve. The relationship predicts a lower adsorption capacity for type 13X molecular sieve. The predicted adsorption capacities are depicted in Fig. 8.13 for comparison to the actual adsorption performance.

The irreversible SO_2 adsorption behavior of the molecular sieves was expected because of previous investigations. Barrer and Rees [71] found that the amount of polar adsorbate bound to the adsorbent was a function of the conditions of adsorbate-adsorbent contacting. This is demonstrated by the adsorption capacity curves depicted in Fig. 8.13. Exposure to binary mixtures of SO_2 and water resulted in adsorption capacities less than those predicted by Equation 8.1 and those measured for SO_2 exposure only.

While a complete theory concerning SO_2 retention by types 13X and AW500 molecular sieve zeolites cannot be formulated, the fact that a relationship between Al_2O_3/SiO_2 and adsorption capacity exists may be useful in determining the role of zeolite composition on retained SO_2.

8.4 Summary of Regeneration Studies

The significance of the regeneration studies was that for single adsorbate adsorption, regeneration degradation was not as severe as

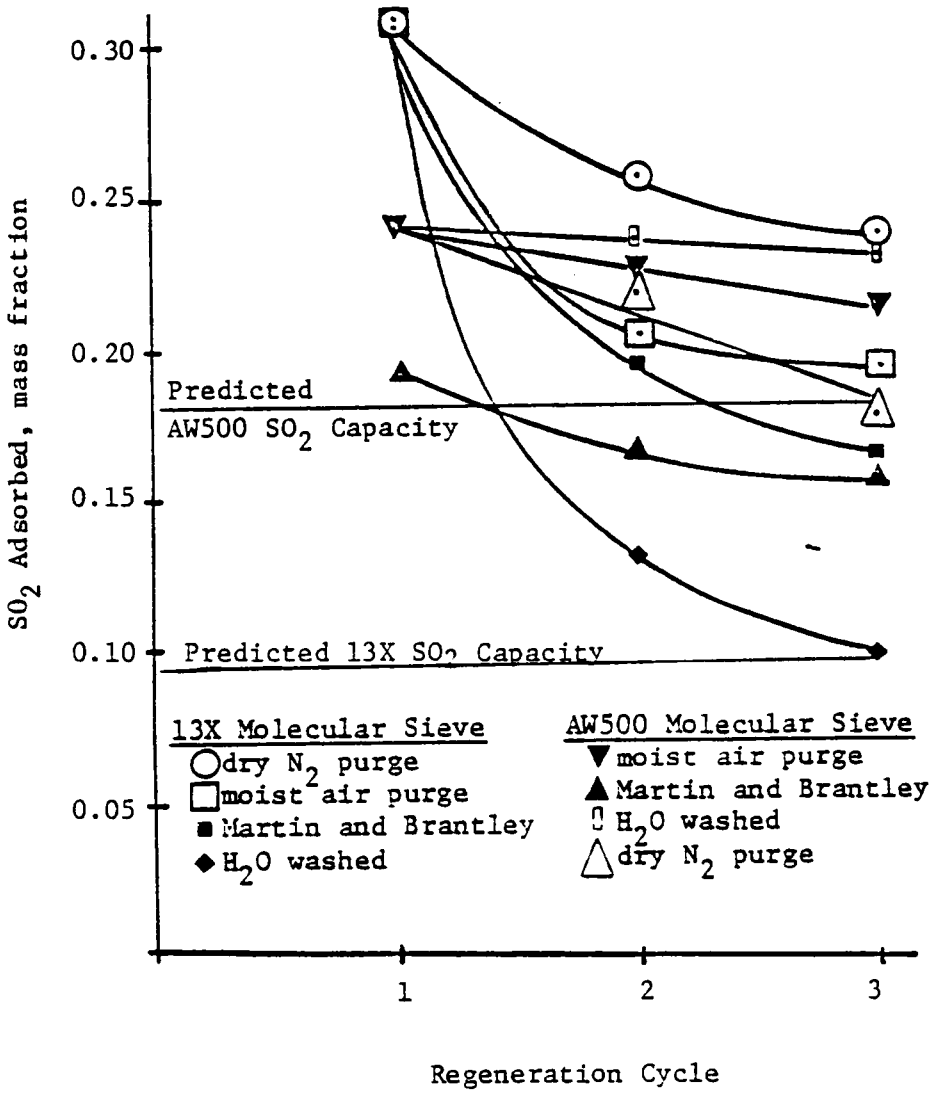

Figure 8.13 Comparison of Measured and Predicted SO_2 Adsorption Capacity after Adsorbent Regeneration.

that measured by Martin and Brantley. When binary adsorption of SO_2 and water vapor occurred, reduction in adsorption capacity after the first regeneration was in agreement with the results of Martin and Brantley for type 13X molecular sieves. However the use of lower regeneration temperatures prevented adsorption capacity losses similar to those measured by Martin and Brantley for both 13X and AW500 molecular sieves.

Tests were performed with an x-ray electron microprobe analyzer to determine if the binder material used had a significant effect on SO_2 adsorption and also determine residual sulfur homogeneity. Surface morphology and subsequent chemical analysis showed that the residual SO_2 was bound primarily by the zeolite crystal. Binding energies of SO_2 on the molecular sieves using x-ray photoelectron spectroscopy could not be obtained.

A relationship was obtained indicating that SO_2 adsorption capacity is a function of the Al_2O_3/SiO_2 ratio of the zeolite and the conditions of gas contacting and regeneration.

IX. CONCLUSIONS

The utilization of synthetic molecular sieve zeolites for combustion gas desulfurization was investigated for a variety of gas contacting conditions. Based on the results obtained, the following conclusions were made:

1) The kinetic adsorption of SO_2 on types 13X and AW500 molecular sieves and silica gel have been measured for SO_2 concentrations representative of an effluent combustion gas stream.
2) SO_2 loadings were greatest for the type 13X molecular sieve followed by the AW500 molecular sieve. As gas temperature was increased, a decrease in SO_2 breakthrough time occurred. The effect of gas velocity was minimal suggesting that mass transfer was adsorbent-side controlling. As SO_2 concentration was increased the asymptotic loading capacity for both molecular sieves was found to be a linear function of temperature. Silica gel SO_2 adsorption capacity was very low compared to that of the types 13X and AW500 molecular sieves.
3) Simultaneous adsorption of SO_2 and water vapor caused a reduction in SO_2 adsorbent loading capacity which was a function of the inlet SO_2/H_2O mole ratio. For equal mole ratios of SO_2 and water vapor, SO_2

breakthrough time for type 13X molecular sieve was decreased by 44 percent of the water vapor free case. SO_2 breakthrough time for type AW500 molecular sieve was decreased by 11 percent.

4) SO_2 adsorption isotherms for both the 13X and AW500 molecular sieve were correlated with a modified Langmuir isotherm of the form

$$q/q_m = \frac{kp^{1/n}}{(1 + kp^{1/n})}$$

Isosteric heats of adsorption were determined for both 13X and AW500 molecular sieves.

5) Adsorbent degradation was found to be dependent on the conditions of gas contacting and regeneration. Use of lower regeneration temperatures increased SO_2 adsorbent capacity for both the 13X and AW500 molecular sieves. Exposure to air-water vapor-SO_2 mixtures led to substantially decreased SO_2 adsorption capacity.

6) Adsorbent degradation was found to be directly related to the Al_2O_3/SiO_2 ratio of zeolite crystal.

While several important questions concerning SO_2 adsorption behavior need to be resolved, this investigation has revealed sufficient data that can be used to determine process feasibility.

The results obtained from this investigation indicate the SO_2 adsorption performance that would result under the restrictions imposed by the required operating conditions.

X. RECOMMENDATIONS

The results of this study have demonstrated the SO_2 adsorption performance of type 13X and AW500 molecular sieves in single and binary adsorbate systems. Before implementation of a large scale SO_2 adsorber, several additional factors should be considered.

10.1 Adsorbent Contamination by Combustion Products

Aside from the water vapor-SO_2 interactions, the adsorbent capacity and regeneration in an actual combustion gas stream should be performed. Since actual combustion gas streams are complex, studies of pellet life and integrity should be considered. Also since SO_3 is present in the gas stream, the effects of adsorption of SO_3 and water vapor deserves attention.

More knowledge of the chemical and physical changes occurring in the pellet during adsorption and regeneration is needed to confirm possible interaction between SO_2 and the adsorbent. A complete study of the SO_2 bonding mechanism with the zeolite crystal could contribute significantly to the evaluation and possible modification of the zeolite composition.

10.2 Scaling and Adsorber Design

A complete theoretical description of the process would be useful for scaling and parametric studies of adsorber operation. The main advantage would be the ability to predict effluent gas compositions and temperatures for a specified inlet gas temperature and

concentration. This description should include the capability for describing the flow field throughout the bed.

10.3 Cost of New Adsorbents

Any adsorbent obtained from other than natural deposits will cost more than limestone on a cost/ton basis. However, only through a complete analysis of the total cost of the unit can it be possible to determine if the adsorbent is economically competitive. The cost factors that must be considered are

1. Quantity of makeup adsorbent required (amount will depend on regeneration cycles).
2. Regeneration costs.
3. Waste adsorbent disposal cost.
4. Comparative cost of gas contacting unit.
5. Credit for recovered product.

Only through a complete consideration of the process and cost can the zeolite be evaluated.

10.4 Pore Excluding Capability

Electron microscopy used to study pellet utilization after exposure to real complex gas streams.

10.5 Optimization of Regeneration

By use of a Thermal Gravimetric Analyzer coupled to a mass spectrometer etc. . . the temperature of the pellets could be changed and the gaseous release analyzed. Also the purge gas flowrate could be changed and the effect studied.

11. BIBLIOGRAPHY

1. Cullis, C. F. and M. F. R. Mulcahy, "The Kinetics of Combustion of Gaseous Sulfur Compounds," Combustion and Flame, Vol. 18, No. 2, April 1972, p. 264.

2. Schroeter, L. C., Sulfur Dioxide, Pergamon Press, 1966, p. 275.

3. Elliot, T. C., "SO_2 Removal From Stack Gases," Power, September 1974, p. s-2.

4. Jimeson, R. M. and R. R. Maddocks, "Trade-offs in Selecting SO_x Emission Controls," Chemical Engineering Progress, August 1976, p. 84.

5. Rieber, M., "Low Sulfur Coal, A Revision of Reserve and Supply Estimates," Journal of Environmental Economics and Management, Vol. 2, No. 1, September 1975, p. 44.

6. Princiotta, F. T., "Flue Gas Technology," Health, Environmental Effects and Control Technology of Energy Use, Report No. 600/7-76-002, U.S. Environmental Protection Agency, February 1976, p. 254.

7. Monsanto Research Corporation, "Efficiencies in Power Generation," prepared for the U.S. Environmental Protection Agency, N.T.I.S. No. Pb-234160, March 1974, p. 6.

8. Elliot, op. cit., p. s-5.

9. Ponder, W. H. and G. G. McGlammery, "SO_2 - Control Methods Compared," The Oil and Gas Journal, December 13, 1976, p. 60.

10. Ross, F. F., "A British Approach to Sulfur Oxide Emissions," Mechanical Engineering, August 1978, pp. 42-45.

11. Stern, R. D., "Regenerable Flue Gas Desulfurization Technology for Stationary Combustion Sources," Health, Environmental Effects, and Control Technology of Energy Use, Report No. 600/7-76-002, U.S. Environmental Protection Agency, February 1976, p. 267.

12. Tennessee Valley Authority, "Sulfur Oxide Removal from Power Plant Stack Gas: Use of Limestone in Wet Scrubbing Processes," N.T.I.S. Report No. Pb183-908, p. 30.

13. Slack, A. V. and G. A. Hollinden, Sulfur Dioxide Removal From Waste Gases, Noyes Data Corporation, 1975, p. 19.

14. Bettelheim, J., B. Billingee, and A. Collins, "Some Problems of Dry Processes For Removing SO_2 From Flue Gases," Energy Digest, Vol. 1, No. 1, August/September, 1972, p. 29.

15. Andrews, R. L., "Current Assessment of Flue Gas Desulfurization Technology," Ebasco Services Incorporated, New York, paper presented at the thirty-ninth annual meeting of the American Power Conference, April 1977, p. 14.

16. Letter from E. J. Plyler, Director, Utilities and Industrial Power Division, U.S. Environmental Protection Agency, November 17, 1976.

17. Engdahl, R. B., "The Status of Flue Gas Desulfurization," ASME Air Pollution Control Division News, Newsletter, No. 5, April 1977, p. 5.

18. Slack, A. V., "Flue Gas Desulfurization: An Overview," Chemical Engineering Progress, August 1976, p. 95.

19. Bienstock, D. J., and J. G. Myers, "Process Development in Removing Sulfur Dioxide from Hot Flue Gases," U.S. Dept. of Interior, Bureau of Mines, Report of Investigations, No. 5735, 1961.

20. Bienstock, D. and F. Field, "Bench-Scale Investigations on Removing Sulfur Dioxide From Flue Gases," Journal of the Air Pollution Control Association, Vol. 10, No. 2, April 1960.

21. Conser, R. E., "The Shell Flue Gas Desulfurization Process - How Does It Stack Up?" Petroleum and Petrochemical International, Vol. 13, No. 7, July 1973, pp. 62-79, and No. 8, August 1973, pp. 46-49.

22. Bischoff, W. F. and Y. Habib, "The FW-BF Dry Adsorption System," Chemical Engineering Progress, Vol. 7, No. 5, May 1975, p. 59.

23. Ball, F. J., S. L. Torrence, and A. J. Repik, "Dry Fluidized Activated Carbon Processes For Stack SO_2 Recovery as Sulfur," Journal of the Air Pollution Control Journal, Vol. 22, No. 1, January, 1972, p. 20.

24. Pierce, F. J., Memorandum to the head of the Mechanical Engineering Dept., Virginia Polytechnic Institute and State University, Blacksburg, Va., May 1976.

25. Śmivek, M., and S. Verny, Active Carbon, Elsevier Publishing Company, 1970, pp. 75-162.

26. Joubert, J. I., "Adsorption of Inorganic Gases and their Mixtures on H-Mordenite," Ph.D. dissertation, Worcester Polytechnic Institute, May 1971, p. 6.

27. Breck, D. W., Zeolite Molecular Sieves, John Wiley and Sons, 1974, p. 10.

28. Union Carbide Corporation, "Linde Molecular Sieves," Publication F - 1979C p. 4.

29. Barrer, R. M., "Molecular Sieves," p. 171, Society and Chemical Industry, London 1968.

30. Sameshima, J. and H. Hemmi, "Sorption of Gas by Mineral IV. Zeolites and Bentonite," Bulletin of the Chemical Society of Japan, No. 9, 1934, pp. 27-41.

31. Bienstock, D., J. Field, and J. G. Myers, "Process Development in Removing Sulfur Dioxide from Hot Flue Gases," U.S. Department of Interior, Bureau of Mines, Report of Investigations No. 5735, 1961.

32. Martin, D. and F. Brantley, "Selective Adsorption and Recovery of Sulfur Dioxide from Industrial Gases by Using Synthetic Zeolites," U.S. Department of the Interior, Bureau of Mines, Report of Investigations, No. 6321, April 1963.

33. Tamboli, J. K. "SO_2 - Adsorption Properties and Acid Stability of Molecular Sieve Zeolites," Master of Science Thesis, Worcester Polytechnic Institute, 1970.

34. Anurov, S. A., N. V. Kel'tsev, V. I. Smola, and N. S. Torocheshnikov, "Rate of Adsorption of Sulfur Dioxide on CaY Zeolite," Zhurnal Prikladnoi Khimi, Vol. 48, No. 2, February, 1975, pp. 405-407.

35. Anurov, S. A., N. V. Kel'tsev, V. I. Smola, and N. S. Torocheshnikov, "Kinetics of the Adsorption of Sulphur Dioxide on Natural Zeolites," Zhurnal Fizicheskoi Khimi, Vol. 48, 1974, pp. 2586-2587.

36. Friedman, L. D., "Applicability of Inorganic Solids other than Oxides to the Development of New Processes For Removing SO_2," FMC Research Corp., N.T.I.S. No. PCR-829, December 1970.

37. Vinnikov, L. I., I. P. Mukhlenov, I. G. Lesokhin, and G. N. Buzanova, "Adsorption of Sulfur Dioxide From Wet Air by Industrial Adsorbents," The Soviet Chemical Industry, No. 2, February 1973, pp. 114-117.

38. Brown, J. W., D. W. Pershing, J. H. Wasser, and E. E. Berkau "Interaction of Stack Gas Sulfur and Nitrogen Oxides on Dry Sorbents," National Environmental Research Center, N.T.I.S. No. PB-224-208, September 1973.

39. Davison Chemical Division - W. R. Grace and Co., "Davison Silica Gels," Publication 5C-IC-15-1077.

40. McGavack, J. and W. A. Patrick, "The Adsorption of Sulfur Dioxide By the Gel of Silicic Acid," Journal of the American Chemical Society, Vol. 42, 1920, pp. 946-977.

41. Cole, R., and H. L. Shulman, "Adsorbing Sulfur Dioxide on Dry Ion Exchange Resins," Industrial and Engineering Chemistry, Vol. 52, No. 10, October 1960, pp. 859-860.

42. Joubert, J. I., op. cit., p. 284.

43. Jones, W. J., and R. A. Ross, "The Sorption of Sulfur Dioxide on Silica Gel," Journal of the Chemical Society, 1967, pp. 1021-1026.

44. Galan, M. A. and J. M. Smith, "Adsorption of Sulfur Dioxide on Silica Gel - Rate and Equilibrium Parameters," Journal of Catalysis, Vol. 38, 1975, pp. 206-213.

45. Minachev, Kh. M. and Ya. I. Isakov, "Catalytic Properties of Metal-Containing Zeolites," Zeolite Chemistry and Catalysis, American Chemical Society Monograph, 1976, p. 578.

46. Collins, J. J., "A Report On Acid-Resistant Molecular Sieves Types AW 300 and AW 500," Oil and Gas Journal, Vol. 52, No. 3, December 2, 1963, p. 118.

47. Johnstone, H. F., "Progress in the Removal of Sulphur Compounds From Waste Gases," Combustion, August 1933, pp. 19-30.

48. Charm, S. E., C. C. Matteo, and R. A. Carlson, "Scaling Up of Elution in Chromatography Columns," AICHE Symposium Series, Vol. 86, Bioengineering p. 9-11.

49. Schwartz, C. E. and J. M. Smith, "Flow distribution in Packed Beds," Industrial and Engineering Chemistry, Vol. 45, No. 6, pp. 1209-1218.

50. Slowik, A. A. and E. B. Sansone, "Diffusion Losses of Sulfur Dioxide in Sampling Manifolds," Journal of the Air Pollution Control Association, Vol. 24, No. 3, p. 247.

51. Villalobos, R. and E. A. Houser, "On-Line Analysis of SO_2 in Flue Gas and Other Process Streams by Gas Chromatography," Instrument Society of America Transactions, Vol. 12, No. 1, 1973, p. 71.

52. Hodges, C. T. and R. G. Matson, "Gas Chromatographic Separation of Carbon Dioxide, Carbon Oxysulfide, Hydrogen Sulfide, Carbon Disulfide, and Sulfur Dioxide," Analytical Chemistry, Vol. 37, No. 8, July 1965, p. 1066.

53. McNair, H. M. and E. J. Bonelli, Basic Gas Chromatography, Varian Aerograph, 5th Ed., 1969, p. 59.

54. Wechter, S. G.,"Preparation of Stable Pollution Gas Standards Using Treated Aluminum Cylinders," Paper presented at ASTM Calibration Symposium, Boulder, Colorado, August 5, 1975.

55. Wexler, A., "Humidity Standards," Precision Measurement and Calibration, U.S. National Bureau of Standards Handbook 77, Vol. II, February, 1961, p. 741.

56. Wexler, A., op. cit.

57. Wood, H. L., Personal Communication, Department of Mechanical Engineering, Virginia Polytechnic Institute and State University, Blacksburg, Virginia, March 1978.

58. van Deemter, J. J., F. J. Zuiderweg and A. Klinkenberg, "Longitudinal Diffusion and Resistance to Mass Transfer as Causes of Nonideality in Chromatography," Chemical Engineering Science, Vol. 5, 1956, pp. 271-289.

59. Giddings, J. C., Dynamics of Chromatography - Part I, Marcel Dekker, Inc., 1965, p. 18.

60. Robell, A. J. and R. R. Merrill, "Gaseous Cantaminant Removal by Adsorption: II. Adsorption Dynamics in Fixed Beds," AICHE Symposium Series, Vol. 65, No. 96, p. 101.

61. Acrivos, A., "Method of Characteristic Technique - Application to Heat and Mass Transfer Problems," Industrial and Engineering Chemistry, Vol. 48, No. 4, April 1956, p. 703.

62. Bullock, C. E. and J. L. Threlkeld, "Dehumidification of Moist Air by Adiabatic Adsorption," ASHRAE Transactions, Vol. 72, No. 1, 1966, p. 301.

63. Rachinskii, V. V., The General Theory of Sorption Dynamics and Chromatography, Consultants Bureau, New York, 1965, pp. 13-50.

64. Szekely, J., J. W. Evans, and H. Y. Sohu, Gas-Solid Reactions, Academic Press, Inc., 1976.

65. Mahefkey, E. T., J. D. Pinson, and J. N. Crisp, "Analysis of Transient Heat Transfer in Porous Solids with Application Toward Phase Separation Processes," ASME Paper 77-WA/HT-13.

66. Perry, R. and C. Chilton, Chemical Engineers Handbook, Fifth Edition, McGraw-Hill-11:11, 1973, Chapter 16, p. 14.

67. Joubert, J. I., op. cit., p. 13.

68. Joubert, J. I., op. cit., p. 14.

69. Yon, C. M. and P. H. Turnock, "Multicomponent Adsorption Equilibria on Molecular Sieves," AICHE Symposium Series, Vol. 67, 1971.

70. McDaniel, C. V. and P. K. Maher, "Zeolite Stability and Ultrastable Zeolites," Zeolite Chemistry and Catalysis, American Chemical Society Monograph, 1976, p. 295.

71. Barrer, R. M. and L. V. Rees, Transactions of the Faraday Society, Vol. 50, 1954, p. 852.

APPENDICES

APPENDIX A. MEASUREMENT SO_2 BREAKTHROUGH CURVES

Adsorbent pellets were weighted and then placed in a furnace to desorb water vapor and minimize water vapor adsorption during transfer to the adsorption column. After exposure to dry nitrogen at 260°C (500 F) for at least three hours, the adsorbent was transferred to an insulated glass adsorption column. To reduce thermal shock the column was preheated using a heated bed of glass spheres. The packed column was then installed on the adsorption test apparatus and purged with dry nitrogen until a specified bed temperature was reached.

The main air supply was diverted through a by-pass valve and adjusted to simulate the bed pressure drop and back pressure. For specified bed gas flow conditions, the SO_2 and/or water vapor injection rates were set by diverting a mixed gas sample to the gas chromatograph. Chromatograph calibration was checked before and after each breakthrough curve test. Stability and verification of the gas analysis method was obtained by noting that for each breakthrough curve test no discrepancy between calibration was observed.

Once the test gas conditions (gas concentration, flowrate, gas temperature) were established the flow was diverted to the adsorption column by using a three-way valve. Arrival of the SO_2 front was detected using a phenolred on sodium hydroxide indicator. As the test proceeded, gas temperature, bed pressure drop, inlet air flowrate, and inlet air relative humidity were monitored.

Measured breakthrough curves of SO_2 adsorption on types 13X and AW500 molecular sieves are presented in Figs. A1-A11.

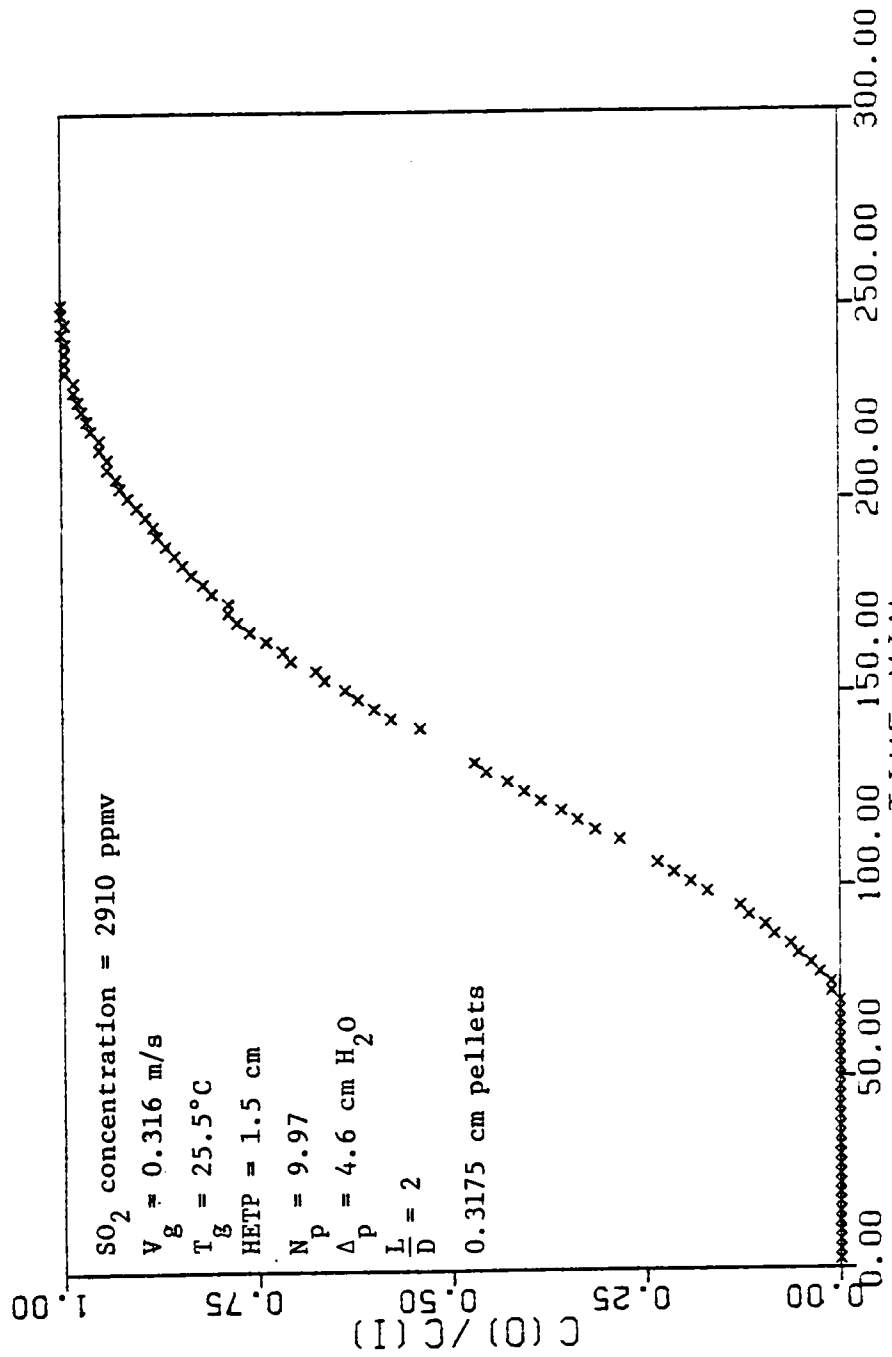

Figure A1. SO_2 Adsorption on 13X Linde Molecular Sieve.

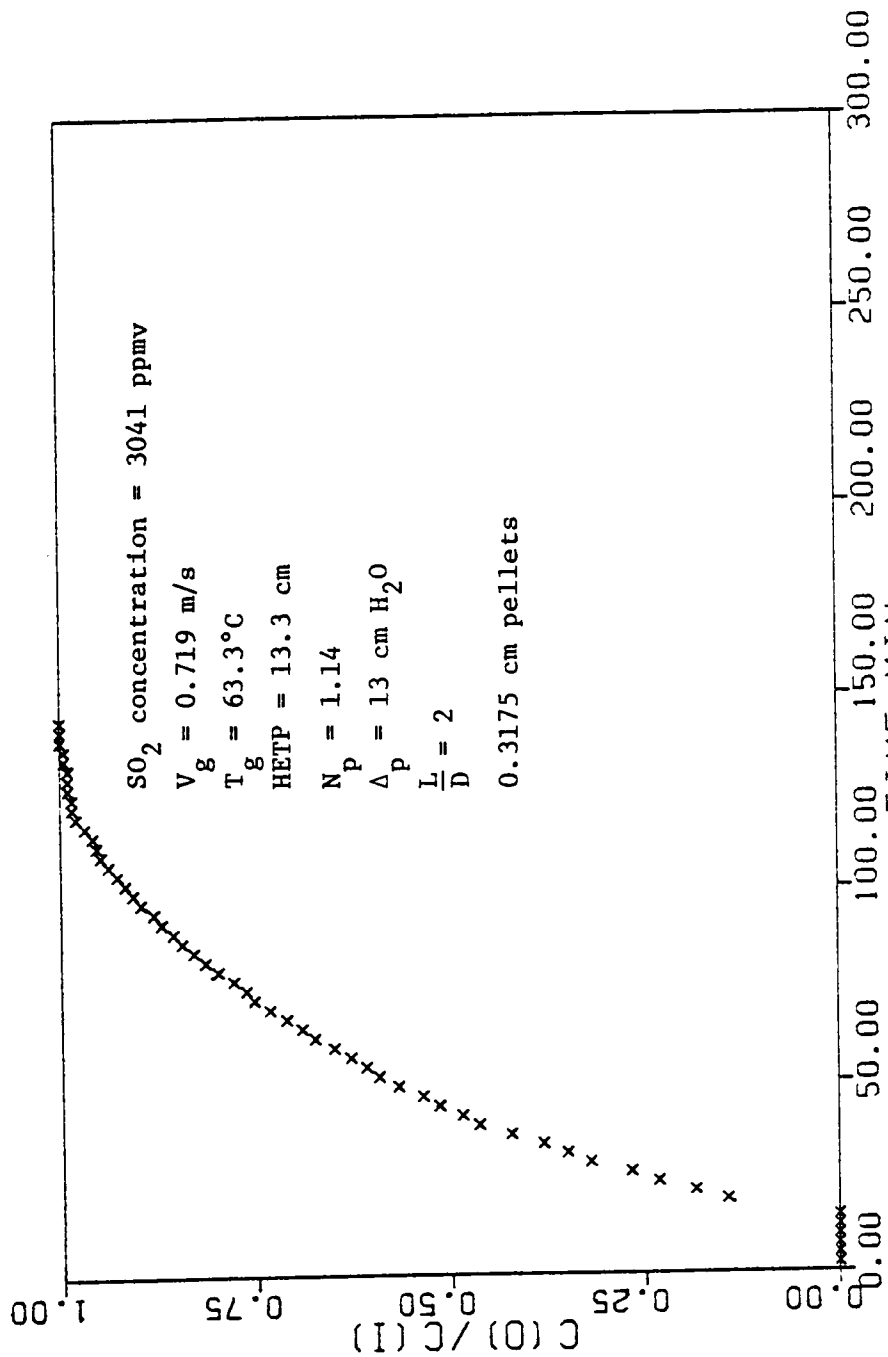

Figure A2. SO_2 Adsorption on Linde 13X Molecular Sieve.

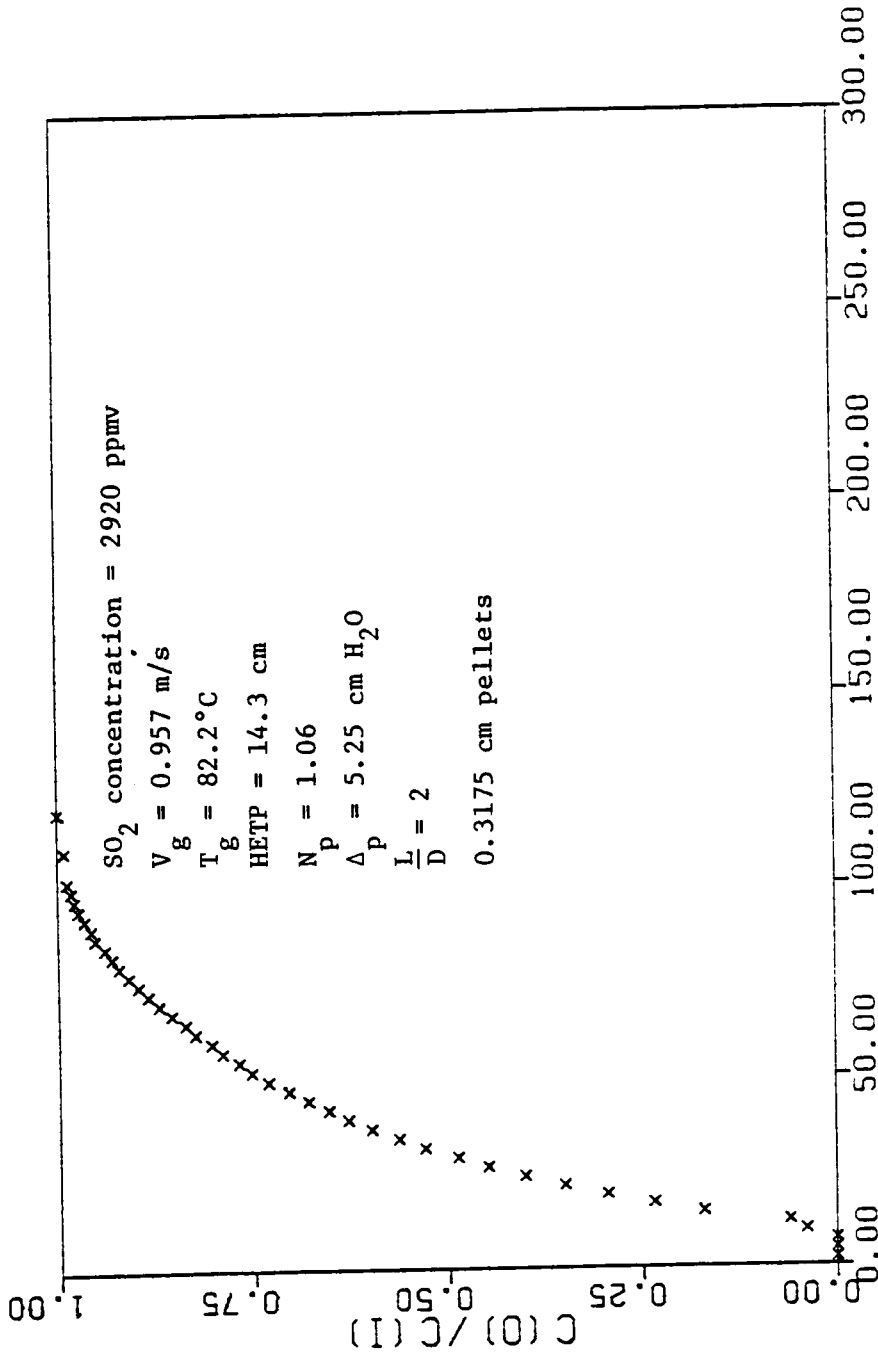

Figure A3. SO_2 Adsorption on Linde 13X Molecular Sieve.

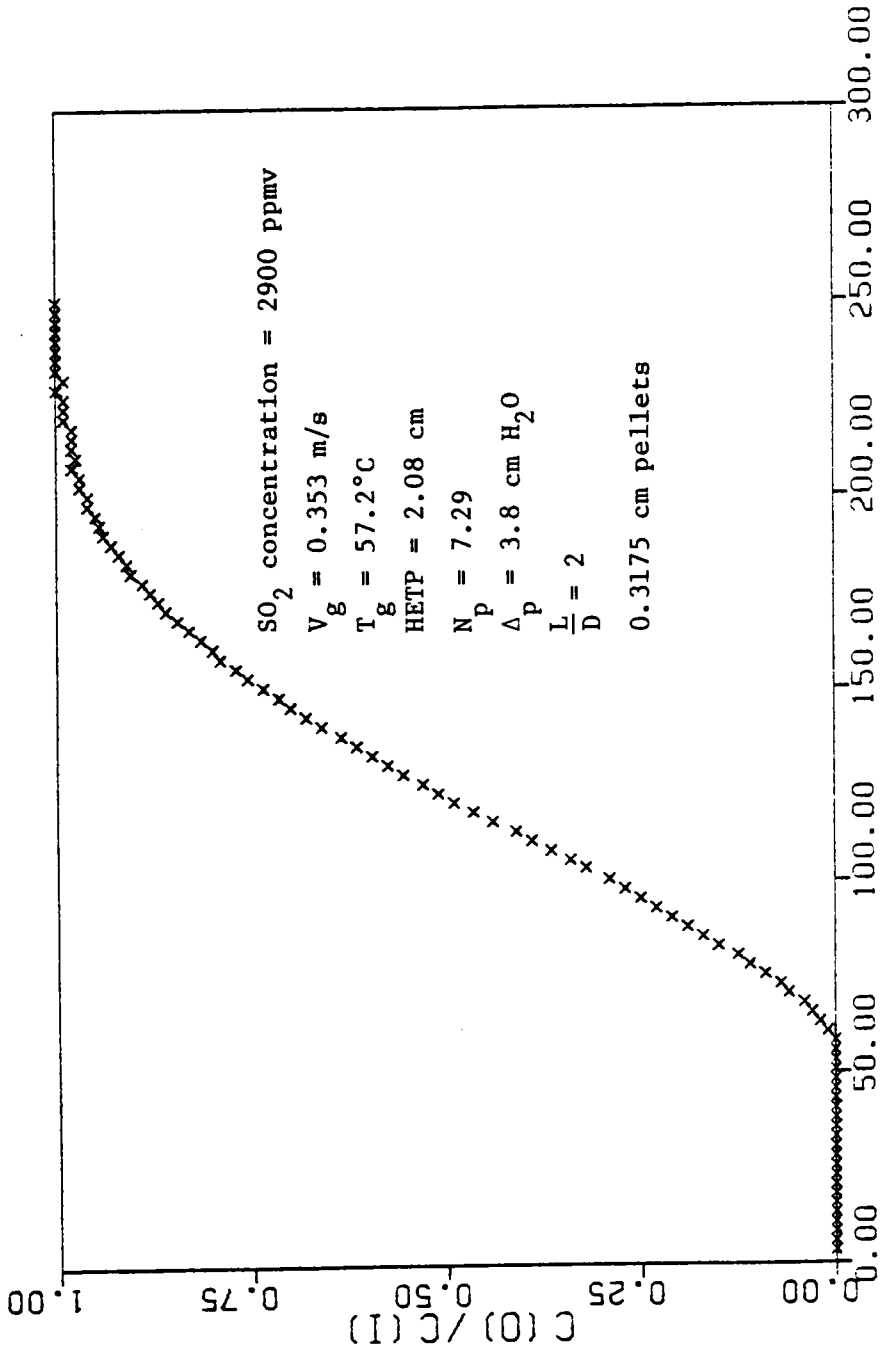

Figure A4. SO_2 Adsorption on 13X Linde Molecular Sieve.

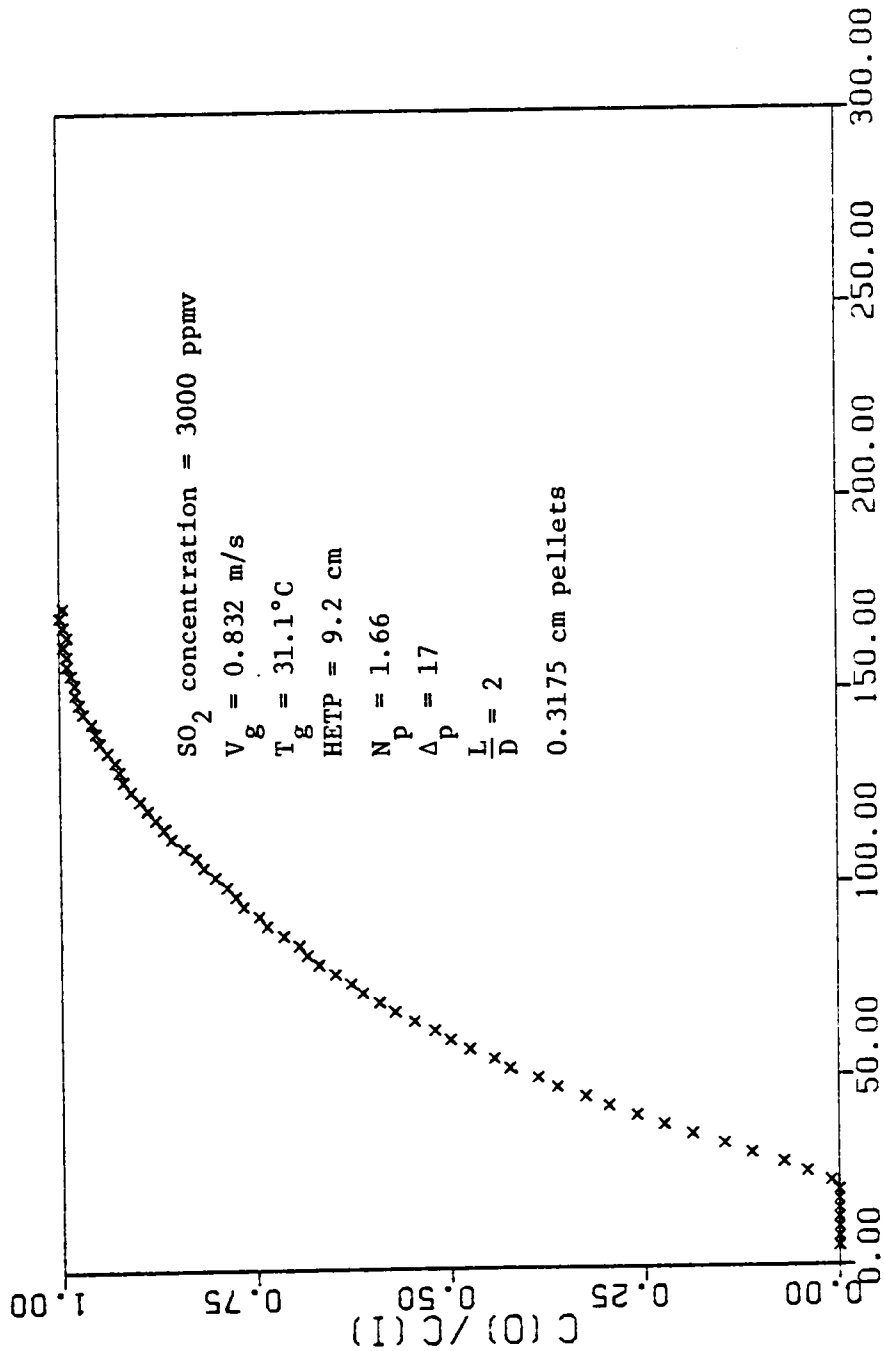

Figure A5. SO_2 Adsorption on 13X Linde Molecular Sieve.

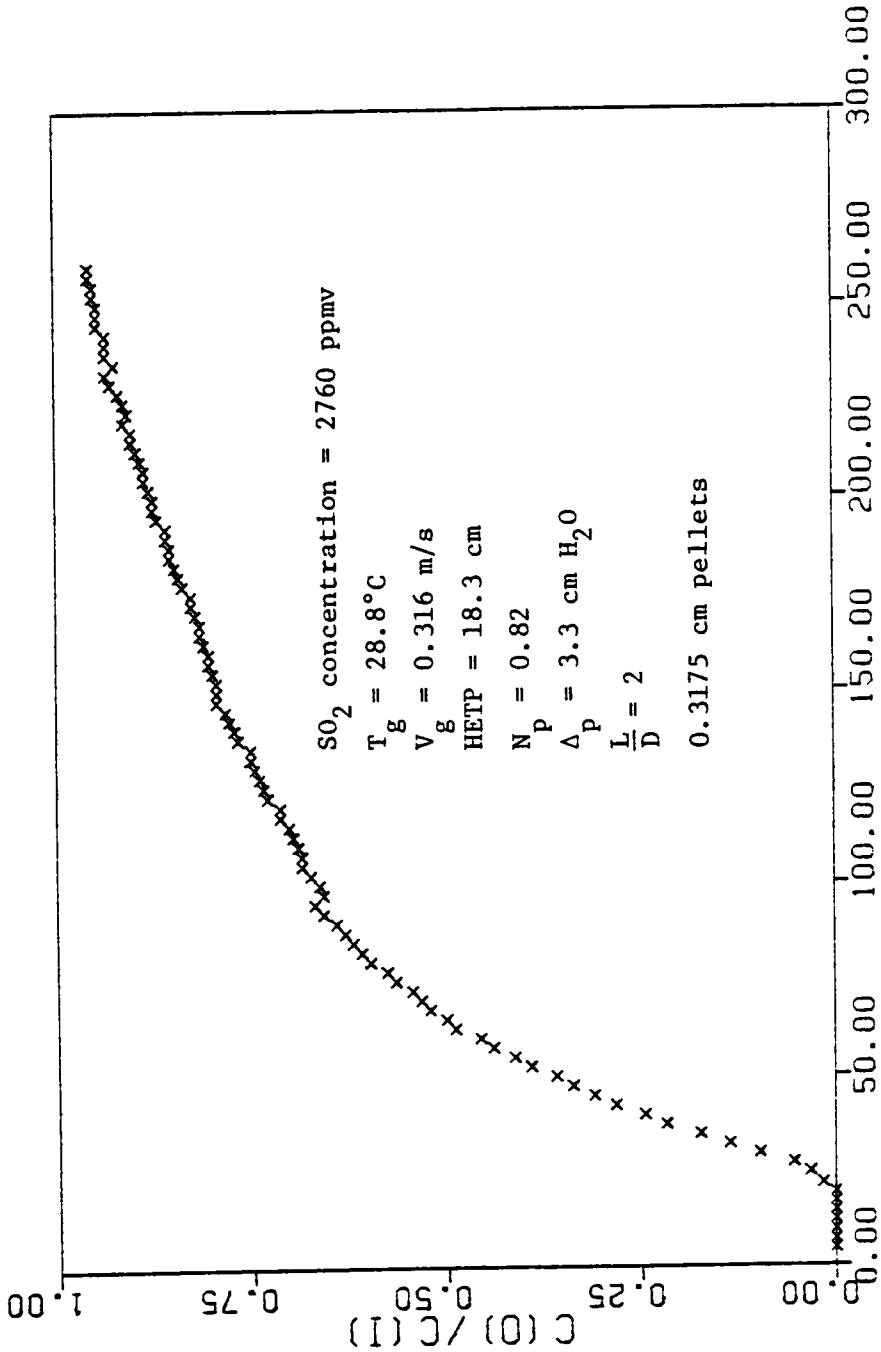

Figure A6. SO_2 Adsorption on AW500 Linde Molecular Sieve.

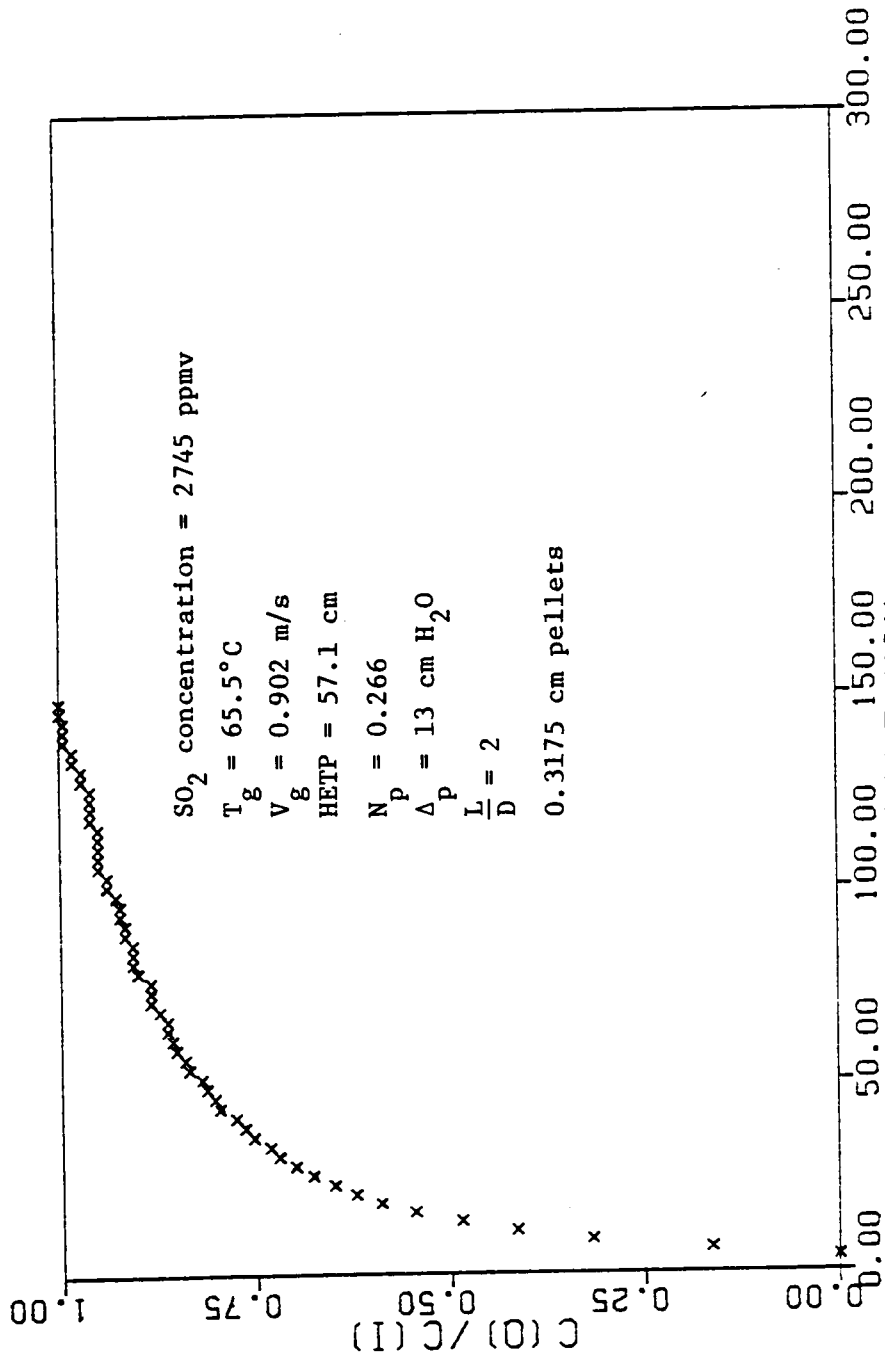

Figure A7. SO_2 Adsorption on AW500 Linde Molecular Sieve.

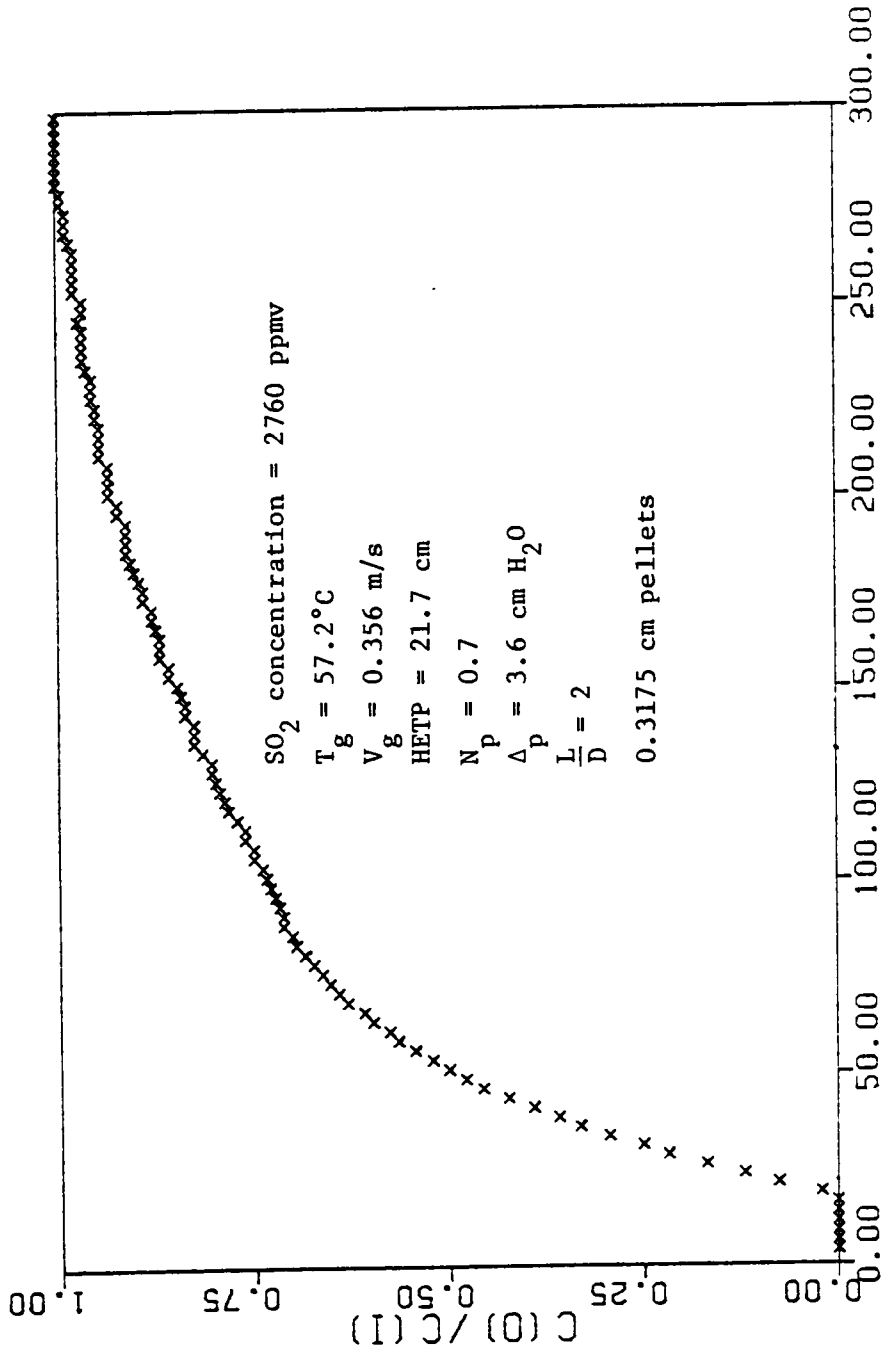

Figure A8. SO_2 Adsorption on AW500 Linde Molecular Sieve.

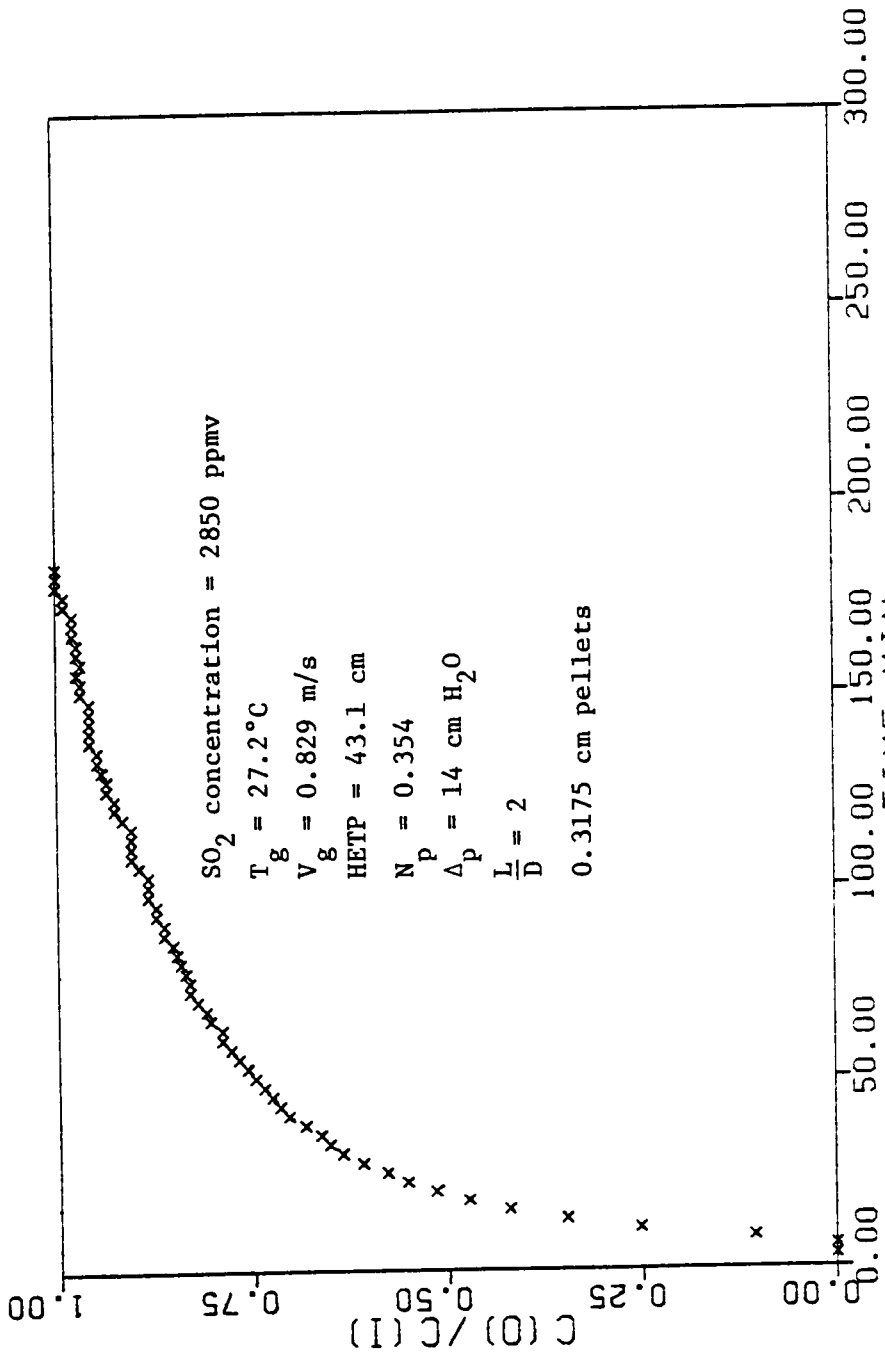

Figure A9. SO_2 Adsorption on AW500 Linde Molecular Sieve.

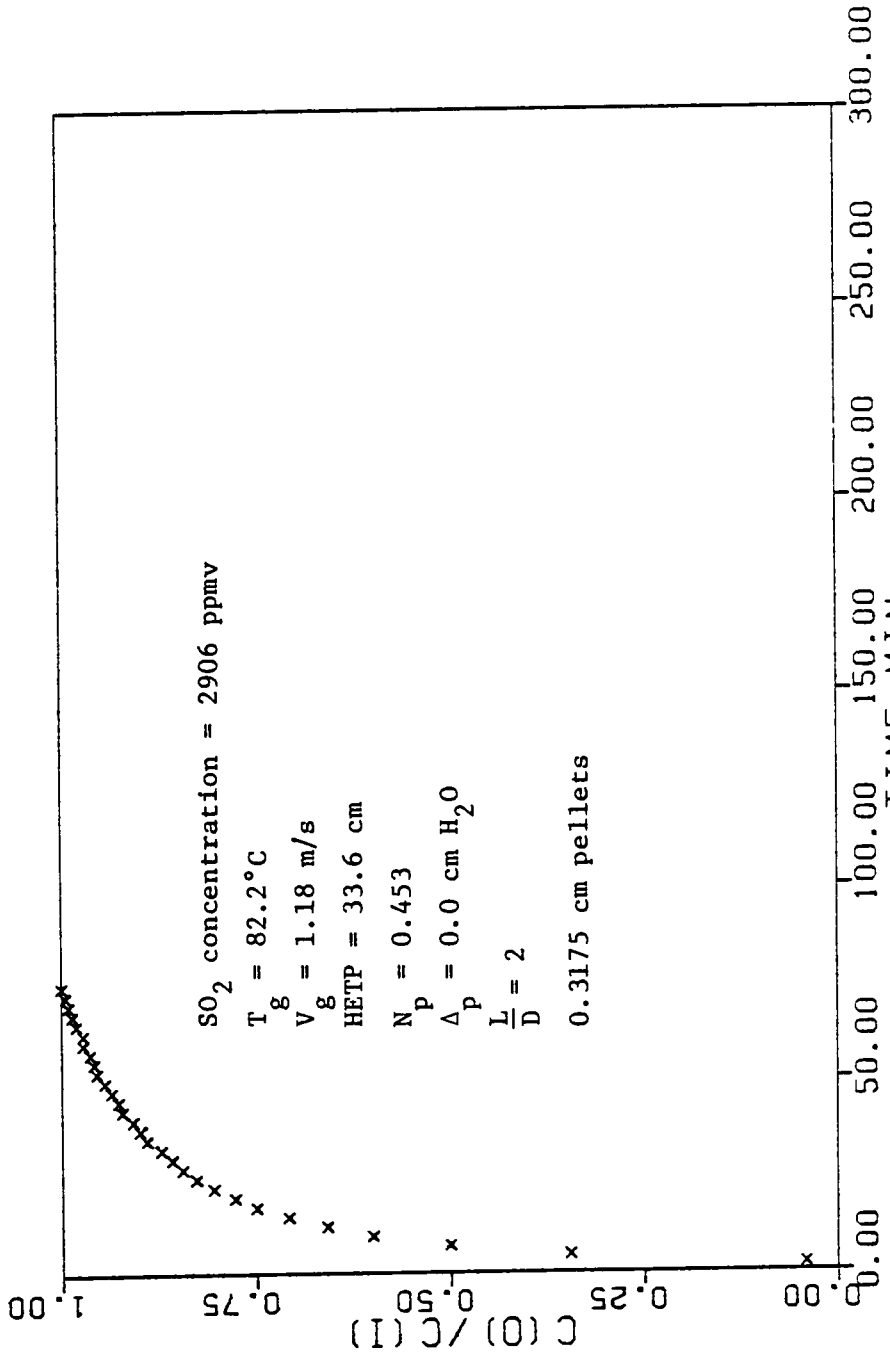

Figure A10. SO_2 Adsorption on AW500 LInde Molecular Sieve.

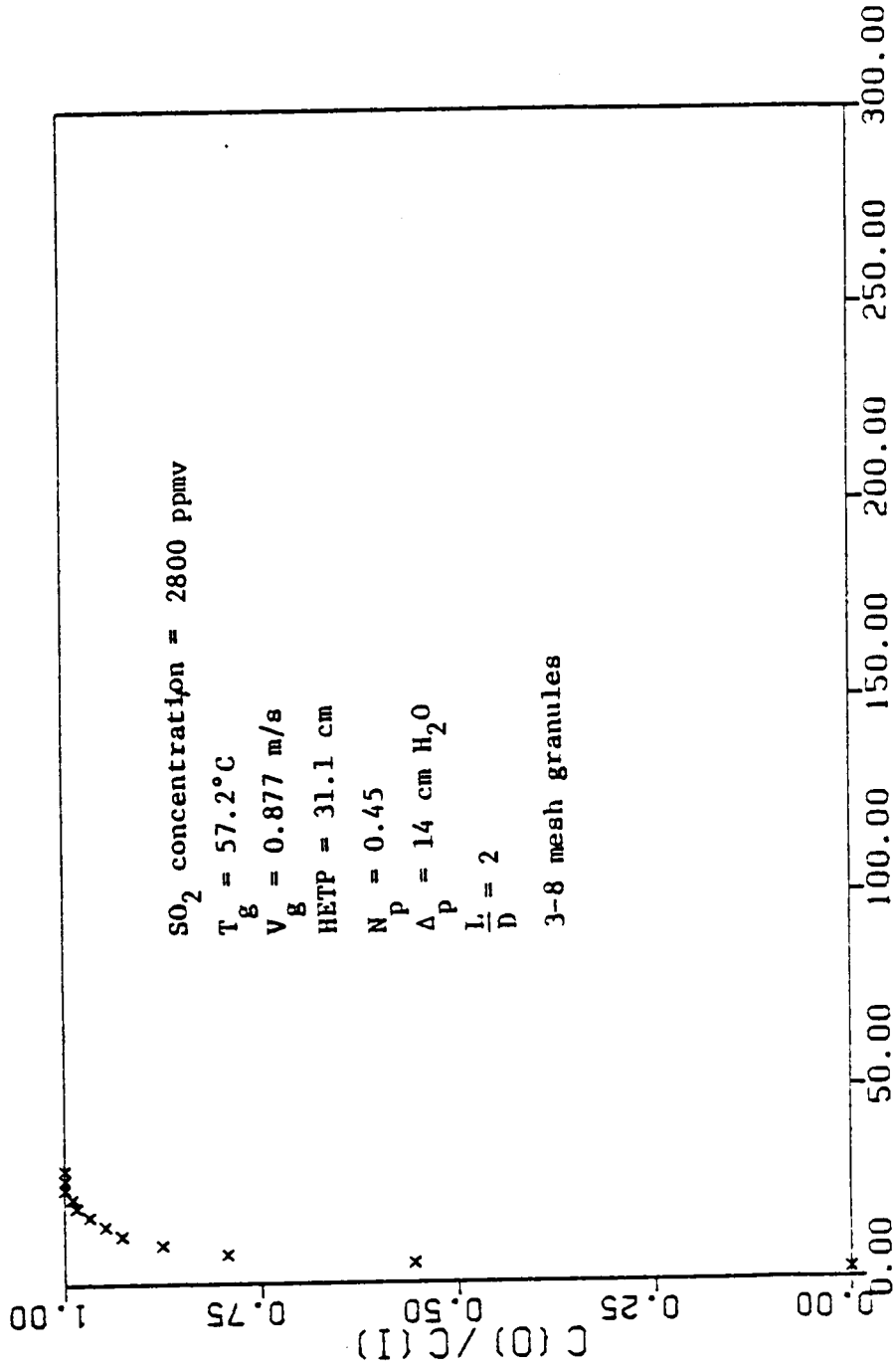

Figure A11. SO_2 Adsorption on Davison Grade 01 Silica Gel.

APPENDIX B. SUMMARY OF REGENERATION DATA

Table B1. Summary of 13X Molecular Sieve Regeneration -- SO_2 Exposure

	SO_2 Adsorbed weight percent x 100		
Adsorption Cycle	1	2	3
	31.6	26.2	24.2
	31.7	27.5	24.0
	31.82	27.1	24.9
	31.98	23.8	22.9
	31.5	24.5	23.5
$\bar{q}_m$	31.72	25.8	23.9
σ	0.1876	1.62	0.752
σ_m^*	0.083	0.724	0.336
Desorption Cycle	1	2	3
	87.72	95.3	--
	88.3	95.2	--
	86.8	92.5	--
	74.7	95.6	--
	78.4	96.0	--
$\bar{q}_m$	83.2	94.9	--
σ	0.622	1.39	--
σ_m^*	0.278	0.622	--

* $\sigma_m = \frac{\sigma}{\sqrt{n}}$

Regeneration conditions: purge using N_2 at 260°C (500 F) for 3 hrs

Table B2. Summary of AW500 Molecular Sieve Regeneration

-- SO_2 Exposure

	SO_2 Adsorption weight percent x 100		
Adsorption Cycle	1	2	3
	24.2	22.9	21.1
	24.37	23.1	22.0
	24.18	22.9	21.4
$\bar{q}_m$	24.25	23.0	21.5
σ	0.104	0.0984	0.464
σ_m^*	0.06	0.0568	0.267
Desorption Cycle	1	2	3
		96.5	--
		96.7	--
		96.9	--
$\bar{q}_m$	94.7	96.7	--
σ	0.157	0.199	--
σ_m^*	0.091	0.114	--

* $\sigma_m = \frac{\sigma}{\sqrt{n}}$

Regeneration Conditions: N_2 purge at 260°C (500 F)

APPENDIX C. MEASUREMENT OF VELOCITY PROFILES

The existance of a radial porosity gradient within the packed bed results in decreased utilization of interior bed materials. Also bed performance can be changed drastically depending on the exothermicity of the reactions occurring in regions of low bulk gas flowrate. To quantify the effect of packing technique on exit velocity profile, several radial velocity profiles were measured at the bed exit plane.

The purposes for measuring bed exit velocity profiles are

1) to aid in the proper design of gas sampling probes,
2) classify the dynamic SO_2 breakthrough measurements,
3) justify formulations used for development of theoretical adsorption model.

Velocity profiles were obtained by traversing the bed exit plane 2.54cm (1 in.) from the bed packing with a hot film anemometer. Measurements were taken at 0.3175cm (1/8 in.) intervals to ensure acquisition of representative profiles. Measured profiles are shown in Figs. C1-C5. Before each profile was measured the bed was repacked and gently tapped to settle the bed packing material.

Calibration of the anemometer sensor consisted of measuring reference velocities from a low speed wind tunnel and using King's equation to provide calibration values for a range of gas velocities.

The measured anemometer data are related to the fluid properties and velocity by King's equation

$$\frac{E_b^2 R}{(R + R_3)} = P = [A + B(V)^{1/n}](t_s - t_e) \qquad (C.1)$$

where E_b = bridge voltage

R = probe resistance

R_3 = resistance of probe lead in series with sensor

P = power input to sensor

V = flow velocity

n = constant which depends on sensor Reynolds number

t_s = sensor temperature

t_e = environment temperature

$A = 0.42\pi K_f L Pr_f^{0.2}$

$B = 0.57\pi K_f L Pr_f^{0.33}(do/\nu_f)^{0.5}$

L = sensor length

do = sensor diameter

K_f = fluid thermal conductivity

Calibration values and reference velocity data are shown in Table C.1.

Table C.1 Calibration of Hot Film Sensor*

Reference Velocity m/s	(ft/s)	Bridge Voltage volts	Bridge Current amps	Manometer cm H_2O	(in. H_2O)
2.1	(6.9)	3.36	0.071	0.0254	(0.01)
3.38	(11.1)	3.56	0.076	0.0635	(0.025)
3.68	(12.1)	3.65	0.078	0.076	(0.03)
3.99	(13.1)	3.66	0.078	0.0889	(0.035)
1.49	(4.9)	3.18	0.068	0.0127	(0.005)
1.06	(3.5)	3.12	0.066	0.0063	(0.0025)
6.03	(19.8)	3.94	0.084	0.203	(0.08)
8.81	(28.9)	4.22	0.089	0.43	(0.17)
11.0	(36.1)	4.37	0.093	0.673	(0.265)
12.3	(40.2)	4.45	0.094	0.838	(0.33)
13.2	(43.3)	4.6	0.097	1.19	(0.47)
17.6	(57.8)	4.74	0.01	1.74	(0.685)
13.8	(45.5)	4.63	0.098	1.34	(0.52)

* Constant Temperature Anemometer
TSI Heat Flux Model 1010A
Serial No. 16610

TSI Probe (Hot Film)
Probe Model:1210
Sensor Code -20
Serial No. E471

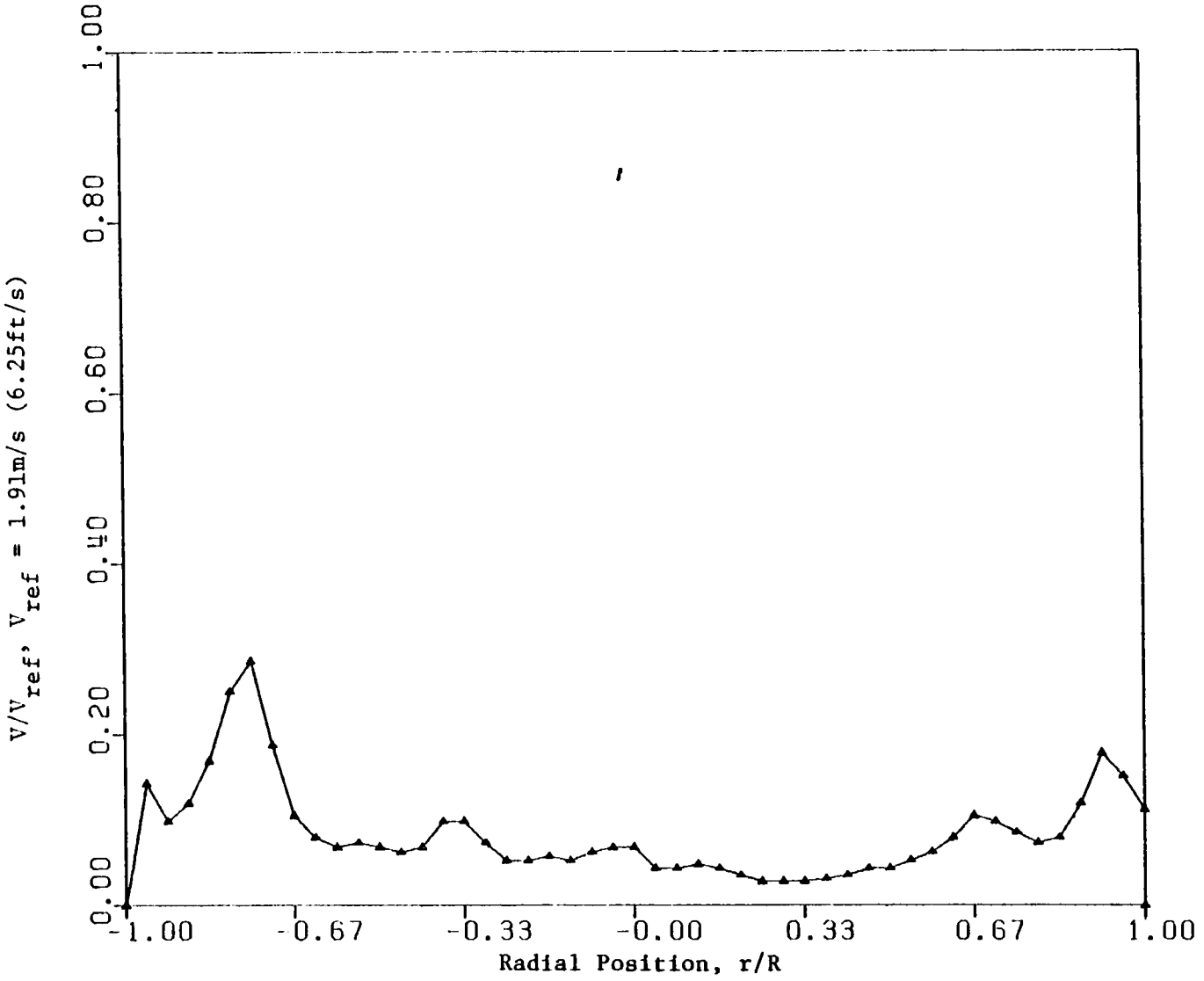

Figure C1. Measured Velocity Profile for Flow Through a 0.153m(0.5ft) Packed Bed--Run 01.

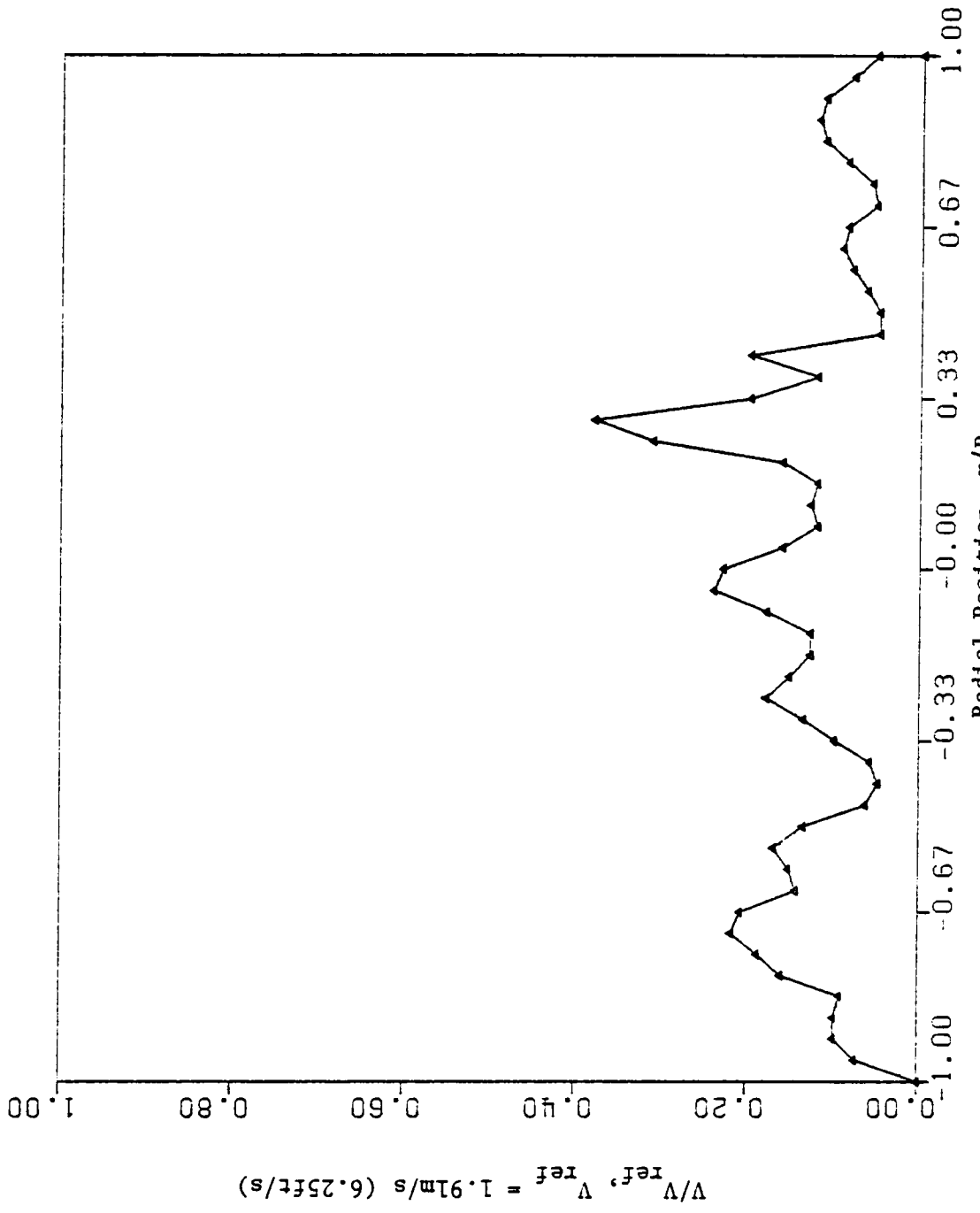

Figure C2. Measured Velocity Profile for Flow Through a 0.153m(0.5ft) Packed Bed--Run 02.

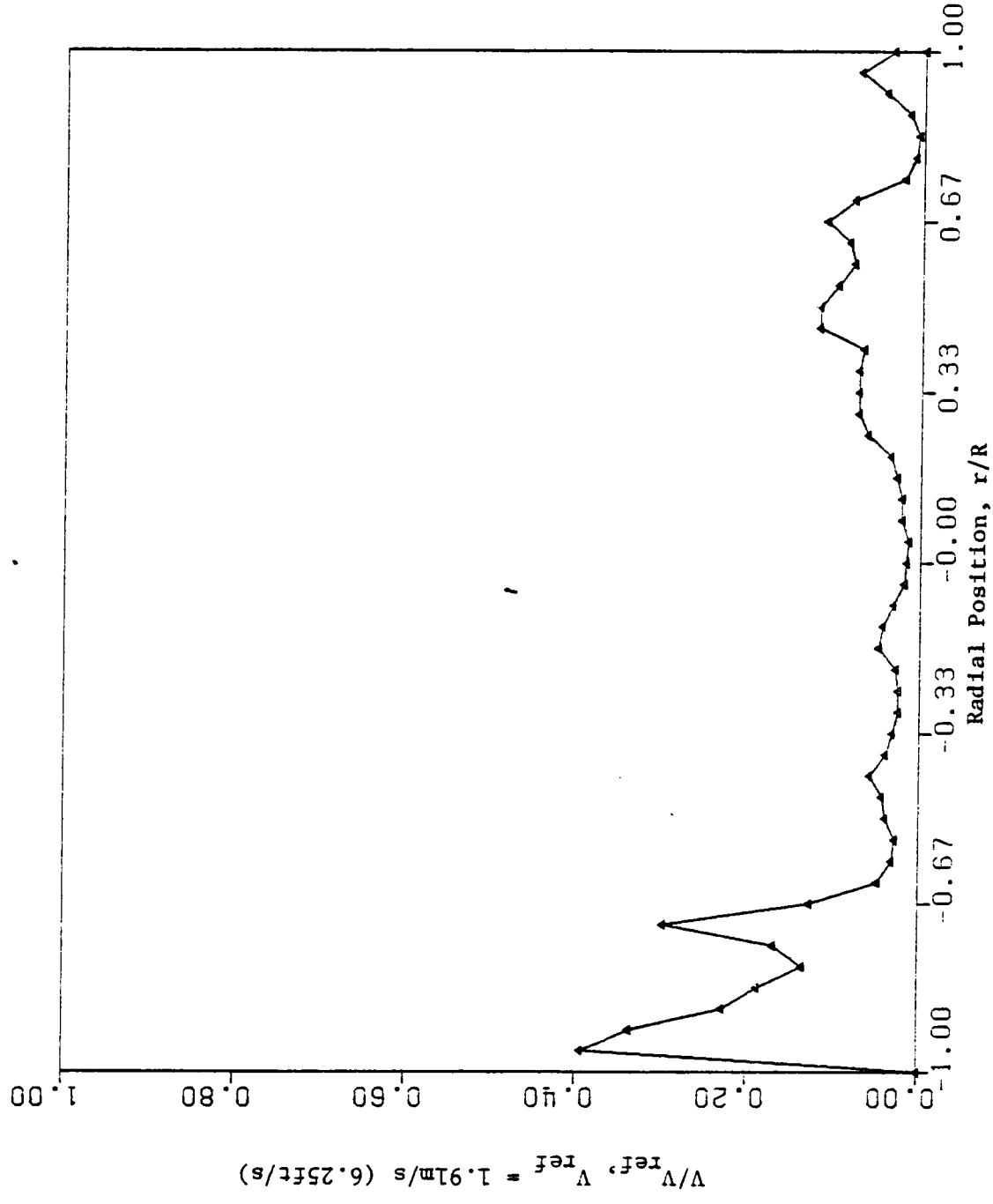

Figure C3. Measured Velocity Profile for Flow Through a 0.153m(0.5ft) Packed Bed--Run 03.

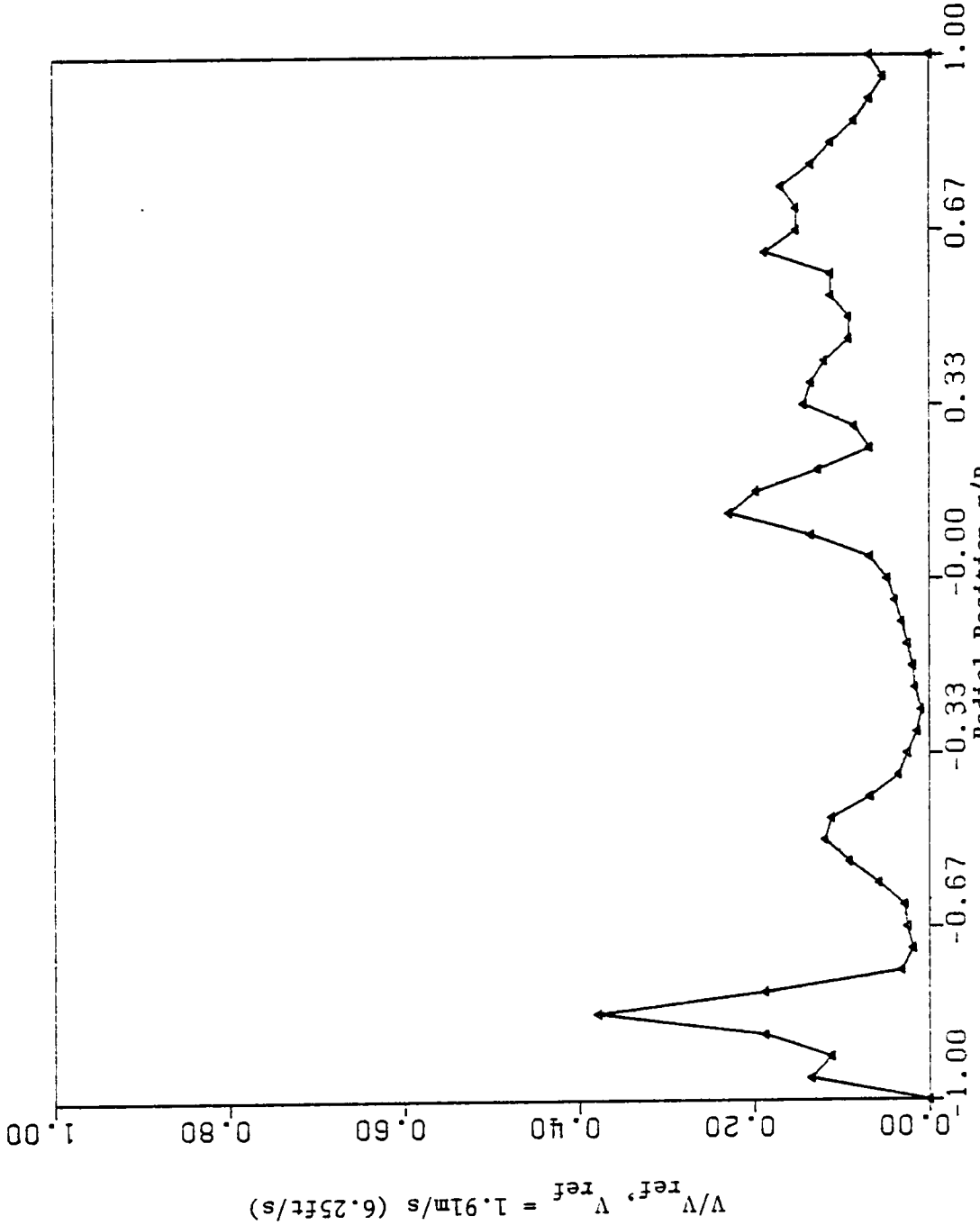

Figure C4. Measured Velocity Profile for Flow Through a 0.153m(0.5ft) Packed Bed--Run 04.

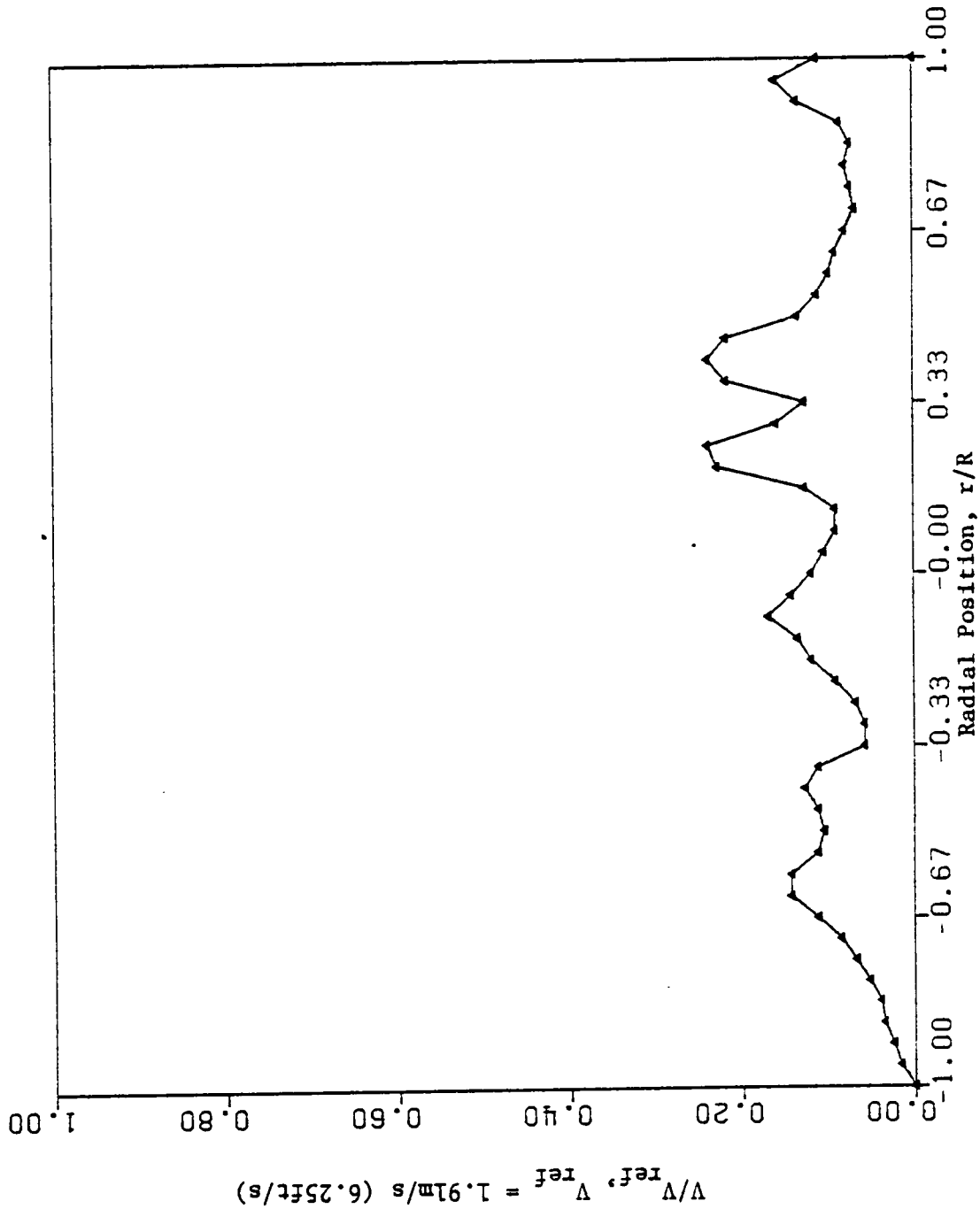

Figure C5. Measured Velocity Profile for Flow Through a 0.153m(0.5ft) Packed Bed--Run 05.

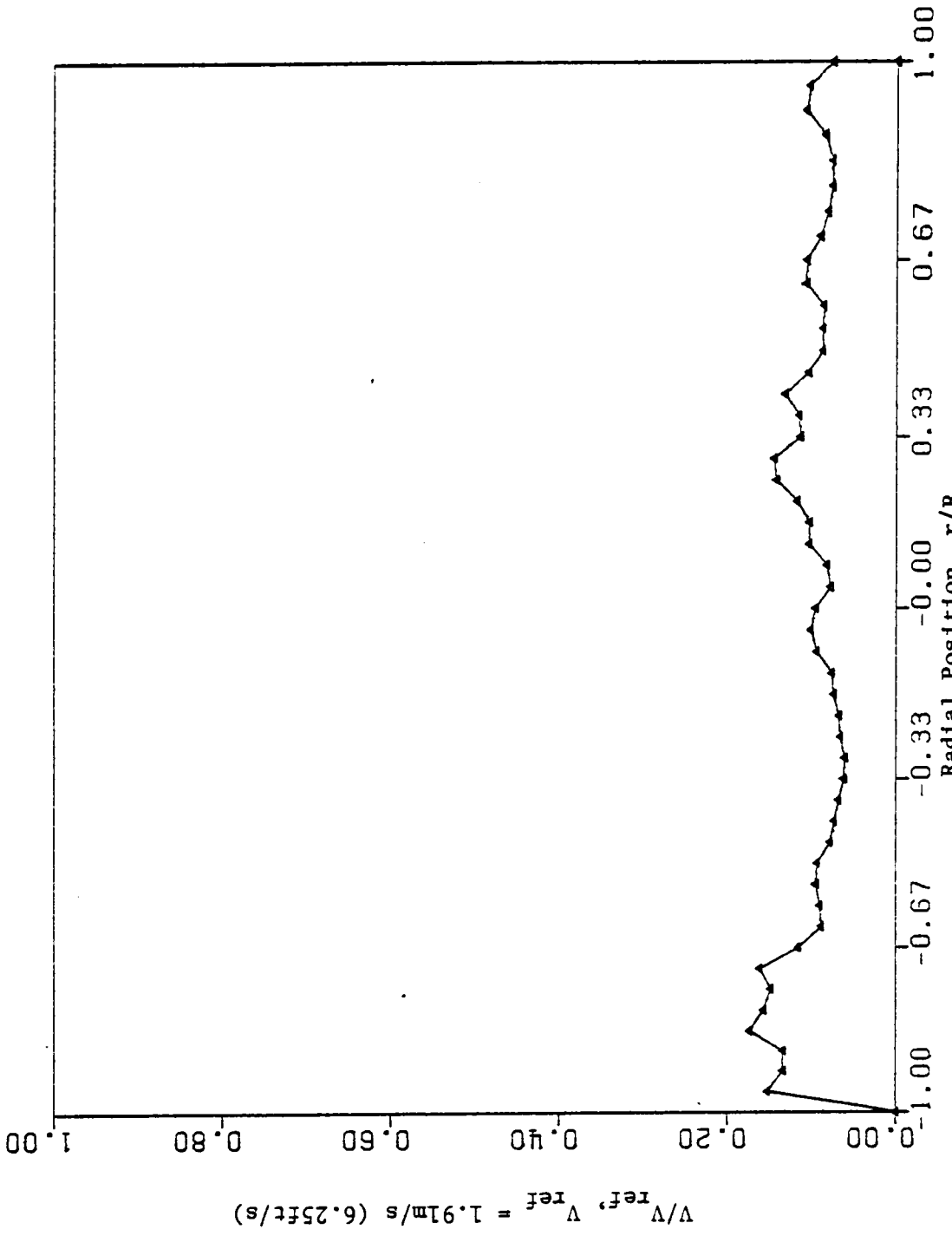

Figure C6. Measured Velocity Profile for Flow Through a 0.153m(0.5ft) Packed Bed--Run 06.

APPENDIX D. GAS CHROMATOGRAPH CALIBRATION

1. SO_2 Calibration Procedure

To ensure linearity and reproducibility of the chromatograph calibration, several samples were analized by a variety of methods. Reproducibility of SO_2 measurements using two prepared gas mixtures (Airco cylinders No. LL1990 and CC5785) were 29.9 ± 0.12 mm and 98.0 ± 0.07 mm corresponding to SO_2 concentrations of 921.1 and 2880 ppmv, respectively. An analysis of a representative calibration curve is presented in Table D.1. Recorder response was verified by comparing the response for known millivolt inputs. The results of a least squares regression analysis is presented in Table D.2.

2. Water Vapor Calibration Procedure

The mole fraction of water vapor used for calibrating the gas chromatagraph was obtained by injecting known volumes of water into sampling flask containing a specified volume of nitrogen. The apparatus used for obtaining water vapor-nitrogen mixtures is shown in Fig. D.1. For comparison, values were obtained from a large environmental chamber where water vapor concentrations were determined using a psychrometer and also a Gastek Gas Monitor.

The humity ratio of the air-water vapor sample was calculated using the expression

$$W = \frac{C_{pa}(t_{wb} - t_{db}) + W_{ws} - wbt(hfg - wbt)}{hwv - dbt - h_{wl} - wbt}$$

Table D.1. Analysis of Representative SO_2 Calibration

Peak Height mm	Estimated Height	Residual	Percent Error
12	12.2	-0.18	0.015
20*	17.9	2.10	-0.105
30	28.9	1.01	-0.034
43	46.8	-3.3	0.088
52.5*	58.2	-5.7	0.109
65	61.1	3.93	-0.060
73.5	71.4	2.1	-0.028
99.5	98.9	0.59	-0.006

Least Squares Regression Analysis

Intercept	-3.88 mm
Regression Coefficient	0.0357 mm/ppmv
Correlation Coefficient	0.994

* Values obtained using Gastek Gas Monitor

Table D.2. Gas Chromatograph Recorder* Linearity

Input Voltage mv	Recorder Response mm	Estimated Response	Residual	Percent Error
0.1	28	27.07	0.928	-0.033
0.2	55	55.28	-0.286	0.005
0.3	88	83.5	-0.50	0.006
0.4	111	111.7	-0.714	0.006
0.5	140	139.9	0.071	-0.001
0.6	168	168.1	-0.143	0.001
0.7	197	196.4	0.643	-0.003

Linear Regression Model	Ph = A + BX
Intercept	A = -1.143 mm
Regression Coefficient	B = 282.1 mm/mv
Correlation Coefficient	1.000

* Westronic Recorder
Model: SSAZ-3
Serial: 2689

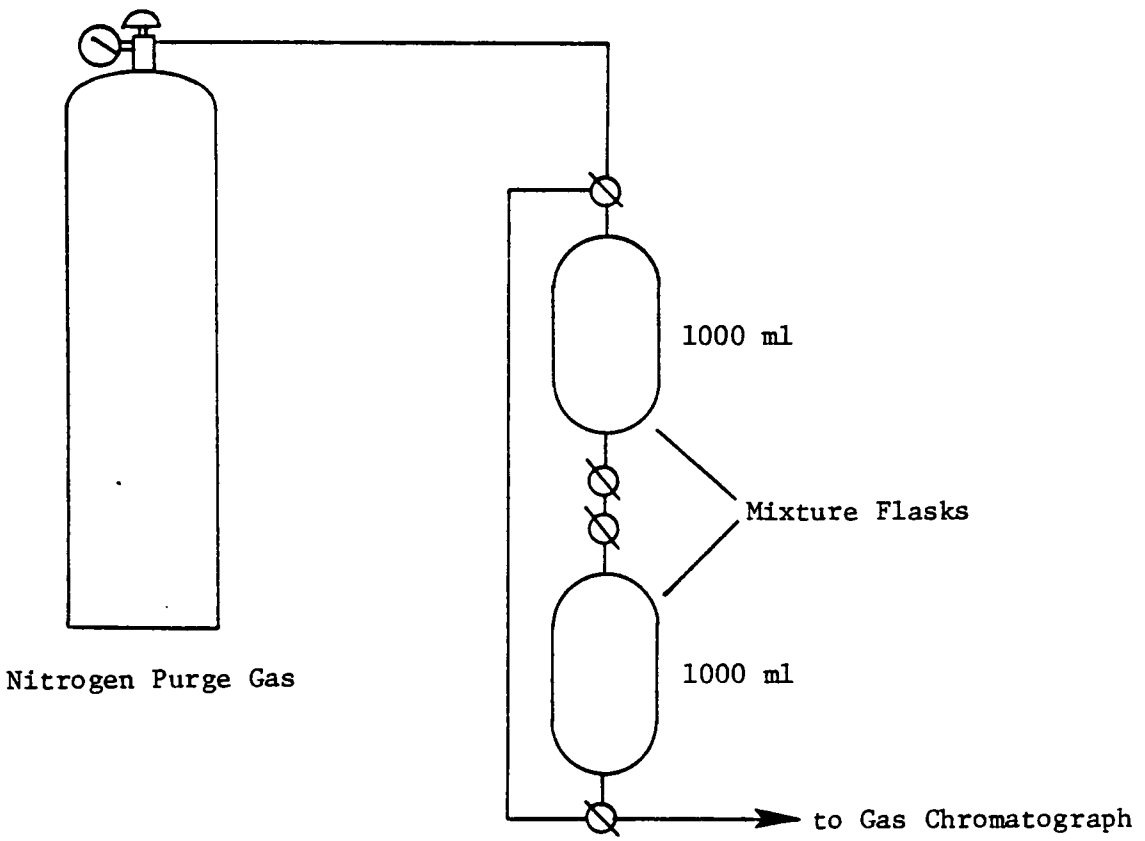

Figure D.1. Configuration Used for Calibrating Gas Chromatograph for Water Vapor.

where

C_{pa} = air specific heat

twb = wet-bulb temperature

tdb = dry-bulb temperature

h_{fg} - wbt = phase change enthalpy

h_{wv} - dbt = water vapor enthalpy at dry-bulb temperature

hwl - wbt = liquid water enthalpy at wet-bulb temperature

The relative humidity was obtained using

$$\phi = \frac{P_{wv} - dbt}{P_{ws} - dbt}$$

where

P_{wv} - dbt = partial pressure of water at dry-bulb temperature

P_{ws} - dbt = partial pressure of saturated water vapor at the dry-bulb temperature

The mole fraction of water vapor then is given by

$$x_{H_2O} = \frac{(P_{ws} - dbt)\phi}{P}$$

A least squares regression analysis of the linear transform for the water vapor calibration curve model yielded

$$Ph = 10^{(-1.46 + 0.9 \log x_{H_2O})}$$

where

Ph = chromatograph response, peak height (mm)

x_{H_2O} = water vapor mole fraction.

Several combinations of carrier gas flowrate, cell current, and oven temperature were varied to obtain the most suitable settings for measurement of a range of SO_2 - water vapor mixtures. A representative chromatogram of an N_2-SO_2-water vapor mixture is shown in Fig. D.2. Resolution of SO_2 and water vapor was 1.25 for the conditions specified. During actual breakthrough curve measurements this was not crucial since water vapor retention time was greater for the adsorbents tested in this investigation.

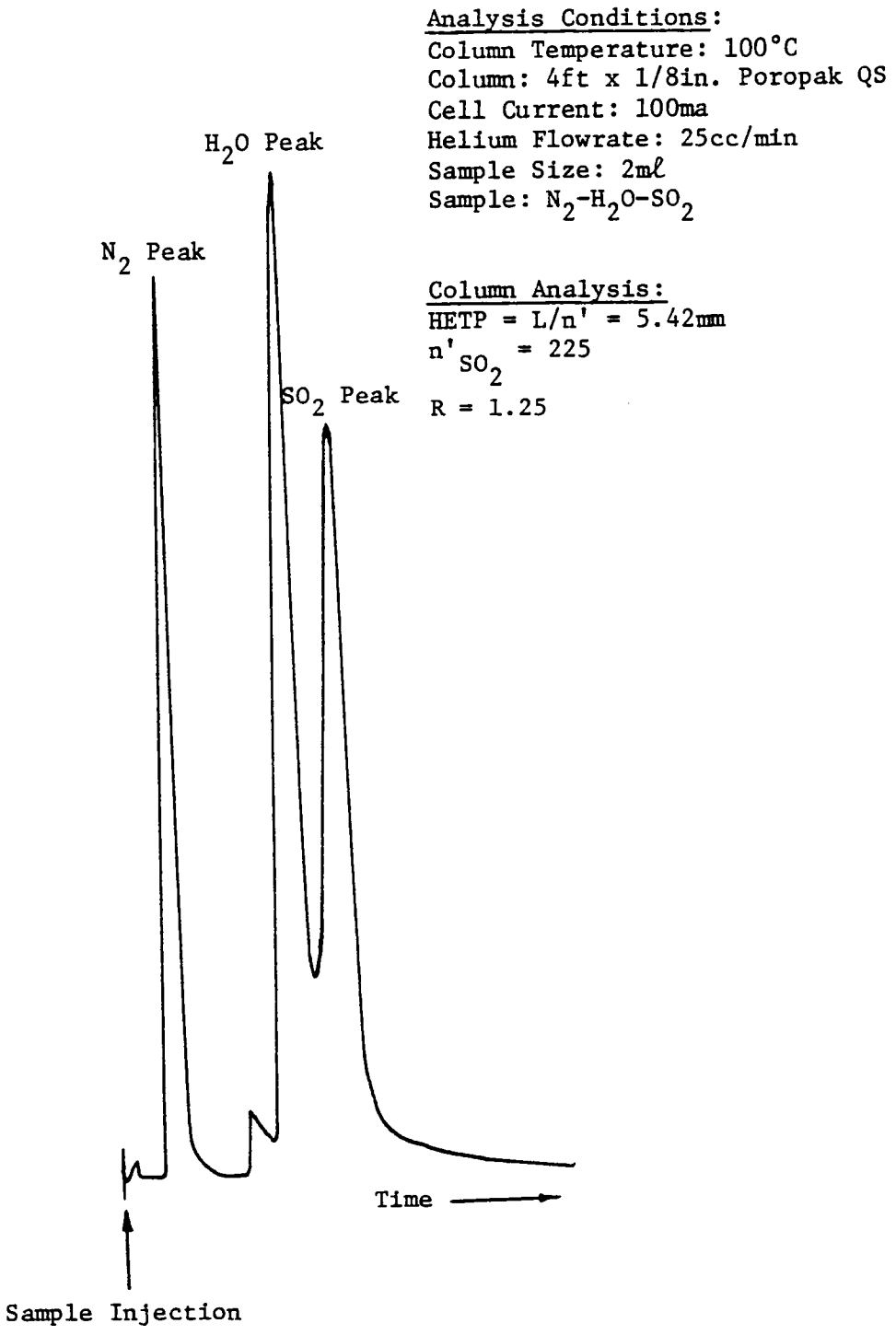

Figure D2. Representative Chromatogram for Analysis of SO_2 and Water in Air.

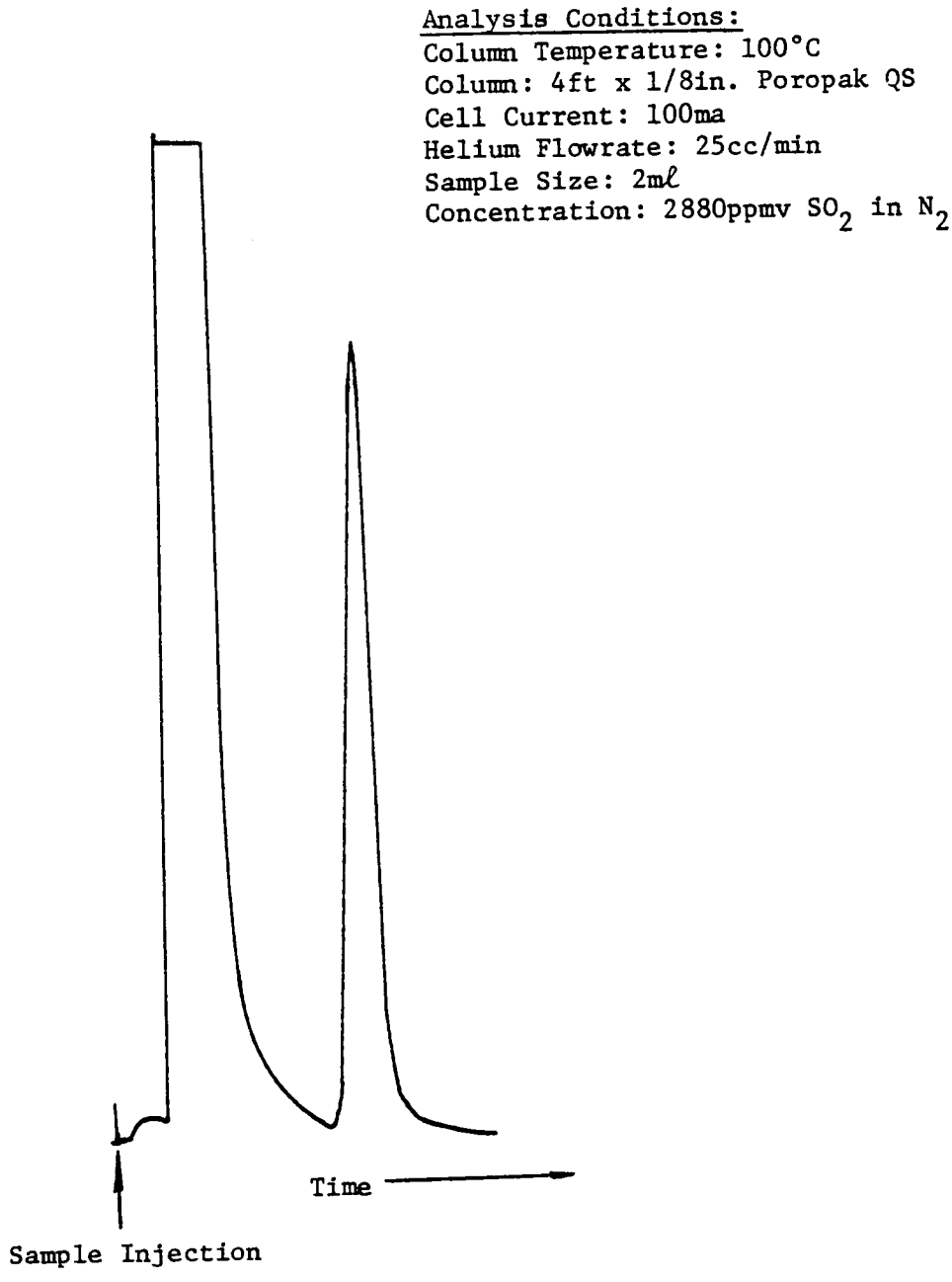

Figure D3. Representative Chromatogram for SO_2 Analysis.

APPENDIX E. SUMMARY OF BINARY ADSORPTION TESTS

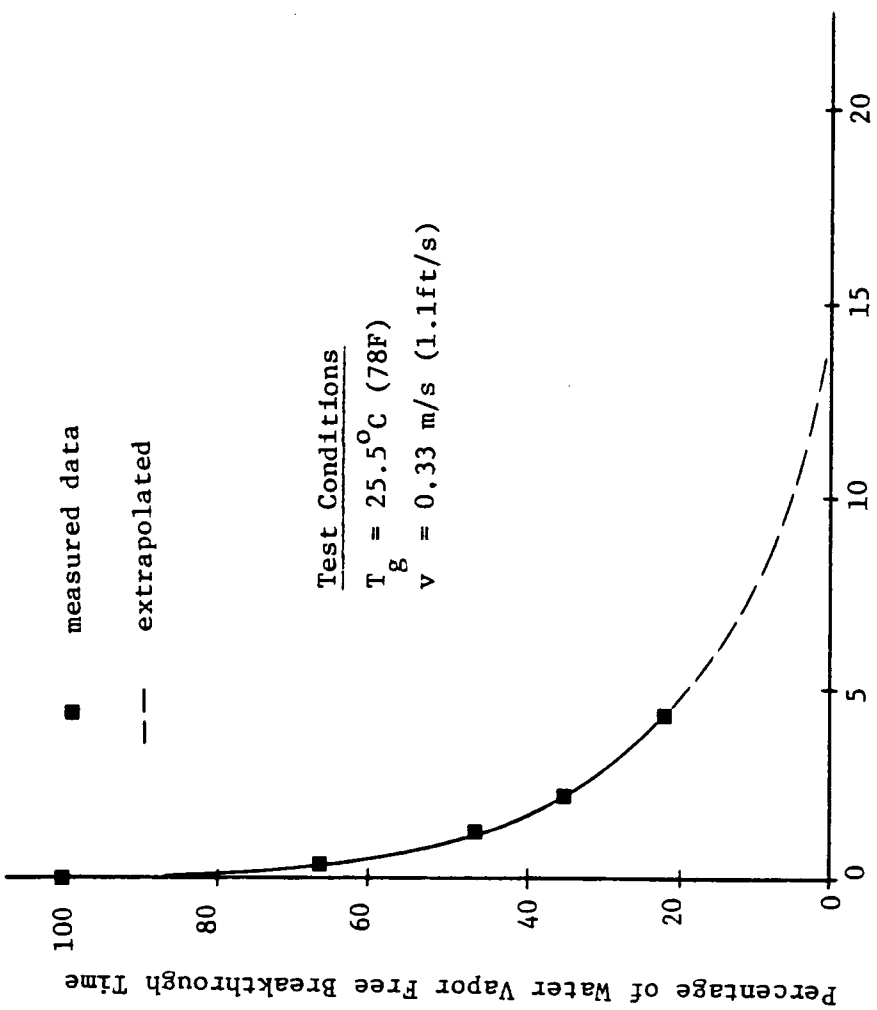

Figure E1. Variation in SO_2 Breakthrough Time with Inlet Vapor Concentration on 13X Molecular Sieve.

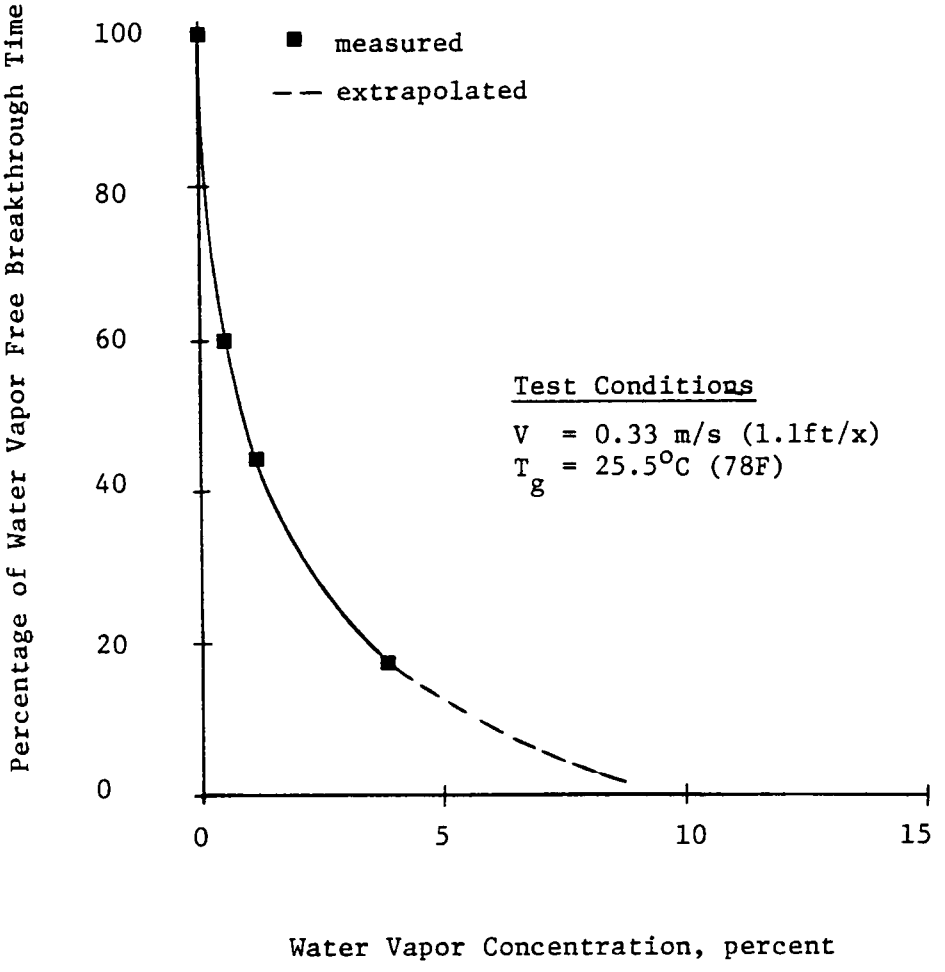

Figure 2. Variation in SO_2 Breakthrough Time with Water Vapor Concentration on AW500 Molecular Sieve.

APPENDIX F. SUMMARY OF ELECTRONPROBE ANALYSIS OF 13X AND AW500 MOLECULAR SIEVES

Table F.1. Summary of Electron Microprobe Analysis of 13X and AW500 Molecular Sieves -- No SO_2 Exposure

Sample	SiO_2/Al_2O_3 weight percent	SO_3[1] weight percent	Analysis Location* μm
13X Molecular Sieve	1.449	0.283	1
	1.464	0.537	3
	1.375	0.759	6
	1.461	0.962	2
	1.439	0.818	8
AW500 Molecular Sieve	3.715	0.323	1
	3.918	0.27	5
	3.911	0.381	8
	3.794	0.334	12
	3.978	0.392	15
	3.946	0.433	19
	3.783	0.471	22
	3.868	0.501	26
	3.907	0.574	29
	4.065	0.555	33

Summary of Microprobe Analysis

	$(SiO_2/Al_2O_3)_{avg}$	T	T_m
13X Molecular Sieve	1.438	0.0368	0.0165
AW500 Molecular Sieve	3.888	0.1026	0.0324

* Beam Location with respect to first sample analyzed

[1] used to reference SO_2 exposed samples

APPENDIX G. MEASUREMENTS OF SO_2 EQUILIBRIUM ADSORPTION CAPACITY ON 13X AND AW500 MOLECULAR SIEVES

Several methods can be used for obtaining the equilibrium adsorption capacity of an adsorbent. Gas chromatographic pulse response techniques, low pressure adsorption flask apparatus, and gravimetric methods would be capable of obtaining adsorption equilibrium data. For this investigation the gravimetric method was chosen because of the simple fabrication required.

Data acquisition consisted of exposing a known weight of adsorbent to a gas of known concentration. The flask temperature was maintained by a constant temperature bath. After equilibrium was obtained, the adsorption flask was weighted on an electronic balance and the adsorbent weight gain recorded. Corrections for gas weight and void volume of the flask were also measured. A summary of the results for the ultimate SO_2 adsorption capacity of type 13X and AW500 molecular sieves is shown in Tables G.1. and G.2.

Table G.1. Ultimate SO_2 Adsorption Capacity of 13X Molecular Sieve*

Gas Temperature °C	(F)	SO_2 Adsorption weight percent	Estimated Adsorption weight percent	Residual	Percent Error	95% Confidence Intervals	
25.5	(78)	0.316	0.317	-0.001	-0.2	0.313	0.320
71.1	(160)	0.2903	0.288	-0.002	0.7	0.285	0.292
87.7	(190)	0.277	0.270	0.007	-0.1	0.274	0.281
112.7	(235)	0.261	0.262	0.001	-0.3	0.258	0.265

Least Squares Regression Model

Intercept	0.50597
Regression Coefficient	0.0003514/°R
Correlation Coefficient	-0.998

* Linde Molecular Sieve Lot No. 13945450038

Table G.2. Ultimate SO_2 Adsorption Capacity of AW500 Molecular Sieve*

Gas Temperature °C	(F)	SO_2 Adsorption weight percent	Estimated Adsorption weight percent	Residual	Percent Error	95% Confidence Intervals	
25.5	(78)	0.242	0.242	-0.000	0.0	0.239	0.245
71.1	(160)	0.208	0.209	-0.001	-0.5	0.206	0.212
87.7	(190)	0.199	0.197	0.002	1.0	0.194	0.200
112.7	(235)	0.178	0.179	-0.001	-0.4	0.175	0.182

Least Squares Regression Model

Intercept	0.4586
Regression Coefficient	-0.0004025/°R
Correlation Coefficient	-0.999

* Linde Molecular Sieve Lot No. 5943556040

APPENDIX H. PROPERTIES OF MOLECULAR SIEVE ZEOLITES

Table H.1. Adsorbent Data of Linde 13X Molecular Sieve Zeolite -- 0.3175 cm (1/8 in.) pellets

Nominal Pore Diameter	10 Å
Bulk Density	38 lbm/cu ft
Particle Diameter	0.115-0.135 in.
Crush Strength	18 lbf
Heat of Adsorption (maximum)	1800B/lbm H_2O
Equilibrium H_2O Capacity	28.5% wt
Water Content (as shipped)	<1.5% wt

Application: general gas drying, air purification, removal of H_2S and mercaptans from liquid hydrocarbons and natural gas

Table H.2. Adsorbent Data for AW500 Molecular Sieve Zeolite

Nominal Pore Diameter	5.0 Å
Bulk Density	45.4 lbm/cu ft
Pellet Density	72.7 lbm/cu ft
Heat of Adsorption	1450 B/lbm H_2O
Specific Heat	0.15 B/lbm-F - 60F
	0.19 B/lbm-F - 100F
	0.24 B/lbm-F - 460F
Thermal Conductivity (vacuum)	0.08B/ft-hr-F

Application: Reformer Recycle Hydrogen Drying and H_2S and CO_2 removal from natural gas

Table H.3. Adsorption Data for Davison GR1 Silica Gel

Nominal Pore Diameter (average)	22 Å
Bulk Density	45 lbm/cu ft
Thermal Conductivity	0.08 Btu/hr-ft-F

Chemical Analysis

	weight percent
Silica as SiO_2	99.71
Iron as Fe_2O_3	0.03
Aluminum as Al_2O_3	0.10
Titanium as TiO_2	0.09
Calcium as CaO	0.01
Sodium as Na_2O	0.02
Zirconium as ZrO_2	0.01

Application: general gas drying, polar molecules favorably adsorbed

Relative Adsorbability (decreasing order of adsorption):

water
alcohols
aromatics
di-olefins
olefins
paraffins

(for hydrocarbons of similar molecular weight, adsorbability increases with the number of double bonds per molecule)

The vita has been removed from the scanned document

APPLICATION OF SYNTHETIC MOLECULAR SIEVE ZEOLITES AND SILICA GEL TOWARDS THE SEPARATION OF SULFUR DIOXIDE FROM COMBUSTION GASES

by

George Todd Wright

(ABSTRACT)

An evaluation of several commercial adsorbents for use as contacting media in a process for combustion gas desulfurization was performed. Linde Synthetic Molecular Sieves types 13X and AW500 and Davison Silica Gel were the materials studied. The motivation for this investigation was based on the premise that a suitable method for removing sulfur dioxide from combustion gas streams has not been realized.

Sulfur dioxide adsorption capacities were obtained for equilibrium (non-flow) and dynamic flow conditions. Sulfur dioxide adsorption on the molecular sieves could be described by a modified Langmuir expression of the form

$$\frac{q}{q_m} = \frac{kc^{1/n}}{1 + kc^{1/n}}$$

Calculated isosteric heats of adsorption were found to agree with measured data.

Small scale dynamic studies consisted of contacting the adsorbents in a packed column with a simulated combustion gas. Evaluation of the adsorbent materials consisted of monitoring the effluent gas concentration after exposure to a step change in sulfur dioxide concentration.

Sulfur dioxide loadings were greatest for the type 13X molecular sieve followed by AW500 molecular sieve. The effect of gas throughput was minimal which suggests that mass transfer was adsorbent side controlling. As gas temperature increased, sulfur dioxide adsorption decreased linearly for 100 percent sulfur dioxide concentration and non-linearly for low concentrations (0.003 percent).

The effect of water vapor on sulfur dioxide adsorption capacity was determined by monitoring the effluent gas composition for specified sulfur dioxide-water vapor mixtures. Breakthrough time for sulfur dioxide was found to be an inverse function of the inlet water vapor concentration. For a typical combustion gas stream, (8 percent water vapor) the breakthrough time is roughly 10 percent of the water vapor free value.

Based on the results obtained, a shallow bed (0.15m, 0.5 ft) of either type 13X or AW500 molecular sieve removed 5 to 3 times that of activated charcoal for a gas temperature of 57.2°C (135 F) and low gas pressure drop 4.6 cm H_2O (1.85 in. H_2O).

Adsorption degradation studies were performed to determine the loss in sulfur dioxide adsorption capacity after adsorbent regeneration. Both the 13X and AW500 molecular sieve could be regenerated, but the

loss in adsorption capacity depended on the gas contacting conditions. X-ray spectroscopy was used to determine the homogeneity of the sulfur distribution within the adsorbents. The sulfur dioxide adsorption capacity for subsequent regeneration cycles was found to be a function of the $A\ell_2O_3/SiO_2$ ratio of the molecular sieve.

Application of the molecular sieve adsorbents in a simulated combustion gas for sulfur dioxide removal was found to be superior to several adsorbents for the temperature range 21-76°C (70-170 F). However, as gas temperature increases, sulfur dioxide adsorption decreases. No adsorption of sulfur dioxide above 148°C (300 F) could be measured.